ISSN 1881-7815 Online ISSN 1881-7823

BST
BioScience Trends

Volume 13, Number 5
October, 2019

IRCA
BSSA

IACMHR

www.biosciencetrends.com

BST
BioScience Trends

ISSN: 1881-7815
Online ISSN: 1881-7823
CODEN: BTIRCZ
Issues/Year: 6
Language: English
Publisher: IACMHR Co., Ltd.

BioScience Trends is one of a series of peer-reviewed journals of the International Research and Cooperation Association for Bio & Socio-Sciences Advancement (IRCA-BSSA) Group and is published bimonthly by the International Advancement Center for Medicine & Health Research Co., Ltd. (IACMHR Co., Ltd.) and supported by the IRCA-BSSA and Shandong University China-Japan Cooperation Center for Drug Discovery & Screening (SDU-DDSC).

BioScience Trends devotes to publishing the latest and most exciting advances in scientific research. Articles cover fields of life science such as biochemistry, molecular biology, clinical research, public health, medical care system, and social science in order to encourage cooperation and exchange among scientists and clinical researchers.

BioScience Trends publishes Original Articles, Brief Reports, Reviews, Policy Forum articles, Case Reports, News, and Letters on all aspects of the field of life science. All contributions should seek to promote international collaboration.

Editorial Board

Editorial Office

Pearl City Koishikawa 603,
2-4-5 Kasuga, Bunkyo-ku, Tokyo 112-0003, Japan
Tel: +81-3-5840-8764 Fax: +81-3-5840-8765
E-mail: office@biosciencetrends.com

BioScience Trends

Editorial and Head Office

Pearl City Koishikawa 603, 2-4-5 Kasuga, Bunkyo-ku,
Tokyo 112-0003, Japan

Tel: +81-3-5840-8764, Fax: +81-3-5840-8765
E-mail: office@biosciencetrends.com
URL: www.biosciencetrends.com

Editorial Board Members

CONTENTS

Volume 13, Number 5, 2019

Review

Original Article

Brief Report

Communication

Retraction

Guide for Authors

Copyright

Review

DOI: 10.5582/bst.2019.01244

The toxicity and safety of traditional Chinese medicines: Please treat with rationality

Pingping Cai[1], Hua Qiu[2], Fanghua Qi[1], Xiaoyi Zhang[1,*]

[1] *Department of Traditional Chinese Medicine, Shandong Provincial Hospital affiliated to Shandong University, Ji'nan, China;*
[2] *Department of gynecology, Jinan Municipal Hospital of Traditional Chinese Medicine, Ji'nan, China.*

Summary **For a long time, many people have believed that traditional Chinese medicines (TCMs) are safe because they derive from natural products. However, this belief has been greatly challenged in recent years especially after some reports on aristolochic acid involved in the genesis of cancer. According to the Chinese pharmacopoeia, many TCMs are known to be toxic, causing damage to the nervous, liver, renal, respiratory, and reproductive system. How to reduce the toxicity of TCMs and how to avoid abuse of TCMs in daily practice is the question? Here, we will give a brief summary and some tips on these issues. First, the accurate differentiation of a specific syndrome is the foundation of an effective and individualized treatment strategy, as well as the key to applying TCMs. Second, through standard processing, proper compatibility, rational decoction, and appropriate dose for TCMs, the harm of TCMs can be effectively avoided. Third, it should be remembered that Chinese herbs cannot be taken continuously as dietary supplements. Finally, Chinese patent medicines should be used with caution. In addition, the dosage of TCMs should not exceed the limit prescribed by the current China Pharmacopoeia, which will ensure the balance of efficacy and toxicity. Taken together, it is necessary to treat the toxicity and safety of TCMs with rationality. The more toxicity we can find, the more safety patients will have.**

Keywords: Traditional Chinese medicines (TCMs), Chinese patent medicines, dietary supplements, toxicity, safety, rationality

1. Introduction

Over the centuries, traditional Chinese medicines (TCMs) have been widely used to treat numerous diseases in China and other ancients from the orient since they are relatively low cost, widely available and have reliable therapeutic efficacy (*1*). Currently, TCMs are receiving increasing attention worldwide as alternative and supplemental medicines (*2*). The World Health Organization estimates that 80% of the world population uses herbal medicine. For a long time, many people have believed that TCMs are safe because they are derived from natural products. However, this belief has been greatly challenged in recent years especially after some reports on aristolochic acid involved in the genesis of cancer (*3*). Thus, the toxicity and safety issues of TCMs have aroused increasing concern by the international community in recent years.

Are TCMs really toxic? As practitioners and researchers of traditional Chinese medicine (TCM), their answers are yes. In fact, many TCMs are really toxic. Shennong's Herbal Classic (Shennong Bencao Jing), finished in the Eastern Han Dynasty of China (24-220 AD), is the oldest pharmacopoeia in the world (*4*). It records 365 TCMs and these TCMs are divided into top, middle and lower of three grades (Table 1): (*i*) 120 TCMs belonging to the top grade are non-toxic, nourishing and strong products, such as ginseng, licorice, rehmannia, jujube, *etc*.; (*ii*) 120 TCMs belonging to the middle grade are non-toxic or toxic products, some of which can help the weak, such as lily, angelica, longan, antler, *etc*., some can fight evil and disease, such as berberine, ephedra, white

Released online in J-STAGE as advance publication September 30, 2019.

**Address correspondence to:*
Dr. Xiaoyi Zhang, Department of Traditional Chinese Medicine, Shandong Provincial Hospital affiliated to Shandong University, No. 324, Jingwuweiqi Road, Ji'nan 250021, Shandong, China.
E-mail: zhangxiaoyi6257@sina.com

Table 1. A brief introduction about Shennong's Herbal Classic (Shennong Bencao Jing)

Grade	Number of herbs	Characteristic	Common herbs
Top	120	Non-toxic, nourishing and strong products	Ginseng, licorice, rehmannia, jujube, *etc*.
Middle	120	Non-toxic or toxic products, some of which can help the weak	Berberine, ephedra, white peony, jaundice, *etc*.
Lower	150	poisonous products which can destroy evil spirits	Rhubarb, aconite, croton, *etc*.

peony, jaundice and so on; (*iii*) 125 TCMs belonging to the lower grade are poisonous products which can destroy evil spirits, such as rhubarb, aconite, and croton. Although many TCMs are toxic, as long as they are used properly, the toxicity is exactly their role. In TCM, the human body is divided into Yin and Yang (*5*). Diseases occur when the Yin and Yang balance is disrupted. Different herbs with toxicity are used to restore this balance. That is to say, for symptomatic treatment, toxic drugs are also safe; for non-symptomatic treatment, non-toxic drugs are also harmful. Therefore, it is necessary to treat the toxicity and safety of TCMs with rationality. But how to reduce the toxicity of TCMs and how to avoid abuse of TCMs in daily use? These issues deserve to be seriously considered by everyone. Here, we will give a brief summary and some tips on these issues (Table 2).

Table 2. Some tips on treating the toxicity of traditional Chinese medicines (TCMs)with rationality

Tips	How to reduce the toxicity of TCMs?
1	Syndrome differentiation and treatment of TCM
2	Rational preparation
3	Reasonable compatibility
4	Proper processing
5	Correct decoction
6	Appropriate dose
Tips	**How to avoid improper use of TCMs in daily practice?**
1	Do not regard TCMs as dietary supplements
2	Do not abuse Chinese patent medicines

2. How to reduce the toxicity of TCMs?

Many common drugs in the Chinese materia medica are known to be toxic, causing damage to nervous, liver, renal, respiratory system, and reproductive system (Table 3) (*6-14*). The toxic components from TCM herbs include alkaloids, anthraquinones, aristolochic acids, cardiac glycosides and others (*15*). Among the TCM-induced side effects, aconite toxicity is of major concern, which derives from Aconitum species (*16*). Although many TCMs are toxic, in clinical practice, their toxicity can be avoided and their efficacy can be enhanced by rational preparation, decoction, interaction with other herbal medicines and so on (*17*). Moreover, practitioners of TCM should pay more attention to treating diseases with TCM syndrome differentiation theory, mastering reasonable doses of TCMs, and ceasing in time after recovery. In addition, the dosage of TCMs should not exceed the limit prescribed by the current China Pharmacopoeia, and also should be strictly controlled by considering various factors, which will ensure the balance of efficacy and toxicity. The more toxicity we can find, the more safety patients will have.

2.1. *Syndrome differentiation of TCM*

Syndrome differentiation and treatment of TCM is a process of understanding diseases and solving diseases using TCM theory and methods. TCM Syndrome, also known as "ZHENG" in Chinese, is an integral and essential part of TCM theory. The TCM syndrome can be observed by a clinical TCM practitioner using the traditional four diagnostic methods including inspection, listening, inquiry, and palpation rather than micro-level laboratory tests or imaging examination (*18*). The accurate differentiation of a specific syndrome is the foundation of an effective and individualized treatment strategy, as well as the key to recognizing the disease state (*19*). Therefore, syndrome differentiation plays the most important role in the TCM system. It is the essence of TCM, consistent with modern "precise medicine". However, many people ignore the TCM practitioner's advice on syndrome differentiation and treatment theory, and regard TCMs as general ingredients to boil soup or tea. In fact, if not following the theory of TCM, using some medicated diet or herbal tea for a long time can cause liver and kidney damage and some other toxicities.

In addition, according to the difference of a patient's physical condition, TCMs should be used with caution especially for the elderly, children and pregnant women. As the body's function of the elderly is degenerative, the distribution, absorption, metabolism and excretion capacity of TCMs will be affected. For the elderly, the dosage of TCMs should be strictly controlled, generally starting with the "minimum dose" and reducing it as appropriate. More importantly, as we all know, for pregnant patients, the improper use of some Chinese herbs can be harmful to the fetus, affect the growth of the fetus, or cause the fetus to be teratogenic or aborted, such as tripterygium, safflower, and so on. Using TCMs during pregnancy, the TCM practitioners should not only consider its therapeutic effects according to syndrome differentiation and treatment theory, but also consider the impact of these drugs on the growth and development of the fetus or the newly born baby (*20*).

Table 3. Some common Traditional Chinese medicines (TCMs) with severe toxicities

Common name	Scientific name	Source	Activity	Toxicity							Ref.
				liver	Renal	Cardiologic	Neurologic	Respiratory	Carcinogenic	Reproductive	
Fu-zi	*Aconitum carmichaeli*	Lateral root	Analgesic; anti-inflammatory			•	•				*6,7*
Chuan-wu	*Radix Aconiti*	Mother root	Anti-inflammatory; analgesic; cardiotonic			•	•				*6,8,9*
Cao-wu	*Radix Aconiti kusnezoffii*	Tuberous root	Anti-inflammatory; analgesic; cardiotonic			•	•				*6,9,10*
Ma-huang	*Ephedra sinica*	Grass stem	Anti-inflammatory; cardiotonic; antiallergic; vasoconstrictive;	•	•	•	•				*6,11,12*
Xi-xin	*Asarum sieboldii*	Whole herb	Analgesic; anti-inflammatory; cardiotonic; Antiasthma				•	•			*6,13*
Guan-mu-tong	*Caulis aristolochiae*	Stem	Diuretic; anti-inflammatory; anti-cancer		•				•		*6,11,13*
Guang-fang-ji	*Aristolochia fangchi*	Root	Analgesic; antiallergic; anti-inflammatory;		•				•		*6,11,13*
He-shou-wu	*Polygonum multiflorum*	Tuberous root	Anticancer; anti-hyperlipidemia; anti-aging; hair-blacking	•						•	*6,14*

2.2. *Preparation of TCMs*

Prior to sale as TCMs, raw herbs must undergo physical and/or chemical pretreatment processes (Paozhi in Chinese) after harvesting, for preservation, detoxification, or enhancing efficacy (*17,21*). According to Pharmacopoeia of the People's Republic of China 2015, the processes of preparation include sun drying, stir frying, roasting, honey frying, wine frying, soil frying, vinegar frying, steaming, fumigation, calcination and so on, which are the key methods for reducing toxicity (*6*). Using methods of rational preparation, reasonable compatibility, and proper processing based on traditional experiences and new technologies, can enable TCMs to be used safely and effectively. In the following section, we will use aconitum species as examples to give a brief introduction to the importance of rational preparation and proper processing for TCMs.

Aconitum species, including including Chuan-wu (Radix Aconiti), Cao-wu (Radix Aconiti kusnezoffii), and Fu-zi (Aconitum carmichaeli), are well known for their medicinal value and high lethal toxicity in many Asian countries, notably China, India and Japan. Aconitum carmichaelii, known as Fu-zi in China, "bushi" in Japan, and "Kyeong-Po Buja" in Korea, is the processed lateral root of Aconitum carmichaelii Debeaux (Ranunculaceae) (*22*). It is an officially recognized TCM with characteristic analgesic and anti-inflammatory activities, whose principal pharmacological ingredients are considered to be aconitine-type diterpene alkaloids. Both Radix Aconiti kusnezoffii (known as Cao-wu in China), the root of Aconitum kusnezoffii Reichb., and Radix Aconiti (known as Chuan-wu in China), the mother root of Aconitum carmichaelii Debx., are believed to possess anti-inflammatory, analgesic and cardiotonic effects and have been widely used clinically in the treatment of musculoskeletal disorders such as rheumatic arthritis and painful joints for thousands of years (*23*). The problem of toxicity is a constraint for effective application of these aconitum species and are sometimes life threatening. The heart and the central nervous system are the primary toxicity targets (*9*). Modern research has shown that the toxic components of these aconite roots are diester diterpenoid alkaloids, including aconitine, mesaconitine, hypaconitine, neoline, talatizamine, beiwutine, and deoxyaconitine, which are neurotoxins and cardiotoxins (*24*).

Aconitum species are only used after processing. They can be used safely and effectively with the methods of decoction, rational compatibility, and correct processing based on traditional experiences and new technologies (*25*). Moreover, current metabolomics is vitally significant to evaluate toxicity and finding detoxification methods for TCMs (*26*). A clear understanding of the toxicity mechanism of aconitum species and the influence on the metabolome are

essential for clinical safety. Yan *et al*. conducted a study to analyze the toxicity and detoxification effects of herbal Cao-wu *via* HPLC/MS metabolomics using a pattern recognition method (*10*). The research determined the main target organs for toxicity are the heart and liver after long-term administration of Cao-wu. Cao-wu mainly affected glucuronate interconversions, nucleotide sugar metabolism, fatty acid metabolism, and proline metabolism associated with the liver; affected taurine transformation, amino sugar metabolism associated with the heart; and affected tryptophan metabolism associated with the nervous system.

2.3. *Proper compatibility of TCMs*

Compatibility is a feature of the theoretical system of TCM, which embodies the concept of syndrome differentiation and treatment. The interaction between compatible medicines includes mutual reinforcement and the opposite, mutual restraint and detoxication, mutual assistance and inhibition according to Shennong's Herbal Classic (*27*). It can play a role of detoxification or increased efficiency through proper compatibility. Here, we will use aconitum species as examples to give a brief introduction to the importance of proper compatibility for TCMs.

Screened from classical TCM prescriptions, combinatorial intervention of Cao-wu with Gancao (Radix Glyeyrrhizae), Baishao (Radix Paeoniae Alba), Ganjiang (Rhizoma Zingiberis), and Renshen (Radix Ginseng) are the most extensively used combinatorial intervention drugs in the clinical setting to decrease toxicity and enhance efficacy (*28*). Modern research has shown that metabolomics is vitally significant to evaluate toxicity and find detoxification methods for TCMs. Dong *et al* conducted a study using urinary metabolomics, which were examined by UPLC-Q-TOF-HDMS and the mass spectra signals of the detected metabolites were systematically analyzed using pattern recognition methods (*25*). The expression levels of toxicity biomarkers in the urine were analyzed to evaluate the detoxification of Cao-wu combined with Gancao (Radix Glyeyrrhizae), Baishao (Radix Paeoniae Alba) and Ganjiang (Rhizoma Zingiberis). They found that three compatible drugs could effectively detoxify Cao-wu. After compatibility, the content of ester alkaloids showed a descending tendency, which decreases the toxicity of aconitum plants. Another study indicated that after administration of Gancao, Baishao, and Renshen (Radix Ginseng), the metabolic markers of metabolic pathways and metabolic direction associated with toxicity of Cao-wu decreased, which then had no toxic effect on the body (*10*).

2.4. *Correct decocting methods for TCMs*

Most TCMs are used as a decoction and the correct decocting method can be effectively used to remove the toxicity of some TCMs. Decoction for a longer time represents a traditional way to detoxify toxic TCM herbs. The process of decoction can make the toxic components changes after boiling.

Some poisonous TCMs such as aconitum species (Chuan-wu, Cao-wu, and Fu-zi), and raw Pinellia ternata (Banxia in Chinese) should be decocted first for 1-2 h to reduce toxicity and increase safety and effectiveness (*6*). As mentioned above, the toxic components of these aconitum species roots are diester diterpenoid alkaloids, including aconitine, mesaconitine, hypaconitine, deoxyaconitine, and so on, which are neurotoxins and cardiotoxins (*24*). The toxicity of these diester diterpenoid alkaloids are hydrolyzed into non-toxic derivatives by water decoction. Therefore, long-time decoction was commonly applied as a traditional way to detoxify TCMs from aconitum species roots before use. Why has long-time decoction been used as a traditional way for detoxifying aconitum species? Why has it been widely applied in many aconitum species such as Fu-zi-contained in TCM prescriptions? Some modern pharmacological studies have given a scientific explanation for these questions. Water-decoction hydrolyzes diester diterpenoid alkaloids into non-toxic derivatives by removing their acetyl group and benzoyl ester group (*29*). However, some reports indicated that Fu-zi is not sufficiently safe even after long-time decoction. Sun *et al*. (*30*) applied both rodent and zebrafish models to thoroughly evaluate the safety of the traditional detoxification method and applied chemoprofile analyses to analyze the underlying phytochemical basis. They concluded that Fu-zi is not sufficiently safe even after long-time decoction. This indicates that the detoxifying effect of long-time decoction on some poisonous TCMs remains controversial and needs to be further studied.

Rhubarb (Rheum rhabarbarum, Dahuang in Chinese) is a species of plant in the family Polygonaceae. Anthraquinones are the main components of Rhubarb. Rhubarb is well known for its cathartic effect and has been used as a laxative for several thousand years. It has been widely prescribed to treat gastrointestinal disease, hepatitis, blood diseases, chronic renal failure, and especially constipation due to its effective purgative activity (*31*). To better play its role as a purgative, Rhubarb is usually given a short time decoction. That is to say, after some other Chinese herbs of a TCM prescription have been boiled for a while Rhubarb will then be added and boiled together (*32*). If Rhubarb is given a long time decoction, its active components anthraquinones will be destroyed and its purgative activity will be decreased. Rhubarb has been reported to have diarrhoeogenic and anti-diarrhoeal bidirectional effects due to the coexistence of anthraquinones and tannins. The bidirectional effects might be the reason or one of the reasons for the adverse effects of long-term

use of rhubarb as a purgative (*33*).

3. How to avoid improper use of TCMs in daily practice

As can be seen from the above, through strict syndrome differentiation and treatment, standard processing, proper compatibility, rational decoction, and appropriate dose for TCMs, the harm of Chinese herbal medicine can be effectively avoided by clinical TCM physicians and practitioners. Nevertheless, for the majority of non-TCM professionals, they are often harmed by some TCMs unconsciously. Here, we will give a brief summary and some tips on how to avoid improper use of TCMs in daily practice.

3.1. *Do not regard TCMs as dietary supplements*

Currently, with the increasing popularity of herbal products and traditional Chinese medicine as alternative and supplemental medicines in the Western world, therapeutic effects of some Chinese herbs have been exaggerated or distorted, and the herbs are usually regarded as dietary supplements and misused (*34*). Chinese herbs can be toxic, which has been proven through laboratory research. Both clinical practice and research have demonstrated that TCMs are a special type of natural materia medica, and not dietary supplements. In contrast, dietary supplements are preparations intended to provide nutrients that are missing or are not consumed in sufficient quantity in a person's diet (*35*). Therefore, it is of significance to properly use TCMs.

Ginseng Radix (Renshen in Chinese or Ginseng in Korea) is a well-known and popular TCM, which is believed to be the king of the herbs in the Orient particularly in China, Korea and Japan. It has been used for several thousand years with mysterious powers as a tonic, prophylactic and restorative agent (*36*). It has a good therapeutic effect with cardiovascular benefits especially for convalescent patients, and has become one of the most popular herbal supplements on the US market. Nevertheless, some reports of adverse effects from products containing ginseng have been filed with the US Food and Drug Administration (FDA). These adverse effects are named "Ginseng abuse syndrome" and is manifested by diarrhea, skin lesions, central nervous system stimulation, and interference with homeostasis (*37*). Ginseng may increase the anti-platelet effect of Coumadin, aspirin, and NSAIDs and taking these drugs with Ginseng may pose surgical risks. Ginseng may also elevate blood pressure and increase irritability with long term use (*34*).

Radix Astragali (Huangqi in Chinese), is the dried root of Astragalus membranaceus Bge. Var. mongholicus, and one of the most famous and frequently used herbal medicines and healthy food supplements used as a tonic. It has been used for over 2000 years in TCM prescriptions for the treatment of animal bites and poisons, wounds and burns, nephritis, diabetes, albuminuria, hypertension, cirrhosis, and various cancers (*37*). However, it is reported that products containing Huangqi have some adverse effects if used for a long time. Huangqi may induce bleeding when used with another anticoagulant, anti-platelet, or anti-thrombotic agents. Furthermore, it is incompatible with opiates (*34*).

Therefore, it looks to be dangerous for patients to self-administer Chinese herbs improperly and to not inform their physician. Moreover, it should be remembered that herbs cannot be taken continuously as dietary supplements. From time to time, doctors of TCM must be consulted for proper herbal dosage adjustment, to meet individual needs and provide necessary warnings. In addition, a public health campaign should be launched by the government to educate users about the merits and hazards of improper use of TCMs.

3.2. *Do not abuse Chinese patent medicines*

Chinese patent medicines are a form of Chinese herbal medicine that are isolated from single herbs or their active compounds or herbal formulations and prepared using modern advanced pharmaceutical technology. There are various dosage forms including injections, tablets, pills, capsules, and liquids (*6*). Chinese patent medicines are developed by combining modernized pharmaceutical technologies with ancient TCM theories. Compared to traditional herbal decoctions, refined dosage forms and relative standardization in composing the main effective components are considered to be advantages of Chinese patent medicines (*38*). Therefore, Chinese patent medicines are becoming increasingly popular in China and are attracting worldwide attention (*39*). In recent years, people have realized the hazards of hormones and antibiotics, but they still abuse Chinese patent medicines. They insist that Chinese patent medicines are safer, non-toxic and more effective. This misunderstanding has led to the abuse of Chinese patent medicines and is getting worse.

Polygonum multiflorum Thunb., known as He-shou-wu in Chinese, is traditionally valued and reported for hair-blacking, liver and kidney-tonifying and anti-aging effects as well as low toxicity. Pharmacokinetic studies have demonstrated that the main components of Polygonum multiflorum are various stilbenes, quinones, flavonoids, phospholipids and other compounds. It has been used in conditions like Alzheimer′s disease, Parkinson′s disease, hyperlipidemia, inflammation and cancer. On the other hand, it can lead to hepatotoxicity, nephrotoxicity and embryonic toxicity (*40*). Areca nut, known as Binlang in Chinese, is obtained from the fruit of the Areca catechu (Palmae), which is

widely distributed in southeast Asia and southern China. Areca nuts are regarded as a TCM usually used for the treatment of indigestion, liver disorders, and also used as a vermifuge. Pharmacological studies have demonstrated it has antibacterial, antioxidant, anti-inflammatory, antifungal, and anthelmintic activities (*41*). However, Areca nut chewing can cause dreaded diseases primarily oral submucous fibrosis, cardiovascular disease, and cancers, and has been listed as a primary carcinogen by American Joint Committee on Cancer (*42*). Therefore, Chinese patent medicines containing these ingredients such as Polygonum multiflorum and Areca nuts, should be used with caution.

In addition, some traditional Chinese patent medicines including Zhusha Anshen pills, Niuhuang Qingxin pills, Angong Niuhuang pills, Tianwang Buxin pills, and so on, contain cinnabar. Cinnabar is widely used in the clinic and shows a unique efficacy for calming and soothing the nerves. It has been used in treating diseases for thousands of years either as a single-use or in combination with other traditional Chinese medicines. Cinnabar mainly contains mercury, which displays obvious hepatotoxicity and nephrotoxicity (*43*). The safety of Chinese patent medicines containing cinnabar and rational use causes extensive attention. Excessive or over use will lead to poisoning reactions. Thus, these Chinese patent medicines should not be taken over-dosage or for a long time.

4. Conclusion

According to the Chinese pharmacopoeia, many TCMs are known to be toxic, causing damage to the nervous, liver, renal, respiratory, and reproductive system. How to reduce the toxicity of TCMs and how to avoid improper use of TCMs in daily practice? These should be paid more attention by everyone. First, the accurate differentiation of a specific syndrome is the foundation of an effective and individualized treatment strategy, as well as the key to applying TCMs. Second, through standard processing, proper compatibility, rational decoction, and appropriate dose for TCMs, the harm of TCMs can be effectively avoided. Third, it should be remembered that Chinese herbs cannot be taken continuously as dietary supplements. Finally, Chinese patent medicines should be used with caution according to the theory of syndrome differentiation and treatment. In addition, the dosage of TCMs should not exceed the limit prescribed by the current China Pharmacopoeia, which will ensure the balance of efficacy and toxicity. Moreover, a public health campaign should be launched by the government to educate users about the merits and hazards of improper use of TCMs. Taken together, it is necessary to treat the toxicity and safety of TCMs with rationality. The more toxicity we can find, the more safety patients will have.

Acknowledgements

This study was funded by National Natural Science Foundation of China (No. 81603449) and Key Research and Development Project of Shandong Province (No. 2019GSF108197).

References

1. Cheung F. TCM: Made in China. Nature. 2011; 480:S82-S83.
2. Wang ZX, Qi FH, Cui YG, Zhao L, Sun XG, Tang W, Cai PP. An update on Chinese herbal medicines as adjuvant treatment of anticancer therapeutics. Biosci Trends. 2018; 12:220-239.
3. Bara T Jr, Gurzu S, Sugimura H, Bara T, Beleaua MA, Jung I. A systematic review of the possible carcinogenic role of the aristolochic acid. Rom J Morphol Embryol. 2017; 58:41-44.
4. Xin T, Zhang Y, Pu X, Gao R, Xu Z, Song J. Trends in herbgenomics. Sci China Life Sci. 2019; 62:288-308.
5. Chua YT, Ang XL, Zhong XM, Khoo KS. Interaction between warfarin and Chinese herbal medicines. Singapore Med J. 2015; 56:11-18.
6. The State Pharmacopoeia Commission of the People's Republic of China. Pharmacopoeia of the People's Republic of China 2015. China Medical Science and Technology Press, Beijing, China, 2015.
7. Yang M, Ji X, Zuo Z. Relationships between the Toxicities of Radix Aconiti Lateralis Preparata (Fuzi) and the Toxicokinetics of Its Main Diester-Diterpenoid Alkaloids. Toxins (Basel). 2018; 10(10). pii: E391.
8. Zhang Y, Bian X, Yang J, Wu H, Wu JL, Li N. Metabolomics of Clinical Poisoning by Aconitum Alkaloids Using Derivatization LC-MS. Front Pharmacol. 2019; 10:275.
9. Chan TY. Aconite poisoning. Clin Toxicol (Phila). 2009; 47:279-285.
10. Yan Y, Zhang A, Dong H, Yan G, Sun H, Wu X, Han Y, Wang X. Toxicity and Detoxification Effects of Herbal Caowu *via* Ultra Performance Liquid Chromatography/ Mass Spectrometry Metabolomics Analyzed using Pattern Recognition Method. Pharmacogn Mag. 2017; 13:683-692.
11. Brown AC. Kidney toxicity related to herbs and dietary supplements: Online table of case reports. Part 3 of 5 series. Food Chem Toxicol. 2017; 107(Pt A):502-519.
12. Lee AY, Jang Y, Hong SH, Chang SH, Park S, Kim S, Kang KS, Kim JE, Cho MH. Ephedrine-induced mitophagy *via* oxidative stress in human hepatic stellate cells. J Toxicol Sci. 2017; 42(4):461-473.
13. Duan L, Guo L, Wang L, Yin Q, Zhang CM, Zheng YG, Liu EH. Application of metabolomics in toxicity evaluation of traditional Chinese medicines. Chin Med. 2018; 13:60.
14. Wang Y, Wang L, Saxena R, Wee A, Yang R, Tian Q, Zhang J, Zhao X, Jia J. Clinicopathological features of He Shou Wu-induced liver injury: This ancient anti-aging therapy is not liver-friendly. Liver Int. 2019; 39:389-400.
15. Xu XL, Yang LJ, Jiang JG. Renal toxic ingredients and their toxicology from traditional Chinese medicine. Expert Opin Drug Metab Toxicol. 2016;12:149-159.
16. Poon WT, Lai CK, Ching CK, Tse KY, So YC, Chan

YC, Hau LM, Mak TW, Chan AY. Aconite poisoning in camouflage. Hong Kong Med J. 2006; 12:456-459.
17. Liu SH, Chuang WC, Lam W, Jiang Z, Cheng YC. Safety surveillance of traditional Chinese medicine: current and future. Drug Saf. 2015; 38:117-128.
18. Su SB, Jia W, Lu A, Li S. Evidence-Based ZHENG: A Traditional Chinese Medicine Syndrome 2013. Evid Based Complement Alternat Med. 2014; 2014:484201.
19. Gu Z, Qi X, Zhai X, Lang Q, Lu J, Ma C, Liu L, Yue X. Study on TCM Syndrome Differentiation of Primary Liver Cancer Based on the Analysis of Latent Structural Model. Evid Based Complement Alternat Med. 2015; 2015:761565.
20. Chen HQ, Zou SH, Yang JB, Cai J, Zhang Y, Wang ZL. A survey and analysis of using traditional Chinese medicine during pregnancy. Int J Clin Exp Med. 2015; 8:19496-19500.
21. Simon RA. Adverse reactions to drug additives. J Allergy Clin Immunol. 1984; 74:623.
22. Zhou G, Tang L, Zhou X, Wang T, Kou Z, Wang Z. A review on phytochemistry and pharmacological activities of the processed lateral root of Aconitum carmichaelii Debeaux. J Ethnopharmacol. 2015; 160:173-193.
23. Chan TY, Tomlinson B, Tse LK, Chan JC, Chan WW, Critchley JA. Aconitine poisoning due to Chinese herbal medicines: a review. Vet Hum Toxicol. 1994; 36(5):452-455.
24. Sun H, Wang M, Zhang A, Ni B, Dong H, Wang X. UPLC-Q-TOF-HDMS analysis of constituents in the root of two kinds of Aconitum using a metabolomics approach. Phytochem Anal. 2013; 24:263-276.
25. Dong H, Yan GL, Han Y, Sun H, Zhang AH, Li XN, Wang XJ. UPLC-Q-TOF/MS-based metabolomic studies on the toxicity mechanisms of traditional Chinese medicine Chuanwu and the detoxification mechanisms of Gancao, Baishao, and Ganjiang. Chin J Nat Med. 2015; 13:687-698.
26. Liu S, Li F, Li Y, Li W, Xu J, Du H. A review of traditional and current methods used to potentially reduce toxicity of Aconitum roots in Traditional Chinese Medicine. J Ethnopharmacol. 2017; 207:237-250.
27. Yang YY, Yang FQ, Gao JL. Differential proteomics for studying action mechanisms of traditional Chinese medicines. Chin Med. 2019; 14:1.
28. Zhang XM, Lin ZJ, Zhang B, Li A. Traditional prescription rules of Aconitum herbs in treatment of Bi syndrome. Zhongguo Zhong Yao Za Zhi. 2018; 43:211-215. (in Chinese)
29. Tong P, Wu C, Wang X, Hu H, Jin H, Li C, Zhu Y, Shan L, Xiao L. Development and assessment of a complete-detoxication strategy for Fuzi (lateral root of Aconitum carmichaeli) and its application in rheumatoid arthritis therapy. J Ethnopharmacol. 2013; 146:562-571.
30. Sun W, Yan B, Wang R, Liu F, Hu Z, Zhou L, Yan L, Zhou K, Huang J, Tong P, Shan L, Efferth T. In vivo acute toxicity of detoxified Fuzi (lateral root of Aconitum carmichaeli) after a traditional detoxification process. EXCLI J. 2018; 17:889-899.
31. Li F, Wang SC, Wang X, Ren QY, Wang W, Shang GW, Zhang L, Zhang SH. Novel exploration of cathartic pharmacology induced by rhubarb. Zhongguo Zhong Yao Za Zhi. 2008; 33:481-484. (in Chinese)
32. Peng Y, Wu C, Yang J, Li X. Gut microbial diversity in rat model induced by rhubarb. Exp Anim. 2014; 63:415-422.
33. Qin Y, Wang JB, Kong WJ, Zhao YL, Yang HY, Dai CM, Fang F, Zhang L, Li BC, Jin C, Xiao XH. The diarrhoeogenic and antidiarrhoeal bidirectional effects of rhubarb and its potential mechanism. J Ethnopharmacol. 2011; 133:1096-1102.
34. Lu WI, Lu DP. Impact of chinese herbal medicine on american society and health care system: perspective and concern. Evid Based Complement Alternat Med. 2014; 2014:251891.
35. Bao K. Non-scientific classification of Chinese herbal medicine as dietary supplement. Chin J Integr Med. 2017; 23:166-169.
36. Qi FH, Zhao L, Zhou AY, Zhang B, Li AY, Wang ZX, Han JQ. The advantages of using traditional Chinese medicine as an adjunctive therapy in the whole course of cancer treatment instead of only terminal stage of cancer. Biosci Trends. 2015; 9:16-34.
37. Siegel RK. Ginseng abuse syndrome. Problems with the panacea. JAMA. 1979; 241:1614-1615.
38. Wang Q, Li C, Di S, Han L, Zhao L, Tong X. Clinical efficacy and safety of traditional Chinese patent medicine for hyperthyroid heart disease: study protocol for a systematic review and meta-analysis. Medicine (Baltimore). 2018; 97:e13076.
39. He J, Tang M, Ye Z, Jiang X, Chen D, Song P, Jin C. China issues the National Essential Medicines List (2018 edition): Background, differences from previous editions, and potential issues. Biosci Trends. 2018;12:445-449.
40. Lin L, Ni B, Lin H, Zhang M, Li X, Yin X, Qu C, Ni J. Traditional usages, botany, phytochemistry, pharmacology and toxicology of Polygonum multiflorum Thunb.: a review. J Ethnopharmacol. 2015; 159:158-183.
41. Cao M, Yuan H, Daniyal M, Yu H, Xie Q, Liu Y, Li B, Jian Y, Peng C, Tan D, Peng Y, Choudhary MI, Rahman AU, Wang W. Two new alkaloids isolated from traditional Chinese medicine Binglang the fruit of Areca catechu. Fitoterapia. 2019; 138:104276.
42. Mehrtash H, Duncan K, Parascandola M, David A, Gritz ER, Gupta PC, Mehrotra R, Amer Nordin AS, Pearlman PC, Warnakulasuriya S, Wen CP, Zain RB, Trimble EL. Defining a global research and policy agenda for betel quid and areca nut. Lancet Oncol. 2017; 18:e767-e775.
43. Ding T, Luo JY, Han X, Yang SH, Lin RC, Yang MH. Advances of toxicity evaluation of cinnabar and compatibility necessity analysis. Zhongguo Zhong Yao Za Zhi. 2016; 41:4533-4540. (in Chinese)

(Received September 2, 2019; Revised September 15, 2019; Accepted September 18, 2019)

Review

DOI: 10.5582/bst.2019.01153

The clinical safety and efficacy of conventional transcatheter arterial chemoembolization and drug-eluting beads-transcatheter arterial chemoembolization for unresectable hepatocellular carcinoma: A meta-analysis

Tao Han[1,§], Xiaodan Yang[1,§], Yue Zhang[1], Gao Li[2], Lu Liu[1], Tingsong Chen[3,*], Zhendong Zheng[1,*]

[1] *Department of Oncology, Cancer Center, General Hospital of Northern Theater Command, Shenyang, Liaoning, China;*
[2] *Department of Clinical Pharmacy, Shenyang Pharmaceutical University, Shenyang, China;*
[3] *Department of Invasive Technology, The Seventh People's Hospital of Shanghai University of Traditional Chinese Medicine, Shanghai, China.*

Summary **Transcatheter arterial chemoembolization (TACE) plays an important role in the treatment of unresectable liver cancer. We conducted this meta-analysis to compare the clinical safety and efficacy of conventional TACE (C-TACE) and drug-eluting beads (DEB)-TACE. A search for those procedures was performed using the PubMed, EMBASE, and Cochrane Library databases. A meta-analysis of patients who underwent C-TACE or DEB-TACE was conducted. Odds ratios (ORs) and 95% confidence intervals (CIs) were calculated. Of 334 studies, 30 were analyzed. The complete response rate, disease control rate, objective response rate, 3-year survival rate, and non-response rate were significantly higher in patients who underwent DEB-TACE than those in patients who underwent C-TACE. The 1-year survival rate, 2-year survival rate, 30-day mortality rate, complete response rate, disease control rate, complete necrosis rate, non-response rate, objective response rate, progressive disease rate, and recurrence did not differ significantly between patients who underwent C-TACE and patients who underwent DEB-TACE. Patients who undergo DEB-TACE might have a higher complete response rate, disease control rate, and 3-year survival rate than patients who undergo C-TACE. Safety did not differ significantly between C-TACE and DEB-TACE.**

Keywords: TACE, DEB-TACE, liver cancer, objective response rate, survival, safety

1. Introduction

Hepatocellular carcinoma (HCC) is the 6th most common malignant tumor, and it ranks 3rd in terms of cancer-related deaths, with an overall survival rate of 3-5% (*1*). Unfortunately, its incidence is still rising around the world (*2*). Hepatitis viral infections and alcoholism are the dominant factors that trigger HCC. Diabetes, obesity, and metabolic disorders are also associated with HCC (*3*). Common treatments include resection, ablation, chemoembolization, radiotherapy, and chemotherapy (*4*). The preferred approach, surgical resection can increase the 5-year survival rate to 60% (*5*). However, most patients exhibit nonspecific clinical symptoms, so when the condition is ultimately diagnosed they are unable to undergo radical surgery (*6*). Only 10-15% of patients with HCC are eligible for surgical resection. As a downstaging therapy, transcatheter arterial chemoembolization (TACE) has been widely used to treat unresectable HCC, and it can improve the overall survival of patients with HCC (*7,8*).

Released online in J-STAGE as advance publication October 14, 2019.

[§]These authors contributed equally to this work.

*Address correspondence to:
Dr. Zhendong Zheng, Department of Oncology, Cancer Center, General Hospital of Northern Theater Command, Shenyang, Liaoning, No.83, Wenhua Road, Shenhe, Shenyang, Liaoning 110840, China.
E-mail: zhengzhdong@163.com

Dr. Tingsong Chen, Department of Invasive Technology, The Seventh People's Hospital of Shanghai University of Traditional Chinese medicine, Shanghai 200120, China.
E-mail: cts552052597@163.com

In TACE, a suspension consisting of a chemotherapy drug and lipiodol is delivered via a catheter to the hepatic artery branch of the diseased liver. The released chemotherapy drug then plays an antagonistic role. Drug-eluting beads transcatheter arterial chemoembolization (DEB-TACE) has often been performed over the past decade. Its major differences compared to conventional TACE (C-TACE) are a higher adsorption capacity of the chemotherapy drug and a slower and more consistent release (*9*). Considering the rapid metabolism of chemotherapy drugs in C-TACE, drug use should theoretically be better in DEB-TACE. However, its therapeutic efficacy and safety are debated. Therefore, this meta-analysis was performed.

2. Methods

2.1. *Search strategy*

A search of the PubMed, EMBASE, and the Cochrane Library databases was conducted. The last search was conducted on July 30, 2016. Search terms were as follows: "TACE," "DEB-TACE," and "hepatocellular carcinoma." The full text of each identified article was read, and irrelevant articles were discarded. If the same subjects were referenced across multiple articles or if an article included more subjects or provided more overall information than another article, then the article was selected for meta-analysis.

2.2. *Eligibility criteria*

Eligible studies were randomized controlled trials (RCTs) or prospective or retrospective cohort and case-control studies published prior to June 2016 that met the following inclusion criteria: *i*) directly compared C-TACE and DEB-TACE in patients with HCC; *ii*) reported at least one of the following data: response rate and survival rate; *iii*) reported the relative odds ratio (OR) and hazard ratio (HR) or provided data for their calculation; and iv) articles written in English.

Case reports and abstracts or studies with insufficient data were excluded. If multiple articles included the same subjects, only the most recent and complete article was analyzed. When information was incomplete, attempts were made to contact the corresponding authors for additional data.

2.3. *Data extraction*

Once the researchers agreed on the articles to include, a flow chat was created. The relevant information was as follows: first author, date of publication, country, study design, enrollment period, type of patients, groups, number of patients, number of procedures, previous TACE, locoregional treatment, Child-Pugh stage, Barcelona Clinic Liver Cancer Center (BCLC) stage, Okuda stage, ECOG performance status, and Milan tumor criteria.

2.4. *Assessment of study quality*

The quality of eligible RCTs and non-RCTs was respectively evaluated using the Cochrane Handbook for Systematic Reviews of Interventions and the Newcastle-Ottawa scale. The Cochrane Handbook for Systematic Reviews of Interventions consists of 6 items: adequacy of the generation of allocation sequence, allocation concealment, blinding, the presence of incomplete outcome data, selective outcomes, and other sources of bias. The Newcastle-Ottawa scale consists of 3 items including selection (4 points), comparability (2 points), and exposure (3 points).

2.5. *Data analysis*

Odds ratios (ORs) with 95% confidence intervals (CIs) were calculated to compare C-TACE and DEB-TACE, and only a random-effects model was used. All tests were two-tailed, and p values of less than 0.05 were statistically significant. The I^2 statistic and Chi-square test were used to evaluate heterogeneity. When $I^2 > 50\%$ or $p < 0.10$, heterogeneity was statistically significant. All statistical analyses were performed using Stata.

3. Results

3.1. *Study selection and characteristics*

As shown in Figure 1, 334 studies were initially identified. After preliminary exclusion of abstracts or papers not fulfilling the search criteria, 46 potentially relevant articles were examined. Of these studies, 14 were excluded due to incomplete data. Two studies reported information on the same subjects, and two other studies were published by the same group with overlapping recruitment periods. Ultimately, 30 studies, including 5 RCTs and 25 observational studies, involving 3,195 patients (1,444 treated with DEB-TACE and 1746 with C-TACE) were included in the meta-analysis.

Eight studies were conducted in Italy, 4 studies were conducted in Germany, 4 in the US, 3 in South Korea, 3 in Spain, 2 in Australia, 2 in the UK, 1 in Belgium, 1 in Taiwan, and 1 in Saudi Arabia. Baseline data and the characteristics of studies and patients are shown in Table 1. Five studies were of high quality, one study was of moderate quality, and one study was of poor quality.

3.2. *Comparison of the complete response rate*

Two studies involving 167 subjects reported the complete response rate. The complete response rate was

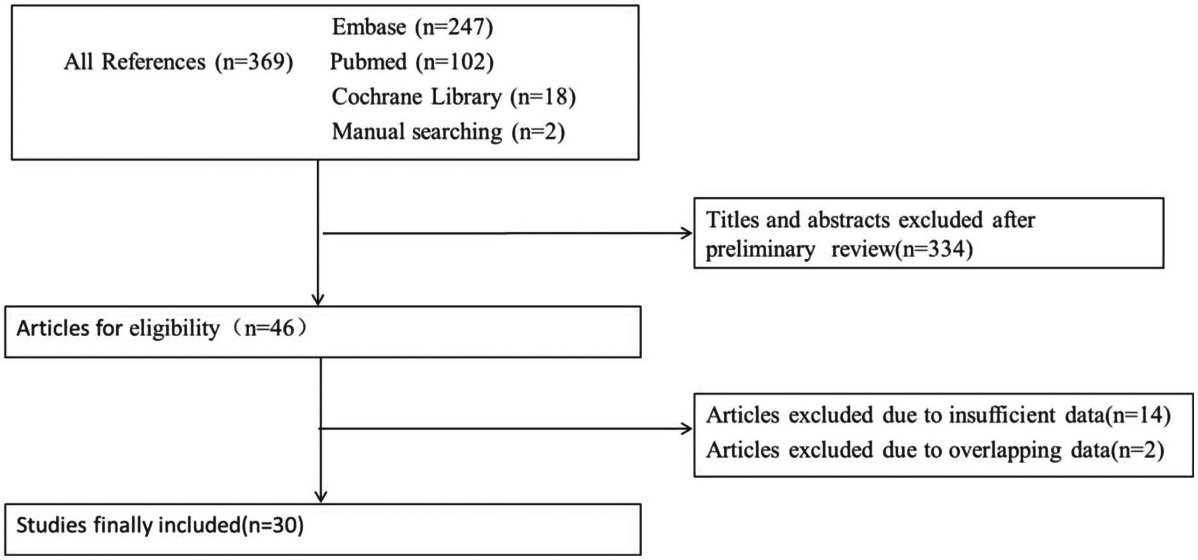

Figure 1. The search strategy used in this meta-analysis.

significantly higher in patients who underwent DEB-TACE than that in patients who underwent C-TACE (OR = 3.59, 95% CI = 1.48-8.72, $p = 0.0048$) without any significant heterogeneity ($p = 0.91$, $I^2 = 0\%$).

3.3. *Comparison of the disease control rate*

Nine studies involving 909 subjects reported the disease control rate (*19,21,25,26,30,32,35,36,38*). Of those studies, 2 were published by the same group. Ultimately, eight studies involving 869 patients were analyzed. The disease control rate was significantly higher in patients who underwent DEB-TACE than that in patients who underwent C-TACE (OR = 2.17, 95% CI = 1.22-3.87, $p = 0.0082$), and statistical heterogeneity was evident ($p = 0.08$, $I^2 = 44.8\%$).

3.4. *Comparison of the objective response rate*

The overall response rate (ORR) was reported in 13 studies (*12,17,19,21,25,26,30-32,34,35,36,38*). Due to the high heterogeneity found among the included studies ($\chi^2 = 6.67$, d.f. = 10, $I^2 = 71\%$; $p = 0.011$), the DerSimonian and Laird test for the random-effects models was used. The objective response rate was significantly higher in patients who underwent DEB-TACE than that in patients who underwent C-TACE (OR = 2.05, 95% CI = 1.17-3.55, $p = 0.011$), and statistical heterogeneity was evident ($p = 0.0001$, $I^2 = 71\%$). Subgroup analyses of RCTs and observational studies confirmed the non-significant OR in favor of DEB-TACE (OR = 1.27, 95% CI = 0.78-2.07 and OR = 2.40, 95% CI = 1.17-4.90, respectively) and detected, as expected, a high heterogeneity among the observational studies (Figure 2). The high heterogeneity may be caused by response assessment, namely, the timing of the response assessment, the response criteria, and the study design and quality.

3.5. *Comparison of the survival rate*

Fourteen studies involving 1,645 patients estimated the overall survival (OS) and compared the two groups using log-rank tests (*13,16,17,19,21,23,24,26,28,31,34,35,38*). As described in Table 2, the two groups had a similar 1-year survival rate (SR) that tended to be higher, albeit not significantly so, in patients who underwent DEB-TACE (OR 1.51, 95% CI 0.48-1.21, $p = 0.08$) (Figure 3). With treatment, survival was prolonged and the OR tended to decrease, albeit not significantly so, thus indicating better long-term outcomes in patients who underwent DEB-TACE (2-year SR: OR 1.32, 95% CI 0.74-2.36, $p = 0.34$; 3-year SR: OR 1.92, 95% CI = 1.00-3.68, $p = 0.049$). The meta-analysis of plotted HRs revealed no significant differences in the 1-year survival rate and 2-year survival rate. The 3-year survival rate was significantly higher in patients who underwent DEB-TACE than that in patients who underwent C-TACE (OR = 1.92, 95% CI = 1.00-3.67, $p = 0.049$), and statistical heterogeneity was evident ($p = 0.043$, $I^2 = 51.7\%$).

4. Discussion

This meta-analysis included a large number of studies on the efficacy and safety of TACE and DEB-TACE. A total of 30 studies (5 RCTs and 25 observational studies) involving 2,920 patients were analyzed. The DEBs, from 150 to 650 nm in size, were loaded with doxorubicin in all of the studies. The C-TACE arms widely differed with regard to the drugs used (Table 1). The current study indicated that patients who underwent DEB-TACE might have a higher complete response rate and disease control rate than patients who underwent C-TACE. In addition, meta-analysis indicated that the 1-year survival rate and 2-year survival rate did not differ significantly between

Table 1. Characteristics of the included studies

Study (*Ref.*)	Arm	Drug	Sample size	Study period	Design	Region	Previous TACE[a]	CP (A/B/C)	BCLC (0/A/B/C/)	Okuda (I/II/III)
Alsina 2011 (*10*)	C-TACE	Cisplatin Adryamicin Mytomicin-C	74	1996-2010	R	USA	NA	NA	NA	NA
	DEB-TACE	LC Beads	28				NA	NA	NA	NA
Arabi 2015 (*11*)	C-TACE	Cisplatin	19	2006-4014	R	Saudi	0	17/2/0	NA	NA
	DEB-TACE	Doxorubicin	35			Arabia	4	24/11/0	NA	NA
Bloom 2012 (*12*)	C-TACE	NA	15	2008-2011	R	Australia	NA	NA	NA	NA
	DEB-TACE	NA	15				NA	NA	NA	NA
Burrell 2014 (*13*)	C-TACE	NA	80	2006-2011	R	NA	NA	NA	NA	NA
	DEB-TACE	NA	26				NA	NA	NA	NA
Castelli 2013 (*14*)	C-TACE	NA	60	NA	NA	Italy	NA	NA	NA	NA
	DEB-TACE	NA	28				NA	NA	NA	NA
Cuomo 2011 (*15*)	C-TACE	Doxorubicin	45	2007-2010	R	Italy	NA	NA	NA	NA
	DEB-TACE	Doxorubicin	68				NA	NA	NA	NA
Dhanasekaran 2010 (*16*)	C-TACE	Doxorubicin Cisplatin Mitomycin	26	1998-2008	R	USA	NA	11/11/4	NA	11/10/5
	DEB-TACE	Doxorubicin	45				NA	22/11/12	NA	17/13/15
Facciorusso 2016 (*17*)	C-TACE	Doxorubicin	104	2007-2011	R	Italy	NA	93/11/0	2/39/63/0	NA
	DEB-TACE	Doxorubicin	145				NA	129/16/0	5/53/81/6	NA
Farris 2010 (*18*)	C-TACE	NA	13	NA	R	NA	NA	NA	NA	NA
	DEB-TACE	NA	13				NA	NA	NA	NA
Ferrer Puchol 2011 (*19*)	C-TACE	Adriamycin	25	2000-2009	R	Spain	NA	NA	NA	NA
	DEB-TACE	Adriamycin	47				NA	NA	NA	NA
Frenette 2012 (*20*)	C-TACE	NA	148	2005-2010	R	USA	NA	83/52/13	12/62/71/3	NA
	DEB-TACE	NA	127				NA	72/50/5	7/46/65/9	NA
Golfieri 2014 (*21*)	C-TACE	Epirubicin	88	2008-2010	RCT	Italy	NA	77/11/0	0/41/23/24	NA
	DEB-TACE	Doxorubicin	89				NA	75/14/0	0/41/26/22	NA
Gorodetski 2015 (*22*)	C-TACE	NA	95	2000-2013	R	USA	NA	NA	NA	NA
	DEB-TACE	NA	38				NA	NA	NA	NA
Kloeckner 2015 (*23*)	C-TACE	Mitomycin-C	174	2002-2013	R	Germany	NA	103/64/7	30/59/77/8	NA
	DEB-TACE	NA	76				NA	51/22/3	8/34/30/4	NA
Kumar 2013 (*24*)	C-TACE	NA	38	2002-2011	R	UK	NA	NA	NA	NA
	DEB-TACE	NA	81				NA	NA	NA	NA
Lammer 2010 (*25*)	C-TACE	Doxorubicin	108	2005-2007	RCT	Austria	NA	89/19/0	0/29/79/0	74/19/0
	DEB-TACE	Doxorubicin	93				NA	77/16/0	0/24/69/0	80/28/0
Liu 2015 (*26*)	C-TACE	Doxorubicin	105	2010-2011	R	Taiwan,	NA	NA	0/7/98/0	NA
	DEB-TACE	Doxorubicin	53			R.O.C.	NA	NA	0/53/0/0	NA
Malenstein 2011 (*27*)	C-TACE	Doxorubicin	14	2006-2009	RCT	Belgium	NA	14/0/0	1/10/3	NA
	DEB-TACE	Doxorubicin	16				NA	14/2/2	2/9/5	NA
Megías Vericat 2015 (*28*)	C-TACE	Cisplatin	30	2008-2009	R	Spain	NA	19/11/0	NA	NA
	DEB-TACE	Doxorubicin	30				NA	14/16/0	NA	NA
Monier 2014 (*29*)	C-TACE	Doxorubicin	67	NA	RCT	NA	NA	NA	NA	NA
	DEB-TACE	Doxorubicin	63				NA	NA	NA	NA
Nicolini 2010 (*30*)	C-TACE	Embosphere particles	8	2003-2007		Italy	NA	6/2/0	NA	NA
	DEB-TACE	Epirubicin	8				NA	5/3/0	NA	NA
Nicolini 2013 (*31*)	C-TACE	Epirubicin	16	2005-2011	R	Italy	NA	NA	7/9/0/0	NA
	DEB-TACE	Doxorubicin	22				NA	NA	14/8/0/0	NA
Park 2010 (*32*)	C-TACE	NA	52	2008-2010	R	South	NA	NA	NA	NA
	DEB-TACE	NA	20			Korea	NA	NA	NA	NA
Recchia 2012 (*33*)	C-TACE	Lipiodol	70	2008-2010	P	Italy	NA	NA	NA	24/14/0
	DEB-TACE	Doxorubicin	35				NA	NA	NA	46/21/0
Sacco 2011 (*34*)	C-TACE	Doxorubicin	34	2006-2009	RCT	Italy	NA	25/9/0	0/22/12/0	NA
	DEB-TACE	Doxorubicin	33				NA	29/4/0	0/22/11/0	NA
Song 2012 (*35*)	C-TACE	Doxorubicin	69	2008-2011	R	Korea	NA	63/6/0	0/28/41/0	NA
	DEB-TACE	Doxorubicin	60				NA	56/4/0	0/27/33/0	NA
Song 2011 (*36*)	C-TACE	Cisplatin Doxorubicin Epirubicin	20	2008-2010		Korea	NA	16/4/0	0/7/6/7	NA
	DEB-TACE	Doxorubicin	20				NA	18/2/0	0/6/10/4	NA
Vogl 2011 (*37*)	C-TACE	Doxorubicin	108	2005-2007	RCT	Germany	NA	89/19/0	29/81/0	104/6/0
	DEB-TACE	Doxorubicin	93				NA	77/16/0	26/76/0	88/14/0
Wiggermann 2011 (*38*)	C-TACE	Cisplatin	22	2003-2008	R	Germany	NA	22/0/0	4/15/2	NA
	DEB-TACE	Epirubicin	22				NA	22/0/0	1/17/3	NA
Zwaka 2011 (*39*)	C-TACE	NA	19	2010-2011	R	Germany	NA	NA	NA	NA
	DEB-TACE	NA	15				NA	NA	NA	NA

[a]Number (percentage) of patients who had already undergone TACE before enrollment in the study. C-TACE, conventional transarterial chemoembolization; DEB-TACE, drug-eluting beads-TACE; R, retrospective; RCT, randomized controlled trial; P, prospective; CP, Child–Pugh; BCLC, Barcelona Clinic Liver Cancer; Okuda, Okuda stage; NA, not assessed.

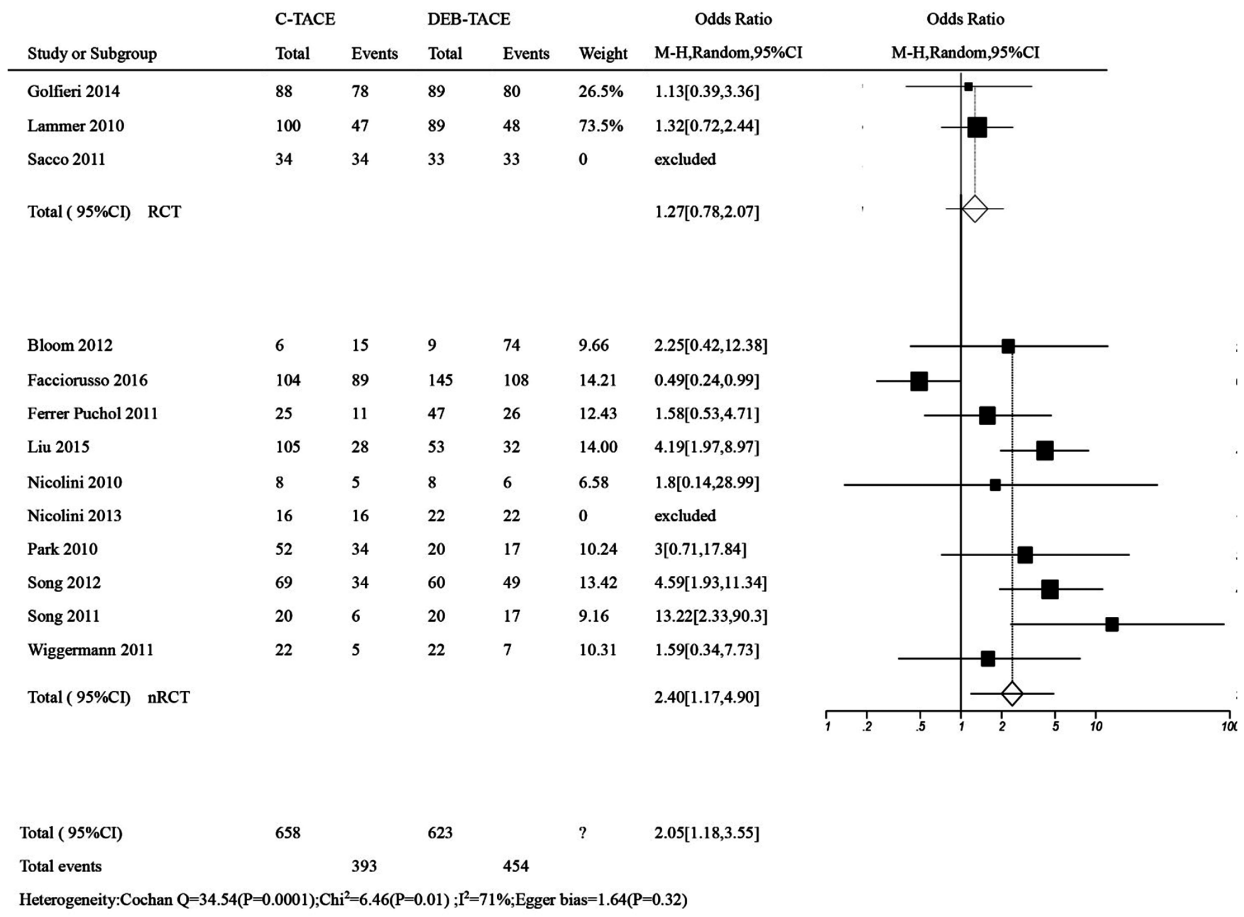

Figure 2. Forest plot comparing objective response rate for DEB-TACE to that for C-TACE. A random effect DerSimonian Laird model showed a summary odds ratio significantly higher after DEB-TACE than that in c-TACE. Subgroup analyses of the RCTs and observational studies confirmed the non-significant OR in favor of DEB-TACE and detected statistical heterogeneity. DEB-TACE, drug-eluting bead transarterial chemoembolization; C-TACE, conventional transarterial chemoembolization; RCT, randomized controlled trial; nRCT, non-randomized controlled trial.

Table 2. Odds ratios and heterogeneity of 1-year, 2-year, and 3-year survival rates

Estimate survival rate	No. of studies	No. of patients	OR (95% CI)	*p* value	Heterogeneity I^2	*p*
1-year SR	14	1604	1.51 (0 .95-2.41)	0.08	73.0%	< 0.0001
2-year SR	13	1422	1.32 (0.74-2.36)	0.34	73.6%	< 0.0001
3-year SR	8	840	1.92 (1.00-3.68)	0.049	51.7%	= 0.04

SR, survival rate; OR, odds ratio; CI, confidence interval.

patients who underwent C-TACE or DEB-TACE. However, the 3-year survival rate was significantly higher in patients who underwent DEB-TACE than that in patients who underwent C-TACE. This finding probably suggests that DEB-TACE results in a better OS than TACE. However, this finding is not consistent with the conclusions of a systematic review recently published in this field (*17*), perhaps because the current meta-analysis analyzed more studies. However, long-term follow-up needs to be conducted and more standard randomized studies need to be assembled to assess the survival benefit of DEB-TACE. The complete response rate, disease control rate, full necrosis rate, non-response rate, objective response rate, progressive disease rate, and recurrence did not differ significantly between patients who underwent C-TACE and patients who underwent DEB-TACE.

Safety did not differ significantly between C-TACE and DEB-TACE. Many clinical research studies suggest that tumor eradication cannot readily be achieved with TACE and that HCC can only be controlled by palliative treatment. Therefore, a low adverse reaction rate and a high tumor response rate in DEB-TACE therapy will be advantageous to patients needing to undergo radical surgery in the short term. Because this population of patients is in the early stage of disease, DEB-TACE can

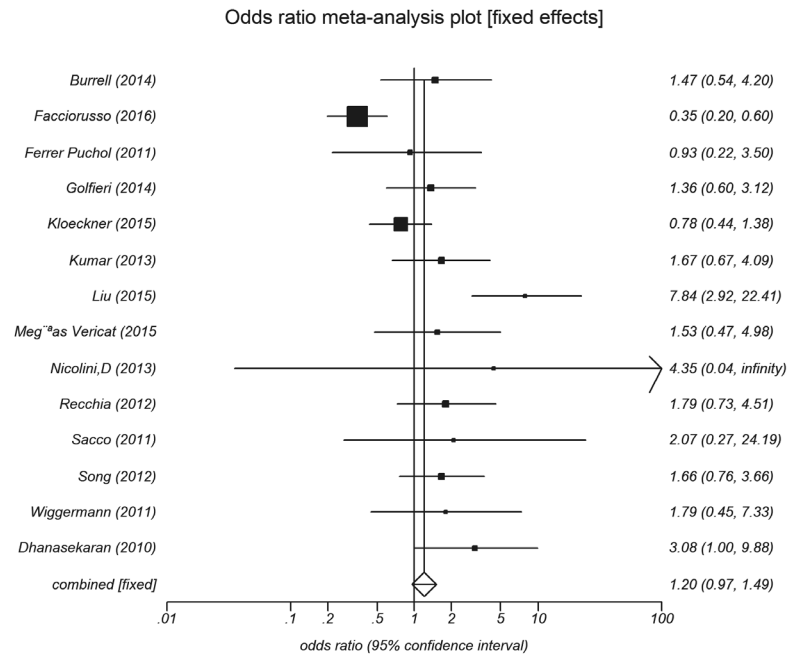

Figure 3. Forest plot of hazard ratios for patient 1-year survival rate after DEB-TACE and C-TACE. A fixed effect Mantel-Haenszel model yielded a summary odds ratio not significantly in favor of DEB-TACE with a low heterogeneity. DEB-TACE, drug-eluting bead transarterial chemoembolization; C-TACE, conventional transarterial chemoembolization; RCT, randomized controlled trial; nRCT, non-randomized controlled trial.

be an efficient and safe way to control the tumor, down-regulate the tumor stage, and protect liver function to the greatest extent. In theory, therefore, DEB-TACE will lay a better foundation for radical surgery and possibly prolong long-term survival.

This meta-analysis provides relatively comprehensive evidence of the benefits of DEB-TACE compared to C-TACE for the treatment of primary liver cancer, but there are still some limitations to this study. First, the evaluation criteria for tumor response in the included literature were not entirely consistent, and mRECIST and EASL standards assess tumor response differently, which may lead to different interpretations. Second, treatment with conventional technology has matured, but many of the RCT designs lacked conventional standardization of evaluation metrics, and this was especially true for C-TACE involving conventional technology and chemotherapy drugs for embolism.

In conclusion, this meta-analysis has shown that patients who underwent DEB-TACE might have a higher complete response rate, disease control rate, and 3-year survival rate than patients who underwent C-TACE. Safety did not differ significant between C-TACE and DEB-TACE. Therefore, DEB-TACE may be a better choice for patients with primary HCC than liver transplantation, liver resection, or partial ablation in the short term.

Acknowledgements

This work was supported by the National Natural Science Foundation (grant no. 81702622), Key Projects of the Liaoning Natural Science Foundation (2018010153-301), and the Guiding Projects of the Liaoning Natural Science Foundation (20170540981).

References

1. Boyle DA. Hepatocellular Carcinoma: Implications for Asia-Pacific oncology nurses. Asia Pac J Oncol Nurs. 2017; 4:98-103.
2. Xie H, Yu H, Tian S, Yang X, Wang X, Yang Z, Wang H, Guo Z. What is the best combination treatment with transarterial chemoembolization of unresectable hepatocellular carcinoma? A systematic review and network meta-analysis. Oncotarget. 2017; 8:100508-100523.
3. Torre LA, Bray F, Siegel RL, Ferlay J, Lortet-Tieulent J, Jemal A. Global cancer statistics, 2012. CA Cancer J Clin. 2015; 65:87-108.
4. Kaneko R, Nakazaki N, Omori R, Yano Y, Ogawa M, Sato Y. The effect of new therapeutic and diagnostic agents on the prognosis of hepatocellular carcinoma in Japan - An analysis of data from the Kanagawa Cancer Registry. Asian Pac J Cancer Prev. 2017; 18:2471-2476.
5. Pascual S, Herrera I, Irurzun J. New advances in hepatocellular carcinoma. World J Hepatol. 2016; 8:421-438.
6. Ji J, Shi J, Budhu A, *et al*. MicroRNA expression, survival, and response to interferon in liver cancer. N Engl J Med. 2009; 361:1437-1447.
7. Chung GE, Lee JH, Kim HY, Hwang SY, Kim JS, Chung JW, Lee HS, Kim YJ. Transarterial chemoembolization can be safely performed in patients with hepatocellular carcinoma invading the main portal vein and may improve

the overall survival. Radiology. 2011; 258:627-634.
8. Izumoto H, Hiraoka A, Ishimaru Y, *et al*. Validation of newly proposed time to transarterial chemoembolization progression in intermediate-stage hepatocellular carcinoma cases. Oncology. 2017; 93 Suppl 1:120-126.
9. Luz JH, Luz PM, Martin HS, Gouveia HR, Levigard RB, Nogueira FD, Rodrigues BC, de Miranda TN, Mamede MH. DEB TACE for intermediate and advanced HCC - Initial experience in a Brazilian cancer center. Cancer Imaging. 2017; 17:5.
10. Alsina A, Franco E, Leone J, Osman-Mohamed H, Huang J, Bowers V, Rojas H, McGhee B, Mendoza A, Kemmer N, Neff G. Collateral damage of liver transplantation in the well compensated cirrhotic with hepatocellular carcinoma. Hepatology. 2011; 54 Suppl 1: 414A.
11. Arabi M, BenMousa A, Bzeizi K, Garad F, Ahmed I, Al-Otaibi M. Doxorubicin-loaded drug-eluting beads versus conventional transarterial chemoembolization for nonresectable hepatocellular carcinoma. Saudi J Gastroenterol. 2015; 21:175-180.
12. Bloom S, Cheng RKY, Lim L, Gow P, Lubel JS. Conventional transarterial chemoembolization versus doxorubicin bead transarterial chemoembolization for the treatment of hepatocellular carcinoma, a retrospective cohort study. J Gastroenterol Hepatol. 2012; 27(Suppl.4):70.
13. Burrell MA, Anderson M, Singal A, Yopp A, Kalva SP, Pillai A. Retrospective analysis of traditional chemoembolization compared with drug-eluting beads in the treatment of hepatocellular carcinoma at varying Barcelona clinic liver cancer stages. J Gastroenterol Hepatol. 2014.5 811.e24.
14. Castelli G, Cardin R, Piciocchi M, Vanin V, Pozzan C, Iurilli V, Giacomin A, Gazzola A, Maddalo G, Farinati F. Neoangiogenesis after TACE: Any difference between conventional and DC-Beads-mediated transarterial chemoembolization? Dig Liver Dis. 2013; 45 Suppl 1:S44-S45.
15. Kumar P, Bryant T, Breen D, Stedman B, Hacking N. Transarterial embolization and doxorubicin eluting beads-transarterial chemoembolization (DEB-TACE) of malignant extra-adrenal pheochromocytoma. Cardiovasc Intervent Radiol. 2011; 34:1325-1329.
16. Dhanasekaran R, Kooby DA, Staley CA, Kauh JS, Khanna V, Kim HS. Comparison of conventional transarterial chemoembolization (TACE) and chemoembolization with doxorubicin drug eluting beads (DEB) for unresectable hepatocellular carcinoma (HCC). J Surg Oncol. 2010. 101: 476-480.
17. Facciorusso A, Mariani L, Sposito C, Spreafico C, Bongini M, Morosi C, Cascella T, Marchianò A, Camerini T, Bhoori S, Brunero F, Barone M, Mazzaferro V. Drug-eluting beads versus conventional chemoembolization for the treatment of unresectable hepatocellular carcinoma. J Gastroenterol Hepatol. 2016; 31:645-653.
18. Farris AB, Dhanasekaran R, Dursun N, *et al*. Tumoral and angiogenesis factors in hepatocellular carcinoma (HCC) after drug eluting bead (DEB) transarterial chemoembolization (TACE) with doxorubicin. J Clin Oncol. 2010; 28(15 Suppl):4162.
19. Ferrer Puchol, la Parra C, Esteban E, Vaño M, Forment M, Vera A, Cosín O. Comparison of doxorubicin-eluting bead transarterial chemoembolization (DEB-TACE) with conventional transarterial chemoembolization (TACE) for the treatment of hepatocellular carcinoma. Radiologia. 2011. 53:246-253. (in Spanish)
20. Burrel M, Reig M, Forner A, Barrufet M, de Lope CR, Tremosini S, Ayuso C, Llovet JM, Real MI, Bruix J. Survival of patients with hepatocellular carcinoma treated by transarterial chemoembolisation (TACE) using Drug Eluting Beads. Implications for clinical practice and trial design. J Hepatol. 2012; 56:1330-1335.
21. Golfieri R, Giampalma E, Renzulli M, Cioni R, Bargellini I, Bartolozzi C, Breatta AD, Gandini G, Nani R, Gasparini D, Cucchetti A, Bolondi L, Trevisani F; Precision Italia Study Group. Randomised controlled trial of doxorubicin-eluting beads vs conventional chemoembolisation for hepatocellular carcinoma. Br J Cancer. 2014; 111:255-264.
22. Schernthaner RE, Haroun RR, Duran R, Lee H, Sahu S, Sohn JH, Chapiro J, Zhao Y, Gorodetski B, Fleckenstein F, Smolka S, Radaelli A, van der Bom IM, Lin M, Geschwind JF. Improved visibility of metastatic disease in the liver during intra-arterial therapy using delayed arterial phase cone-beam CT. Cardiovasc Intervent Radiol. 2016; 39:1429-1437.
23. Kloeckner R, Weinmann A, Prinz F, Pinto dos Santos D, Ruckes C, Dueber C, Pitton MB. Conventional transarterial chemoembolization versus drug-eluting bead transarterial chemoembolization for the treatment of hepatocellular carcinoma. BMC Cancer. 2015; 15:465.
24. Kumar P, Bryant T, Breen D, Stedman B, Hacking N. Transarterial embolization and doxorubicin eluting beads-transarterial chemoembolization (DEB-TACE) of malignant extra-adrenal pheochromocytoma. Cardiovasc Intervent Radiol. 2011; 34:1325-1329.
25. Lammer J, Malagari K, Vogl T, *et al*. Prospective randomized study of doxorubicin-eluting-bead embolization in the treatment of hepatocellular carcinoma: Results of the PRECISION V study. Cardiovasc Intervent Radiol. 2010; 33:41-52.
26. Liu YS, Ou MC, Tsai YS, Lin XZ, Wang CK, Tsai HM, Chuang MT Transarterial chemoembolization using gelatin sponges or microspheres plus lipiodol-doxorubicin versus doxorubicin-loaded beads for the treatment of hepatocellular carcinoma. Korean J Radiol. 2015; 16:125-132.
27. Van Malenstein H, Maleux G, Vandecaveye V, Heye S, Laleman W, van Pelt J, Vaninbroukx J, Nevens F, Verslype C. A randomized phase II study of drug-eluting beads versus transarterial chemoembolization for unresectable hepatocellular carcinoma. Onkologie. 2011; 34:368-376.
28. Megías Vericat JE, García Marcos R, López Briz E, Gómez Muñoz F, Ramos Ruiz J, Martínez Rodrigo JJ, Poveda Andrés JL. Trans-arterial chemoembolization with doxorubicin-eluting particles versus conventional trans-arterial chemoembolization in unresectable hepatocellular carcinoma: A study of effectiveness, safety and costs. Radiologia. 2015; 57:496-504. (in English, Spanish)
29. Monier A, Guiu B, Duran R, Aho S, Bize P, Deltenre P, Dunet V, Denys A. Liver and biliary damages following transarterial chemoembolization of hepatocellular carcinoma: Comparison between drug-eluting beads and lipiodol emulsion. Eur Radiol. 2017; 27:1431-1439.
30. Nicolini A, Martinetti L, Crespi S, Maggioni M, Sangiovanni A. Transarterial chemoembolization with epirubicin-eluting beads versus transarterial embolization before liver transplantation for hepatocellular carcinoma. J Vasc Interv Radiol. 2010; 21: 327-332.

31. Nicolini D, Svegliati-Baroni G, Candelari R, Mincarelli C, Mandolesi A, Bearzi I, Mocchegiani F, Vecchi A, Montalti R, Benedetti A, Risaliti A, Vivarelli M. Doxorubicin-eluting bead vs conventional transcatheter arterial chemoembolization for hepatocellular carcinoma before liver transplantation. World J Gastroenterol. 2013; 19:5622-5632.
32. Park SJ, Lim YS, Hwang S, Heo NY, Lee HC, Suh DJ, Yu E, Lee SG. Emergency adult-to-adult living-donor liver transplantation for acute liver failure in a hepatitis B virus endemic area. Hepatology. 2010; 51:903-911.
33. Recchia F, Passalacqua G, Filauri P, Doddi M, Boscarato P, Candeloro G, Necozione S, Desideri G, Rea S. Chemoembolization of unresectable hepatocellular carcinoma: Decreased toxicity with slow-release doxorubicin-eluting beads compared with lipiodol. Oncol Rep. 2012; 27:1377-1383.
34. Sacco R, Bargellini I, Bertini M, *et al*. Conventional versus doxorubicin-eluting bead transarterial chemoembolization for hepatocellular carcinoma. J Vasc Interv Radiol. 2011; 22:1545-1552.
35. Song MJ, Park CH, Kim JD, Kim HY, Bae SH, Choi JY, Yoon SK, Chun HJ, Choi BG, Lee HG. Drug-eluting bead loaded with doxorubicin versus conventional Lipiodol-based transarterial chemoembolization in the treatment of hepatocellular carcinoma: A case-control study of Asian patients. Eur J Gastroenterol Hepatol. 2011; 23:521-527.
36. Song MJ, Chun HJ, Song DS, Kim HY, Yoo SH, Park CH, Bae SH, Choi JY, Chang UI, Yang JM, Lee HG, Yoon SK. Comparative study between doxorubicin-eluting beads and conventional transarterial chemoembolization for treatment of hepatocellular carcinoma. J Hepatol. 2012; 57:1244-1250.
37. Vogl TJ, Lammer J, Lencioni R, Malagari K, Watkinson A, Pilleul F, Denys A, Lee C. Liver, gastrointestinal, and cardiac toxicity in intermediate hepatocellular carcinoma treated with PRECISION TACE with drug-eluting beads: Results from the PRECISION V randomized trial. AJR Am J Roentgenol. 2011; 197: W562-70.
38. Wiggermann P, Sieron D, Brosche C, Brauer T, Scheer F, Platzek I, Wawrzynek W, Stroszczynski C. Transarterial chemoembolization of Child-A hepatocellular carcinoma: Drug-eluting bead TACE (DEB TACE) vs. TACE with cisplatin/lipiodol (cTACE). Med Sci Monit. 2011; 17: CR189-95.
39. Koike Y, Takizawa K, Ogawa Y, Muto A, Yoshimatsu M, Yagihashi K, Nakajima Y. Transcatheter arterial chemoembolization (TACE) or embolization (TAE) for symptomatic bone metastases as a palliative treatment. Cardiovasc Intervent Radiol. 2011; 34:793-801.

(Received June 24, 2019; Revised August 21, 2019; Accepted September 26, 2019)

Original Article

DOI: 10.5582/bst.2019.01181

Anti-oxidant, anti-apoptotic, anti-hypoxic and anti-inflammatory conditions induced by PTY-2 against STZ-induced stress in islets

Shivani Srivastava[1], Harsh Pandey[1], Surya Kumar Singh[2], Yamini Bhusan Tripathi[1,*]

[1] *Department of Medicinal Chemistry, Institute of Medical Sciences, Banaras Hindu University, Varanasi, India;*
[2] *Department of Endocrinology and Metabolism, Institute of Medical Sciences, Banaras Hindu University, Varanasi, India.*

Summary **The earlier assessment of *Pueraria tuberosa* (PT) has shown anti-diabetic effects through enhancing incretin action and DPP-IV (Dipeptidyl peptidase-IV) inhibition. The aim of this work was to further explore the protective role of aqueous extract of *Pueraria tuberosa* tuber (PTY-2) against streptozotocin (STZ) induced islet stress in rats. Diabetes was induced by STZ (65 mg/kg body weight) in charles foster male rats. After 60 days of STZ administration, animals with blood glucose levels > 200 g/dL were considered as diabetic. All the rats were later divided into three groups: Group-1 (STZ untreated normal rats), Group-2 (Diabetic control), and Group-3 (PTY-2 [50 mg/100 g bw treatment for next 10 days to diabetic rats). The rats were then sacrificed after the 10th day of treatment accordingly. STZ treatment led to an increase in expression of Matrix metalloproteinases-9 (MMP-9), Tumour necrosis factor-α (Tnf-α), Hypoxia inducible factor-α (HIF-1α), Vascular endothelial growth factor (VEGF), Interleukin-6 (IL-6), Protein kinase C-ε (PKC-ε), Nuclear factor kappa-light-chain-enhancer of activated B-cells (NFkB), and Caspase-3. Reverse Transcriptase-PCR (RT-PCR), Immunohistochemistry and Western-Blot analysis showed an increase in the expressions of Superoxide Dismutase (SOD) and Nephrin, and a decrease in the expressions of NFkB, PKC-ε, TNF-α, MMP-9, HIF-1α, VEGF, Caspase-3 and IL-6 after 10 days of PTY-2 treatment. The results showed that PTY-2 favorably changed all the expressions *via* anti-oxidant, anti-apoptotic, anti-hypoxic and anti-inflammatory pathways, making itself as a protective agent against STZ induced islet stress. Further evaluation of PTY-2 might be helpful in establishing its role in the management of diabetes mellitus.**

Keywords: STZ, PTY 2, stress, expressions, diabetes, islets

1. Introduction

Mortality and morbidity due to diabetes mellitus (DM) are rising rapidly worldwide (*1,2*). Type 2 DM (T2DM) increases the risk of acute pancreatitis by 1.5-3 folds, and the use of anti-diabetic drugs decreases this excess risk (*2*). On the other hand, pancreatitis is one of the known risk factors for the onset of DM (*3-5*). Additionally, the onset of DM can be a symptom of pancreatic cancer as the latter is more common among newly diagnosed cases of T2DM. Furthermore, long-standing DM can increase the risk of occurrence of pancreatic cancer (*6-9*). Apart from the known etiological factors, pathological changes due to environmental factors or other unknown reasons can alter the gene expression and lead to diseases like DM, pancreatic cancer, acute or chronic pancreatitis (*10*). Both *in-vivo* and *in-vitro* models are being developed to understand the mechanisms underlying the profile change in gene expression. Many synthetic drugs and herbal formulations have been developed for the prevention and treatment of DM.

PTY-2, is being evaluated for its protective role in STZ induced islet stress. In our earlier studies, we had evaluated the role of PT in animal models of streptozotocin (STZ)-induced DM and in normoglycemic rats (*11-13*). PT has also been studied for its anti-

Released online in J-STAGE as advance publication October 8, 2019.

*Address correspondence to:
Prof. Yamini Bhusan Tripathi, Department of Medicinal Chemistry, Institute of Medical Sciences, Banaras Hindu University, Varanasi, Uttar Pradesh 221005, India.
E-mail: yamini@bhu.ac.in, or yaminibiochemist6@gmail.com

inflammatory, anti-oxidant, nephro-protective, intestine-protective, hepato-protective, anti-hypertensive and anti-diabetic properties (*11-20,44*). The analysis of the actions makes hypothesis that there must be interconnected signaling pathways between anti-inflammatory, anti-hypoxic, anti-apoptotic, antioxidants and anti-diabetic genes for the effect of PT. Taking our research forwards, we have attempted to study the signaling pathways to understand the protective role of PTY-2 in islet damage.

Various markers like Nephrin, SOD, HIF-1α, TNF-α, MMP-9, Caspase-3, NF-kB, VEGF, PKC-ε, Caspase-3 and IL-6 have been used to study the effect of drugs or herbal products on DM. Earlier studies have demonstrated increased levels of VEGF, TNF-α, MMP-9, IL-6, NF-kB, PKC, and HIF-1α in inflammatory conditions, vascular lesions and DM (*21-25*). Excess generation of reactive oxygen species (ROS) and oxidative stress is one of the common etiological pathways in the development and progression of DM (*26,27*). Nephrin, a member of immunoglobulin super family, is a surface receptor that is specifically expressed in kidney, brain and pancreas (*28*). Nephrin plays an important role in beta cell survival signaling through the association with PI3-kinase, reported in mouse islet β-cells and mouse pancreatic beta-cell line (βTC-6 cells) (*29*). VEGF is a vital regulator of vascularization of islet cells, and the islet vascular system is critical for a normal secretion of insulin (*30,31*). Genetic studies have shown that normal VEGF and vascularization are important for adult islet cell function and β cell mass (*25*). The β cell-specific overexpression of VEGF causes rapid hypervascularization and hyperinnervation of the islet, leading to increased production of extracellular matrix components (ECM) (*32*). Hence, we can say that increased amount of VEGF is responsible for defective angiogenesis. MMPs are a large family of endopeptidases, and these are produced by stromal and inflammatory cells. Pancreatic MMPs (especially MMP-9) induce inflammation, and serum MMP-9 levels are an assessment marker of severity of pancreatitis (*33*). MMP-9 is usually involved in degradation and remodeling of ECM components (*22,34,35*). NF-kB, a nuclear transcription factor, regulates the transcription of various genes involved in inflammation mediation (*36*). The activation of NF-kB is an early pathological event in the development of insulin resistance (*37*). TNF-α, an inflammatory marker, is rapidly produced intracellularly with the activation of NF-kB and is known to have effects on diabetes and obesity (*21,38*). The PKC-ε belongs to the superfamily of isoforms of protein kinases. PKC-ε is involved in the development of insulin resistance, and its inhibition is associated with the improvement in glucose homeostasis in animal models (*39*). PKC-ε has a strong presence in islet cells, acinar cells, and ductal epithelium (*40*). Similarly, both IL-6 and HIF-1α are also known to play a pro-inflammatory role in the mediation of acute pancreatitis and pancreatic cancer (*23,24*). Hypoxia is an important cause of beta-cell loss and is measured by an increase in HIF-1α expression (41). Various gene knockout experiments have shown that caspase-3 is involved in beta cell apoptosis and that $Casp^{-/-}$ are protected from the development of DM (*42*).

As PT has multiple medicinal properties with several beneficial compositions, we have studied the protective effect of its total water extract rather than on its individual components. Because PT contains many steroids, triterpenoid, glycosides, carbohydrates, alkaloids, flavanoid, tannin, protein and amino acids, *e.g.*, daidzin, puerarin, puerarone, genistein, puetuberosanol, tuberostan, tuberosin, and puerarin 4',6'-diacetate as the main constituents (*12,14,43*). We planned to study the multi-targeted protective effect of PTY-2 on the islet damage among rats with STZ-induced stress.

2. Materials and Methods

2.1. *Materials*

The antibody of rabbit IL-6 (23 Kda) (08310): SAB1408591, mouse monoclonal VEGF (21 Kda) (JH-121): sc-57496, NF-κB p65 (D14E12) XP® Rabbit mAb #8242, rabbit polyclonal PKC-ε (SAB1300094), mouse monoclonal β-actin (A2228), mouse monoclonal Hif-1α (H6536-100 UG), rabbit monoclonal Caspase-3 (CASP 3 [D175] invitrogen), Mouse monoclonal MMP-9 and monoclonal anti-rabbit IgG (γ-chain specific)-peroxidise (A1949), pre-stained protein ladder (from Hi-Media Pvt. Ltd, Kolkata, India) along with PVDF membranes (from Millipore, catalog no. IPVH20200) were used for proteins expression analysis. STZ-S0130 was bought from Sigma-Aldrich, St Louis, USA. For RT-PCR, Trizol (Himedia, Pvt. Ltd, Kolkata, India), cDNA Kit (Fermentas), and Taq-polymerase (Genaxy Scientific Pvt.Ltd) were used.

2.2. *Sample preparation*

PT was purchased from Ayurvedic Pharmacy, Banaras Hindu University. Its authenticity has already been ascertained in our previous research (*44*). We extracted 30 g powder with eight volumes of distilled water. When the volume was reduced to ¼th, it was filtered with cloth. The total yield of PTY-2 obtained by this process was 30%.

2.3. *Study Design*

The protocol was approved by the Institute Ethical Committee (Dean/2015/CAEC/1266), Institute of Medical Sciences, Banaras Hindu University. After overnight fasting, Charles foster male rats of the same age group with body weight in the range of 120-130 grams were injected STZ (65 mg/kg body weight). STZ was prepared in chilled and fresh citrate buffer of pH

4.5. The blood glucose levels were checked using strips (Dr. Morepen) on the 5th day. Rats with blood glucose levels > 200 mg/dL were placed under diabetic group. In order to induce severe diabetes, we further left the rats (three rats per cage) for 55 days. On the 61st day, we divided the rats into three groups (n = 6): Group-1 (STZ untreated rats, *i.e*., age-matched normal rats), Group-2 (diabetic control), and Group-3 (PTY-2 at 50 mg/100 g bw treatment for next 10 days to diabetic rats). The rats were then sacrificed after 10 days of treatment. The pancreas was isolated and rinsed with PBS. Then, these were cut into two parts; one for histology (preserved in 10% formaldehyde) and the other was first crushed in liquid nitrogen and then stored in -80°C freezer for molecular study.

2.4. *RT-PCR*

RNA was extracted using trizol reagent from about 50 mg of pancreatic tissue with a homogenizer. Then 5 µg of total RNA was reverse-transcribed with superscript II RNase H-reverse transcriptase (RT) using random hexamers according to the instructions provided by the manufacturers (Fermentas Pvt. Ltd.). For SOD, 2 µL c-DNA, 0.2 mmol/L deoxynucleotide triphosphates (dNTPs), 1.5 mmol/L $MgCl_2$, 0.5 µmol/L of each primer, 2.5 µL 10X PCR buffer and 1 U Taq DNA polymerase were used. For Nephrin, 1 µL c-DNA, 0.2 mmol/L dNTPs, 1.5 mmol/L $MgCl_2$, 1.2 µmol/L of each primer, 2.5 µL 10X PCR buffer and 1U Taq DNA polymerase were used. For matrix metallopeptidase 9 (MMP-9), 2 µl c-DNA, 200 umol/L dNTPs, 1.5 mmol/L $MgCl_2$, 0.4 µmol/L of each primer, 2 µL 10X PCR buffer and 2.5 U Taq DNA polymerase were used. For Tnf-α, 1 µL c-DNA, 200 umol/L dNTPs, 1.2 mmol/L $MgCl_2$, 0.6 µmol/L of each primer, 2 µL 10X PCR buffer and 2 U Taq DNA polymerase were used. For glyceraldehyde 3-phosphate dehydrogenase (GAPDH), 0.1 µmol/L of each primer was used. The optical density of each expression was determined *via* alpha imager 2200 and presented as the ratio against GAPDH. All RT-PCR experiments were performed in triplicates (Table 1).

2.5 *Western blot analysis*

Pancreatic tissue was homogenized with chilled lysis buffer (50 mMTris pH 7.6, 150 mM NaCl, 1 mM EDTA, 1 mM EGTA, 1% triton, 0.1% SDS, 1 mM sodium orthovanadate, protease inhibitor cocktail and 1 mM PMSF). The homogenate was then centrifuged at 12,000 rpm at 4°C for 30 min. The protein estimation was done by Bradford method. 40 µg proteins with loading dye were separated in the polyacrylamide gel. The gel was then electro-transferred to PVDF membranes in transfer buffer (10X Tris-glycine-methanol and SDS-PAGE buffer) to stay overnight at 4°C at 45 V. The next day, PVDF membrane was blocked with 5% non-

Table 1. Details of PCR primer sequences, product size and thermal steps for expressions of TNF α, SOD, Nephrin, MMP 9 and GAPDH

Primers	Sequence	Product Size (bp)	RT PCR Thermal steps					
			Initial denaturation	Denature	Anneal	Extention	Final Extention
TNF α FORW	5'- CACCACGCTCTTCTGTCTACTGAAC -3'	546	No. of Cycle		30		1
TNF α REV	5'- CCGGACTCCGTGATGTCTAAGTACT -3'		Temp.(°C)	95	63	72	72
			Time	1 min	1 min	2 min	5 min
SOD FORW	5'-TCTAAGAAACATGGCGGTCC-3'	387	No. of Cycle		35		1
SOD REV	5'-CAGTTAGCAGGCCAGCAGAT-3'		Temp.(°C)	94	55	72	72
			Time	45 sec	30 sec	1.3 min	10 min
Nephrin FORW	5'-GTT CAG CTG GGAGAGACT GG-3'	340	No. of Cycle		43		1
Nephrin REV	5'-TTG GAC ATC CAG AGG GAC C-3'		Temp.(°C)	94	56	72	72
			Time	45 sec	45 sec	1 min	10 min
MMP 9 FORW	5'-TGTACCGTATGGTTACAC-3'	371	No. of Cycle		35		1
MMP 9 REV	5'CCGCGACACCAAACTGGAT3'		Temp.(°C)	94	58	72	72
			Time	1 min	90 sec	90 sec	7 min
GAPDH FORW	5'-CACGGCAAGTTCAATGGCACA-3'	244	No. of Cycle		35		1
GAPDH REV	5'-GAATTGTGAGGGAGATGCTC-3'		Temp.(°C)	94	58	72	75
			Time	30 sec	30 sec	45 sec	5 min

fat milk powder. The membrane was then incubated overnight with primary antibody diluted in TBST [IL-6 (1:1,000), PKC ε (1:500), VEGF (1:1,000), NF-kB (1:1,000), HIF 1α (1:1,000) & housekeeping gene β-actin (1:500)]. Then, on the next day, the blots were incubated with secondary antibody in TBST for one hour. Protein expression was detected through enhanced chemiluminescence (ECL) in LAS 500 Image Quant system (Wipro GE Healthcare, Hong Kong). The quantification was done by alpha imager 2200. The experiments were done in triplicates.

2.6. *Immunostaining*

The paraffin sections of pancreas were treated with xylene for 10 minutes to remove paraffin. The sections were rehydrated through 90%, 70% alcohol, and water by putting them for 5 minutes in each. Antigen retrieval was done by putting the citrate buffer dipped slides in EZ Retrieval System V.3 (Bio Genex). Sections were washed twice in citrate buffer and two times in 1X PBS (130 mM NaCl, 7 mM Na_2HPO_4, 3 mM KH_2PO_4, pH 7.4) for 10 minutes each, following which the sections were incubated in blocking solution [0.1% Triton X-100, 0.1% BSA, 10% FCS, 0.1% sodium deoxycholate and 0.02% Thiomersal (an anti-fungal agent), in 1X Phosphate Buffered Saline (PBS)] for 2 hours at room temperature and then transferred in primary antibodies, for overnight at 4°C. Tissues were washed in PBST (0.1% triton X in 1X PBS) with three changes of 10 minutes each. After the washing, the sections were incubated with anti-rabbit AF 546 (Red) and anti-mouse AF 488 (Green) (Invitrogen, USA) secondary antibody for 2 hours at room temperature. Sections were washed in PBS with Tween 20 (PBST) with three changes for 10 minutes each, counterstained with DAPI (1 µg/mL DAPI in 1X PBS), mounted in DABCO and examined under Zeiss LSM510 Meta confocal microscope. Image analysis was done by using Zen Black (2012) software.

2.7. *Statistical analysis*

One-way ANOVA test followed by post hoc analysis with Dunnett's test was done for each experiment. All results were expressed as means ± SD. Statistical significance was taken at $p \leq 0.05$.

3. Results

3.1. *PTY-2 response to islet stress*

3.1.1. *mRNA Expressions*

As compared to normal rats, the STZ-treated diabetic group showed a significant increase in TNF-α in pancreatic tissue, whereas the PTY-2 treatment significantly decreased the TNF-α expression as compared to diabetic control and increase as compared to normal. The MMP-9 expression also increased significantly in diabetic control as compared to normal rats, and there was a significant decrease after 10 days of PTY-2 treatment. On the contrary, both SOD and Nephrin expression decreased significantly in diabetic control rats as compared to normal. However, the PTY-2 treated group showed a significant increase in SOD expression as compared to diabetic control and a significant decrease as compared to normal. The Nephrin expression in PTY 2 treated rats increased significantly as compared to both normal and diabetic control (Figure 1 (a) and (b))

These results clearly indicate that in chronic diabetes, there is a significant increase in free radicals/ stress accompanied by an increase in pancreatic inflammation. Treatment with PTY-2 significantly reversed all these changes. Thus, any severe complications of severe diabetes like pancreatitis could be prevented by using PTY-2 as medicinal supplement.

3.2. *Protein Expressions*

3.2.1. *Western blot*

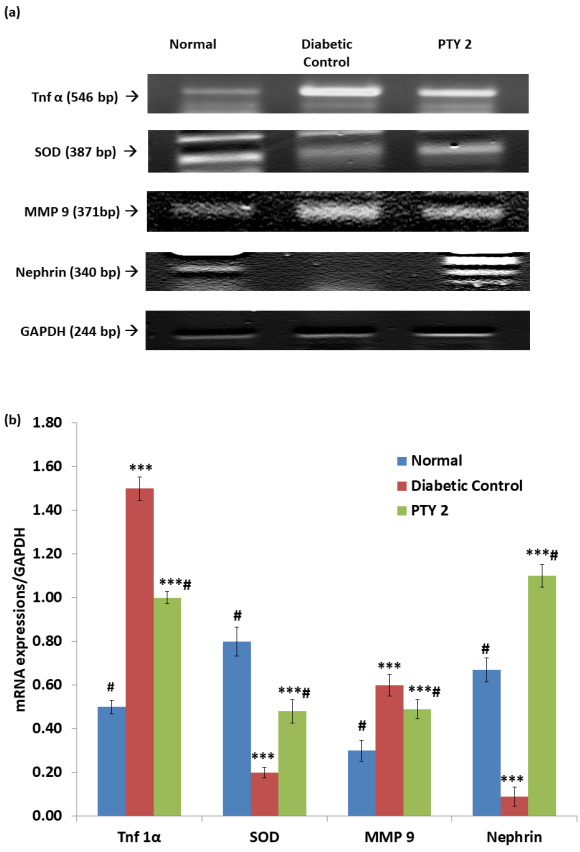

Figure 1. (a) mRNA expressions to investigate the effect of PTY-2 on STZ induced islet stress; (b) Densitometric analysis of RT-PCR product. Each value represents mean ± SD ($n = 6$); $^{***}p < 0.05$ compared with Normal, $^{\#}p < 0.05$ as compared with Diabetic Control.

For further validation, the protein expressions responsible for the induction of oxidative stress, hypoxia, apoptosis and inflammation of pancreatic tissues were estimated. The expressions of NF-kB, PKC ε, HIF-1α, VEGF and IL-6 were significantly increased in diabetic control as compared to normal rats. However, PTY-2 treatment significantly decreased all these expressions (Figure 2 (a) and (b)).

3.2.2. *Immunohistochemistry*

The expressions of MMP-9, HIF-1α, VEGF, IL-6, PKC-ε, NF-kB and Caspase-3 were significantly enhanced in diabetic control islets. The hazardous effects of STZ were down-regulated by 10 days of PTY-2 treatment. The Caspase-3, HIF-1α, MMP-9, IL-6, VEGF and PKC-ε expressions decreased significantly in PTY-2 treated group as compared to diabetic control and increased significantly as compared to the normal. The expression of NF-kB in PTY 2 treated group decreased significantly as compared to diabetic control, but non-

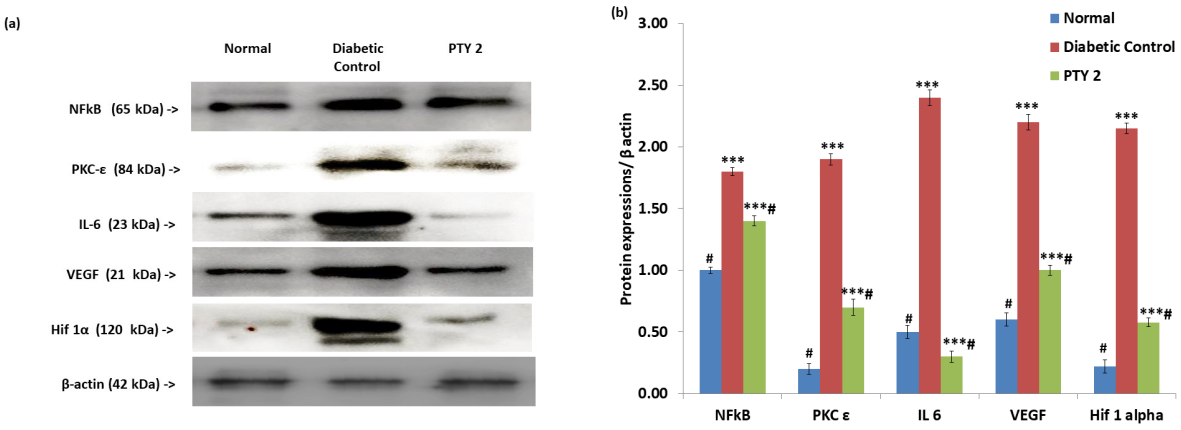

Figure 2. (a) Protein expressions to investigate the effect of PTY-2 on STZ induced islet stress; (b) Densitometric analysis of western blot product. Each value represent the mean ± SD (n = 6); $^{***}p < 0.05$ compared with Normal, $^{\#}p < 0.05$ compared with Diabetic Control.

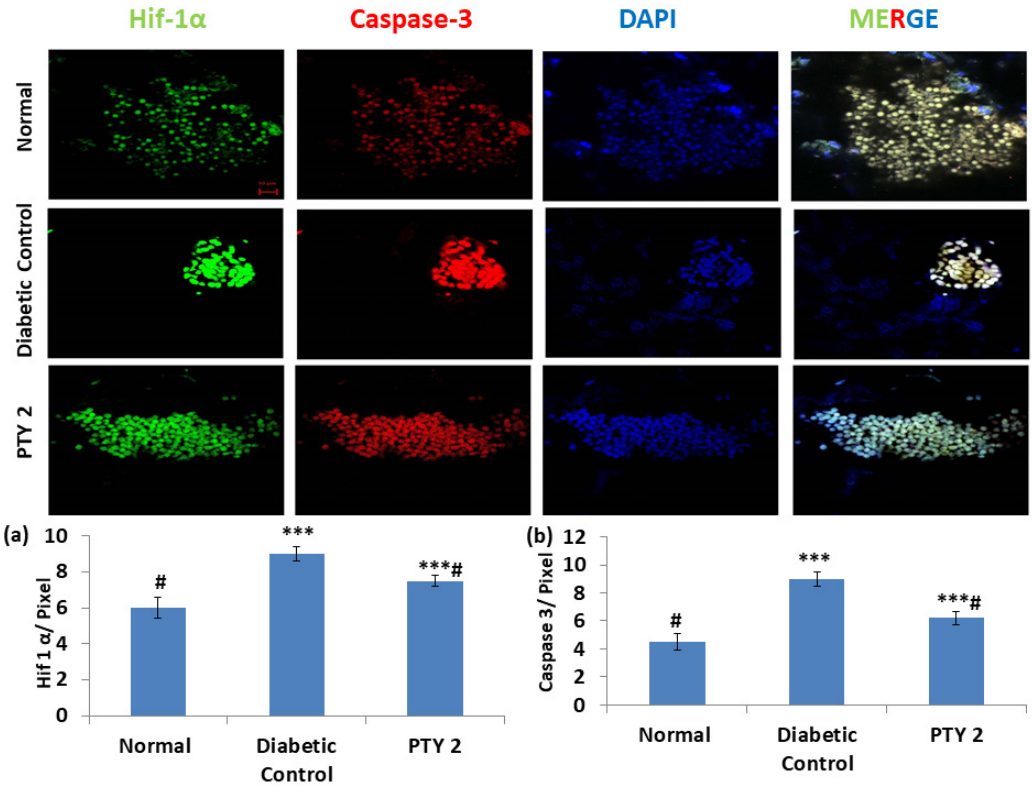

Figure 3. Immunohistochemistry analysis showed the effect of PTY-2 on the expression of (a) HIF-1α (green) and (b) Caspase 3 (red) in the islets of normal, diabetic control, and PTY-2-treated rats' pancreatic tissues. Both the expressions were merged with DAPI (blue). In comparison to diabetic control, PTY-2 down regulated the expression of both HIF-1α and Caspase 3. The images were taken at 63X magnification. Scale bar was 10 µm. The intensity was measured in pixel values. Each value represent the mean ± SD (n = 6); $^{***}p < 0.05$, compared with Normal, $^{\#}p < 0.05$, compared with Diabetic Control.

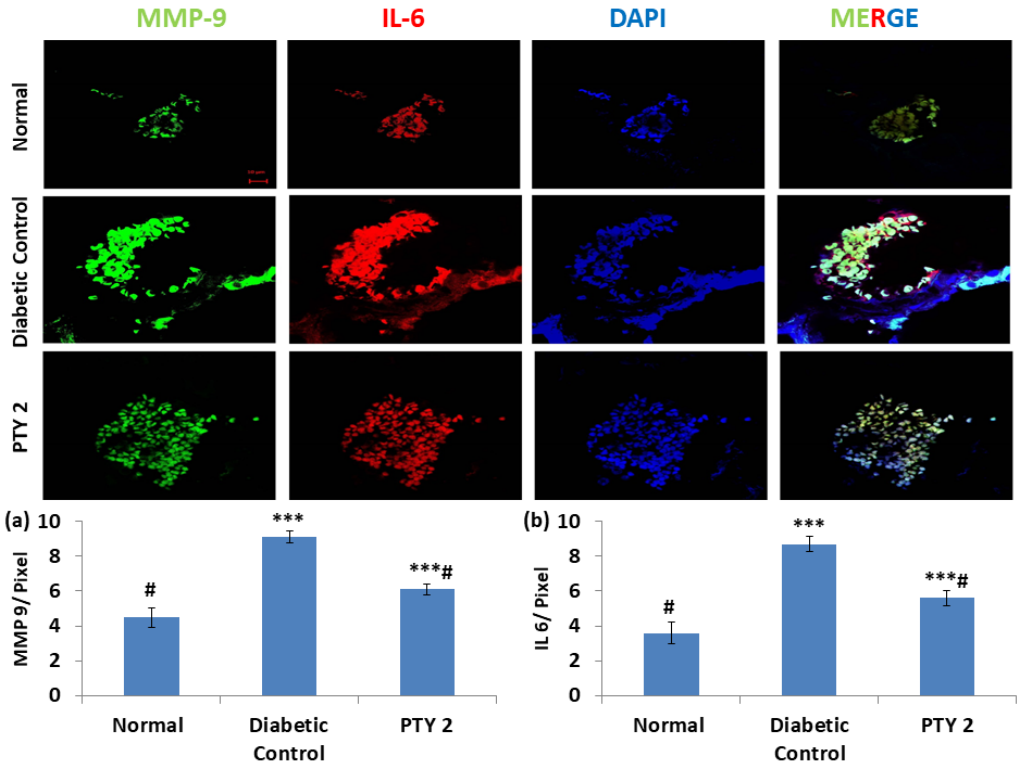

Figure 4. Immunohistochemistry analysis showed the effect of PTY-2 on the expression of (a) MMP-9 (green) and (b) IL-6 (red) in the islets of normal, diabetic control, and PTY-2-treated rats' pancreatic tissues. Both the expressions were merged with DAPI (blue). In comparison to diabetic control, PTY-2 down regulated the expression of both MMP-9 and IL-6. The images were taken at 63X magnification and scale bar was 10 μm. The intensity was measured in pixel values. Each value represent the mean ± SD ($n = 6$); $^{***}p < 0.05$, compared with Normal, $^{\#}p < 0.05$, compared with Diabetic Control.

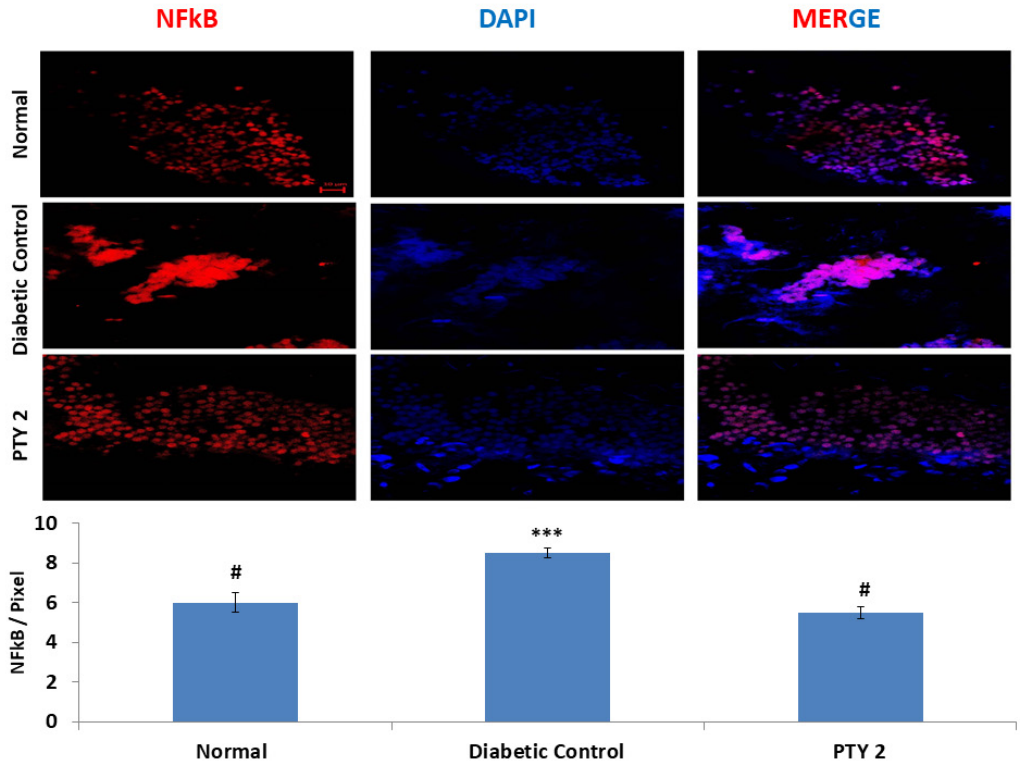

Figure 5. Immunohistochemistry analysis showed the effect of PTY-2 on the expression of NFkB (red) in the islets of normal, diabetic control, and PTY-2-treated rats' pancreatic tissues. The expression was merged with DAPI (blue) In comparison to diabetic control, PTY-2 down regulated the expression of NF-kB. The images were taken at 63X magnification and scale bar was 10 μm. The intensity was measured in pixel values. Each value represent the mean ± SD ($n = 6$); $^{***}p < 0.05$, compared with Normal, $^{\#}p < 0.05$, compared with Diabetic Control.

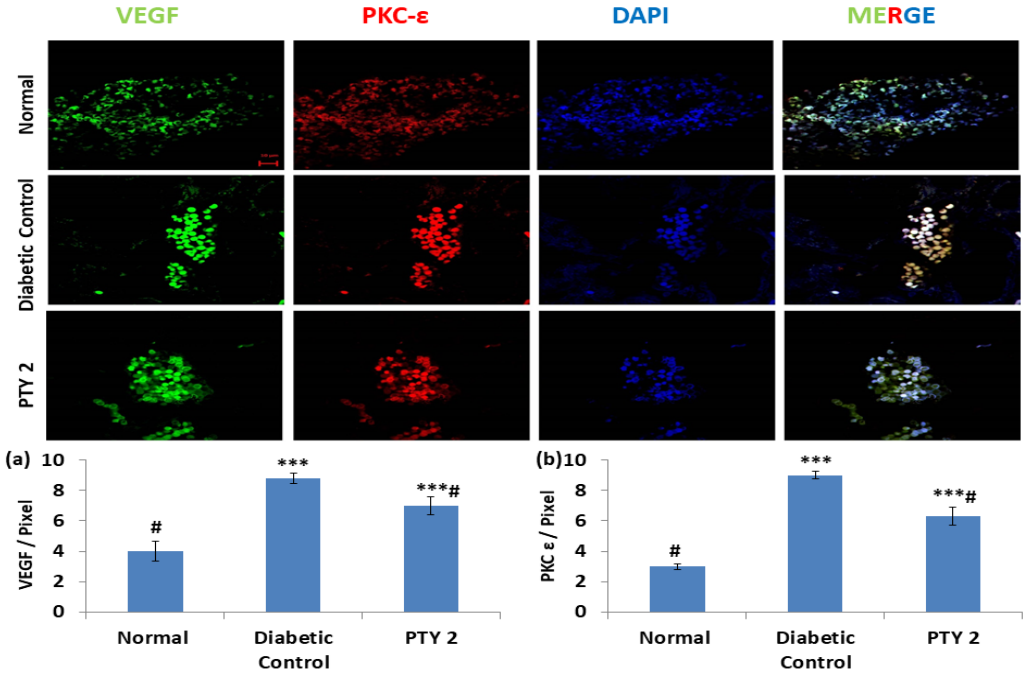

Figure 6. Immunohistochemistry analysis showed the effect of PTY-2 on the expression of (a) VEGF (green) and (b) PKC-ε (red) in the islets of normal, diabetic control, and PTY-2-treated rats' pancreatic tissues. Both the expressions were merged with DAPI (blue). In comparison to diabetic control, PTY-2 down regulated the expression of both VEGF and PKC ε. The images were taken at 63X magnification and scale bar was 10 μm. The intensity was measured in pixel values. Each value represent the mean ± SD ($n = 6$); $^{***}p < 0.05$, compared with Normal, $^{\#}p < 0.05$, compared with Diabetic Control.

significant to normal rats (Figures 3, 4, 5 and 6).

4. Discussion

The results of our study showed that, compared to the diabetic control group, the PTY-2 group had a favorable change in the expressions of biomarkers as assessed by RT-PCR, Western blot and Immunohistochemistry techniques. Analysis showed that STZ increased the expressions of MMP-9, TNF- α, HIF-1α, VEGF, IL-6, PKC-ε, NFkB and Caspase-3, which leads to the development of diabetic pathogenesis. But these expressions were significantly decreased by the treatment with PTY-2 for 10 days. Expression of SOD and Nephrin were significantly decreased among diabetic control rats, and these increased significantly after the administration of PTY-2. Thus, PTY-2 favorably changed the expressions of the biomarkers against islet stress.

Our earlier research had focused on the antidiabetic role of PT in STZ-induced diabetic model. We found that PT has an effect on inflammation (*15*) and hyperglycemia (*11-13*). Initially, the results showed that PTY-2 had hypoglycemic action because of inhibition of DPP-IV activity. In further research, we evaluated the effect on incretin receptors GLP-1R (Glucagon-like peptide 1 receptor), GIP-R (Glucose-dependent insulinotropic peptide receptor), and insulin. The results showed a significantly higher increase in plasma GLP-1 and GIP levels and a significant decrease in blood glucose concentrations after PTY-2 treatment (50 mg/100 g body weight) for 10 days. In the second study of chronic diabetes induced with STZ among rats, there was also a significant decrease in intestinal DPP-IV activity and an enhanced basal plasma insulin concentration in PTY-2 (earlier mentioned as PTWE) treated diabetic rats. Additionally, there was an increase in the number of islet cells and a significant increase in protein expression of insulin and B-cell lymphoma-2 (Bcl-2) in islet. According to *in silico* studies in our lab, Puerarone and Robinin were the two most effective phytochemicals for DPP-IV inhibition, and Tuberostan & Puererone of PTY-2 identified as the active component for GLP-1 and GIP receptors. Moreover, an *in-vivo* experiment showed that anti-inflammatory property of *Pueraria tuberosa* might be because of the scavenging of free radicals by increase in activity of SOD, and decrease in C-reactive protein levels (*15*).

Moving in the same direction of evaluation of the role of PTY-2 in chronic diabetes, we studied the effect of PTY-2 on the markers of oxidative stress, hypoxia, apoptosis and inflammation, which are known to play a significant role in the development and progression of pancreatitis and DM.

To understand and assimilate the results, the pathological changes in chronic diabetes along with the hypothetical mechanism of action of PTY-2 according to our study and previous reports have been diagrammatically shown in Graphical abstract (Figure 7). DM is a manifestation of abnormal metabolism and transport of glucose, and is associated with a decrease in insulin secretion and presence of insulin resistance. Further on, this leads to hyperglycemia and an increase

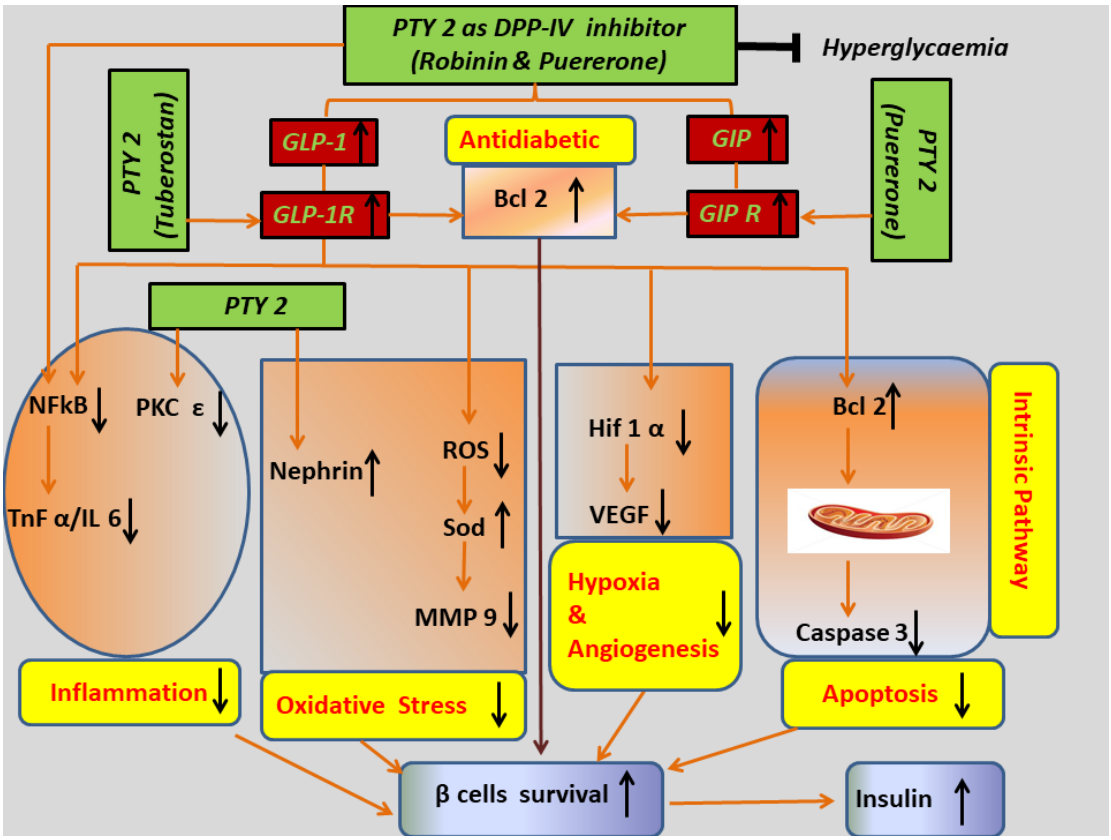

Figure 7. Mechanism of action of PTY-2 against STZ induced islet stress.

in the release of free fatty acids (FFAs) (*45*). All these inter-related steps decrease β-cell function and number, increase oxidative stress, induce apoptosis and endoplasmic reticulum stress, and increase the release of inflammatory cytokines (*45*). FFAs are known to induce the release of various interleukins, including IL-6, which further increase the release of free radicals and activate caspases. As shown in graphical abstract, NFκB, PKC-ε, TNF-α, and IL-6 are mediators of inflammation, and the administration of PTY-2 in our study was associated with a decrease in the expression of all these mediators. With the progression of diabetes, the balance between the pro-inflammatory, anti-inflammatory or protective mediators is disturbed (*45*). The increase in oxidative stress, measured by a decrease in SOD activity and an increase in ROS, was also decreased by PTY-2 administration. Other mediators of oxidative stress, *i.e.*, MMP-9 and VEGF, were also decreased. Hypoxia, which is measured with HIF 1α, is also an inducible factor of DM and was decreased by PTY-2 administration. Apoptosis, one of the critical pathological changes, is mediated by an increase in activity of caspases (*42*). PTY-2 led to a decrease in caspase-3 expression. Taking into consideration of our earlier evidence, it can be proposed that PTY-2 acts as a DPP-IV inhibitor, potentiates GLP-1 and GIP (*13*) mediated responses, and decreases inflammation, oxidative stress, apoptosis and hypoxia. GLP-1 agonists showed an inhibition of pro-inflammatory mediators in DM and other inflammatory conditions as well, in addition to their glucose-lowering potential (*46,47*).

MMP-9, one of the markers estimated in our study, deteriorates the inflammatory condition as it causes vascular injury, increases migration and cellular invasion by inflammatory cells (*22,33*). Both animal and human studies have shown an increase in MMP-9 expression in pancreatitis (*48,49*). MMP-9 acts as a diabetogenic factor by increasing proteolytic cleavage of insulin (*48,49*). Similar to our results, earlier studies have also shown an increase of MMP-9 activity in STZ induced models of DM (*22,48*). It is assumed that hyperglycemia induced oxidative stress induces the expression of MMP-9 in pancreas, and this can be counterbalanced with GLP-1 agonists (*22,50*). However, MMP-9 along with other paracrine factors is required for normal islet matrix turnover (*51*). IL-6, another biomarker, is also known to perform both inflammatory and protective roles (*45*). In type 1 DM, IL-6 participates in the regulation of balance between peripheral blood's regulatory T cells and Th17. In addition to this, IL-6 may contribute to both enhanced tissue insulin sensitivity and insulin resistance. Also, the increase of glucose concentration were found to co-exits with enhanced blood IL-6 concentration in patients with T2DM (*45*). However, PKC-ε inhibition/deletion is associated with an improvement in glucose homeostasis

(*39*). In a previous study, when the Psammomys (sand rats) were fed with high energy diet, they developed insulin resistance mimicking T2DM. Treatment with PKC-ε abrogated peptides prevented insulin resistance, hyperinsulinemia and pancreatic beta cell loss. It shows that the enhanced expression of PKC-ε in T2DM is associated with beta cell loss (*52*). In another study with culture of lipid-treated islets isolated from PKC-ε knockout (PKC-ε KO) mice, there occurred amplification of GSIS (glucose-stimulated-insulin-secretion), reinforcing the benefit of inhibition of PKC-ε (*39*). Our results also showed a significant increase of PKC-ε in the diabetic group, followed by a significant decrease in the PTY-2 group.

Pro-inflammatory and pro-apoptotic cytokines like IL-1β and TNF-α are involved in the development and progression of diabetes. NFκB is a transcription factor for mediating the cellular responses of inflammatory cytokines like IL-1β and TNF-α (*45*). NFkB pathways control cellular proliferation, inflammation, and immune responses through signal transduction (*21,53*). The activity of NFkB is increased in acute pancreatitis, and the longer duration of increased activity is associated with chronic diseases (*54-57*). Sitagliptin, a DPP-IV inhibitor used among T2DM patients, has shown anti-inflammatory action through the inhibition of NFκB, inflammatory cytokines and cell apoptosis (*58*). Mice deficient in NFκB have shown to be resistant to STZ induced diabetes (*59*).

TNF-α is a part of diabetes pathologenesis (*60*). The effects of TNF-α are mediated through the activation of NFkB pathway. An increase in the expression of TNF-α gene can enhance the risk of onset and progression of DM (*21*). Although the administration of TNF-α to animals is associated with insulin resistance and the regulation of TNF-α levels can improve insulin sensitivity, the status of TNF-α as a drug target for DM is still being evaluated. This might be possible with more understanding of the inter-relationships of the mediators in the pathogenesis of DM (*61*). A novel transcriptional inhibitor of TNF-α, MDL 201.449, has been found to reduce TNF-α mRNA levels dose dependently and prevent the development of hyperglycemia among mice following STZ injections (*73*).

Hyperglycemia also leads to the destabilization of HIF-1α, which is responsible for the regulation of the cellular responses to hypoxia. (*62,6*3). Hypoxia is an important cause of apoptosis and beta cell loss, and HIF-1α is an important indicator of beta cell loss (*64*). It is known that GLP-1R agonists (Extendin-4) improve islets survival through the activation of transcription factor, cAMP response element binding protein (CREB). A combination of CREB and Extendin-4 exerted enhanced anti-apoptotic action in cultured islets against hypoxia and cytokines. In an early phase, HIF-1α comes as a metabolic adaptation, but its prolonged activation enhances the expression of proapoptotic genes (64). Increased levels of caspases, along with the hypoxic state, are involved in beta cell apoptosis (*65*). Caspase-3, an important effector of the apoptotic pathways of DM, was also evaluated in our study *(42*). A study among Caspase-3 knockout ($Casp^{-/-}$) mice has shown that these mice were protected from the development of DM with a multiple low-dose administration of STZ, which, otherwise, causes selective β cell destruction and further triggers the immune reactions against islets (*42*). Studies with GLP-1 analogs among the animal models, *in-vitro* cell lines and human islet cells have shown a reduction in apoptosis, which was associated with a significant down-regulation of caspase-3 and up-regulation of bcl-2, and an increase in intracellular insulin content (*47,64,66,67*). In an earlier study, Puerarin, one of the components of PTY-2, decreased the expression of caspase-3 in osteoblasts of diabetic rats and improved the pathological changes (*68*).

HIF-1α is also a transcriptional activator of VEGF (*69*). VEGF, a pro-angiogenic growth factor, helps in the vascularization of the pancreatic islets (*31,70*). But overexpression of VEGF is fatal, as stated earlier. Oxidative stress, measured by the presence of ROS, is a promoter of angiogenesis (*70*). Currently, anti-VEGF therapy is approved for use in diabetic retinopathy (*71*). Additionally, the effect of DPP-IV inhibition and GLP-1 are being evaluated in diabetic ulcers and for cardiovascular protective role (*69,72*).

Hyperglycemia also impairs nephrin signaling by increasing its internalization and upregulates PKC-α expression. Thus, these expressions playing an interesting role against pancreatic β-cell loss in T2DM (*29*).

Currently, there is a need of antidiabetic agents with a wider spectrum of actions. As the roles of inflammation, oxidative stress, hypoxia, and apoptosis have become clearer over years, the currently available drugs should be re-evaluated for their effects on newer targets. Additionally, there is a need of newer agents which have action beyond the glucose-lowering potential. Various compounds have been studied for their role in the treatment of DM.

PTY-2 is a herbal medicine under evaluation for its role in DM. Along with these results, PTY-2 has also shown anti-diabetic action by inhibition of DPP-IV enzyme, by acting as incretins receptor agonist, and by decreasing β cell apoptosis. Further pre-clinical and clinical research can help in the utilization of PTY-2 as a treatment option in DM. PTY-2 can be a less costly treatment option as compared to the already available anti-diabetic synthetic drugs in market. As PTY-2 extract is composed of many phytochemicals, it can be effective for multiple diseases. On the other hand, the limitations of work shows that this study did not evaluate the role of individual phytochemicals of PTY-2 in DM. Overall, further post-translational studies are required to completely understand the protective effect of PTY-2 on islet.

5. Conclusion

Administration of PTY-2 for 10 days decreased the expressions of various biomarkers of oxidative stress, hypoxia, apoptosis and inflammation such as MMP-9, SOD, NFκB, VEGF, TNF-α, Caspase-3, IL-6, and HIF-1α as well as increased the expression of SOD and Nephrin among STZ-induced diabetic rats. Thus, PTY-2 protects diabetic islet through multi-targeted pathways. Further clinical research is needed to establish the role of PTY-2 in the treatment of DM.

Acknowledgements

We are thankful to the Head of Department, Dr. Amrita G. Kar, and all laboratory technicians of the Department of Pathology, IMS, BHU for their help in tissue slide preparations. Heartfelt thanks to ISLS, BHU for providing us the facility to perform Confocal Microscopy. Last but not least, we are grateful to Mrs. Durgavati Yadav, Mr. Vivek Pandey, Mrs. Rashmi Shukla, Mrs. Prerna Aditi and my escort Satish for helping us in sample processing.

References

1. World Health Organization. India: First to adapt the global monitoring framework on noncommunicable diseases (NCDs), 2015.
2. Yadav D, Lowenfels AB. The epidemiology of pancreatitis and pancreatic cancer. Gastroenterology. 2013; 144:1252-1261.
3. DiMagno MJ, DiMagno EP. Chronic pancreatitis. Curr Opin Gastroenterol. 2012; 28:523-531.
4. Alsamarrai A, Das SLM, Windsor JA, Petrov MS. Factors that affect risk for pancreatic disease in the general population: A systematic review and meta-analysis of prospective cohort studies. Clin Gastroenterol Hepatol. 2014; 12:1635-1644.e5.
5. Das SLM, Singh PP, Phillips ARJ, Murphy R, Windsor JA, Petrov MS. Newly diagnosed diabetes mellitus after acute pancreatitis: a systematic review and meta-analysis. Gut. 2014; 63:818-831.
6. Gupta S, Vittinghoff E, Bertenthal D, Corley D, Shen H, Walter LC, McQuaid K. New-onset diabetes and pancreatic cancer. Clin Gastroenterol Hepatol. 2006; 4:1366-1372.
7. Ben Q, Xu M, Ning X, Liu J, Hong S, Huang W, Zhang H, Li Z. Diabetes mellitus and risk of pancreatic cancer: A meta-analysis of cohort studies. Eur J Cancer. 2011; 47:1928-1937.
8. Perrin MC, Terry MB, Kleinhaus K, Deutsch L, Yanetz R, Tiram E, Calderon R, Friedlander Y, Paltiel O, Harlap S. Gestational diabetes as a risk factor for pancreatic cancer: A prospective cohort study. BMC Med. 2007; 5:25.
9. Girman CJ, Kou TD, Cai B, Alexander CM, O'Neill EA, Williams-Herman DE, Katz L. Patients with type 2 diabetes mellitus have higher risk for acute pancreatitis compared with those without diabetes. Diabetes, Obes Metab. 2010; 12:766-771.
10. Rosendahl J, Bödeker H, Mössner J, Teich N. Hereditary chronic pancreatitis. Orphanet J Rare Dis. 2007; 2:1.
11. Srivastava S, Shree P, Pandey H, Tripathi YB. Incretin hormones receptor signaling plays the key role in antidiabetic potential of PTY-2 against STZ-induced pancreatitis. Biomed Pharmacother. 2018; 97:330-338.
12. Srivastava S, Koley TK, Singh SK, Tripathi YB. The tuber extract of *Pueraria tuberosa* Linn. competitively inhibits DPP-IV activity in normoglycemic rats. Int J Pharm Pharm. Sci. 2015; 7:7-11.
13. Srivastava S, Shree P, Tripathi YB. Active phytochemicals of *Pueraria tuberosa* for DPP-IV inhibition: *in silico* and experimental approach. J Diabetes Metab Disord. 2017; 16:46.
14. Tripathi AK, Kohli S. Anti-diabetic activity and phytochemical screening of crude extracts of *Pueraria tuberosa* DC. (FABACEAE) grown in India on STZ -induced diabetic rats. Asian J Med Pharm Res. 2013; 3:66-73.
15. Pandey N, Yadav D, Pandey V, Tripathi YB. Anti-inflammatory effect of *Pueraria tuberosa* extracts through improvement in activity of red blood cell anti-oxidant enzymes. Ayu. 2013; 34:297-301.
16. Srivastava S, Yadav D, Tripathi YB. DPP-IV Inhibitory potential of methanolic extract of *Pueraria tuberosa* in liver of alloxan induced diabetic model. Biosci Biotechnol Res Asia. 2018; 15:1-4.
17. Shukla R, Pandey N, Banerjee S, Tripathi YB. Effect of extract of *Pueraria tuberosa* on expression of hypoxia inducible factor-1α and vascular endothelial growth factor in kidney of diabetic rats. Biomed Pharmacother. 2017; 93:276-285.
18. Shukla R, Banerjee S, Tripathi YB. *Pueraria tuberosa* extract inhibits iNOS and IL-6 through suppression of PKC-α and NF-kB pathway in diabetes-induced nephropathy. J Pharm Pharmacol. 2018; 70:1102-1112.
19. Verma SK, Jain V, Singh DP. Effect of *Pueraria tuberosa* DC. (Indian Kudzu) on blood pressure, fibrinolysis and oxidative stress in patients with stage 1 hypertension. Pakistan J Biol Sci. 2012; 15:742-747.
20. Srivastava S, Pandey H, Singh SK, Tripathi YB. PTY 2 as DPP-IV inhibitor prevents intestinal cell's apoptosis. bioRxiv. 2019; doi:10.1101/670430.
21. Burke SJ, Lu D, Sparer TE, Karlstad MD, Collier JJ. Transcription of the gene encoding TNF-α is increased by IL-1β in rat and human islets and β-cell lines. Mol Immunol. 2014; 62:54-62.
22. Uemura S, Matsushita H, Li W, Glassford AJ, Asagami T, Lee KH, Harrison DG, Tsao PS. Diabetes mellitus enhances vascular matrix metalloproteinase activity: role of oxidative stress. Circ Res. 2001; 88:1291-1298.
23. Shibaji T, Nagao M, Ikeda N, Kanehiro H, Hisanaga M, Ko S, Fukumoto A, Nakajima Y. Prognostic significance of HIF-1 alpha overexpression in human pancreatic cancer. Anticancer Res. 2003; 23:4721-4727.
24. Pini M, Rhodes DH, Castellanos KJ, Hall AR, Cabay RJ, Chennuri R, Grady EF, Fantuzzi G. Role of IL-6 in the resolution of pancreatitis in obese mice. J Leukoc Biol. 2012; 91:957-966.
25. Reinert RB, Brissova M, Shostak A, Pan FC, Poffenberger G, Cai Q, Hundemer GL, Kantz J, Thompson CS, Dai C, McGuinness OP, Powers AC. Vascular endothelial growth factor-A and islet vascularization are necessary in developing, but not adult, pancreatic islets. Diabetes. 2013; 62:4154-4164.
26. Singh N, Bhardwaj P, Pandey RM, Saraya A. Oxidative

stress and antioxidant capacity in patients with chronic pancreatitis with and without diabetes mellitus. Indian J Gastroenterol. 2012; 31:226-231.
27. Dabhi B, Mistry KN. Oxidative stress and its association with TNF-α-308 G/C and IL-1α-889 C/T gene polymorphisms in patients with diabetes and diabetic nephropathy. Gene. 2015; 562:197-202.
28. Putaala H, Soininen R, Kilpeläinen P, Wartiovaara J, Tryggvason K. The murine nephrin gene is specifically expressed in kidney, brain and pancreas: inactivation of the gene leads to massive proteinuria and neonatal death. Hum Mol Genet. 2001; 10:1-8.
29. Kapodistria K, Tsilibary EP, Politis P, Moustardas P, Charonis A, Kitsiou P. Nephrin, a transmembrane protein, is involved in pancreatic beta-cell survival signaling. Mol Cell Endocrinol. 2015; 400:112-128.
30. Watada H. Role of VEGF-A in pancreatic beta cells. Endocr J. 2010; 57:185-191.
31. Brissova M, Shostak A, Shiota M, Wiebe PO, Poffenberger G, Kantz J, Chen Z, Carr C, Jerome WG, Chen J, Baldwin HS, Nicholson W, Bader DM, Jetton T, Gannon M, Powers AC. Pancreatic islet production of vascular endothelial growth factor-A is essential for islet vascularization, revascularization, and function. Diabetes. 2006; 55:2974-2985.
32. Reinert RB, Cai Q, Hong JY, Plank JL, Aamodt K, Prasad N, Aramandla R, Dai C, Levy SE, Pozzi A, Labosky PA, Wright CVE, Brissova M, Powers AC. Vascular endothelial growth factor coordinates islet innervation *via* vascular scaffolding. Development. 2014; 141:1480-1491.
33. Zhen GD, Zhao LB, Wu SS, Chen MY, Li ZH, Zhou SZ, Li ZF. Associations of MMP-2 and MMP-9 gene polymorphism with ulinastatin efficacy in patients with severe acute pancreatitis. Biosci Rep. 2017; 37:BSR20160612.
34. De Palma AM, Verbeken E, Van Aelst I, Van den Steen PE, Opdenakker G, Neyts J. Increased gelatinase B/matrix metalloproteinase 9 (MMP-9) activity in a murine model of acute coxsackievirus B4-induced pancreatitis, Virology. 2008; 382:20-27.
35. Opdenakker G, Van den Steen PE, Van Damme J. Gelatinase B: a tuner and amplifier of immune functions. Trends Immunol. 2001; 22:571-579.
36. Rakonczay Z, Hegyi P, Takacs T, McCarroll J, Saluja AK. The role of NF- B activation in the pathogenesis of acute pancreatitis. Gut. 2008; 57: 259-267.
37. Patel S, Santani D. Role of NF-kappa B in the pathogenesis of diabetes and its associated complications. Pharmacol Rep. 2009; 61:595-603.
38. Swaroop JJ, Rajarajeswari D, Naidu JN. Association of TNF-α with insulin resistance in type 2 diabetes mellitus. Indian J Med Res. 2012; 135:127-130.
39. Cantley J, Burchfield JG, Pearson GL, Schmitz-Peiffer C, Leitges M, Biden TJ. Deletion of PKC epsilon selectively enhances the amplifying pathways of glucose-stimulated insulin secretion *via* increased lipolysis in mouse beta-Cells. Diabetes. 2009; 58:1826-1834.
40. Kim MJ, Lee YS, Lee KH, Min DS, Yoon SH, Hahn SJ, Kim MS, Jo YH. Site-specific localization of protein kinase C isoforms in rat pancreas. Pancreatology. 2001; 1:36-42.
41. Moritz W, Meier F, Stroka DM, Giuliani M, Kugelmeier P, Nett PC, Lehmann R, Candinas D, Gassmann M, Weber M. Apoptosis in hypoxic human pancreatic islets correlates with HIF-1α expression. FASEB J. 2002; 16:745-747.
42. Liadis N, Murakami K, Eweida M, Elford AR, Sheu L, Gaisano HY, Hakem R, Ohashi PS, Woo M. Caspase-3-dependent beta-cell apoptosis in the initiation of autoimmune diabetes mellitus. Mol Cell Biol. 2005; 25:3620-3629.
43. Asthana S, Agarwal T, Singothu S, Samal A, Banerjee I, Pal K, Pramanik K, Ray SS. Molecular docking and interactions of *Pueraria tuberosa* with vascular endothelial growth factor receptors. Indian J Pharm Sci. 2015; 77:439-445.
44. Pandey N, Tripathi YB. Antioxidant activity of tuberosin isolated from P*ueraria tuberose* Linn. J Inflamm (Lond). 2010; 7:47.
45. Cieślak M, Wojtczak A, Cieślak M. Role of pro-inflammatory cytokines of pancreatic islets and prospects of elaboration of new methods for the diabetes treatment. Acta Biochim Pol. 2015; 62:15-21.
46. Lee YS, Jun HS. Anti-inflammatory effects of GLP-1-based therapies beyond glucose control. Mediators Inflamm. 2016; 2016:1-11.
47. Farilla L, Hui H, Bertolotto C, Kang E, Bulotta A, Di Mario U, Perfetti R. Glucagon-like peptide-1 promotes islet cell growth and inhibits apoptosis in Zucker Diabetic rats. Endocrinology. 2002; 143: 4397-4408.
48. Descamps FJ, Martens E, Ballaux F, Geboes K, Opdenakker G. *In vivo* activation of gelatinase B/MMP-9 by trypsin in acute pancreatitis is a permissive factor in streptozotocin-induced diabetes. J Pathol. 2004; 204:555-561.
49. Descamps FJ, Van den Steen PE, Martens E, Ballaux F, Geboes K, Opdenakker G. Gelatinase B is diabetogenic in acute and chronic pancreatitis by cleaving insulin. FASEB J. 2003; 17: 887-889.
50. Ceriello A, La Sala L, De Nigris V, Pujadas G, Rondinelli M, Genovese S. GLP-1 reduces metalloproteinase-9 induced by both hyperglycemia and hypoglycemia in type 1 diabetes. The possible role of oxidative stress. Ther Clin Risk Manag. 2015; 11:901-903.
51. Christoffersson G, Waldén T, Sandberg M, Opdenakker G, Carlsson PO, Phillipson M. Matrix Metalloproteinase-9 is essential for physiological Beta cell function and islet vascularization in adult mice. Am J Pathol. 2015; 185:1094-1103.
52. Mack E, Ziv E, Reuveni H, Kalman R, Niv MY, Jörns A, Lenzen S, Shafrir E. Prevention of insulin resistance and beta-cell loss by abrogating PKCε-induced serine phosphorylation of muscle IRS-1 in Psammomys obesus. Diabetes Metab Res Rev. 2008; 24:577-584.
53. Croft M, Benedict CA, Ware CF. Clinical targeting of the TNF and TNFR superfamilies. Nat Rev Drug Discov. 2013; 12:147-168.
54. Chen W, Zheng Z, Duan J, Wang X, Wu S, Wang W, Xu L, Han S, Qiao Z. Quantitation of nuclear factor kappa B activation in pancreatic acinar cells during rat acute pancreatitis by flow cytometry. Int J Clin Exp Med. 2015; 8:10143-10151.
55. Steinle AU, Weidenbach H, Wagner M, Adler G, Schmid RM. NF-κB/Rel activation in cerulein pancreatitis. Gastroenterology. 1999; 116:420-430.
56. Algül H, Treiber M, Lesina M, Nakhai H, Saur D, Geisler F, Pfeifer A, Paxian S, Schmid RM. Pancreas-specific RelA/p65 truncation increases susceptibility of acini to inflammation-associated cell death following cerulein pancreatitis. J Clin Invest. 2007; 117:1490-1501.

57. Fantini L, Tomassetti P, Pezzilli R. Management of acute pancreatitis: Current knowledge and future perspectives. World J Emerg Surg. 2006; 1:16.
58. Hu X, Liu S, Liu X, Zhang J, Liang Y, Li Y. DPP-4 (CD26) inhibitor sitagliptin exerts anti-inflammatory effects on rat insulinoma (RINm) cells *via* suppressing NF-κB activation. Endocrine. 2017; 55:754-763.
59. Liuwantara D, Elliot M, Smith MW, Yam AO, Walters SN, Marino E, McShea A, Grey ST. Nuclear factor-kappaB regulates beta-cell death: a critical role for A20 in beta-cell protection. Diabetes. 2006; 55:2491-2501.
60. Mandrup-Poulsen T. Apoptotic signal transduction pathways in diabetes. Biochem Pharmacol. 2003; 66:1433-1440.
61. DE M. Potential role of TNF-alpha in the pathogenesis of insulin resistance and type 2 diabetes. Trends Endocrinol Metab. 2000; 11: 21-27.
62. Catrina SB, Okamoto K, Pereira T, Brismar K, Poellinger L. Hyperglycemia regulates hypoxia-inducible factor-1alpha protein stability and function. Diabetes. 2004; 53:3226-3232.
63. Bento CF, Pereira P. Regulation of hypoxia-inducible factor 1 and the loss of the cellular response to hypoxia in diabetes. Diabetologia. 2011; 54:1946-1956.
64. Velmurugan K, Balamurugan AN, Loganathan G, Ahmad A, Hering BJ, Pugazhenthi S. Antiapoptotic actions of exendin-4 against hypoxia and cytokines are augmented by CREB. Endocrinology. 2012; 153:1116-1128.
65. Greijer AE, van der Wall E. The role of hypoxia inducible factor 1 (HIF-1) in hypoxia induced apoptosis. J Clin Pathol. 2004; 57:1009-1014.
66. Farilla L, Bulotta A, Hirshberg B, Li Calzi S, Khoury N, Noushmehr H, Bertolotto C, Di Mario U, Harlan DM, Perfetti R. Glucagon-like peptide 1 inhibits cell apoptosis and improves glucose responsiveness of freshly isolated human islets. Endocrinology. 2003; 144:5149-5158.
67. Li Y, Hansotia T, Yusta B, Ris F, Halban PA, Drucker DJ. Glucagon-like Peptide-1 receptor signaling modulates β cell apoptosis. J Biol Chem. 2003; 278:471-478.
68. Liang J, Chen H, Pan W, Xu C. Puerarin inhibits caspase-3 expression in osteoblasts of diabetic rats. Mol Med Rep. 2012; 5:1419-1422.
69. Marfella R, Sasso FC, Rizzo MR, Paolisso P, Barbieri M, Padovano V, Carbonara O, Gualdiero P, Petronella P, Ferraraccio F, Petrella A, Canonico R, Campitiello F, Della Corte A, Paolisso G, Canonico S. Dipeptidyl peptidase 4 inhibition may facilitate healing of chronic foot ulcers in patients with type 2 diabetes. Exp Diabetes Res. 2012; 2012:892706.
70. El-Refaei MF, Abduljawad SH, Alghamdi AH. Alternative medicine in diabetes – role of angiogenesis, oxidative stress, and chronic inflammation. Rev Diabet Stud. 2014; 11:231-244.
71. Osaadon P, Fagan XJ, Lifshitz T, Levy J. A review of anti-VEGF agents for proliferative diabetic retinopathy. Eye. 2014; 28:510-520.
72. Xiao-Yun X, Zhao-Hui M, Ke C, Hong-Hui H, Yan-Hong X. Glucagon-like peptide-1 improves proliferation and differentiation of endothelial progenitor cells *via* upregulating VEGF generation. Med Sci Monit. 2011; 17:BR35-41.
73. Holstad M, Sandler S, A transcriptional inhibitor of TNF-α prevents diabetes induced by multiple low-dose streptozotocin injections in mice, J Autoimmun. 2001; 16:441-447.

(Received July 16, 2019; Revised September 24, 2019; Accepted October 4, 2019)

Original Article

DOI: 10.5582/bst.2019.01186

Dioscin improves postmenopausal osteoporosis through inducing bone formation and inhibiting apoptosis in ovariectomized rats

Shan Wu[1,§], Fan Zhao[2,§], Jing Zhao[1], Hui Li[3], Junyu Chen[1], Yang Xia[1], Junwei Wang[1], Benzheng Zhao[1], Shuhua Zhao[1,*], Na Li[4]

[1] *The Second Hospital of Jilin University, Changchun, Jilin province, China;*
[2] *China-Japan Union Hospital of Jilin University, Changchun, Jilin province, China;*
[3] *Qian Wei Hospital of Jilin Province, Changchun, Jilin province, China;*
[4] *Jilin Ginseng Academic, Changchun University of Chinese Medicine, Changchun, Jilin province, China.*

Summary **Postmenopausal osteoporosis (PMO) has become a public health problem worldwide. Hormonal replacement therapy (HRT) is the most popular treatment for PMO at present, but the side effects, including increased risk of endometrial cancer and breast cancer, limit its clinical use. Therefore, finding a new medication with high efficiency and less side-effects is urgently required. Dioscin is the main ingredient of some medicinal plants such as Dioscorea nipponica Makino and Dioscorea zingiberensis Wrigh. It is reported that dioscin has anti-tumoral and anti-atherosclerotic activity as well as an inhibitory effect on hepatic fibrosis. In this study, the effects of dioscin on PMO were examined and the mechanisms were analyzed. The results indicated that the bone mineral density and ultimate load of PMO rats were increased after being treated with dioscin. H&E staining and immunohistochemical staining showed the bone trabeculae formation and bone differentiation of PMO rats were promoted by dioscin. Western blots revealed that dioscin could activate the PI3K/P38/AKT signaling pathway and inhibit the apoptosis signaling pathway in bone tissue cells of PMO rats. In addition, MTT assays showed that MC3T3-E1 cell viability could be improved by dioscin. These results suggest dioscin is a potential therapeutic reagent for osteoporosis and deserves further investigation.**

Keywords: Dioscin, postmenopausal osteoporosis, PI3K/P38/AKT pathway, apoptosis

1. Introduction

Osteoporosis is a prevalent systemic metabolic bone disease characterized by decreased bone mass, bone microstructure degradation, bone fragility and susceptibility to pathological fractures (*1*). Osteoporosis has been paid more attention, because of the progressive aging of society (*2*). According to a report from World Health Organization, osteoporosis has become a global health issue with high morbidity and mortality, similar to cardiovascular diseases, diabetes, and cancer. More than 200 million people in the world have osteoporosis, and at least 9 million of them suffer from fractures. The financial burden of fractures has been increasing and is expected to rise 29% by 2020 compared to 2005 (*3*).

There are numerous issues that can cause osteoporosis, such as endocrine or nutritional factors, age, and a myriad of chronic systemic diseases. It can occur at any age but is especially frequent in postmenopausal women (*4*). Postmenopausal women suffer from osteoporosis primarily due to decreased gonadal function, which, in conjunction with advanced age, promotes postmenopausal osteoporosis (PMO) (*5*). Both the pain and skeletal deformation caused by PMO decrease the quality of life of female patients. Moreover, PMO sufferers place a financial burden on both families and society due to the disabilities

Released online in J-STAGE as advance publication October 15, 2019.

[§]These authors contributed equally to this work.

**Address correspondence to:*
Dr. Shuhua Zhao, Department of Gynecology and Obstetrics, the Second Hospital of Jilin University, Changchun 130041, Jilin province, China.
E-mail: zhaoshuhua-1966@163.com

Table 1. The pharmacological treatment of rats

Treatments	Model group	Low dose group	High dose group	Control group
Dioscin	/	150 mg/kg daily (*i.g.*)	300 mg/kg daily (*i.g.*)	/
Operations	Ovariectomy	Ovariectomy	Ovariectomy	Sham-operation

associated with PMO. Therefore, PMO is a serious problem that still needs to be adequately addressed. It is necessary to find new remedies for the disease that will be both effective and safe, to complete the existing therapeutic arsenal.

Estrogen (E) deficiency caused by ovarian dysfunction is the major factor in the development of osteoporosis after menopause (*6,7*), and hormone replacement therapy (HRT) has been applied widely in recent decades. However, long term HRT is associated with an increased risk of thrombosis, breast cancer, and endometrial cancer, which limits the clinical application of HRT. Furthermore, HRT-induced sodium and water retention affect patient compliance. Apart from HRT, other treatments for PMO include calcitonin, bisphosphonates, statins, and monoclonal antibodies. However, the clinical applications are all restricted by high price and side effects, including osteonecrosis and venous thromboembolism (VTE) (*8*). Considering these problems, herbal drugs, which might be cable of assuaging concerns about treatment risks, have received attention in PMO management and are of great interest to both public and medical professionals.

Dioscin is the main ingredient of some medicinal plants such as Dioscorea nipponica Makino and Dioscorea zingiberensis Wright (*9*) and has therapeutic uses in various diseases. It is reported that dioscin has anti-tumoral activity (*10,11*), anti-atherosclerotic activity (*12*) and inhibitory effects on hepatic fibrosis (*13*). In recent years, several studies have showed dioscin alleviates the impact of osteoporosis (*4*). Interestingly, it does not cause endometrium proliferation (*3*), which indicates that dioscin could be used in women with intact uteri.

In this study, osteoporotic ovariectomized rat model, as well as a cultured osteoblast precursor cell line, was made to investigate the effects of dioscin on PMO. Moreover, possible molecular mechanisms of action were proposed to further verify the feasibility of clinical application of dioscin.

2. Materials and Methods

2.1. *Materials*

Dioscin (purity > 98%) was purchased from Shanxi Hengcheng Pharmaceutical company. In cell experiments, dioscin was added into phosphate buffered saline (PBS) with a final concentration of less than 0.1% fetal bovine serum (FBS) and penicillin-streptomycin were obtained from Hyclone. Dimethyl sulfoxide (DMSO) was purchased from Amresco. Alkaline phosphatase (ALP), bone morphogenetic protein (BMP), PI3K, P38, p-P38, ERK, p-ERK, AKT, p-AKT, Bcl-2, Bax, Caspase3 and c-Caspase3 antibodies were purchased from Affinity.

2.2. *Animal preparation*

Forty female Sprague Dawley (SD) rats were provided by Basic Medical College of Jilin University. The animal study was conducted following internationally recognized guidelines and was approved by the Animal Research Committee of Norman Bethune College of Medicine, Jilin University. Apart from this, all rats were allowed seven days to adapt to the new environment and were housed in a room with a 12-hour light/dark cycle at a temperature between 22-25°C and controlled humidity between 40-50%.

2.3. *Pharmacological treatment*

As shown in Table 1, the study was performed on 40 female SD rats (200 ± 20 g). At about 4 to 6 weeks of age, the rats were randomly divided into four groups (of 10 animals each): Model group and control group received PBS intragastrically (*i.g.*) at a rate of 4 mL/kg daily. The other two groups were treated *i.g.* with dioscin at either 150 mg/kg daily (low dose group) or 300 mg/kg daily (high dose group) in PBS.

With the exception of the control group (which underwent the same procedure but without ovariectomy), the other 30 rats all underwent a complete bilateral ovariectomy. Five days after the operation, dioscin was administered *i.g.* for 60 days.

After intraperitoneal injection of chloral hydrate (350 mg/kg), the rats' serum was collected and used for culturing MC3T3-E1 cells. Then, the rats were euthanized, and the right femurs were dissected, cleaned, and fixed in 10% buffered formalin for 24 hrs. After that, the bones were kept in 70% ethanol and stored at 4°C to be sliced.

2.4. *BMD measurement*

Before euthanizing the rats, the bone mineral density (BMD) of femur and lumbar vertebra were measured *via* Dual-energy X-ray (LUNAR, USA) absorptiometry using software for small animals.

2.5. *Three-point bending test*

The mechanical properties of the femoral diaphysis

were studied using a three-point bending test. After being placed at room temperature for 1h, the left femurs were placed under vertical load in the testing machine. The load increased at the rate of 2 mm/min until the bone broke, and the load under which the bone broke (the ultimate load) was recorded.

2.6. *Histomorphological assay*

The right femurs of the rats were fixed in 10% buffered formalin for 24 hrs and then decalcified in 10% ethylenediaminetetraacetic acid for 14 days. The bones were then treated with ethanol and xylene for dehydration. After being embedded in paraffin and sliced, several 4 μm-thin histological slices stained with hematoxylin and eosin (H&E) were prepared. The images were subsequently acquired using a light microscope with 200× magnification.

2.7. *Immunohistochemical (IHC) staining*

After 60 days of treatment, histological slices from the right femurs of rats were prepared for ALP and BMP IHC staining, as previously described (*14*). The slices were analyzed using a microscope Image-Pro Plus 6.0, and positive cells were identified as the cells with brown staining.

2.8. *Western blo*t

The protein samples from fresh rat femoral bone tissue were extracted with cold lysis buffer, resolved in 12% SDS-PAGE gels, separated electrophoretically and transferred onto Polyvinylidene Fluoride (PVDF) membranes (Millipore, USA). The non-specific binding sites of the membrane were blocked with 5% dried skim milk at 37°C for 1hr. After that, the membrane was incubated with primary antibodies (PI3K, P38, p-P38, ERK, p-ERK, AKT, p-AKT, Bcl-2, Bax, Caspase3, c-Caspase3 and β-actin antibody) overnight at 4°C and then incubated with horseradish peroxidase (HRP) tagged secondary antibody at room temperature for 2hrs. Finally, the protein level was detected with an ECL plus kit (Millipore, USA) and developed *via* ChemiDoc XRS (BIO-RAD, USA).

2.9. *Cell cultures and MTT assay*

The MC3T3-E1 cells were purchased from the Cell Bank of the Chinese Academy of Sciences (Shanghai, China), and were cultured in IMDM supplemented with 10% FBS and 1% penicillin-streptomycin. The cells were all maintained in a humidified incubator containing 5% CO_2 at 37°C. Cell viability was evaluated with MTT assay. After being adjusted to a concentration of 5×10^4 /mL, the MC3T3-E1 cells were seeded onto 96-well plates at 100 μL per well and cultured in an incubator overnight. After being incubated with the serum of rats respectively for 72 hrs, the MTT solution (10 μL per well, 5 mg/mL) was added into each well, and the cells were incubated at 37°C for 4 hrs. Finally, DMSO solution was added at 150 μL per well. After shaking for 10 minutes, the absorbance was analyzed at 490 nm using a Microplate Reader.

2.10. *Statistical analysis*

All data was analyzed with the statistical software SPSS 18.0 and the results expressed as means ± SD. The differences among groups were analyzed using a student's *t*-test. $p < 0.05$ and $p < 0.01$ indicated statistically significant differences.

3. Results

3.1. *Dioscin increased the BMD of PMO rats*

To assess the effect of dioscin on PMO, the BMD of PMO rats were measured. As shown in Figure 1A-C, rats in the model group showed a lower level of femur BMD (f-BMD) and lumbar vertebra BMD (v-BMD) compared with the control group ($p < 0.01$). Meanwhile, low-dose treatment with dioscin increased the level of f-BMD and v-BMD ($p < 0.01$) compared with the model group. Furthermore, high-dose treatment with dioscin increased the level of BMDs significantly ($p < 0.05$ in both BMDs). These results indicate that the PMO rat model has been established successfully, and dioscin can increase the BMD of PMO rats by promoting formation of bone.

3.2. *Dioscin enhanced the mechanical properties of bone in PMO rats*

To further investigate whether dioscin improves mechanical properties of bone in the PMO rats, maximum bone stress was compared between groups. As shown in Figure 1D, the femurs from the model group show a significant decrease in ultimate load compared with the control group ($p < 0.01$), and a substantial increase in the ultimate load has been observed in both the low-dose group ($p < 0.05$) and high-dose group ($p < 0.01$) compared with the model group, suggesting dioscin is capable of providing significant protection against ovariectomy-induced bone fragility.

3.3. *Dioscin increased bone trabeculae formation in PMO rats*

H&E staining was employed to observe the morphological features of bone trabeculae in PMO rats. Compared with the control group, there were more spaces within the bone marrow than bone trabeculae in the cancellous bone of femurs in the model group,

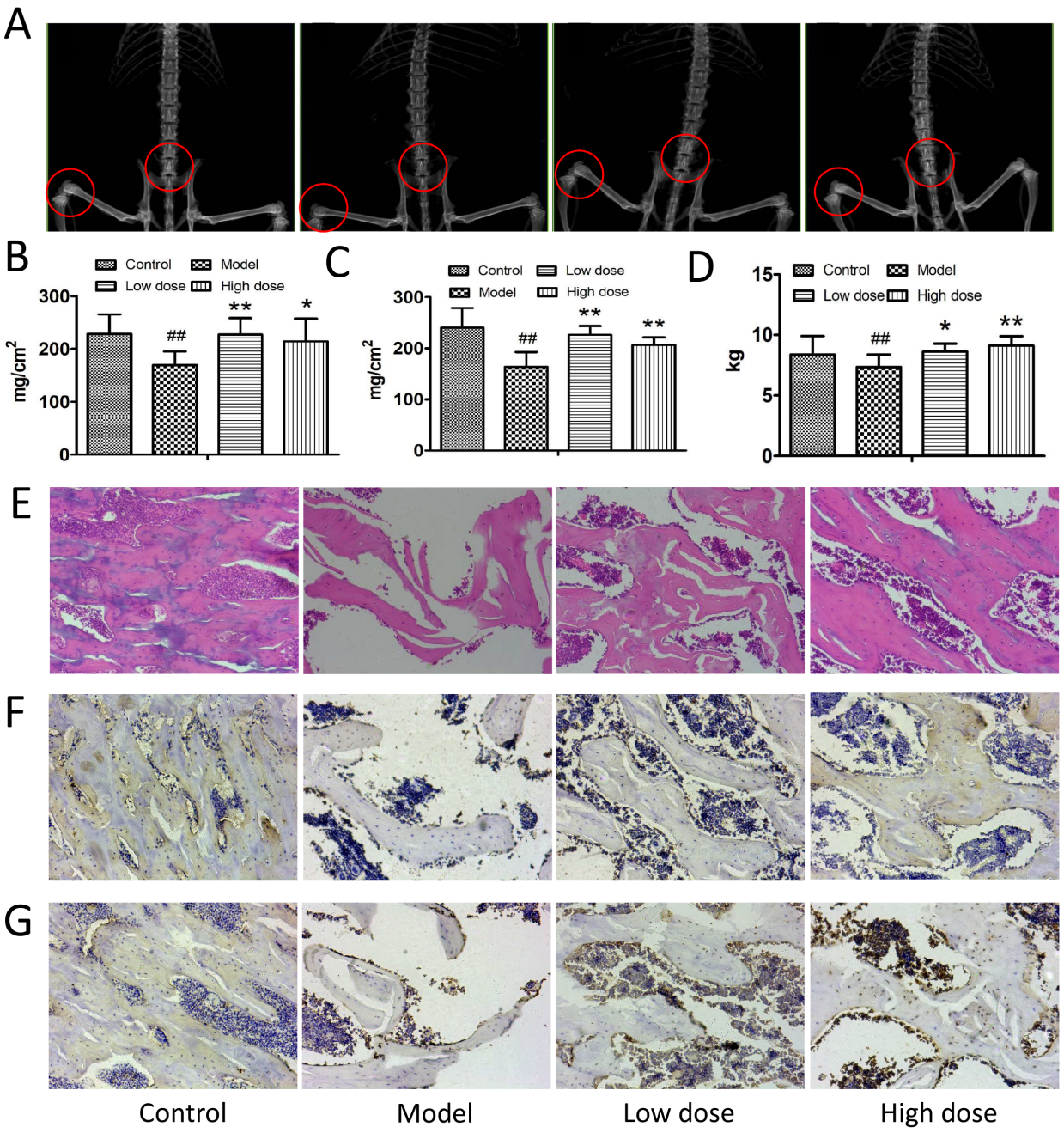

Figure 1. Effects of dioscin on BMD, ultimate load and histopathological evaluation in rats. (A-C), Effects of dioscin on the BMD of femur **(A,B)** and lumbar vertebra **(A,C),** respectively. **(D),** Effects of dioscin on the ultimate load of rat femurs. **(E),** H&E staining of rat femur tissue. **(F),** IHC staining of ALP in rat femur tissue. **(G),** The IHC staining of BMP in rat femur tissue. Results were obtained from three independent experiments and are expressed as mean ± SD. #: $p < 0.05$; ##: $p < 0.01$ *vs*. control group; *: $p < 0.05$; **: $p < 0.01$ *vs*. model group.

which could be significantly restored by dioscin regardless of dose (Figure 1E). These results demonstrate the protective role of dioscin in the prevention of ovariectomy-induced trabecular bone loss.

3.4. *Dioscin promoted bone differentiation*

To further verify the efficacy of dioscin in the promotion of bone differentiation, IHC staining was conducted to determine the levels of ALP and BMP. As shown in Figure 1F, the expression of ALP in rats from the model group is lower than control group, while this decrease has been prevented by dioscin. The same change can be observed in the expression of BMP (Figure 1G). Therefore, the conclusion can be drawn that dioscin is capable of up-regulating the levels of ALP and BMP, which have been down-regulated in PMO rats.

3.5. *Dioscin promoted bone formation via PI3K/P38/AKT signaling pathway*

To investigate the mechanism of dioscin promoting the

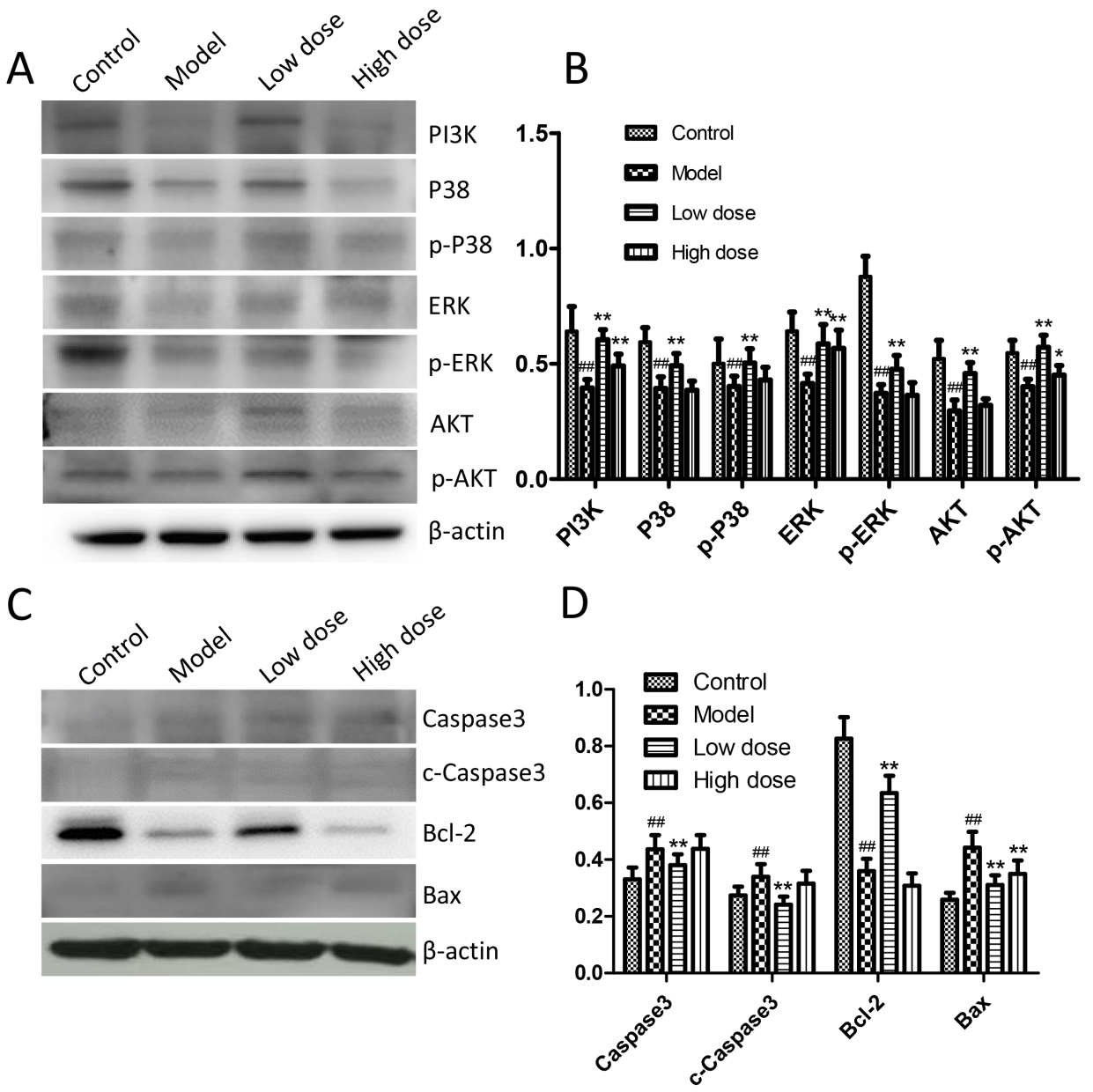

Figure 2. Effects of dioscin on proliferation, differentiation and apoptosis-associated proteins in bone tissue. (A and **B),** Effects of dioscin on PI3K, P38, p-P38, ERK, p-ERK, AKT and p-AKT levels in bone tissue. **(C** and **D),** Effects of dioscin on Caspase3, c-Caspase3, Bcl-2 and Bax levels in bone tissue. Results were obtained from three independent experiments and are expressed as mean ± SD. #: $p < 0.05$; ##: $p < 0.01$ *vs*. control group; *: $p < 0.05$; **: $p < 0.01$ *vs*. model group.

formation of bone, Western blots were used to detect the expression of proliferation-associated proteins in bone tissue. As shown in Figure 2A and Figure 2B, the expression of PI3K, P38, p-P38, ERK, p-ERK, AKT, p-AKT of rats in the model group was decreased compared with the control group ($p < 0.01$). Except that the level of P38, p-P38, p-ERK and AKT was only increased by low-dose dioscin ($p < 0.01$), the increase of the other proteins were observed at both the low and high dose of dioscin, compared to the model group. These results reveal that the promoting effect of dioscin in bone formation might be associated with the activation of the PI3K/P38/AKT signaling pathway.

3.6. *Dioscin inhibited the apoptosis of bone tissue*

To further explore the mechanism of dioscin promoting the formation of bone, the expression of apoptosis-associated proteins in bone tissue was detected using Western blots. Results are represented in Figure 2C and Figure 2D: in the model group, the level of Bcl-2 was decreased, and the level of Caspase3, c-Caspase3 and Bax was increased compared with the control group ($p < 0.01$). While it was expected only low-dose dioscin would effectively down-regulate the level of Caspase3 and c-Caspase3, as well as up-regulate the level of Bcl-2, both dosages of dioscin inhibited the expression of

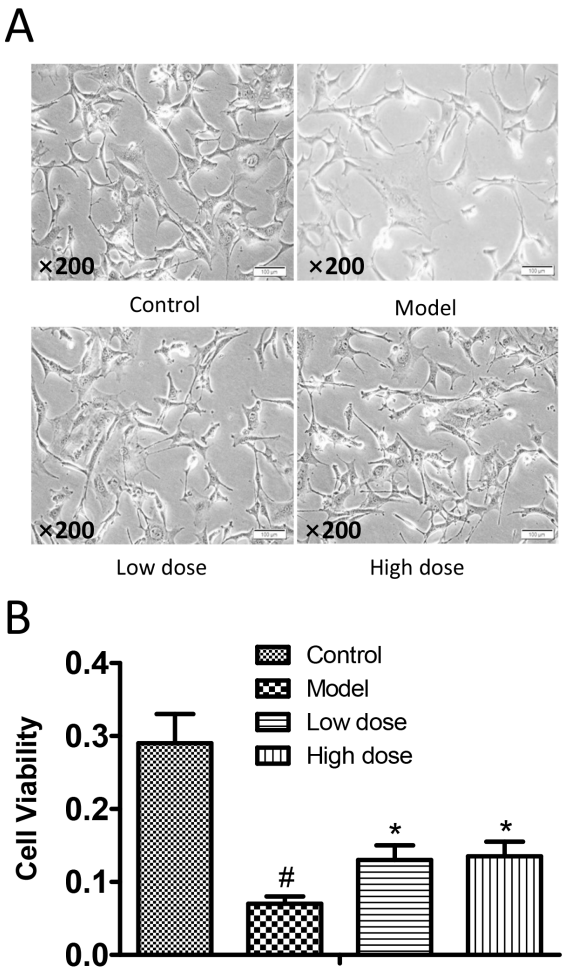

Figure 3. Effects of dioscin on the proliferation of MC3T3-E1 cells. Effects of dioscin on cell viabilities of MC3T3-E1 cells. Results are expressed as mean ± SD. #: $p < 0.05$; ##: $p < 0.01$ *vs*. control group; *: $p < 0.05$; **: $p < 0.01$ *vs*. model group.

Bax significantly ($p < 0.01$). These results suggest that dioscin could improve osteoporosis through inhibiting the apoptosis signaling pathway.

3.7. *Dioscin enhanced the proliferation of MC3T3-E1 cells*

MC3T3-E1 cells were used to identify whether dioscin could enhance osteoblast proliferation *in vitro*. As shown in Figure 3A and Figure 3B, the MTT assay showed that the cell viability of the model group is much lower than that of the control group. Meanwhile, the viability of cells incubated with the serum of rats treated with dioscin at different doses increased significantly, compared to the model group. The above results show that osteoblast proliferation was promoted by dioscin, which indicates dioscin might promote bone formation *via* osteoblast activation.

4. Discussion

Bone metabolic balance depends on the interaction of bone formation and bone resorption, indicating the disorder is caused by an imbalance between osteoblasts and osteoclasts (*15,16*), which is also the key cause of PMO. Osteoblasts play a vital role in bone formation and are controlled by several signaling pathways, including PI3K/P38/AKT pathways (*17-19*). This study aimed to evaluate the osteoprotective effects of dioscin on PMO rats and explore dioscin's mechanism of action.

PMO rats, a well-established experimental model of PMO *in vivo*, were confirmed by the decrease of BMD, ultimate load, ALP and BMP expression (all of which were prevented by dioscin in this study). The lower levels of BMD and the reduced stiffness are two principal features in osteoporosis formation, predisposing patients with osteoporosis to a high risk of bone fracture (*8*). ALP, functioning as an osteoblast differentiation marker at an early stage, participates in the beginning of mineralization of bone formation. Additionally, ALP activation could be increased by BMP (*20*), a significant autocrine and paracrine growth factor (*21*).

BMP is a member of the TGF-β superfamily and is derived from osteoblasts. Besides, BMP could influence the differentiation of mesenchymal stem cells (MSCs) to osteoblasts *via* the P38 signaling pathway (*22*). Thus, BMP represents a critical factor in the process of bone formation and bone repair (*23*). Our results indicated that dioscin could up-regulate the expression of osteoblast differentiation-associated proteins including ALP and BMP, which implied that it might increase BMD *via* promoting osteoblast differentiation and hence strengthen the ultimate load of PMO rat femurs.

Obviously, there is a decrease in the expression of PI3K, P38, p-P38, ERK, p-ERK, AKT and p-AKT in PMO rats. Interestingly, although the effectiveness of dioscin varied based on the concentration, it could reverse these decreases in our study. P38 mitogen-activated protein kinase (P38) and extracellular regulated protein kinases (ERK) are members of mitogen-activated protein kinases (MAPK), which are a family of serine/threonine protein kinases. P38 is capable of increasing the proliferation of osteoblasts and inhibiting the differentiation of osteoclasts by activating NF-KB, Max, P53, and Stat1 to improve osteoporosis (*24*). Moreover, P38 is an osteoblast-derived protein with a significant effect on the regulation of cell proliferation (*25*). Also, ERK has an essential impact on maintaining the balance between bone formation and bone resorption by promoting the differentiation of MSCs to osteoblasts. What's more, protein kinase B (AKT) is the downstream of PI3K (*26*). PI3K/AKT signaling pathway plays a vital role in osteoblast differentiation and mineralization (*27*). Not only does PI3K regulate the differentiation of osteoblasts by interacting with Runx2 (*28-31*), but also could inhibit osteoblast apoptosis by inactivating FoxO (forkhead proteins) (*32-35*). Apart from these, the PI3K/

AKT signaling pathway promotes the proliferation and differentiation of osteoblasts through associated signaling molecules such as ALP and BMP (*36,37*). Our results indicate that dioscin stimulates bone tissue proliferation and differentiation *via* P38 and PI3K/AKT signaling pathways.

Our study demonstrates the expression of Bcl-2 is up-regulated in dioscin-treated rats compared with PMO rats, while the expressions of Caspase3, c-Caspase3 and Bax are down-regulated. Bcl-2, Bax, and Caspase3 as well as c-Caspase3 play a vital role in apoptosis. Apoptosis could be induced by the release of cytochrome C from mitochondria (*38*). The release of cytochrome C could be inhibited by Bcl-2 and be promoted by Bax, then contribute significantly to activate the Caspase family of proteins, especially Caspase3 (*39,40*), which could be activated by Caspase9, cleaved into c-Caspase3 and work as an executor leading to cells apoptosis. Furthermore, by combining with Bax and silencing it, Bcl-2 performs a protective effect on apoptosis. However, the overexpression of Bax could overcome the protective effect of Bcl-2 and lead to apoptosis (*41*). AKT also has a protective effect *via* the inhibition of Caspase9 and activation of Bcl-2. Our results demonstrate the ability of dioscin to alleviate ovariectomy-induced osteoporosis by inhibiting bone tissue apoptosis through the regulation of both Bcl-2/Bax and PI3K/AKT signaling pathways.

Additionally, osteoblast-like MC3T3-E1 cells were used to examine the effects of dioscin on osteoblasts *in vitro*. Our data shows both low and high doses of dioscin significantly increase MC3T3-E1 cell viability. The ability to increase MC3T3-E1 cell viability provides further evidence for the mitigating effect of dioscin on osteoporosis *via* osteoblast proliferation.

Ultimately, it was found that dioscin can improve BMD and strengthen the maximum bone stress of PMO rats. The strengthening can likely be attributed to the activation of osteoblast proliferation and differentiation. Furthermore, dioscin could promote bone tissue proliferation through PI3K/AKT and P38 signaling pathways, and inhibit bone tissue apoptosis *via* regulation of the Bcl-2/Bax signaling pathway in rat models, to perform a protective effect against postmenopausal osteoporosis. The anti-osteoporotic effect of dioscin was also confirmed *in vitro* in this study. Accordingly, dioscin represents a novel candidate for treatment of PMO.

However, considering this study was preclinical, further research is required to support these conclusions. Moreover, the exact mechanisms and the clinical applications of dioscin in PMO treatment need to be further explored in the future.

Acknowledgements

This work was financially supported by the Jilin Province Development and Reform Commission (2016C048-2).

References

1. Rachner TD, Khosla S, Hofbauer LC. Osteoporosis: Now and the future. Lancet. 2011; 377:1276-1287.
2. Liu L, Webster TJ. In Situ Sensor Advancements for Osteoporosis Prevention, Diagnosis, and Treatment. Curr Osteoporos Rep. 2016; 14:386-395.
3. Tao X, Qi Y, Xu L, Yin L, Han X, Xu Y, Wang C, Sun H, Peng J. Dioscin reduces ovariectomy-induced bone loss by enhancing osteoblastogenesis and inhibiting osteoclastogenesis. Pharmacol Res. 2016; 108:90-101.
4. Zhang C, Peng J, Wu S, Jin Y, Xia F, Wang C, Liu K, Sun H, Liu M. Dioscin promotes osteoblastic proliferation and differentiation *via* Lrp5 and ER pathway in mouse and human osteoblast-like cell lines. J Biomed Sci. 2014; 21:30.
5. Xu JH, Yao M, Ye J, Wang GD, Wang J, Cui XJ, Mo W. Bone mass improved effect of icariin for postmenopausal osteoporosis in ovariectomy-induced rats: A meta-analysis and systematic review. Menopause. 2016; 23:1152-1157.
6. Song C, Wang J, Song Q, Li X, Chen Z, Ma Q, Liu Z, Jia H, Dang G. Simvastatin induces estrogen receptor-alpha (ER-alpha) in murine bone marrow stromal cells. J Bone Miner Metab. 2008; 26:213-217.
7. Sample SJ, Racette MA, Hao Z, Thomas CF, Behan M, Muir P. Functional adaptation in female rats: The role of estrogen signaling. PLoS One. 2012; 7:e43215.
8. Tella SH, Gallagher JC. Prevention and treatment of postmenopausal osteoporosis. J Steroid Biochem Mol Biol. 2014; 142:155-170.
9. Lu B, Xu Y, Xu L, Cong X, Yin L, Li H, Peng J. Mechanism investigation of dioscin against CCl4-induced acute liver damage in mice. Environ Toxicol Pharmacol. 2012; 34:127-135.
10. Wei Y, Xu Y, Han X, Qi Y, Xu L, Xu Y, Yin L, Sun H, Liu K, Peng J. Anti-cancer effects of dioscin on three kinds of human lung cancer cell lines through inducing DNA damage and activating mitochondrial signal pathway. Food Chem Toxicol. 2013; 59:118-128.
11. Zhao X, Tao X, Xu L, Yin L, Qi Y, Xu Y, Han X, Peng J. Dioscin Induces Apoptosis in Human Cervical Carcinoma HeLa and SiHa Cells through ROS-Mediated DNA Damage and the Mitochondrial Signaling Pathway. Molecules. 2016; 21: pii: E730.
12. Pan CH, Tsai CH, Liu FC, Fan MJ, Sheu MJ, Hsieh WT, Wu CH. Influence of different particle processing on hypocholesterolemic and antiatherogenic activities of yam (Dioscorea pseudojaponica) in cholesterol-fed rabbit model. J Sci Food Agric. 2013; 93:1278-1283.
13. Zhang X, Han X, Yin L, Xu L, Qi Y, Xu Y, Sun H, Lin Y, Liu K, Peng J. Potent effects of dioscin against liver fibrosis. Sci Rep. 2015; 5:9713.
14. Zheng J, Zhao S, Yu X, Huang S, Liu HY. Simultaneous targeting of CD44 and EpCAM with a bispecific aptamer effectively inhibits intraperitoneal ovarian cancer growth. Theranostics. 2017; 7:1373-1388.
15. Lee YS, Choi EM. Costunolide stimulates the function of osteoblastic MC3T3-E1 cells. Int Immunopharmacol. 2011; 11:712-718.
16. Hou JM, Xue Y, Lin QM. Bovine lactoferrin improves bone mass and microstructure in ovariectomized rats *via*

OPG/RANKL/RANK pathway. Acta Pharmacol Sin. 2012; 33:1277-1284.
17. Xi JC, Zang HY, Guo LX, Xue HB, Liu XD, Bai YB, Ma YZ. The PI3K/AKT cell signaling pathway is involved in regulation of osteoporosis. J Recept Signal Transduct Res. 2015; 35:640-645.
18. Han X, Zhou J, Peng W. Orexins Facilitates Osteogenic Differentiation of MC3T3-E1 Cells. 2018; 70:633-641.
19. Suzuki E, Ochiai-Shino H, Aoki H, Onodera S, Saito A, Saito A, Azuma T. Akt activation is required for TGF-beta1-induced osteoblast differentiation of MC3T3-E1 pre-osteoblasts. PLoS One. 2014; 9:e112566.
20. Komori T, Yagi H, Nomura S, Yamaguchi A, Sasaki K, Deguchi K, Shimizu Y, Bronson RT, Gao YH, Inada M, Sato M, Okamoto R, Kitamura Y, Yoshiki S, Kishimoto T. Targeted disruption of Cbfa1 results in a complete lack of bone formation owing to maturational arrest of osteoblasts. Cell. 1997; 89:755-764.
21. Adapala NS, Barbe MF, Tsygankov AY, Lorenzo JA, Sanjay A. Loss of Cbl-PI3K interaction enhances osteoclast survival due to p21-Ras mediated PI3K activation independent of Cbl-b. J Cell Biochem. 2014; 115:1277-1289.
22. Chen G, Deng C, Li YP. TGF-beta and BMP signaling in osteoblast differentiation and bone formation. Int J Biol Sci. 2012; 8:272-288.
23. Ghosh-Choudhury N, Abboud SL, Nishimura R, Celeste A, Mahimainathan L, Choudhury GG. Requirement of BMP-2-induced phosphatidylinositol 3-kinase and Akt serine/threonine kinase in osteoblast differentiation and Smad-dependent BMP-2 gene transcription. J Biol Chem. 2002; 277:33361-33368.
24. Choi SW, Son YJ, Yun JM, Kim SH. Fisetin Inhibits Osteoclast Differentiation *via* Downregulation of p38 and c-Fos-NFATc1 Signaling Pathways. Evid Based Complement Alternat Med. 2012; 2012:810563.
25. Liu M, Fan F, Shi P, Tu M, Yu C, Yu C, Du M. Lactoferrin promotes MC3T3-E1 osteoblast cells proliferation *via* MAPK signaling pathways. Int J Biol Macromol. 2018; 107:137-143.
26. Shi X, Miller JS, Harper LJ, Poole RL, Gould TJ, Unterwald EM. Reactivation of cocaine reward memory engages the Akt/GSK3/mTOR signaling pathway and can be disrupted by GSK3 inhibition. Psychopharmacology (Berl). 2014; 231:3109-3118.
27. Mukherjee A, Rotwein P. Akt promotes BMP2-mediated osteoblast differentiation and bone development. J Cell Sci. 2009; 122:716-726.
28. Fujita T, Azuma Y, Fukuyama R, Hattori Y, Yoshida C, Koida M, Ogita K, Komori T. Runx2 induces osteoblast and chondrocyte differentiation and enhances their migration by coupling with PI3K-Akt signaling. J Cell Biol. 2004; 166:85-95.
29. Tandon M, Chen Z, Pratap J. Runx2 activates PI3K/Akt signaling *via* mTORC2 regulation in invasive breast cancer cells. Breast Cancer Res. 2014; 16:R16.
30. Kita K, Kimura T, Nakamura N, Yoshikawa H, Nakano T. PI3K/Akt signaling as a key regulatory pathway for chondrocyte terminal differentiation. Genes Cells. 2008; 13:839-850.
31. Chen J, Yuan K, Mao X, Miano JM, Wu H, Chen Y. Serum response factor regulates bone formation *via* IGF-1 and Runx2 signals. J Bone Miner Res. 2012; 27:1659-1668.
32. Bahia PK, Pugh V, Hoyland K, Hensley V, Rattray M, Williams RJ. Neuroprotective effects of phenolic antioxidant tBHQ associate with inhibition of FoxO3a nuclear translocation and activity. J Neurochem 2012; 123:182-191.
33. Chen AT, Guo C, Dumas KJ, Ashrafi K, Hu PJ. Effects of Caenorhabditis elegans sgk-1 mutations on lifespan, stress resistance, and DAF-16/FoxO regulation. Aging Cell. 2013; 12:932-940.
34. Hamann I, Petroll K, Grimm L, Hartwig A, Klotz LO. Insulin-like modulation of Akt/FoxO signaling by copper ions is independent of insulin receptor. Arch Biochem Biophys. 2014; 558:42-50.
35. Kawamura N, Kugimiya F, Oshima Y, Ohba S, Ikeda T, Saito T, Shinoda Y, Kawasaki Y, Ogata N, Hoshi K, Akiyama T, Chen WS, Hay N, Tobe K, Kadowaki T, Azuma Y, Tanaka S, Nakamura K, Chung UI, Kawaguchi H. Akt1 in osteoblasts and osteoclasts controls bone remodeling. PLoS One. 2007; 2:e1058.
36. Wu CM, Chen PC, Li TM, Fong YC, Tang CH. Si-Wu-tang extract stimulates bone formation through PI3K/Akt/NF-kappaB signaling pathways in osteoblasts. BMC Complement Altern Med. 2013; 13:277.
37. Wu SS, Liang QH, Liu Y, Cui RR, Yuan LQ, Liao EY. Omentin-1 Stimulates Human Osteoblast Proliferation through PI3K/Akt Signal Pathway. Int J Endocrinol. 2013; 2013:368970.
38. Huang Q, Singh B, Sharawy M. Immunohistochemical analysis of Bcl-2 and Bax oncoproteins in rabbit craniomandibular joint. Arch Oral Biol. 2004; 49:143-148.
39. Miura M, Chen XD, Allen MR, Bi Y, Gronthos S, Seo BM, Lakhani S, Flavell RA, Feng XH, Robey PG, Young M, Shi S. A crucial role of caspase-3 in osteogenic differentiation of bone marrow stromal stem cells. J Clin Invest. 2004; 114:1704-1713.
40. Thornberry NA, Lazebnik Y. Caspases: Enemies within. Science. 1998; 281:1312-1316.
41. Tsukahara S, Yamamoto S, Tin Tin Win S, Ahmed S, Kunugita N, Arashidani K, Fujimaki H. Inhalation of low-level formaldehyde increases the Bcl-2/Bax expression ratio in the hippocampus of immunologically sensitized mice. Neuroimmunomodulation. 2006; 13:63-68.

(Received July 21, 2019; Revised October 1, 2019; Accepted October 9, 2019)

Original Article

DOI: 10.5582/bst.2019.01233

Growth-promoting effects of the hydrogen-sulfide compounds produced by *Desulfovibrio desulfuricans* subsp. *desulfuricans* co-cultured with *Escherichia coli* (DH5α) on the growth of *Entamoeba* and *Endolimax* species isolates from swine

Naoko Yoshida[1], Seiki Kobayashi[1,*], Jun Suzuki[2], Yoshiyuki Azuma[3], Namiko Kobayashi-Ogata[4], Dwi Peni Kartikasari[5], Yasuaki Yanagawa[6], Satoshi Iwata[1]

[1] *Department of Infectious Diseases, Keio University School of Medicine, Tokyo, Japan;*
[2] *Division of Food Microbiology, Department of Microbiology, Tokyo Metropolitan Institute of Public Health, Tokyo, Japan;*
[3] *Laboratory of Animal and Human Nutritional Physiology, Kitasato University School of Veterinary Medicine, Towada, Aomori, Japan;*
[4] *Center for Advanced Marine Core Research, Kochi University, Nangoku, Kochi, Japan;*
[5] *Department of Parasitology, Faculty of Medicine, Universitas Airlangga, Surabaya, Indonesia;*
[6] *AIDS Clinical Center, National Center for Global Health and Medicine, Tokyo, Japan.*

Summary **Certain *Desulfovibrio* sp. (anaerobic sulfate-reducing bacteria) are indigenous to swine cecum and colon, which are also common habitats for parasitic amoebae such as *Entamoeba polecki* and *Entamoeba suis*. In this study, we evaluated the growth-promoting effects of *D. desulfuricans* co-cultured with *Escherichia coli* (DH5α) and its products [*e.g.*, hydrogen sulfide (H_2S) and certain iron-sulfide (FeS) compounds] using Robinson's medium, on the 4 amoeba isolates from swine-*Entamoeba polecki* subtype (ST)-1, *E. polecki* ST-3, *Entamoeba suis*, and *Endolimax* sp., and, consequently, a continuous culture system for these amoebae was established. However, this novel culture system was required to regulate the excess H_2S dissolved in the medium by increasing air space as amoeba isolates thrive only in large air spaces (30-40%). The effects of air space and H_2S and FeS compounds on the growth of *E. polecki* ST-1 (TDP-5) were determined. *E. polecki* ST-1 (TDP-5) thrived well in culture bottles with an air space of 30-40% (aerobic) (H_2S: ~250-400 μmoles/L), but did not grow at all in an air space < 5% (microaerobic) (H_2S:~800 μmoles/L) and in anaerobic vessels (H_2S: 20-30 μmoles/L). In both H_2S-depleted and FeS compound-depleted conditions, the amoebae sp. could not thrive either. It was hypothesized that an appropriate concentration of H_2S and FeS compounds might function as important physiologically active components of electron carriers such as FeS and ferredoxin.**

Keywords: Swine amoeba isolate, Robinson's medium, *Desulfovibrio desulfuricans*, hydrogen-sulfide, iron-sulfide compound

1. Introduction

Certain *Desulfovibrio* sp. (anaerobic sulfate-reducing bacteria) are bacteria indigenous to the cecum and colon of swine (*1*), which are also common habitats for parasitic amoebae, such as *Entamoeba polecki* and *Entamoeba suis* (*2-4*). Hydrogen sulfide (H_2S) produced by some enteric bacteria (*e.g.*, *Desulfovibrio* sp., *Clostridium* sp., *etc*.) is sometimes toxic to the aerobic organisms which possess the mitochondrial cytochrome c oxidase enzyme. This is because H_2S binds with iron in the cytochrome c oxidase and prevents the aerobic respiration by mitochondria. However, micro quantities of H_2S are also recognized for their cytoprotective and antioxidant activities along with the physiological

Released online in J-STAGE as advance publication October 9, 2019.

**Address correspondence to:*
Dr. Seiki Kobayashi, Department of Infectious Diseases, Keio University School of Medicine, 35 Shinanomachi, Shinjuku-ku, Tokyo 160-8582, Japan.
E-mail: skobaya@z7.keio.jp

effects on energy metabolism, signal transduction, and neurotransmission. (*5-7*).

Culture strains [*Entamoeba polecki* (subtype (ST)-1 and ST-3), *Entamoeba suis*, and *Endolimax* sp.] were previously isolated from swine using Robinson's medium supplemented with a *Desulfovibrio* sp. derived from these animals. During the culture, ferrous sulfide (FeS)-like black colored precipitate was sometimes observed in the culture media in which amoebae of those isolates thrived. Hence, in the present study, we investigated the growth-promoting effect on *E. polecki* (subtype 1: TDP-5), which exhibits the highest rate of proliferation among the four isolates and is a zoonotic species infecting humans (*8*), and used the reference strain *Desulfovibrio* sp. [*Desulfovibrio desulfuricans* subsp. *desulfuricans* (NBRC13699)] instead of a *Desulfovibrio* sp. derived from swine.

2. Materials and Methods

2.1. *Amoeba isolates from swine*

The present study used amoebae isolated from swine bred at the Kitasato University School of Veterinary Medicine (Towada, Aomori, Japan), and the study was conducted according to the protocols approved by the Institutional Care and Use Committee of Kitasato University (Approval number: 17-123). The isolated culture strains were *E. polecki* ST-1 (TDP-5), *E. polecki* ST-3 (TDP-1; synonym: *Entamoeba struthionis*), *E. suis* (TDP-3), and *Endolimax* sp. (TDP-2). *E. polecki* ST-2 (SZM-1; synonym: *Entamoeba chattoni*) isolated from the stool of a wild monkey (*Macaca fuscata fuscata*) in Shizuoka, Japan, was used as a reference strain of *E. polecki* species that is not indigenous to swine.

2.2. *Robinson's medium and supplements*

Robinson's, R (defined medium for *Escherichia coli*) and BR (R medium precultured with *E. coli*) media were prepared as described by Robinson (*9*). The sulfate-reducing bacterium *Desulfovibrio desulfuricans* subsp. *desulfuricans* (NBRC 13699; NITE Biological Resource Center, Japan) and *E. coli* (type B: DH5α) (Ec) were individually cultured in a modified medium (M-ATCC 207) designed based on ATCC 210-modified Starkey's medium C (ATCC 207 (2016); American Type Culture Collection, USA) (*10*) and R medium by Robinson, respectively (*9*). The modified medium was prepared as follows. The following components were dissolved in 900 mL ultrapure water and brought to a final volume of 1 L: 5 g NaCl, 2 g citric acid monohydrate, 0.5 g KH_2PO_4, 0.1 g $(NH_4)_2SO_4$, 50 mg $MgSO_4 \cdot 7H_2O$, 1 g Na_2SO_4, 0.1 g $CaCl_2$, 50 mg ferrous ammonium sulfate, 4 mL lactic acid, 75 mg L-cysteine hydrochloride, 1 g yeast extract, and 1 mg bromothymol blue. The pH was adjusted to 7.5 using approximately 7.5 mL of 10 N NaOH. After filter-sterilizing the medium, 20-mL aliquots were added to 50-mL culture flasks. *D. desulfuricans* (Dd) and Ec grown in this medium in anaerobic and aerobic conditions, respectively, were mixed at equal volumes in a baffled polycarbonate Erlenmeyer culture flask (Falcon; BD Biosciences, Durham, NC, USA) and cultured at 35.5°C for 2 days. The flask lid was closed and the flask was incubated at 24-27°C, and used within 2 weeks. A suspension containing Dd co-cultured with Ec (Dd/Ec) (H_2S: approximately 1,500 μmoles/L) was added just before the subculture of the amoebic isolates, as a supplement. Anaeropack-Anaero (Mitsubishi Gas Chemical Co., Inc., Chiyoda-ku, Tokyo, Japan) was used to absorb oxygen in the closed vessel. Glass vials (SV-8, 8 ml (exact capacity: 9.5 mL); Nichiden-Rika Glass Co., Ltd., Kobe, Hyogo, Japan) with screw caps, silicon packing, and sloped saline agar (4 mL) were used to cultivate the amoebic isolates.

The FeS-rich compound was obtained from the cultured medium of Dd/Ec by centrifugation (275 × g, 5 min). The precipitate was sterilized with 5 mL of 2N NaOH for over 24 hours. The precipitate was washed with 8 mL of Hanks' balanced salt solution (HBSS), pH7.4, with 0.002% phenol red, by centrifugation (275 × g, 5 min) for 3 times, and finally adjusted to approximately 0.5% (vol/vol) suspension with HBSS.

2.3. *Culture of amoebic isolates*

After establishing the amoeba strains, Dd/Ec (100 μL) was added to 1.5 mL of fresh Robinson's medium, and inoculated with amoeba suspension (1 mL), for subculture. Then, 1 mL of amoeba suspension was aspirated after mixing well and was added back to the first culture medium (final air space: ~37.2%).

The H_2S detectable SIM medium (Nissui Pharmaceutical Co., LTD, Taito-ku, Tokyo, Japan) was used to determine the viability of Dd in Dd/Ec under aerobic culture conditions.

The concentration of H_2S produced by Dd was assayed quantitatively using a HSip-1 kit (Dojindo Molecular Technologies, Inc., Rockville, MD, USA) and a multimode microplate reader (Cytation 5, BioTek; BioTek Japan, Taito-ku, Tokyo, Japan).

Partially purified FeS-rich compounds derived from Dd/Ec were also supplemented, instead of Dd/Ec, under the existence of sufficient H_2S produced by Dd which was spontaneously proliferated and subcultured along with amoeba. The concentration of the FeS-rich compounds in the medium as a supplement was determined by referring to a study on the toxic effects in axenic culture of *Entamoeba dispar* (AS16IR) (*11*). This study was chosen as the growth of AS 16 IR is more easily affected by toxic substances than that of other axenic amoebic culture strains.

2.4. *Trichrome staining*

Trichrome staining was carried out according to the protocol described by Wheatley (*12*). However, a basic solution of Kohn's stain was used as a fixative instead of Shaudin's fixative, which contains mercuric chloride (*13*).

2.5. *DNA isolation and amplification by polymerase chain reaction (PCR)*

DNA was isolated from approximately 1×10^5 - 2×10^5 amoeba cells suspended in 100 μL of 10 mM phosphate-buffered saline (pH 7.4) using a Cica Geneus total DNA prep kit for tissue (Kanto Chemical Co., Chuo-ku, Tokyo, Japan). DNA samples from the isolates of *E. polecki*, *E. suis*, and the *Endolimax* species were used as templates for the PCR amplification of 18S ribosomal RNA (rRNA) genes. Three primer sets each for *E. polecki* ST-1 and ST-3 (Ent-1F and Esuis-1R, Epol-2F and Epol-2R, and Epol-3F and Ent-3R), *E. polecki* ST-2 (Ent-1F and Echat-2R, Echat-1F and Epol-2R, and Epol-3F and Ent-3R), and *E. suis* (Ent-1F and Esuis-1R, Esuis-2F and Esuis-2R, and Esuis-3F and Ent-3R), as well as a separate primer set (Ent-1F and Ent-3R) for the *Endolimax* species, were used (Table 1). Amplification was performed in a 20-μL reaction volume containing 2 μL of 10× Ex Taq buffer, 4 μL of 2.5 mM of each dNTP, 2 μL of each primer (10 μM; Table 1), 0.2 μL of 5 U/μL Ex Taq (Takara Bio, Inc., Kusatsu, Shiga, Japan), and 9.8 μL of H_2O. The following cycle parameters were used: initial denaturation at 94°C for 5 min; 35 cycles of 94°C for 30 s, 58°C for 30 s, and 72°C for 1 min; and a final extension at 72°C for 5 min. The PCR products of the suspected *Endolimax* species were used to obtain clones of the *Endolimax* 18S rRNA gene using a Qiagen PCR cloning kit (Qiagen, Com., Venlo, Netherlands).

2.6. *Sequencing and phylogenetic analysis*

The PCR products were directly sequenced using an ABI Prism BigDye Terminator v3.1 cycle sequencing ready reaction kit and an ABI Prism 3500 genetic analyzer (Applied Biosystems Japan, Ltd., Chuo-ku, Tokyo, Japan). Multiple alignment and phylogenetic analysis of the 18S rRNA gene sequences of the *Entamoeba* and *Endolimax* species were performed using ClustalW and the maximum-likelihood (ML) method using the MEGA version 6 software, respectively (*14,15*). The ML tree was derived using the Tamura-Nei model employing estimates of the proportion of invariable sites and the gamma distribution with five rate categories. Statistical significance was evaluated by bootstrapping with 1,000 replicates. The ML tree data files were visualized using MEGA version 6.

2.7. *Measurement of the individual cysts and trophozoites of each species of amoebic isolate*

The long and short diameters (l.d. and s.d.) of the individual cysts in fresh stool suspensions in deionized water and those of trophozoites isolated using the culture system were measured on a screen display using a microscope digital camera and the measuring tool of imaging software (cellSens, ver. 1.7.1; Olympus Co., Shinjuku-ku, Tokyo, Japan). The mean values were calculated from measurements of 50 trophozoites and cysts of each amoebic isolate.

Table 1. Oligonucleotide primers used for PCR

Species	Primers		Primer sequence (5′–3′)	Positions	Accession no.
Entamoeba polecki	Ent-1F	Forward	GTTGATCCTGCCAGTATTATATG	7 – 29	AF149913
ST-1 and ST-3	Esuis-1R	Reverse	AAAGATGATCATGGATTTTCACCT	864 – 887	DQ286372
	Epol-2F	Forward	CTAATATAAAAAAAGGAGAAAGG	652 – 674	AF149913
	Epol-2R	Reverse	AGATAAAGTCTCGTTCGTTATCGGA	1287 – 1311	AF149913
	Epol-3F	Forward	AGGATTGACAGATTAATAGTTTTTTCA	1199 – 1225	AF149913
	Ent-3R	Reverse	ATCCTTCCGCAGGTTCACCTA	1950 – 1970	DQ286372
Entamoeba polecki	Ent-1F	Forward	GTTGATCCTGCCAGTATTATATG	7 – 29	AF149913
ST-2 (*Entamoeba*	Echat-2R	Reverse	TAAATAACCTTTCTCCTTTTTCTATC	660 – 685	AF149912
chattoni)	Echat-1F	Forward	AGGATTTGTTTTATAACAAGTTC	471 – 493	AF149912
	Epol-2R	Reverse	AGATAAAGTCTCGTTCGTTATCGGA	1287 – 1311	AF149913
	Epol-3F	Forward	AGGATTGACAGATTAATAGTTTTTTCA	1203 – 1229	AF149912
	Ent-3R	Reverse	ATCCTTCCGCAGGTTCACCTA	1950 – 1970	DQ286372
Entamoeba suis	Ent-1F	Forward	GTTGATCCTGCCAGTATTATATG	7 – 29	AF149913
	Esuis-1R	Reverse	AAAGATGATCATGGATTTTCACCT	864 – 887	DQ286372
	Esuis-2F	Forward	ACTCTTTTAAAGCCGTAAGGT	448 – 468	DQ286372
	Esuis-2R	Reverse	ACTACATGAATATCTTTTAGGT	1379 – 1400	DQ286372
	Esuis-3F	Forward	ATTCCGGTAACGAACGAGACTTA	1336 – 1358	DQ286372
	Ent-3R	Reverse	ATCCTTCCGCAGGTTCACCTA	1950 – 1970	DQ286372
Endolimax sp.	Ent-1F	Forward	GTTGATCCTGCCAGTATTATATG	7 – 29	AF149913
	Ent-3R	Reverse	ATCCTTCCGCAGGTTCACCTA	1950 – 1970	DQ286372

2.8. *Correlation between the amount of air space and growth of E. polecki ST-1 (TDP-5)*

The growth-promoting effects of Dd/Ec and FeS compounds were determined by assaying the growth kinetics of the amoebic isolates, which was done by estimating the number of amoebae in cultures using a Fuchs-Rosenthal counting chamber every 24 h.

2.9. *Effect of iron-sulfide compounds on the growth of E. polecki ST-1 (TDP-5)*

Prior to this experiment, the amoebae were washed with HBSS by centrifugation (275 × g, 5 min) twice for removing H_2S from the culture medium. Thereafter, the growth kinetics of the washed amoebae in different culture conditions – without Dd/Ec, with Dd/Ec (100 µL), with ferric ammonium citrate (Fe) (1 mg/mL, 100 µL) – were observed.

3. Results

3.1. *Molecular identification and measurement of the cultured isolates*

The 18S rRNA gene sequences of *E. polecki* ST-1 (TDP-5; LC230016), *E. polecki* ST-3 (TDP-1; LC230018), and *E. suis* (TDP-4; LC230019) were consistent with all the previous reports on these subtypes and species (*16-18*). Phylogenetic analysis results pertaining to the 18S rRNA gene sequences of the three isolates of *E. polecki* (ST-1, ST-2, and ST-3) and *E. suis* are shown in Figure 1. The macaque isolate was identified as *E. polecki* ST-2 (SZM-1; LC230017). However, 0.5% of its sequence was different from the previously reported sequence of *E. polecki* ST-2

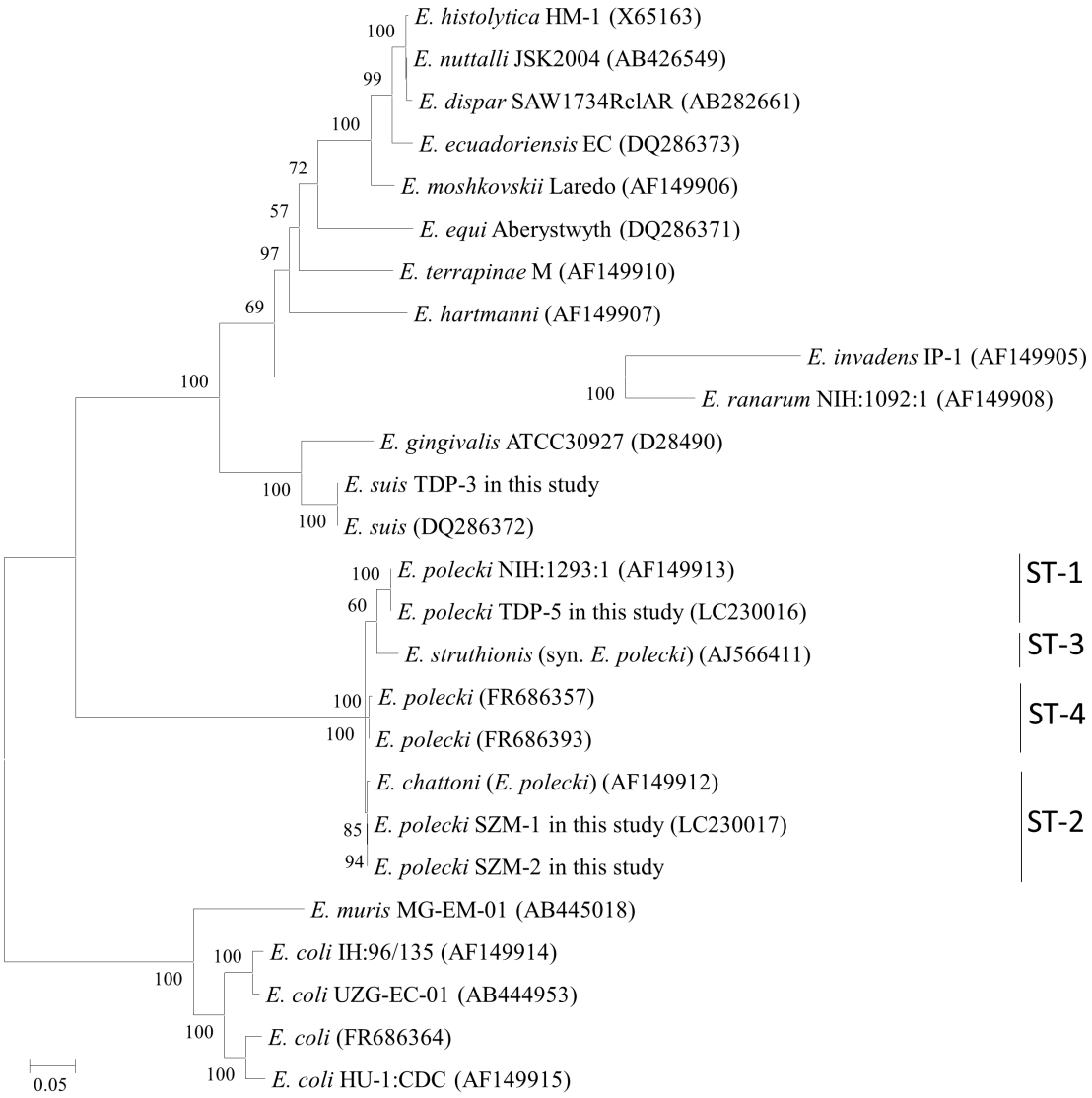

Figure 1. Phylogenetic analysis of 18S rRNA gene sequences of the three isolates of *Entamoeba polecki* (ST-1, ST-2, and ST-3) and *Entamoeba suis*. Maximum-likelihood (ML) tree derived using a Tamura-Nei model with a proportion of invariable sites and gamma distribution of 0.309 and 0.428, respectively. Significant bootstrap support (> 500) from 1,000 replicates is indicated on the left of the supported nodes. The scale bar represents the evolutionary distance for the number of changes per site. Numbers within parentheses represent the GenBank accession numbers.

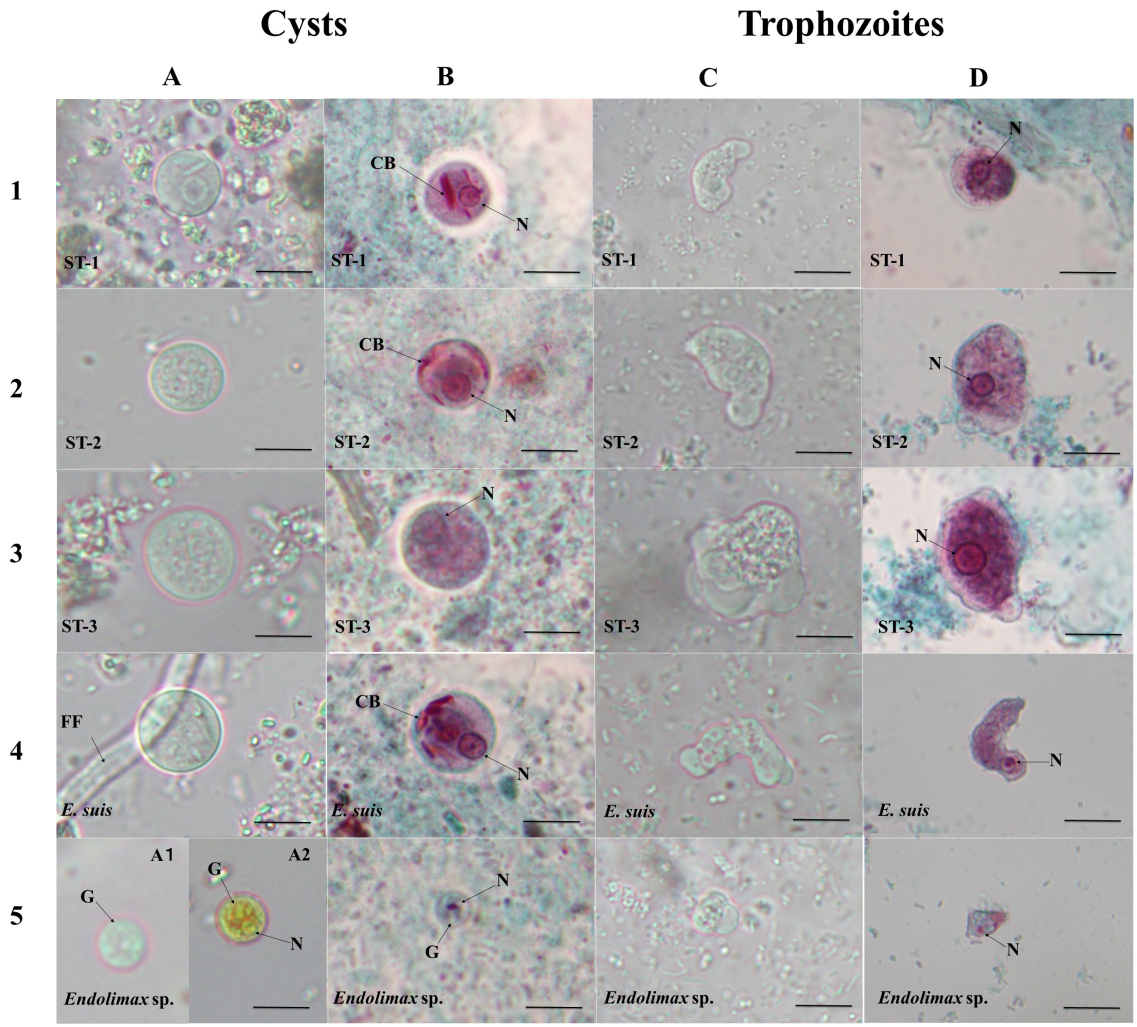

Figure 2. Light microscopy images of fresh and trichrome-stained cysts and cultured trophozoites of *E. polecki* subtypes (ST) 1, 2, and 3; *E. suis*; and the *Endolimax* species isolated from swine and a macaque. Row **1**: *E. polecki* ST-1 (TDP-5); row **2**: *E. polecki* ST-2 (SZM-1); row **3**: *E. polecki* ST-3 (TDP-1); row **4**: *E. suis* (TDP-4); row **5**: *Endolimax* species (TDP-2). Columns **A** and **A1**: fresh cysts in stool samples; column **A2**: fresh cysts stained with iodine-potassium iodide solution in stool samples; column **B**: cysts stained with trichrome dye; column **C**: live trophozoites in the culture medium; column **D**: trophozoites in the culture medium stained with trichrome dye. Scale bar = 10 μm. N, nucleus; CB, chromatoid body; FF, fungal filament; G, granule.

(AF149912) (*16*). Trophozoites of *E. polecki* ST-1 (TDP-5) with a mean length (l.d × s.d.) of 18.30 ± 3.30 × 12.85 ± 2.63 μm (Figure 2 [1C and 1D]) were isolated from small-sized uninucleate cysts with a mean length (l.d × s.d.) of 10.94 ± 1.09 × 10.38 ± 1.75 μm (Figure 2 [1A and 1B]). The latter possessed typical small rod-like chromatoid bodies of *E. polecki*. Large trophozoites of *E. polecki* ST-3 (TDP-1) with a mean length (l.d × s.d.) of 28.65 ± 6.16 × 19.56 ± 4.01 μm (Figure 2 [3C and 3D]) were isolated from uninucleate cysts with a mean length (l.d × s.d.) of 15.43 ± 2.20 × 14.14 ± 1.28 μm (Figure 2 [3A and 3B]) observed among the amoebic species. Trophozoites with a mean length of (l.d × s.d.) 23.87 ± 5.25 × 14.67 ± 3.65 μm (Figure 2 [2C and 2D]) of *E. polecki* ST-2 (SZM-1) were also isolated from the corresponding cysts with a mean length (l.d × s.d.) of 12.98 ± 1.75 × 12.39 ± 0.99 (Figure 2 [2A and 2B]). Intermediate-sized and slender trophozoites with a mean length (l.d × s.d.) of 20.58 ± 3.19 × 7.49 ± 1.04 μm (Figure 2 [4C and 4D]), which were genetically identified as *E. suis* (TDP-4) (*2*), were isolated from the corresponding cysts which were highly transparent, such that fungal filaments could be observed clearly through the cysts covering them, with mean length (l.d × s.d.) 16.13 ± 1.51 × 15.38 ± 1.34 μm (Figure 2 [4A]). The characteristics of the cysts were consistent with those of *E. suis* cysts described in the first report on this species by Clark *et al* (*2*).

Phylogenetic analysis of the five clones of the *Endolimax* species (Figure 3) showed some divergence in the 18S rRNA gene sequences (0.99-1.74%). The cause for this divergence is not clear. The 18S rRNA gene sequences of the five clones of *Endolimax* species (TDP-2; LC230011–LC230015) showed 85.3-85.8% homology with the sequence of *Endolimax nana* NIH:0591:1 (AF149916) registered in the GenBank database (*18*). The significant divergence between these clones and *E. nana* indicated that the *Endolimax* species

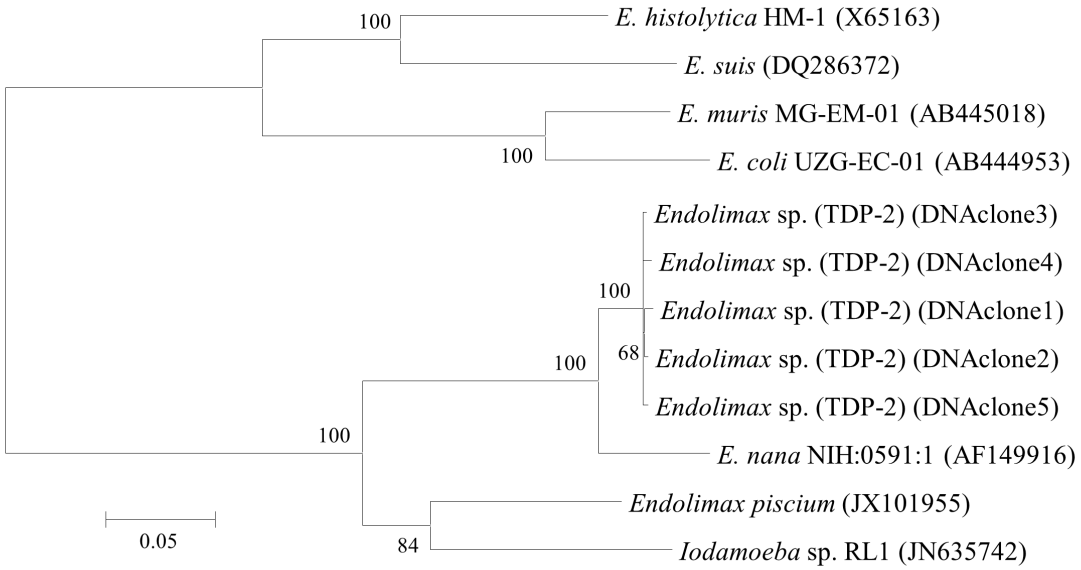

Figure 3. Phylogenetic analysis of 18S rRNA gene sequences of five clones of the new *Endolimax* species obtained by plasmid cloning. Maximum-likelihood (ML) tree derived using a Tamura-Nei model with a proportion of invariable sites and gamma distribution of 0.175 and 0.534, respectively. Significant bootstrap support (> 500) from 1,000 replicates is indicated on the left of the supported nodes. The scale bar represents the evolutionary distance based on the number of changes per site. Numbers in parentheses represent the GenBank accession numbers.

isolated in this study were not *E. nana*.

Very small trophozoites of the *Endolima*x species (TDP-2) with mean length (l.d × s.d.) 8.80 ± 0.97 × 8.15 ± 1.20 μm (Figure 2 [5C and 5D]) were also isolated from very small cysts with mean length (l.d × s.d.) 8.36 ± 1.25 × 7.41 ± 1.26 μm (Figure 2 [5A1, 5A2, and B]).

3.2. *Correlation between the amount of air space with the growth of E. polecki ST-1 (TDP-5)*

H_2S concentrations in the seven conditions examined are shown in Figure 4. The concentration of H_2S in the medium was ~800 μmoles/L, ~ 250-400 μ moles/L, and ~ 20-30 μ moles/L when the air space was < ~ 5%, ~ 30-40%, and in an anaerobic vessel, respectively. The amoebae, when supplemented with Dd/Ec (100 μL), thrived in culture bottles with an air space of 30-40% (aerobic), but did not grow at all when the air space was < 5% (microaerobic) or in anaerobic vessels (data not shown). The growth kinetics of the amoebae when supplemented with Dd/Ec (100 μL), FeS (100 μL), and Fe (50 μL) maintained in culture bottles with 30-40% air space are shown in Figure 5. The growth kinetics of the amoebae were affected by the amount of H_2S dissolved in the medium. The suitable concentration of H_2S for their growth seemed to be around ~ 250-400 μ moles/L with an appropriate amount of FeS compounds. When growth occurred in medium supplemented only with Fe, it is thought that some FeS compound was produced by reacting Fe with H_2S derived from spontaneously subcultured Dd (Dd was confirmed by H_2S-detectable SIM medium).

3.3. *Effect of iron-sulfide compounds on the growth of E. polecki ST-1 (TDP-5)*

As shown in Figure 6, the group without Dd/Ec (100 μL) did not proliferate, but the growth of Dd/Ec (100 μL) and Fe-supplemented groups drastically recovered after 3 days of culture. The results showed that amoebae could not proliferate in either H_2S- or FeS compound- depleted conditions. Surviving Dd in both culture media after 3 days from the group without Dd/Ec (100 μL) and the Fe-supplemented group was confirmed by SIM medium, whereas amoeba was recovered only in the group supplemented with Fe.

4. Discussion

We previously found that an appropriate volume (approximately 400 μL) of Dd/Ec culture suspension in BR or in complete Robinson's medium induced excystation of trophozoites from swine amoeba cysts used in this study, even after the cysts were washed with distilled water by centrifugation (275 × g for 3 min) twice (data not shown).

Based on these results, a culture system supplemented with Dd/Ec was established which enabled the first-time continuous culture of four parasitic amoebic species (*E. polecki* ST-1 and ST-3, *E. suis*, and an *Endolimax* species) from swine, and could be subcultured for over two years.

In this culture system, it was hypothesized that Dd itself, H_2S derived from Dd, and some FeS compounds produced by reaction with exogenous iron might

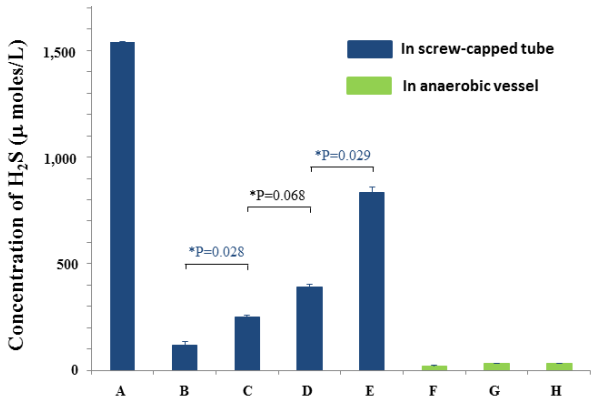

Figure 4. The concentration of H_2S in the media correlates with the seven different conditions. The concentrations of H_2S dissolved in the media were tested under various conditions as follows: **A)** Modified ATCC 207 medium cultured with Desulfovibrio desulfuricans co-cultured with Escherichia coli (Dd/Ec) [air space: 40% (AS 40%)] 7 days after cultivation at 25°C; **B)** Robinson's medium (Rm) (AS 40%); **C)** Rm + Dd/Ec (100 μL: added once without adding Dd/Ec anew during the next three subcultures) (AS 40%); **D)** Rm + Dd/Ec (100 μL: added at each time of subculture) (AS 40%); **E)** The same as **B)** except for AS, which was < 5%; **F), G)** and **H)** were the same conditions as **B), C),** and **D),** respectively, but cultured in anaerobic vessels. **B) – H)** were cultured at 35.5 °C. Data are presented as the mean and standard deviations of two measurements from each culture. Comparisons between two groups **(B** and **C**, **C** and **D**, and **D** and **E)** was made by performing a two-sided Wilcoxon's signed rank test based on the summed data of two experiments to confirm reproducibility. The differences in the medium concentrations of H_2S between **B** and **C** (P = 0.028) and **D** and **E** (P = 0.029) were confirmed as statistically significant.

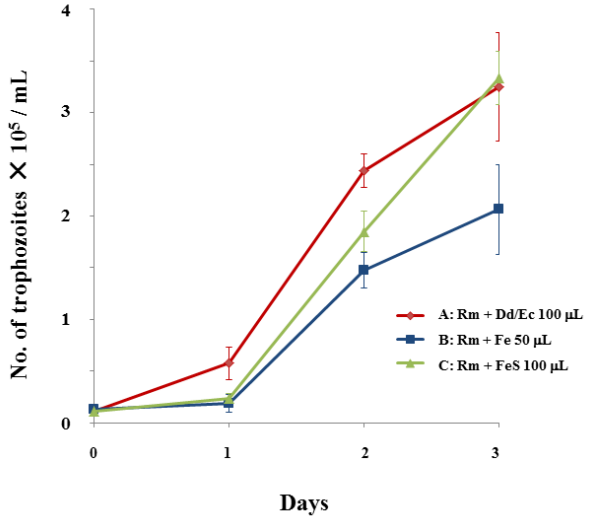

Figure 5. Growth kinetics of *Entamoeba polecki* ST-1 (TDP-5) supplemented with *Desulfovibrio desulfuricans* co-cultured with *Escherichia coli* (Dd/Ec), Fe, and partially purified FeS compounds. The number of trophozoites was counted daily for 4 days after inoculation and after subculturing seven times in the same manner at 35.5°C (AS 40%). Data are presented as the mean and standard deviations of four measurements for each culture. **A)** Rm + Dd/Ec (100 μL); **B)** Rm + ferric ammonium citrate (1mg/mL: 50 μL) (Fe); **C)** Rm + partially purified FeS (0.5% vol/vol, 100 μL). ***A) – C)** were cultured with AS 40% at 35.5°C. Post hoc comparisons of the number of trophozoites among those three different culture conditions were made by performing a Turkey's test (significance level, 5%). The differences in the number of trophozoites among **A**, **B**, and **C** on days 2 and 3 after inoculation were confirmed to be statistically significant.

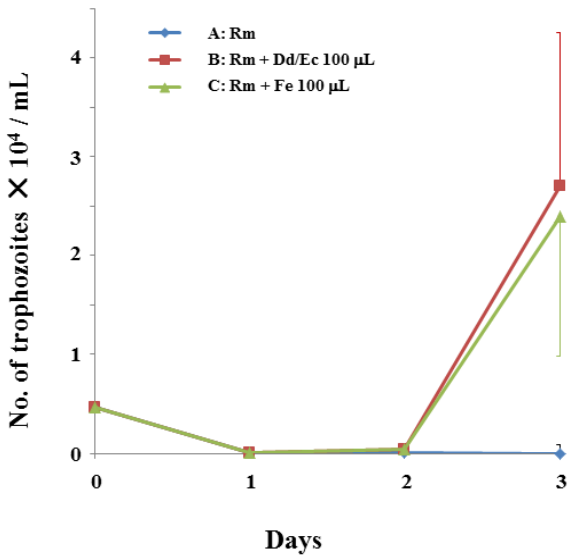

Figure 6. Growth-promoting effect of *Desulfovibrio desulfuricans* co-cultured with *Escherichia coli* (Dd/Ec) and iron on *E. polecki* ST-1 (TDP-5). The number of trophozoites was counted daily for 4 days after inoculation. Data are presented as the mean and standard deviations of four measurements of each culture. **A)** Rm; **B)** Rm + Dd/Ec (100 μL); **C)** Rm + ferric ammonium citrate (1 mg/mL: 100 μL) (Fe). ***A)** – **C)** were cultured with AS 40% at 35.5°C. Post hoc comparisons of the number of trophozoites among those three different culture conditions were made by performing a Turkey's test (significance level, 5%). The differences in the number of trophozoites between **A** and **B** and between **A** and **C**, but not between **B** and **C**, 3 days after inoculation were confirmed to be statistically significant.

function as important physiologically active compounds such as components of electron carriers (*e.g.* FeS, ferredoxin, *etc.*). These electron carriers participate in anaerobic energy metabolism (*19-21*) and are involved in the growth of the amoeba species from swine used in this study and a reference strain of *E. polecki* from macaque. This theory is further supported by an interesting report by Reeves *et al.* (*22*) which stated that ferredoxin isolated from *Entamoeba histolytica* (pathogenic *Entamoeba* species) could be converted to an apoprotein and be experimentally reconstituted with iron and H_2S.

The culture system with aerobic conditions (airspace of 30-40%) provided a suitable condition for the growth of the amoebic isolates. This might result from 1) lactic acid in R mdium; and H_2, aerobic metabolic products of Ec; and ionized H_2 produced from H_2S in the medium by reaction with sufficient oxygen from Dd itself, were available as energy sources for the growth of Dd and 2) large airspace and small liquid phase of the medium can consume the excess H_2S dissolved in the medium. Dissolved H_2S in the culture medium at this concentration (~ 250-400 μ moles/L) practically eliminated the contamination by aerobic fungi and bacteria that often inhibit the growth of amoebic isolates (data not shown).

In these culture conditions, Dd could also be

subcultured in the fresh medium along with the amoebae. However, sometimes Dd/Ec culture suspension, Fe or partially purified FeS compound from the culture suspension had to be added to the medium for successful subculture of the amoeba isolates, even though the medium already had serum iron from the Robinson's medium. *D. desulfuricans* is also known to contain a ferredoxin including the cluster [4Fe-4S] (*23*). Hence, bacterial cells might also represent a source of FeS compounds.

Indeed, a previous case report indicated that the trophozoites of *E. polecki* co-infected with *Lawsonia intracellularis* which belongs to the same family as *D. desulfuricans,* were observed in a lesion of ileitis caused by *L. intracellularis*, an irregular parasitic location (*3*).

The 18S rRNA gene sequences of the five clones of the *Endolimax* species obtained by plasmid cloning were not identical, and the reason for this is unclear. El-Sherry *et al*. (*24*) reported similar differences in the 18S rRNA gene sequences of coccidian protozoan parasites, resulting in multiple 18S rRNA gene sequences obtained from two single oocyst-derived lines of *Eimeria meleagrimitis* and *Eimeria adenoids*. Therefore, this indicates that divergent and paralogous 18S rRNA gene copies clearly exist within the nuclear genome of *E. meleagrimitis*.

The growth-promoting mechanism of this culture system could not be understood entirely. However, sulfur and iron derived from the Dd/Ec cultured medium had a critical and fast-acting effect on the proliferation of the amoeba species. Therefore, if the growth-promoting substance and its physiological activities could be elucidated, it may be utilized for further research on pathogenic mechanisms and the development of therapeutic agents against pathogenic protozoan species that possess an anaerobic energy metabolism involving iron, sulfur, and FeS compounds. While considering the difference between this limited in vitro culture condition and an actual in-vivo state in the intestine, the culture system could also be used to isolate other *Entamoeba* species such as *Entamoeba histolytica*, *Entamoeba coli*, and *Entamoeba muris* (*25*), among others.

Acknowledgements

We would like to thank Mr. Takahiro Nanbu, a member of the Kitasato University School of Veterinary Medicine, for collecting and providing the swine samples. A part of this work was supported by a JSPS KAKENHI Grant-in-Aid for Scientific Research [(C) 24590511 and (B) 16H05819]. The authors declare that there are no conflicts of interest.

References

1. Butine TJ, Leedle JA. Enumeration of selected anaerobic bacterial groups in cecal and colonic contents of growing-finishing pigs. Appl Environ Microbiol. 1989; 55:1112-1116.
2. Clark CG, Kaffashian F, Tawari B, Windsor JJ, Twigg-Flesner A, Davies-Morel MC, Blessmann J, Ebert F, Peschel B, Le Van A, Jackson CJ, Macfarlane L, Tannich E. New insights into the phylogeny of *Entamoeba* species provided by analysis of four new small-subunit rRNA genes. Int J Syst Evol Microbiol. 2006; 56:2235-2239.
3. Matsubayashi M, Kanamori K, Sadahiro M, Tokoro M, Abe N, Haritani M, Shibahara T. First molecular identification of *Entamoeba polecki* in a piglet in Japan and implications for aggravation of ileitis by coinfection with *Lawsonia intracellularis*. Parasitol Res. 2015; 114:3069-3073.
4. Matsubayashi M, Sasagawa Y, Aita T , Tokoro M, Haritani M, Shibahara T. First report of mixed of *Entamoeba polecki* (ST-1) and *E. suis* infection in piglets shedding abnormal feces by histopathological and molecular surveys. Acta Parasitol. 2016; 61:665-670
5. Zheng Y, Ji X, Ji K, Wang B. Hydrogen sulfide prodrugs—a review. Acta Pharm Sin B. 2015; 5:367-377.
6. Benchoam D, Cuevasanta E, Möller MN, Alvarez B. Hydrogen sulfide and persulfides oxidation by biologically relevant oxidizing species. Antioxidants (Basel). 2019; 8:48.
7. Wetzel MD, Wenke JC. Mechanisms by which hydrogen sulfide attenuates muscle function following ischemia-reperfusion injury: Effects on Akt signaling, mitochondrial function, and apoptosis. J Transl Med. 2019; 17:33.
8. Stensvold CR, Winiecka-Krusnell J, Lier T, Lebbad M. Evaluation of PCR method for detection of *Entamoeba polecki*, with an overview of its molecular epidemiology. J Clin Microbiol. 2018; 56:e00154-18.
9. American Type Culture Collection. ATCC medium: 207 Modified Starkey's medium C. *https://www.atcc.org/~/media/8ECF033ECF304CF3B92802660F5046C8.ashx* (accessed February 02, 2018).
10. Robinson GL. The laboratory diagnosis of human parasitic amebae. Trans R Soc Tro Med Hyg. 1968; 62:285-294.
11. Khalifa SA, Imai E, Kobayashi S, Haghighi A, Hayakawa E, Takeuchi T. Growth-promoting effect on iron-sulfur proteins on axenic cultures of *Entamoeba dispar*. Parasite. 2006; 13:51-58.
12. Wheatley WB. A rapid staining procedure for intestinal amoebae and flagellates. Am J Clin Pathol. 1951; 21:990-991.
13. Kohn JA. A one stage permanent staining method for faecal protozoa. Dapim Refuiim Med Q Isr. 1960; 19:160-161.
14. Tamura K, Stecher G, Peterson D, Filipski A, Kumar S. MEGA6: Molecular evolutionary genetics analysis version 6.0. Mol Biol Evol. 2013; 30:2725-2729.
15. Thompson JD, Higgins DG, Gibson TJ. CLUSTAL W: Improving the sensitivity of progressive multiple sequence alignment through sequence weighting, position-specific gap penalties and weight matrix choice. Nucleic Acids Res. 1994; 22:4673-4680.
16. Stensvold CR, Lebbad M, Victory EL, Verweij JJ, Tannich E, Alfellani M, Legarraga P, Clark CG. Increased sampling reveals novel lineages of *Entamoeba*: Consequences of genetic diversity and host specificity for taxonomy and molecular detection. Protist. 2011; 162:525-541.
17. Ponce-Gordo F, Martinez-Diaz RA, Herrera S. *Entamoeba struthionis* n. sp. (Sarcomastigophora: Endamoebidae)

from ostriches (Struthio camelus). Vet Parasitol. 2004; 119:327-335.
18. Silberman JD, Clark CG, Diamond LS, Sogin ML. Phylogeny of the genera *Entamoeba* and *Endolimax* as deduced from small-subunit ribosomal RNA sequences. Mol Biol Evol. 1999; 16:1740-1751.
19. Gillin FD, Diamond LS. *Entamoeba histolytica* and *Giardia lamblia*: Growth responses to reducing agents. Exp Parasitol. 1981; 51:382-391.
20. Diamond LS. Techniques of axenic cultivation of *Entamoeba histolytica* Schaudinn, 1903 and *E. histolytica*-like amebae. J Parasitol. 1968; 54:1047-1056.
21. Reeves RE, Warren LG, Susskind B, Lo HS. An energy-conserving pyruvate-to-acetate pathway in *Entamoeba histolytica*. Pyruvate synthase and a new acetate thiokinase. J Biol Chem. 1977; 252:726-731.
22. Reeves RE, Guthrie JD, Lobelle-Rich P. *Entamoeba histolytica*: Isolation of ferredoxin. Exp Parasitol. 1980; 49:83-88.
23. Zubieta JA, Mason R, Postgate JR. A four-iron ferredoxin from *Desulfovibrio desulfuricans*. Biochem J. 1973; 133:851-854.
24. El-Sherry S, Ogedengbe ME, Hafeez MA, Barta JR. Divergent nuclear 18S rRNA paralogs in a turkey coccidium, *Eimeria meleagrimitis*, complicate molecular systematics and identification. Int J Parasitol. 2013; 43:679-685.
25. Kobayashi S, Suzuki J, Takeuchi T. Establishment of a continuous culture system for *Entamoeba muris* and analysis of the small subunit rRNA gene. Parasite. 2009; 16:135-139.

(Received August 30, 2019; Revised September 30, 2019; Accepted October 4, 2019)

Original Article

DOI: 10.5582/bst.2019.01191

Overexpression of anti-fibrotic factors ameliorates anti-fibrotic properties of Wharton's jelly derived mesenchymal stem cells under oxidative damage

Natakarn Nimsanor[1], Jitrada Phetfong[2], Narisorn Kitiyanant[3], Witchayapon Kamprom[4], Aungkura Supokawej[1,*]

[1] *Department of Clinical Microscopy, Faculty of Medical Technology, Mahidol University, Salaya, Nakhon Pathom, Thailand;*
[2] *Center for Research and Innovation, Faculty of Medical Technology, Mahidol University, Salaya, Nakhon Pathom, Thailand;*
[3] *Stem Cell Research Group, Institute of Molecular Biosciences, Mahidol University, Salaya, Nakhon Pathom, Thailand;*
[4] *Department of Clinical Microbiology and Applied Technology, Faculty of Medical Technology, Mahidol University, Salaya, Nakhon Pathom, Thailand.*

Summary **Transplantation with Wharton's jelly derived mesenchymal stem cells (WJ-MSCs) showed great benefits for restoring myocardial function. However, the outcome of WJ-MSCs transplantation was unsuccessful due to multiple factors including oxidative damage. The presence of oxidative stress due to myocardium injury influences fibrous tissue formation, which causes disability of cardiac muscle. Hepatocyte growth factor (HGF), insulin-like growth factor (IGF1), and sonic hedgehog (SHH) are well-known master regulators in anti-fibrosis when secreted by WJ-MSCs. They showed a beneficial role in the recovery of cardiac fibrosis after WJ-MSCs transplantation. This study hypothesizes whether the reduction of the anti-fibrosis property in WJ-MSCs from oxidative damage can be recovered by overexpression of the HGF, IGF1, or SHH gene. Overexpression was attained by transfection of WJ-MSCs with pCMV3-HGF, pCMV3-IGF1, or pCMV3-SHH followed by H_2O_2 exposure and co-culturing with cardiac fibroblasts. Myofibroblast specific markers comprised of alpha-smooth muscle actin (α-SMA) and collagen type 1 (COL1) were evaluated. The WJ-MSCs treated with H_2O_2 influenced the expression of myofibroblastic markers, whereas the overexpression of HGF, IGF1 or SHH reduced myofibroblastic formation. These results indicate that the oxidative stress impaired anti-fibrotic property of WJ-MSCs, leads to an increase of myofibroblasts. Overexpression of anti-fibrotic genes restored the endogenous HGF, IGF1, and SHH alleviating improvement of cardiac function.**

Keywords: Mesenchymal stem cells, Wharton's jelly, oxidative stress, cardiac fibrosis, anti-fibrosis

1. Introduction

Myocardium infarction (MI) has been reported as a major health problem worldwide. The pathogenesis of MI is from insufficient blood supply to myocardium, which leads to apoptosis, limiting proliferative capability of cardiomyocytes and post-MI fibrosis formation (*1*). Oxidative stress under hypoxic conditions leads to accumulation of reactive oxygen species (ROS), which impacts myocardium function. ROS are toxic cellular radicals, affecting the macrobiological molecules contributing to the induction of cardiomyocyte apoptosis through apoptotic pathways (*2*), mitochondrial damage (*3*) as well as inhibition of cardioprotective functions (*4*).

Nowadays, transplantations are a convincing strategy in myocardium infarction treatment especially mesenchymal stem cells (MSCs) transplantation (*5*).

Released online in J-STAGE as advance publication October 25, 2019.

**Address correspondence to:*
Dr. Aungkura Supokawej, Department of Clinical Microscopy, Faculty of Medical Technology, Mahidol University, 999 Putthamonthon Sai 4, Putthamonthon, Salaya, Nakhon Pathom 73170, Thailand.
E-mail: aungkura.jer@mahidol.ac.th

MSCs that are obtained from a perinatal source such as Wharton' jelly derived mesenchymal stem cells (WJ-MSCs) have been found to have superior biological properties when compared to bone marrow derived MSCs (BM-MSCs) due to high proliferation rates, hypoimmunogenicity (*6*), lower potential of forming teratomas (*7*), non-invasive techniques and avoidance of ethical problems (*8*). Several clinical trial studies showed promising results of treatment, which could be due to the WJ-MSCs properties; immunomodulatory (*9*), transdifferentiation to cardiomyocytes (*10*) and releasing cardioprotective paracrines (*11*) as well as anti-cardiac fibrosis (*12*). The cardiac fibrosis was initiated during myocardium regeneration and characterized by accumulation of myofibroblasts and high amounts of extracellular matrix (ECM) proteins deposition. These alterations are finally leading to stiffening of the heart and cardiac dysfunction. Unsuccessful findings were frequently found with the poor survival rate and dysfunction of transplanted WJ-MSCs and the underlying cause has not been elucidated. The outcome variances were suggested to be from poor survival of transplanted WJ-MSCs by oxidative stress-induced apoptosis (*13*). Oxidative stress was a factor reported as a dangerous insult to cell recovery mechanisms underlying pathogenesis and has a negative impact on survival of transplanted WJ-MSCs (*14*) and fibrosis (*15*).

Activation of cardioprotective cytokines has been shown during tissue regeneration to promote anti-fibrosis *via* induction of metalloproteases (MMP) to degrade ECM, inhibition of the transition from interstitial fibroblasts to myofibroblasts and against proliferation of collagen production of fibroblasts (*16*). Hepatocyte growth factor (HGF) and insulin-like growth factor (IGF1) have been reported as beneficial agents to prevent apoptosis and fibrosis in cardiovascular diseases (*17*), liver diseases (*18*) and pulmonary diseases (*19*). Sonic hedgehog (SHH) plays a role in the development of the heart blood vessels in the embryonic heart and adult heart (*20*) and has potential in cardiac repair after myocardial ischemia (*21*). Therapy of myocardial infarction with WJ-MSCs showed reduction of fibrosis and promotion of near-normalization of cardiac function (*22*). WJ-MSCs released paracrine factors as the signaling mediators of the anti-fibrotic agents. Hepatocyte growth factor and insulin-like growth factor were secreted by WJ-MSCs and have been reported to play a beneficial role in healing of fibrosis (*23*). Sonic hedgehog is a prototypical morphogen that is involved in cardiovascular regeneration *in vivo* by inducing the expression of angiogenic cytokines, including vascular endothelial growth factor-1 (VEGF-1), and angiopoietins-1 and -2 (Ang1, Ang2) from interstitial mesenchymal cells (*24*). Direct injection of SHH has been shown to activate angiogenesis in a critical hindlimb ischemia model (*25*). The delivery of those genes or proteins reduced fibrosis in numerous *in vivo* models (*26,27*).

Here, we investigated the expression level of three candidate anti-fibrotic genes, HGF, IGF1, and SHH in WJ-MSCs during H_2O_2-induced reactive oxygen species (ROS), exposure. Then the genetically engineered WJ-MSCs with each of the anti-fibrotic genes comprised of HGF, IGF1, or SHH pretreated with H_2O_2 were co-cultured with rat cardiac fibroblasts. We observed the effect of the paracrine fibrogenesis on rat fibroblasts and evaluated for myofibroblastic formation. We used this as a model to observe the effect of those paracrine factors on fibrogenesis and improve their therapeutic effect *in vitro*. The understanding of these alterations should show great promise for the future use of WJ-MSCs cell therapy in ischemic heart disease (IHD) patients.

2. Materials and Methods

2.1. *Isolation and culture of WJ-MSCs*

Umbilical cords were collected from mothers with normal labor as previously described (*28*). All participants have read and signed the informed consent, which was approved by the Mahidol University Institutional Review Board (protocol no. 147.1311). To isolate Wharton's jelly MSCs (WJ-MSCs), the umbilical cords were cleaned with 70% ethyl alcohol and washed with 1X phosphate saline buffer (1X PBS). The umbilical veins and arteries were removed before collection of Wharton's jelly matrix. The tissues were chopped and digested with collagenase type II (Worthington Biochemical Corp., Lakewood, NJ, USA) and 0.25% trypsin- ethylenediaminetetraacetic acid (EDTA). The cells suspension was harvested and washed twice with PBS. Cells were suspended in complete medium comprised of Dulbecco's Modified Eagle Medium (DMEM) low glucose, 10% fetal bovine serum (Merck KGaA, Darmstadt, Germany), 1% Penicillin/Streptomycin, and 1% GlutaMAX (Gibco, Scientific, Inc., Waltham, MA, USA). The isolated cells were plated on tissue culture dishes and cultured in a 37˚C, 5% CO_2 incubator with 95% humidified air for 24 hours. The supernatant was removed and fresh medium was changed twice a week.

2.2. *Cell and culture of rat cardiac fibroblasts*

Rat cardiac fibroblasts (CF) (n = 5) were kindly provided by Dr. Tuempong Wongtawan (Department of Preclinic and Applied Animal Science, Faculty of Veterinary Science, Mahidol University, Thailand). Cells were cultured in DMEM high glucose medium supplemented with 10% fetal bovine serum under humidified air with 5% CO_2 in a 37°C incubator. The medium was changed twice a week. Cells were expanded by trypsinization,

when cell confluence reached 80%. Confluent cells were washed twice with 1X PBS and incubated with 0.25% trypsin-EDTA at 37°C for 5 minutes. Afterward, cell suspension was harvested by centrifugation at 1,500 rpm, 25˚C for 5 minutes, and re-suspended with appropriate concentrations in culture medium.

2.3. *WJ-MSCs characterization*

WJ-MSCs in all experiments were performed as previously described (*28*). WJ-MSCs were characterized according to the minimal criteria for defining MSCs, stated by the International Society for Cellular Therapy (*29*). MSCs immunophenotype and mesodermal differentiation potential were performed. Briefly, cell surface markers expression of MSCs were evaluated from WJ-MSCs passage 3^{rd}-5^{th}. Cells were collected and incubated with antibodies specific for CD105, CD73, CD90, CD34 and CD45 (BD Pharmingen™, San Jose, CA, USA) followed by examination with a BD FACSCantoTM II Flow Cytometer and analysis by FACSDIVA Software version 6.1.3 (BD Biosciences, San Jose, CA, USA).

For mesodermal differentiation properties of MSCs, WJ-MSCs were cultured with osteogenic and adipogenic differentiation medium (Stem Cell Technologies, Vancouver, Canada) as previously described (*28*). WJ-MSCs were cultured with differentiation medium for 35 days. The differentiated cells were stained with Alizarin Red S and Oil Red O to evaluate for mineralized calcium deposition and fat deposition, respectively. The cytochemically stained cells were observed using a microscope and photographed.

2.4. *Cell viability assay*

MTT assay was employed to determine percent cell viability of WJ-MSCs during H_2O_2 treatment. WJ-MSCs were cultured with 1×10^3 seeding density for each well of a 96-well plate for 24 hours, followed by culture with growth medium containing 200, 500 and 1,000 μM H_2O_2. Cell viability of treated and control cells were analyzed as described. First, samples were washed with the DMEM twice. 50 μL of MTT (3-(4,5-dimethylthiazol-2-yl)-2,5-diphenyltetrazolium bromide) reagent (1 mg/mL) was added to the sample and incubated at 37o C, in a 5% CO_2 incubator for 4 hours. Then, the supernatant was removed, 100 μL of dimethyl sulfoxide was added, and the plate was shaken for 15 min to completely dissolve the formazan crystals before measuring the absorbance at 570 nm. Cell viability was calculated using the following formula.

$$\% \text{ Cell viability} = \left(\frac{\text{Absorbance of sample-Absorbance of blank}}{\text{Absorbance of control-Absorbance of blank}}\right) \times 100$$

2.5. *Quantitative reverse transcriptase-polymerase chain reaction (qRT-PCR)*

The experimental samples from WJ-MSCs and CF were collected in TRIzol® reagent (Invitrogen; Thermo Fisher Scientific, Inc., Waltham, MA, USA) and RNA isolation was performed using Direct-zol columns (Zymo Research, Irvine, CA, USA). The concentration of RNA was determined with a Nanodrop 2000 spectrophotometer (Thermo Fisher Scientific, Inc.). Next, First-strand cDNA was synthesized with the isolated RNA (1 μg/sample) using a cDNA Synthesis Kit, (Biotechrabbit, Berlin Germany). The expression of anti-fibrotic and myofibroblastic genes were investigated by qPCR using KAPA SYBR® Fast qPCR Kit (KAPABIOSYSTEMS, Massachusetts USA). The quantitative PCR was run with a CFX96 (Bio-Rad Laboratories, Inc.). The conditions of qPCR were set as follows: denaturation; 95˚C for 3 minutes; followed by 40 cycles of 95˚C for 3 seconds, annealing; 60˚C for 30 seconds and elongation; 72˚C for 45 seconds. The primer sequences were designed as follows: HGF forward, 5'-GGGCTGAAAAGATTGGATCA-3' and reverse, 5'-TAATTTTGTGTATCCATTTTGCAT-3'; SHH forward, 5'-GTAAGGACAAGTTGAACGCTTTG-3', and reverse, 5'-ATATGTGCCTTGGACTCGTAGTA -3'; and GAPDH forward, 5'-CAACTACATGGTTTAC ATGTTCCAA-3' and reverse, 5'-CAGCCTTCTCCAT GGTGGT-3'.The primers for CF were as follows: rCOL1 forward, 5'-AGGCATAAAGGGTCATCGTG-3' and reverse, 5'-ACCGTTGAGTCCATCTTTGC-3'; rSMA forward, 5'-ACTGGGACGACATGGAAAAG-3', and reverse, 5'-TACATGGCAGGGACATTGAA-3'; rGA PDH forward, 5'-AGCTCATTTCCTGGTATGACAA -3' and reverse, 5'-GGTATTCGAGAGAAGGGAGGG -3'. The expression of glyceraldehyde-3-phosphate dehydrogenase (GAPDH) were also quantified and applied as internal control in parallel with the target genes. The expression level of each gene was calculated by the ΔΔCt method and presented in fold changes using Bio-Rad CFX Manager version 3.1 (Bio-Rad Laboratories, Inc.) (*30*).

2.6. *Immunofluorescence staining*

Cells were seeded and cultured on coverslips. The coverslips of cells were washed with 1X PBS followed by fixation with 4% paraformaldehyde for 20 minutes and washing with 1X PBS. Permeabilization was carried out using 0.3% Triton™ X-100 (Merck KGaA) for 5 minutes and non-specific reaction blocking was performed with 3% bovine serum albumin (BSA) (Invitrogen; Thermo Fisher Scientific, Inc.) in PBS for 1 hour. Samples were incubated with anti-HGF (Santa Cruz, CA USA), anti-IGF1 (Abcam, NY USA) and anti-SHH (Abcam, NY USA) at 4°C overnight.

Samples were then washed twice with PBS to remove the excess primary antibodies, followed by incubation with Alexa flour 488 conjugated secondary antibody at room temperature for 1 hour. Cells were washed with PBS and mounted with Antifade Mounting with DAPI solution (Invitrogen; Thermo Fisher Scientific, Inc.,). The observation was performed using a confocal laser scanning microscope, the fluorescent micrographs were captured and analyzed with FluoView FV1000 Software version 3.01 (Olympus Corp., Tokyo, Japan).

2.7. *Western blot analysis*

HGF, IGF1, and SHH were quantified by collection of the condition medium and centrifugation at 1,500 rpm for 5 minutes to discard cell residue (*31*). Protein concentration was determined by using Bradford assay (Bio-Rad, CA, USA). The samples were mixed with dye and boiled for 5 minutes to denature the proteins. Samples were loaded in 10% SDS-PAGE and transferred to nitrocellulose membrane (Bio-Rad, CA, USA). Blocking of non-specific antibody binding was performed by incubating with 5% non-fat dried milk in TBST buffer (0.1 M Tris-HCl and 0.1% Tween-20, pH = 7.5) for 1 hour. Membranes were submerged with each antibody as follows; rabbit anti-human HGF polyclonal (Santa Cruz, CA, USA), mouse anti-SHH monoclonal (Abcam, NY, USA) and mouse anti IGF1 monoclonal (Abcam, NY USA). Next, the membranes were incubated with secondary antibody conjugated with horseradish peroxidase (Cell Signaling Technology, MA, USA). The signal of labelled proteins was done using the ECL™ prime Western blotting detection reagent (Amersham, UK). Images were scanned with the ChemiDoc™ MP Imaging System (Bio-Rad, UK).

2.8. *Transfection*

All plasmids, including pCMV3-HGF, pCMV3-IGF1 and pCMV3-SHH were purchased from Sino Biological Inc., China. The plasmids were transformed into Top10 competent *E. coli* and plated on LB agar plates supplemented with ampicillin. The bacterial colonies were picked and plated into LB medium supplemented with ampicillin. The bacteria were inoculated in shaking culture at 37°C for 18 hours. Plasmid DNA was extracted with a FavorPrep™ Plasmid DNA extraction mini kit (Favogen Biotech Corp, Taiwan). PCR and restriction enzyme digestion (XbaI and KpnI) were applied to confirm the correct clone from each plasmid. The correct clones were propagated to obtain a large volume. The desired plasmids were extracted by Geneaid™ Midi Plasmid kit (Geneaid, NY USA) for transfection into WJ-MSCs. WJ-MSCs were cultured in 100-mm dishes at a density of 2×10^6 cells. Next, cells were transfected with 24 μg of plasmid using Lipofectaminne™ 2000 (Invitrogen, CA USA) according to the manufacturer's protocol (*32*). Briefly, 24 μg of plasmid were mixed with Opti-MEM to a final volume of 900 μl and incubated for 5 minutes at room temperature. The mixture of diluted plasmids and the Lipofectamine™ 2000 in Opti-MEM was prepared and incubated for 20 minutes at room temperature to generate the DNA-Lipofectamine 2000 complexes. This mixture was applied to cell culture plates and filled with medium without antibiotic.

2.9. *Amplification of plasmid by polymerase chain reaction (PCR)*

The DNA template for the pCMV3-HGF, pCMV3-IGF1 and pCMV3-SHH containing CDS of interest, was amplified using PCR. The primers of pCMV3 (forward, 5'-CAGGTGTCCACTCCCAGGTCCAAG-3' and reverse, 5'-GGCAACTAGAAGGCACAGTC GAGG-3'); were performed for PCR reaction using I-Taq plus DNA polymerase (iNtRON Biotechnology, Inc., Korea) according to manufacturer's instructions as described. The PCR reaction was performed using the following cycling protocol: initial activation step at 94°C for 2 minutes, followed by 30 cycles of denaturation at 94°C for 20 seconds, annealing at 62°C for 10 seconds, extension at 72°C for 1.30 minutes and final extension at 72°C for 7 minutes.

2.10. *Statistical analysis*

All data of the study were collected from 6 donors, the experiments were performed independently and at least three samples were applied for each experiment. The data is presented as mean ± standard error of the mean. To test statistical difference of mean, Mann-Whitney *U* test was applied and $P < 0.05$ was considered significant difference. Statistical tests were done using PASW software version 18 (IBM Corp., Armonk, NY, USA).

3. Results

3.1. *WJ-MSC characterization*

WJ-MSCs over the first 5-6 days of culture displayed fibroblast-like morphology (Figure 1A). The specific MSC markers (CD90, CD73 and CD105) and hematopoietic cells markers (CD34 and CD45) were analyzed with flow cytometry (Figure 1B). The positive expressions were present on WJ-MSCs; CD90, CD73, CD105. WJ-MSCs were mostly negative for HSC markers; CD34, CD45. To explore the differentiation potential towards osteoblasts and adipocytes, WJ-MSCs were cultured with osteogenic and adipogenic differentiation medium followed by cytochemical staining with Alizarin Red S and Oil Red

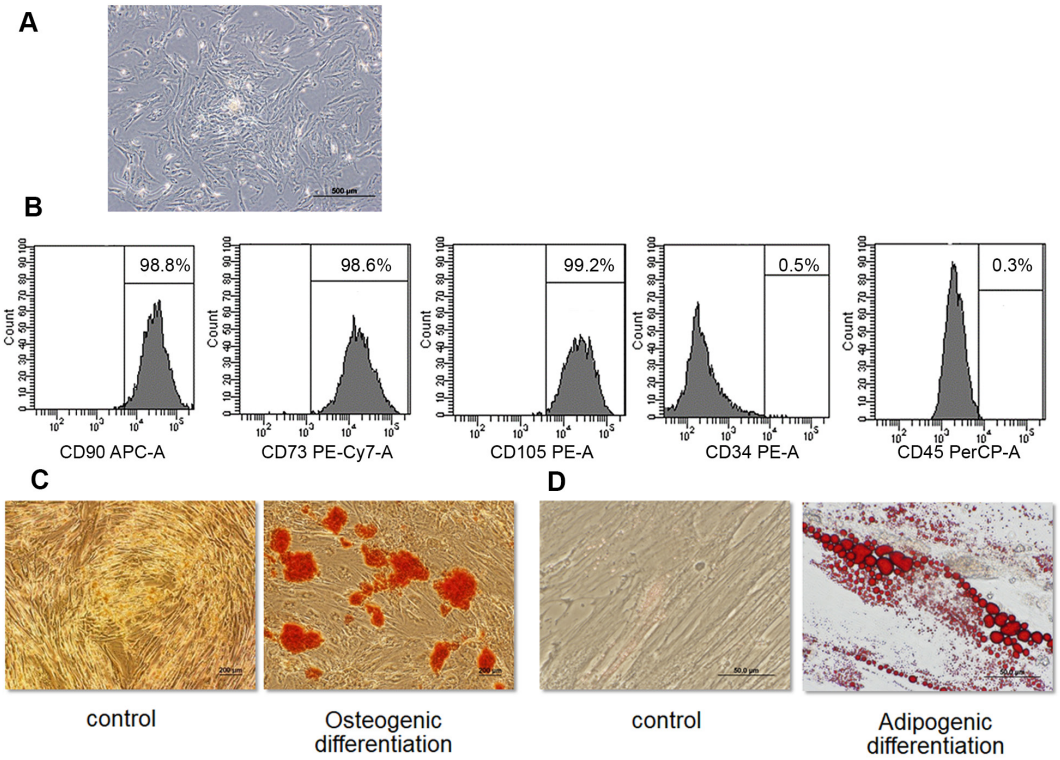

Figure 1. The characterization of WJ-MSCs. (A) The spindle-shaped morphology of WJ-MSCs was observed. **(B)** Flow cytometric analysis of WJ-MSCs are more than 90% positive for MSC markers, CD105, CD90, CD73 and less than 2% positive for hematopoietic markers, CD34, CD45. For the multilineage differentiation study, WJ-MSCs were cultured with osteogenic and adipogenic differentiation medium followed by cytochemical staining, **(C)** Alizarin red S and **(D)** Oil red O, respectively. WJ-MSCs exhibited positive staining under both conditions.

O, respectively. The differentiated cells were positive for both cytochemical stains which indicated cell differentiation toward osteoblast-like (Figure 1C) and adipocyte-like cells (Figure 1D).

3.2. *Cell viability assay*

The effect of H_2O_2 on the viability of WJ-MSCs was investigated. Cells were treated with various concentration of H_2O_2 for 24 and 48 hours before assessing cell viability using MTT assay. The viability of WJ-MSCs after H_2O_2 treatment was expressed as a percentage relative to control (Figure 2A). Results showed that the viability of WJ-MSCs was decreased in a dose- and time-dependent manner after H_2O_2 treatment. At 1,000 μM of H_2O_2 treatment, the viability of WJ-MSCs was significantly decreased compared with control. Microscopic examination of the cells after H_2O_2 treatment for 7 days showed low cell density in 1,000 μM H_2O_2 treatment compared with control (Figure 2B).

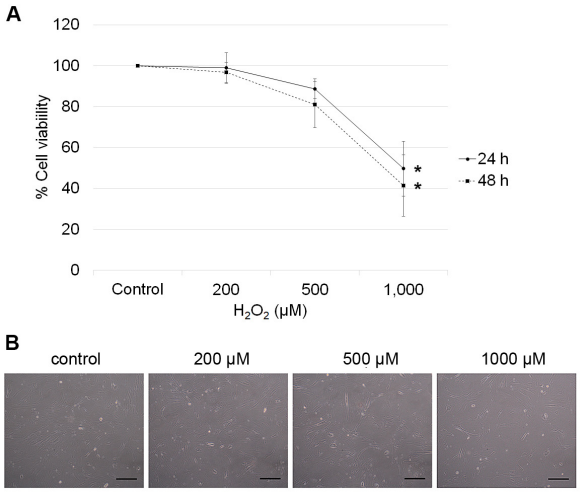

Figure 2. The viability of WJ-MSCs after H2O2 treatment. (A) WJ-MSCs were treated with H_2O_2 at 200, 500 and 1,000 μM for 24 and 48 hours. The viability of the cells was assessed by MTT assay and presented as a mean percentage relative to the control ± SEM of six separate experiments. The viability of WJ-MSCs was reduced by H_2O_2 treatment in a dose- and time-dependent manner. *$p < 0.05$ *vs*. control group. **(B)** Microscopic examination of WJ-MSCs after H_2O_2 treatment for 7 days revealed a low cellular density in H_2O_2 treated cells compared with control group. Scale bar, 200 μm.

3.3. *Anti-fibrotic gene and protein expression in WJ-MSCs under ROS condition*

To determine the expression level of HGF, IGF1, and SHH in WJ-MSCs, real-time PCR and immunofluorescence staining were performed. WJ-MSCs were treated with 200, 500, and 1,000 μM H_2O_2 for 24 hours before harvesting mRNA or staining with anti-fibrotic markers. In comparison with control group,

the expression levels of HGF, IGF1, and SHH were significantly reduced after H_2O_2 treatment in a dose-dependent manner (Figure 3A). Immunofluorescence staining of HGF, IGF1, and SHH showed decreased fluorescence intensity of the three markers in H_2O_2-treated cells compared with control (Figure 3B).

3.4. *Myofibroblastic gene expression in cardiac fibroblasts (CF) after co-culture with H_2O_2-treated WJ-MSCs*

To determine the effect of H_2O_2 on the anti-fibrotic properties of WJ-MSCs, WJ-MSCs were plated in transwells and cultured with medium supplemented with 200, 500, and 1,000 μM H_2O_2 for 24 hours. The H_2O_2 -treated WJ-MSCs were then co-cultured with CF for 48 hours. Myofibroblastic specific markers; alpha-smooth muscle actin (SMA) and collagen type 1 (COL1) were investigated in CF. The gene expression of COL1 and SMA in CF were not significantly different compared with control (Figure 4A), whereas the immunofluorescent micrographs showed the highest fluorescent intensity for COL1 and SMA signal in the 1,000 μM H_2O_2 treatment group indicating an increased myofibroblastic phenotype in CF (Figure 4B). Thus, we decided to use 1,000 μM H_2O_2 treated WJ-MSCs for the subsequent experiments.

3.5. *Anti-fibrosis gene and protein expression of WJ-MSCs after transfection*

In order to improve anti-fibrotic properties of WJ-MSCs, the WJ-MSCs were transfected with pCMV3-HGF, pCMV3-IGF1, or pCMV3-SHH for 48 hours using Lipofectamine™ 2000. The timeline of the

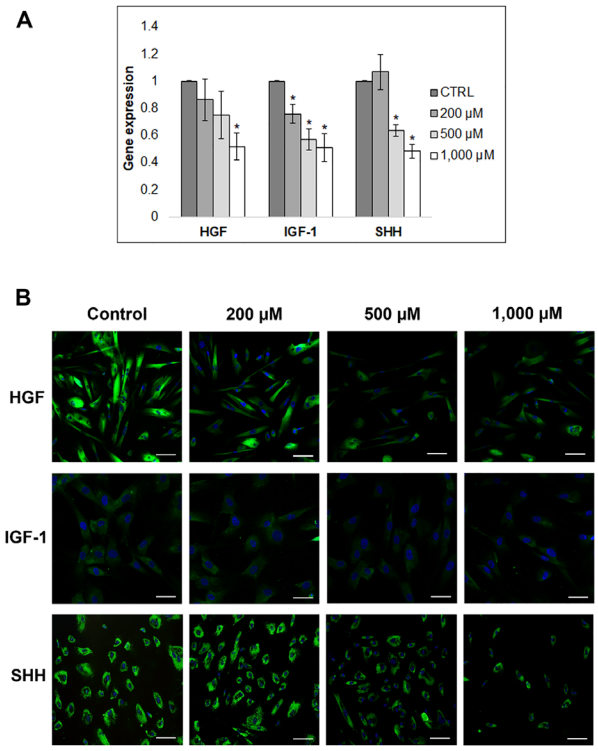

Figure 3. Anti-fibrotic factors expression in WJ-MSCs after H_2O_2 treatment. (A) The levels of HGF, IGF1, and SHH genes were significantly reduced in H_2O_2-treated WJ-MSCs when compared with control group. Data were expressed as mean ± SEM (n = 6), *p < 0.05 *vs*. control. **(B)** Immunofluorescent micrographs of HGF, IGF1, and SHH in WJ-MSCs after treatment with various concentrations of H_2O_2. Low fluorescent intensity of HGF and SHH was obviously observed in 500 and 1,000 μM H_2O_2-treated cells compared with control, whereas the fluorescence intensity of IGF-1 was similar to control. Scale bars, 100 μm. WJ-MSCs, Wharton's jelly-derived WJ-MSCs; HGF, hepatic growth factor; IGF1, insulin-like growth factor; SHH, sonic hedgehog.

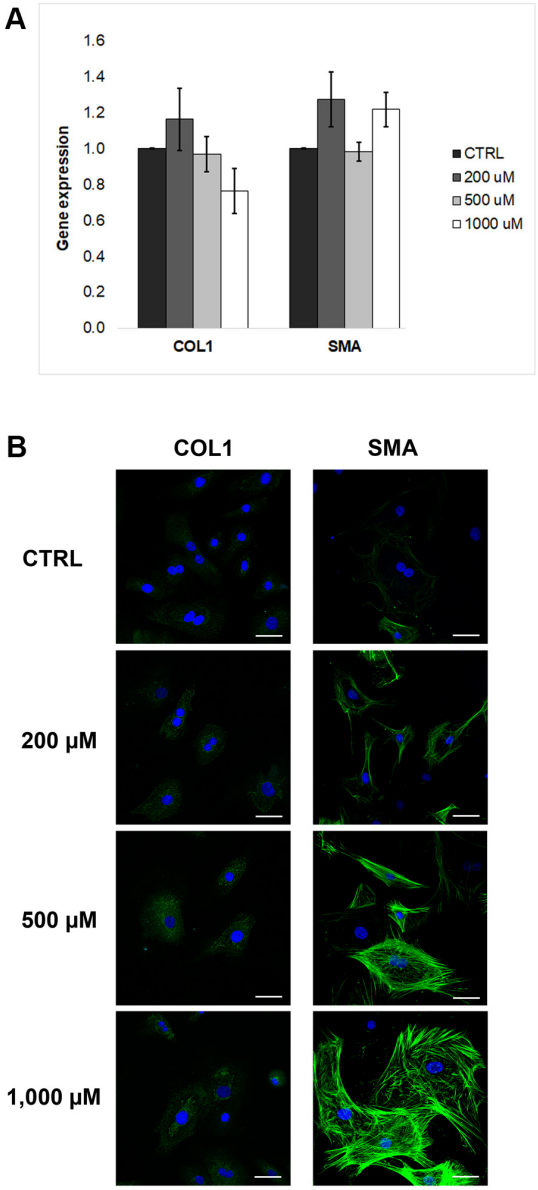

Figure 4. Myofibroblastic gene expression in CF after co-culture with H_2O_2-treated WJ-MSCs. (A) Gene expression of COL1 and SMA in H_2O_2-treated WJ-MSCs were not significantly different when compared with control. Data are expressed as mean ± SEM (n = 3). **(B)** Immunofluorescence micrographs showed the increased fluorescent intensity of COL1 and SMA in CF after co-culture with H_2O_2 –treated WJ-MSCs, in particular at 1,000 μM of H_2O_2. Scale bars, 100 μm. COL1, collagen type I; SMA, smooth muscle actin.

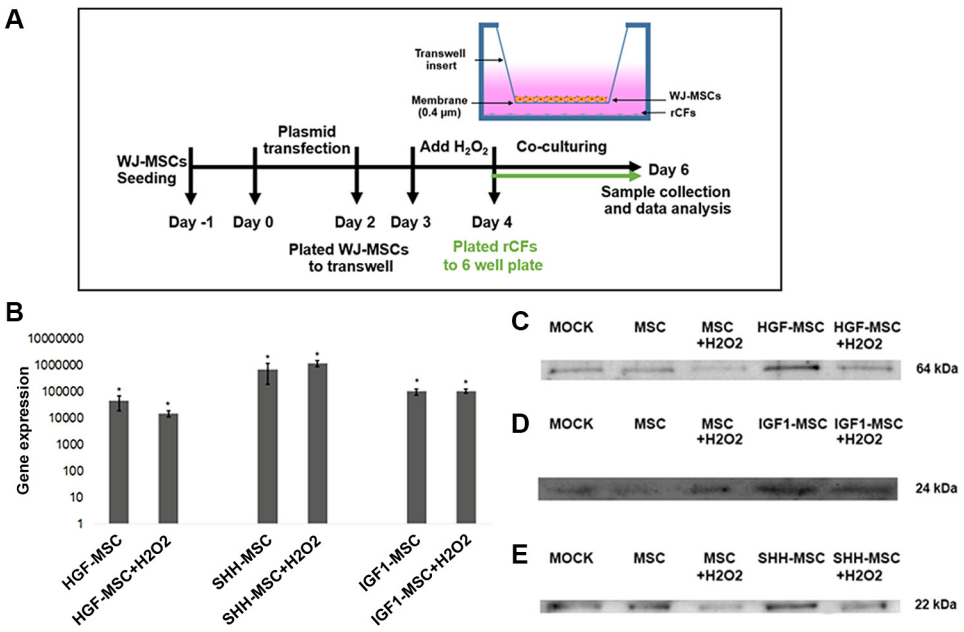

Figure 5. Overexpression of anti-fibrosis factors in WJ-MSCs. (A) Schematic diagram represents the process of WJ-MSC transfection with anti-fibrosis genes. **(B)** Analysis of HGF, IGF1 and SHH mRNA expression in transfected WJ-MSCs at day 6. The levels of HGF, SHH and IGF1 were significantly up-regulated in both transfected MSCs and transfected MSCs after H_2O_2 treatment. Data are expressed as mean ± SEM ($n = 3$), *$p < 0.05$ *vs*. control. Western blot analysis of **(C)** HGF, **(D)** IGF1, **(E)** SHH in conditioned medium of WJ-MSCs are shown. Level of HGF, IGF1, and SHH in conditioned medium from transfected MSCs were higher than those in MSCs. These proteins were decreased after H_2O_2 treatment.

process is shown in Figure 5A. RNA and conditioned medium were collected from transfected MSCs and expression of HGF, IGF1, and SHH were investigated before co-culture with CF. The expression of HGF, SHH, and IGF1 genes in transfected WJ-MSCs were approximately up to 10,000 fold higher than control and were not reduced after H_2O_2 treatment (Figure 5B). The examination of the protein expression in conditioned media performed by Western blot analysis showed decreased HGF, IGF1, and SHH proteins in conditioned media of H_2O_2-treated WJ-MSCs. These proteins were increased in conditioned media of transfected WJ-MSCs (HGF-, IGF1-, SHH-MSC) and decreased after H_2O_2 treatment. However, compared to non-transfected WJ-MSCs, the HGF, IGF1, and SHH protein concentrations tended to be higher in transfected MSCs after H_2O_2 treatment (Figure 5C-E).

3.6. *Myofibroblastic gene and protein expression of CF after co-culture with transfected WJ-MSCs*

To determine whether the expression of anti-fibrotic secreted factors from transfected WJ-MSCs could affect myofibroblast properties in CF, we investigated the myofibroblastic markers; COL1 and SMA in CF after co-culture with WJ-MSCs for 48 hours (Figure 5A). The conditions of WJ-MSCs for co-culture study were as follows; no MSC, -MOCK, -MSC, -MSC+H_2O_2, -MSC+pCMV3 (HGF/IGF1/SHH), -MSC+pCMV3 (HGF/IGF1/SHH) +H_2O_2. As determined by immunofluorescence staining, the fluorescent intensity of COL1 and SMA in CF were lower after co-culture with MSC and MSC+pCMV3 compared with CF (Figure 6-8). The fluorescent signal tended to be increased after co-culture with H_2O_2-treated MSCs compared with MSCs, however, the expression of these myofibroblast markers tended to be decreased after co-culture with MSC+pCMV3+H_2O_2 (Figure 6A,7A, 8A). For the gene expression study, SMA expression was found to have the same trend as the results of fluorescent intensity (Figure 6B, 7B, 8B). The expression of COL1 from all conditions was not much different among the co-culture conditions (Figure 6B, 7B, 8B). All evidence showed the efficacy of anti-fibrotic factors overexpressed-MSC diminished the transformation from fibroblasts to myofibroblasts.

4. Discussion

Stem cell therapy has become a potential novelty for treating degenerative diseases, in particular, cell transplantation in ischemic heart disease (IHD). WJ-MSCs are considered to be a promising stem cell type for treating IHD due to their high number in the tissue, which can easily be isolated by low-invasive methods (*33*). Previous research reported the potential of WJ-MSCs to differentiate into cardiomyocytes, neovascularization and cardioprotective effects *via* paracrine factors (*34*). In the present study, WJ-MSCs exhibited typical MSC characteristics including

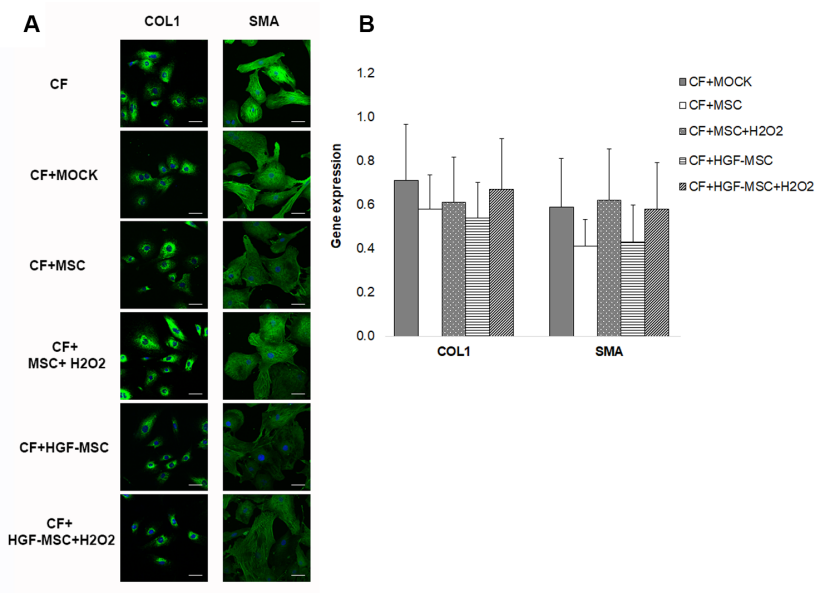

Figure 6. Expression of myofibroblast markers in CF after co-culture with or without HGF-overexpressed WJ-MSCs. **(A)** Immunofluorescence micrographs of CF taken at the 48 hours after co-culture with WJ-MSCs. A low fluorescent intensity of COL1 and SMA was observed in CF+MSC and CF+HGF-MSC. Scale bar, 50 μm. **(B)** The expression of myofibroblastic genes was assessed in CF at 48 hours after co-culture. The expression of COL1 and SMA gene was concordant with the immunofluorescence staining. Data are expressed as mean ± SEM (n = 3).

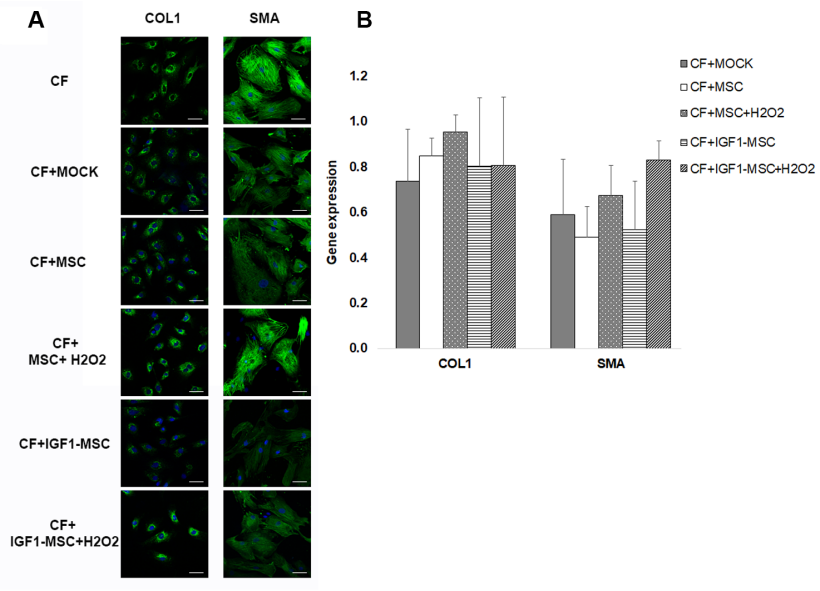

Figure 7. Expression of myofibroblast markers in CF after co-culture with or without IGF1-overexpressed WJ-MSCs. **(A)** Immunofluorescent micrographs of CF taken at the 48 hours after co-culture with WJ-MSCs. A low fluorescent intensity of COL1 and SMA was observed in CF+MSC and CF+IGF1-MSC. Scale bar, 50 μm. **(B)** The myofibroblastic gene level was assessed in CF 48 hours after co-culture. The expression of COL1 and SMA gene was concordant with the immunofluorescence staining. Data are expressed as mean ± SEM (n = 3).

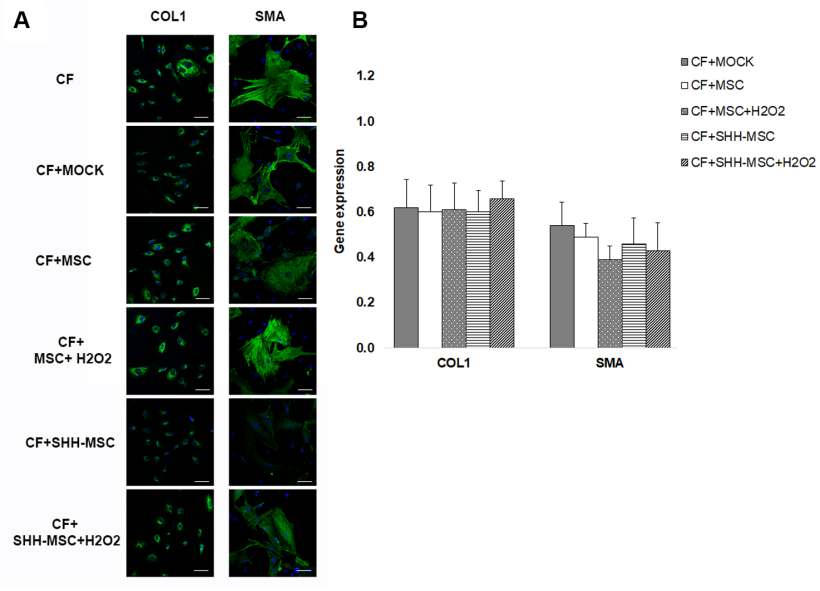

Figure 8. Expression of myofibroblast markers in CF after co-culture with or without SHH-overexpressed WJ-MSCs. **(A)** Immunofluorescent micrographs of CF taken at the 48 hours after co-culture with WJ-MSCs. A low fluorescent intensity of COL1 and SMA was observed in CF+MSC and CF +SHH-MSC. Scale bar, 50 μm. **(B)** The myofibroblastic gene expression was assessed in CF 48 hours after co-culture. The expression of COL1 and SMA gene was not different among tested groups. Data are expressed as mean ± SEM (n = 3).

expression of cell surface markers (CD90, CD73 and CD105) and differentiation potential into mesodermal lineages (osteoblasts and adipocytes). It had been shown that the response of MSCs to oxidative insult was different according to the origin of MSCs (*35*). Therefore, the selection of MSCs used for transplantation must be a concern and appropriate for the specific use. Even though MSCs from different origins have similar characteristics, the type of MSCs must be carefully considered to enhance the outcome of cell transplantation.

WJ-MSCs have been shown to exert anti-fibrotic properties although the underlying mechanism is poorly characterized. WJ-MSCs are able to secrete many anti-fibrotic cytokines including HGF, fibroblast growth factor 2 (FGF2), connective tissue growth factor (CTGF), Tumor necrosis factor-inducible gene 6 (TSG6), IGF1 and SHH, which could account for their therapeutic effects (*36*). Recently, WJ-MSCs treatment for fibrotic diseases has reached clinical trial phase 2, especially in liver fibrosis and cardiac fibrosis. Post myocardial infarction usually develops cardiac fibrosis, which impairs cardiac function. Therefore, the reduction of cardiac fibrosis might be a useful strategy for treatment of heart failure. Even though, it has been demonstrated that administration of WJ-MSCs in a myocardial infarction model decreased cardiac fibrosis (*37*) but unsuccessful findings were frequently found with poor survival rate and dysfunction of transplanted WJ-MSCs.

Oxidative stress was reported to be an important factor influencing the transplanted WJ-MSCs survival and function. Here, we focused on the role of oxidative stress in anti-fibrotic properties of WJ-MSCs. We hypothesized that oxidative stress may diminished the anti-fibrotic property of WJ-MSCs whereas the overexpression of HGF, IGF1 or SHH genes can reconcile this function. Our results demonstrated that the gene and protein levels of anti-fibrosis factors such as HGF, IGF1 and SHH were significantly decreased after exposure to H_2O_2 in a dose dependent manner. HGF, IGF1 and SHH are novel anti-fibrotic cytokines. It has been shown that HGF prevented the progression of fibrogenesis in multiple organs such as lung, liver and heart (*36,38,39*). IGF1 exerts the beneficial effect on cardiac repair by enhancing angiogenesis and improving myocardial function (*40*). Previous studies demonstrated that SHH inhibited cardiac fibrosis, at least in part, by stimulating the production of paracrine factors that exert anti-fibrotic action (*41*). SHH gene therapy also enhanced neovascularization in rat myocardial infarction through the upregulation of angiogenic-associated genes including VEGF, stromal cell-derived factor 1 (SDF-1), angiopoeitin, and IGF1 (*42*). Reactive oxygen species have been shown to activate latent transforming growth factor beta (TGF-β) and induce the expression of profibrogenic cytokines such as TGF-β and angiotensin II (ANG) (*43*), which are negative regulators of HGF (*44*). It is possible that H_2O_2 reduced the expression of anti-fibrosis genes and proteins in WJ-MSCs by stimulating the expression of its antagonist, however, the underlying mechanism was largely unknown. The consequence of downregulation of HGF, IGF1 and SHH under oxidative stress conditions might impair anti-fibrosis properties of WJ-MSCs. Therefore, the anti-fibrosis potential of WJ-MSCs was further investigated by co-culturing with rat cardiac fibroblasts (CF). The results showed that the expression of myofibroblastic specific markers; COL1 and SMA in CF was increased after co-culture with H_2O_2 treated WJ-MSCs. This finding might affect to the activation of interleukin-6 (IL-6) through phosphatidylinositol 3-kinase (PI3K), protein kinase B (Akt), and glycogen synthase kinase 3 beta (GSK3β) downstream molecules (*45*). The upregulation of IL-6 plays a key role in the production of TGF-β *via* the JAK/STAT3 signaling pathway, which enhances the transdifferentiation of fibroblasts to myofibroblasts (*46*). Therefore, oxidative stress might be one important mechanism that attenuates the anti-fibrotic ability of WJ-MSCs. ROS may induce stress in WJ-MSCs and impair its function resulting in transdifferentiation of cardiac fibroblasts to myofibroblasts.

To further elucidate whether the impairment of anti-fibrosis properties can be recovered, we overexpressed anti-fibrosis genes in WJ-MSCs and then co-cultured with CF under ROS conditions. We hypothesized that administration of MSC-HGF, MSC-IGF1 or MSC-SHH might improve anti-fibrotic properties under ROS conditions. The results showed that overexpressed-MSC increased the gene expression levels of HGF, IGF1, and SHH even when cultured under ROS conditions. The conditioned media of overexpressed-MSC co-cultured with CF showed higher HGF, IGF1 and SHH protein expression compared to the others. Therefore, overexpression of anti-fibrosis genes; HGF, IGF1, and SHH in MSC may abolish the effect of H_2O_2 on anti-fibrosis genes and protein expression. MSCs were then co-cultured with CF. Fibrosis is characterized by the accumulation and deposition of collagen type I and SMA produced from myofibroblasts. Therefore, we investigated fibrogenesis *via* evaluation of myofibroblast characteristics of CF during culture. The study was divided into 4 groups as follows; CF+MOCK, CF+MSC+H_2O_2, CF+overexpressed-MSC, CF+overexpressed-MSC+H_2O_2. The results showed that overexpression groups; HGF-MSC, IGF1-MSC or SHH-MSC in the presence of H_2O_2 were able to decrease the expression of myofibroblastic genes and proteins; COL1 and SMA. These results correlated with previous studies that gene transfer of HGF, IGF1, or SHH reduced cardiac fibrosis (*47*). HGF prevents fibrosis *via* the HGF/Met pathway, which antagonize the TGF-β and angiotensin II signaling pathway

(*38,48*). Meanwhile, overexpression of IGF1 in cardiomyocytes reduced fibrosis in the mouse model of dilated cardiomyopathy by inhibiting cardiac fibroblast proliferation and reducing the expression of connective tissue growth factor (CTGF), a downstream mediator of the TGF-β pathway (*49*). However, the role of SHH in cardiac fibrosis has not been clearly elucidated. SHH has been shown to promote fibrosis in some organs such as lung, liver, and kidney *via* its interaction with the receptor Ptch1/Smo, which activates Gli1, a transcription factor regulating the expression of fibrogenic genes; Snail, COL1, SMA, fibronectin, and desmin. Besides, the SHH pathway may promote epithelial-mesenchymal transition (EMT), which is necessary for tissue fibrosis by induction of TGF-β (*50*). Several studies have suggested that SHH may exert beneficial effects on cardiac repair upon tissue injury. It has been elucidated that SHH is involved in the cardio-protective effect after ischemia *via* up-regulation of VEGF, Ang-1, and Ang-2, which can induce neovascularization and angiogenesis (*42*).

Taken together, ROS exerted adverse effects on WJ-MSCs by attenuating its anti-fibrotic properties. Our results suggest the overexpression of anti-fibrosis genes can abolish the ROS affected anti-fibrosis properties of WJ-MSCs. Therefore, WJ-MSCs modified to overexpress anti-fibrosis genes could serve as a novel approach for protecting/treating cardiac fibrosis. However, this finding is only a preliminary study, which revealed that the good outcome of stem cell therapy may originate from multiple factors, particularly, the environment of engrafted cells must be a concern and an *in vivo* study is greatly needed.

Acknowledgements

This project was supported by Mahidol University, Thailand.

References

1. Brown RD, Ambler SK, Mitchell MD, Long CS. The cardiac fibroblast: therapeutic target in myocardial remodeling and failure. Annu Rev Pharmacol Toxicol. 2005; 45:657-687.
2. von Harsdorf R, Li PF, Dietz R. Signaling pathways in reactive oxygen species-induced cardiomyocyte apoptosis. Circulation. 1999; 99:2934-2941.
3. Xu Z, Park SS, Mueller RA, Bagnell RC, Patterson C, Boysen PG. Adenosine produces nitric oxide and prevents mitochondrial oxidant damage in rat cardiomyocytes. Cardiovasc Res. 2005; 65:803-812.
4. Tao L, Gao E, Jiao X, Jiao X, Yuan Y, Li S, Christopher TA, Lopez BL, Koch W, Chan L, Goldstein BJ, Ma XL. Adiponectin cardioprotection after myocardial ischemia/reperfusion involves the reduction of oxidative/nitrative stress. Circulation. 2007; 115:1408-1416.
5. Li L, Zhang Y, Li Y, Yu B, Xu Y, Zhao S, Guan Z. Mesenchymal stem cell transplantation attenuates cardiac fibrosis associated with isoproterenol-induced global heart failure. Transpl Int. 2008; 21:111-1189.
6. Li X, Bai J, Ji X, Li R, Xuan Y, Wang Y. Comprehensive characterization of four different populations of human mesenchymal stem cells as regards their immune properties, proliferation and differentiation. Int J Mol Med. 2014; 34:695-704.
7. Fong CY, Richards M, Manasi N, Biswas A, Bongso A. Comparative growth behaviour and characterization of stem cells from human Wharton's jelly. Reprod Biomed Online. 2007; 15:708-718.
8. Troyer DL, Weiss ML. Wharton's jelly-derived cells are a primitive stromal cell population. Stem Cells. 2008; 26:591-599.
9. Zhou C, Yang B, Tian Y, Jiao H, Zheng W, Wang J, Guan F. Immunomodulatory effect of human umbilical cord Wharton's jelly-derived mesenchymal stem cells on lymphocytes. Cell Immunol. 2011; 272:33-38.
10. Ruan ZB, Zhu L, Yin YG, Chen GC. The mechanism underlying the differentiation of human umbilical cord-derived mesenchymal stem cells into myocardial cells induced by 5-azacytidine. Indian J Med Sci. 2010; 64:402-407.
11. Suzuki YJ. Growth factor signaling for cardioprotection against oxidative stress-induced apoptosis. Antioxid Redox Signal. 2003; 5:741-7499.
12. Li LL, Peng C, Zhang M, Liu Y, Li H, Chen H, Sun Y, Zhu C, Zhang Y. Mesenchymal stem cells overexpressing adrenomedullin improve heart function through antifibrotic action in rats experiencing heart failure. Mol Med Rep. 2018; 17:1437-1444.
13. Turtzo LC, Budde MD, Dean DD, Gold EM, Lewis BK, Janes L, Lescher J, Coppola T, Yarnell A, Grunberg NE, Frank JA. Failure of intravenous or intracardiac delivery of mesenchymal stromal cells to improve outcomes after focal traumatic brain injury in the female rat. PloS One. 2015; 10:e0126551.
14. Song H, Cha MJ, Song BW, Kim IK, Chang W, Lim S, Choi EJ, Ham O, Lee SY, Chung N, Jang Y, Hwang KC. Reactive oxygen species inhibit adhesion of mesenchymal stem cells implanted into ischemic myocardium *via* interference of focal adhesion complex. Stem Cells. 2010; 28:555-563.
15. Zhao W, Zhao T, Chen Y, Ahokas RA, Sun Y. Oxidative stress mediates cardiac fibrosis by enhancing transforming growth factor-β1 in hypertensive rats. Mol Cell Biochem. 2008; 317:43-50.
16. Mohammadi Gorji S, Karimpor Malekshah AA, Hashemi-Soteh MB, Rafiei A, Parivar K, Aghdami N. Effect of mesenchymal stem cells on Doxorubicin-induced fibrosis. Cell J. 2012; 14:142-151.
17. Zhang GW, Gu TX, Guan XY, Sun XJ, Qi X, Li XY, Wang XB, Lv F, Yu L, Jiang DQ, Tang R. HGF and IGF-1 promote protective effects of allogeneic BMSC transplantation in rabbit model of acute myocardial infarction. Cell Prolif. 2015; 48:661-670.
18. Shams S, Mohsin S, Nasir GA, Khan M, Khan SN. Mesenchymal Stem Cells Pretreated with HGF and FGF4 Can Reduce Liver Fibrosis in Mice. Stem Cells Int. 2015; 747245.
19. Kugler MC, Loomis CA, Zhao Z, Cushman JC, Liu L, Munger JS. Sonic Hedgehog Signaling Regulates Myofibroblast Function during Alveolar Septum Formation in Murine Postnatal Lung. Am J Respir Cell Mol Biol. 2017; 57:280-293.

20. Thomas NA, Koudijs M, van Eeden FJ, Joyner AL, Yelon D. Hedgehog signaling plays a cell-autonomous role in maximizing cardiac developmental potential. Development. 2008; 135:3789-3799.
21. Paulis L, Fauconnier J, Cazorla O, Thireau J, Soleti R, Vidal B, Ouille A, Bartholome M, Bideaux P, Roubille F, Le Guennec JY, Andriantsitohaina R, Martinez MC, Lacampagne A. Activation of Sonic hedgehog signaling in ventricular cardiomyocytes exerts cardioprotection against ischemia reperfusion injuries. Sci Rep. 2015; 5:7983.
22. Amado LC, Saliaris AP, Schuleri KH, St John M, Xie JS, Cattaneo S, Durand DJ, Fitton T, Kuang JQ, Stewart G, Lehrke S, Baumgartner WW, Martin BJ, Heldman AW, Hare JM. Cardiac repair with intramyocardial injection of allogeneic mesenchymal stem cells after myocardial infarction. Proc Natl Acad Sci U S A. 2005; 102:11474-11479.
23. Lu F, Zhao X, Wu J, Cui Y, Mao Y, Chen K, Yuan Y, Gong D, Xu Z, Huang S. MSCs transfected with hepatocyte growth factor or vascular endothelial growth factor improve cardiac function in the infarcted porcine heart by increasing angiogenesis and reducing fibrosis. Int J Cardiol. 2013; 167:2524-2532.
24. Wang LC, Liu ZY, Gambardella L, Delacour A, Shapiro R, Yang J, Sizing I, Rayhorn P, Garber EA, Benjamin CD, Williams KP, Taylor FR, Barrandon Y, Ling L, Burkly LC. Regular articles: conditional disruption of hedgehog signaling pathway defines its critical role in hair development and regeneration. J Invest Dermatol. 2000; 114:901-908.
25. Pola R, Ling LE, Silver M, Corbley MJ, Kearney M, Blake Pepinsky R, Shapiro R, Taylor FR, Baker DP, Asahara T, Isner JM. The morphogen Sonic hedgehog is an indirect angiogenic agent upregulating two families of angiogenic growth factors. Nat Med. 2001; 7:706-711.
26. Okayama K, Azuma J, Dosaka N, Iekushi K, Sanada F, Kusunoki H, Iwabayashi M, Rakugi H, Taniyama Y, Morishita R. Hepatocyte growth factor reduces cardiac fibrosis by inhibiting endothelial-mesenchymal transition. Hypertension. 2012; 59:958-965.
27. Choe S, Veliceasa D, Bond CW, Harrington DA, Stupp SI, McVary KT, Podlasek CA. Sonic hedgehog delivery from self-assembled nanofiber hydrogels reduces the fibrotic response in models of erectile dysfunction. Acta Biomater. 2016; 32:89-99.
28. Nimsanor N, Phetfong J, Plabplueng C, Jangpatarapongsa K, Prachayasittikul V, Supokawej. A Inhibitory effect of oxidative damage on cardiomyocyte differentiation from Wharton's jelly-derived mesenchymal stem cells. Exp Ther Med. 2017; 14:5329-5338.
29. Dominici M, Le Blanc K, Mueller I, Slaper-Cortenbach I, Marini F, Krause D, Deans R, Keating A, Prockop D, Horwitz E. Minimal criteria for defining multipotent mesenchymal stromal cells. The International Society for Cellular Therapy position statement. Cytotherapy. 2006; 8:315-317.
30. Livak KJ, Schmittgen TD. Analysis of relative gene expression data using real-time quantitative PCR and the $2(^{-\Delta\Delta C_T})$ Method. Method. Methods: A companion to Methods in enzymology. 2001; 25:402-408.
31. Dowling P, Clynes M. Conditioned media from cell lines: A complementary model to clinical specimens for the discovery of disease-specific biomarkers. Proteomics. 2011; 11:794-804.
32. Maurisse R, De Semir D, Emamekhoo H, Bedayat B, Abdolmohammadi A, Parsi H, Gruenert DC. Comparative transfection of DNA into primary and transformed mammalian cells from different lineages. BMC Biotechnol. 2010; 10:9.
33. Watson N, Divers R, Kedar R, Mehindru A, Mehindru A, Borlongan MC, Borlongan CV. Discarded Wharton jelly of the human umbilical cord: A viable source for mesenchymal stromal cells. Cytotherapy. 2015; 17:18-24.
34. Rahbarghazi R, Nassiri SM, Khazraiinia P, Kajbafzadeh AM, Ahmadi SH, Mohammadi E, Molazem M, Zamani-Ahmadmahmudi M. Juxtacrine and paracrine interactions of rat marrow-derived mesenchymal stem cells, muscle-derived satellite cells, and neonatal cardiomyocytes with endothelial cells in angiogenesis dynamics. Stem Cells Dev. 2013; 22:855-865.
35. Vinoth KJ, Manikandan J, Sethu S, Balakrishnan L, Heng A, Lu K, Poonepalli A, Hande MP, Cao T. Differential resistance of human embryonic stem cells and somatic cell types to hydrogen peroxide-induced genotoxicity may be dependent on innate basal intracellular ROS levels. Folia Histochem Cytobiol. 2015; 53:169-174.
36. Kim MD, Kim SS, Cha HY, Jang SH, Chang DY, Kim W, Suh-Kim H, Lee JH. Therapeutic effect of hepatocyte growth factor-secreting mesenchymal stem cells in a rat model of liver fibrosis. Exp Mol Med. 2014; 46:e110.
37. Elnakish MT, Kuppusamy P, Khan M. Stem cell transplantation as a therapy for cardiac fibrosis. J Pathol. 2013; 229:347-354.
38. Taniyama Y, Morishita R, Nakagami H, Moriguchi A, Sakonjo H, Shokei K, Matsumoto K, Nakamura T, Higaki J, Ogihara T. Potential contribution of a novel antifibrotic factor, hepatocyte growth factor, to prevention of myocardial fibrosis by angiotensin II blockade in cardiomyopathic hamsters. Circulation. 2000; 102:246-252.
39. Cahill EF, Kennelly H, Carty F, Mahon BP, English K. Hepatocyte Growth Factor Is Required for Mesenchymal Stromal Cell Protection Against Bleomycin-Induced Pulmonary Fibrosis. Stem Cells Transl Med. 2016; 5:1307-1318.
40. Gomez-Mauricio G, Moscoso I, Martin-Cancho MF, Crisostomo V, Prat-Vidal C, Baez-Diaz C, Sanchez-Margallo FM, Bernad A. Combined administration of mesenchymal stem cells overexpressing IGF-1 and HGF enhances neovascularization but moderately improves cardiac regeneration in a porcine model. Stem Cell Res Ther. 2016; 7:94.
41. Kusano KF, Pola R, Murayama T, *et al*. Sonic hedgehog myocardial gene therapy: tissue repair through transient reconstitution of embryonic signaling. Nat Med. 2005; 11:1197-1204.
42. Roncalli J, Renault MA, Tongers J, Misener S, Thorne T, Kamide C, Jujo K, Tanaka T, Ii M, Klyachko E, Losordo DW. Sonic hedgehog-induced functional recovery after myocardial infarction is enhanced by AMD3100-mediated progenitor-cell mobilization. J Am Coll Cardiol. 2011; 57:2444-2452.
43. Sullivan DE, Ferris M, Pociask D, Brody AR. The latent form of TGFβ1 is induced by TNFalpha through an ERK specific pathway and is activated by asbestos-derived reactive oxygen species *in vitro* and *in vivo*. J Immunotoxicol. 2008; 5:145-149.
44. Liu RM, Gaston Pravia KA. Oxidative stress and

glutathione in TGF-β-mediated fibrogenesis. Free Radic Biol Med. 2010; 48:1-15.
45. Coudriet GM, He J, Trucco M, Mars WM, Piganelli JD. Hepatocyte growth factor modulates interleukin-6 production in bone marrow derived macrophages: implications for inflammatory mediated diseases. PloS one. 2010; 5:e15384.
46. Seong GJ, Hong S, Jung SA, Lee JJ, Lim E, Kim SJ, Lee JH. TGF-β-induced interleukin-6 participates in transdifferentiation of human Tenon's fibroblasts to myofibroblasts. Mol Vis. 2009; 15:2123-2128.
47. Ishikawa H, Jo J, Tabata Y. Liver anti-fibrosis therapy with mesenchymal stem cells secreting hepatocyte growth factor. J Biomater Sci Polym Ed. 2012; 23:2259-2272.
48. Gallo S, Sala V, Gatti S, Crepaldi T. Cellular and molecular mechanisms of HGF/Met in the cardiovascular system. Clin Sci (Lond). 2015; 129:1173-1193.
49. Touvron M, Escoubet B, Mericskay M, Angelini A, Lamotte L, Santini MP, Rosenthal N, Daegelen D, Tuil D, Decaux JF. Locally expressed IGF1 propeptide improves mouse heart function in induced dilated cardiomyopathy by blocking myocardial fibrosis and SRF-dependent CTGF induction. Dis Model Mech. 2012; 5:481-491.
50. Hu L, Lin X, Lu H, Chen B, Bai Y. An overview of hedgehog signaling in fibrosis. Mol Pharmacol. 2015; 87:174-182.

(Received July 22, 2019; Revised October 8, 2019; Accepted October 14, 2019)

Original Article

DOI: 10.5582/bst.2019.01274

Elevated level of miR-17 along with decreased levels of TIMP-1 and IL-6 in plasma associated with the risk of in-stent restenosis

Feng Jiang[1,2,§], Xi Zhang[1,§], Ying-Min Lu[3], Yi-Gang Li[4], Xin Zhou[1,*], Yao-Sheng Wang[1,4,*]

[1] *Clinical Research Unit, Xinhua Hospital Affiliated with Shanghai Jiao Tong University School of Medicine, Shanghai, China;*
[2] *Scientific Research Center, Xinhua Hospital Affiliated with Shanghai Jiao Tong University School of Medicine, Chongming Branch, Shanghai, China;*
[3] *Cardiology, Xinhua Hospital Affiliated with Shanghai Jiao Tong University School of Medicine, Chongming Branch, Shanghai, China;*
[4] *Cardiology, Xinhua Hospital Affiliated with Shanghai Jiao Tong University School of Medicine, Shanghai, China.*

Summary **In-stent restenosis is highly related to the deposition of inflammatory extracellular matrix and the migration of endothelial and vascular smooth muscle cells. The miR-17/TIMP-1/interleukin pathway regulates vascular matrix remodeling and plays an important role in the inflammatory reaction. This study identified miR-17 and its related biomarkers in serum that potentially indicated susceptibility to in-stent restenosis (ISR) after coronary artery stenting. Subjects were 42 patients with single de novo coronary artery lesions who underwent regular coronary angiography one year after percutaneous coronary intervention. The clinical baseline information was recorded. Serum levels of biomarkers (including miR-17, TIMP-1, IL-6, IL-8, IL-2R, TNF-alpha, IL-10, and IL-1beta) were measured with real-time PCR or ELISA. Intergroup comparisons were used to compare patients with or without ISR. Compared to levels in the non-restenosis group, the serum miR-17 level was significantly higher (3.13 ± 0.22 *vs*. 1.06 ± 0.04, $p < 0.01$) and the serum TIMP-1 and IL-6 levels were significantly lower in the ISR group (TIMP-1: 0.33 ± 0.04 *vs*. 1.00 ± 0.05, $p < 0.01$; IL-6: 1.64 ± 0.18 *vs*. 3.52 ± 0.11, $p < 0.01$). Moreover, the levels of TIMP-1 and IL-6 decreased as the level of miR-17 increased. Spearman's correlation analysis indicated that the miR-17 level was inversely correlated with TIMP-1 and IL-6 levels. Findings suggest that an elevated level of miR-17 and decreased levels of TIMP-1 and IL-6 may be associated with the risk of ISR, which is in accordance with vascular matrix remodeling and an inflammatory reaction during the pathologic process of ISR. This study highlighted the potential for miR-17, TIMP-1, and IL-6 to serve as biomarkers for ISR.**

Keywords: miR-17, TIMP-1, IL-6, in-stent restenosis

Released online in J-STAGE as advance publication October 30, 2019.

[§]These authors contributed equally to this work.
**Address correspondence to:*
Dr. Yao-Sheng Wang, Cardiology, Xinhua Hospital Affiliated with Shanghai Jiao Tong University School of Medicine, Yangpu District, Shanghai 200092, China.
E-mail: wangyaosheng@xinhuamed.com.cn

Dr. Xin Zhou, Clinical Research Unit, Xinhua Hospital Affiliated with Shanghai Jiao Tong University School of Medicine, Yangpu District, Shanghai 200092, China.
E-mail: zhouxin@xinhuamed.com.cn

1. Introduction

Percutaneous coronary intervention (PCI) is currently the main method to treat coronary heart disease. Stent implantation is commonly used as for coronary intervention. There is a certain proportion of in-stent restenosis (ISR) after stent implantation that causes problems clinically. ISR involves many pathologic mechanisms, including intraplaque inflammation, lipid deposition, proliferation of vascular smooth muscle cells, endoluminal thrombus formation, and intraplaque

angiogenesis. These induce endothelial dysfunction and the instability of plaque. The recent incidence of ISR has decreased with the widespread use of drug-eluting stents (DESs). However, ISR still occurs in approximately 10% of patients receiving DESs, and ISR during the long-term period after stent implantation (more than 6 months) has not effectively improved (*1,2*). Given to the pathological characteristics of ISR after intracoronary stent implantation with PCI, potential biomarkers to indicate susceptibility to ISR need to be identified.

The inflammatory properties of the permanent coating applied on stent struts that allows controlled drug release are one of the key factors for ISR in patients receiving DESs. However, a nonselective anti-proliferative drug that is released on endothelial regeneration increases the risk of late and very late stent thrombosis (*3*).

MicroRNA (miRNA, miR) is highly conserved short non-coding RNA. miRNA can bind to the 3' end untranslated region (UTR) of the corresponding target mRNA and inhibit translation or promote degradation of mRNA at the post-transcriptional level (*4*). Recent studies have indicated that an imbalance in expression of miRNAs is closely related to the occurrence and development of diseases (*5*). To some extent, specific miRNAs can be considered as biomarkers of various cardiovascular diseases and may inspire effective ways to diagnose and evaluate cardiovascular diseases. Because of the stability of miRNAs in whole blood, plasma, or serum, numerous studies have speculated that specific miRNAs in peripheral circulating blood can be used as early warning indicators of various cardiovascular diseases (*6,7*). Basic studies have revealed significant changes in the expression of miRNAs that relate to endothelial growth and smooth muscle proliferation after balloon injury (*8*). miR-17, miR-21, miR-125, and miR-126 have been widely reported as regulators of inflammation and angiogenesis. Such miRNAs can be used as biomarkers and possible targets for interventions in the process of arterial injury and repair (*9-11*). Thus, ISR may also be accompanied by the expression of specific miRNAs. The molecular biological mechanism of ISR after PCI can be described at the level of identifying a series of miRNAs and corresponding downstream gene targets.

In light of these previous studies, the current study measured the levels of several key miRNAs, as well as corresponding specific targets, in patients with and without ISR. The aim of this study was to assess their value as potential molecular markers for ISR.

2. Materials and Methods

2.1. *Study subjects*

Subjects were 14 patients who underwent PCI one year earlier. Patients had single de novo coronary artery lesions and underwent regular coronary angiography (CAG) at Xinhua Hospital from October 2014 to October 2017. All 14 patients had ISR. Patients received standard dual therapy with aspirin 100 mg/day and clopidogrel 75 mg/day. Patients who suffered an acute myocardial infarction within one year of PCI were excluded. Twenty-eight patients without ISR who had single de novo coronary artery lesions and similar baseline characteristics served as the control group. ISR was defined as the presence of > 50% diameter stenosis in the stented segment. The study followed the principles outlined in the Declaration of Helsinki and it was approved by the ethics committee.

2.2. *Plasma collection*

Patients routinely underwent CAG one year after coronary artery PCI stent implantation. Some blood samples are left for clinical biochemical examination when blood vessels are punctured during CAG. The residual blood from clinical tests was collected at the time of routine follow-up. Plasma samples were collected by centrifugation (15 minutes at 1,200 × g) within 30 minutes, preserved in RNase-free tubes, and stored at -80°C for extraction of RNA.

2.3. *RNA isolation*

Total RNA was extracted using a Trizol-based miRNA isolation protocol (Tiangen, China). Plasma was lysed with Trizol at a 1:3 ratio. After 5 min, 0.8 mL of chloroform per 1 mL of sample was added. The three phases (aqueous, inter, and organic) were obtained by centrifugation at 4°C and 12,000 rpm for 15 min. The aqueous phase was then transferred to a fresh tube, and 2.0 mL of isopropanol per 1 mL of sample was added and incubated for 10 min. Total RNA was precipitated after samples were centrifuged at 12,000 × g for 10 min at 4°C. The supernatant was removed, and the RNA pellet was washed with 1 mL of 75% ethanol and subsequently centrifuged at 7,500 × g for 5 min at 4°C. After the ethanol was removed, the RNA pellet was briefly air-dried and dissolved in RNase-free water. The RNA concentrations were measured with a NanoDrop ND-1000 spectrophotometer (NanoDrop Technologies, USA), and the RNA samples were stored at −80°C for future use.

2.4. *Detection and analysis of miRNAs and TIMP-1 mRNA by qRT-PCR*

A real-time quantitative reverse-transcription polymerase chain reaction (qRT-PCR) was used to determine the expression of miRNAs. Pure RNA (OD 1.8-2.2) was reverse-transcribed (RT) to cDNA at 42°C for 30 min using mirVana™ miRNA detection

Table 1. Nucleotide sequences of primers used for PCR amplification

Primer name	Forward primer(5'-3')	Reverse primer(5'-3')
miR-17	GCGGCCAAAGTGCTTACAGTG	CAGCCACAAAAGAGCACAAT
miR-21	ACACTCCAGCTGGGTAGCTTATCAGACTGA	TGGTGCGTGGAGTCG
miR-125	GTCCCTGAAGCCCTTTAACC	AACCTCACCTGTGACCCTG
miR-126	CATTATTACTTTTGGTACGC	GTCGTATCCAGTGCGTGTCGTG
TIMP-1	CTTCTGGCATCCTGTTGTTG	GGTATAAGGTGGTCTGGTTG
U6	GTGCTCGCTTCGGCAGCACATATAC	AAAAATATGGAACGCTTCACGAATTTG

Table 2. Characteristics of patients with or without restenosis

Items	With restenosis (n = 14)	Without restenosis (n = 28)	p value
Gender (% male)	50.00	64.29	0.374
Age (years)	66.29 ± 1.61	67.54 ± 1.72	0.645
BMI (kg/m^2)	24.22 ± 0.58	23.66 ± 0.48	0.490
Hypertension, %	71.43	75.00	0.804
Hypercholesterolemia, %	78.57	71.43	0.620
Diabetes, %	35.71	32.14	0.817
Current smoker, %	35.71	39.29	0.822
Current alcohol drinker, %	35.71	42.86	0.675
Family history of CVD, %	50.00	57.14	0.661

kits (Thermo Fisher Scientific, USA), according to the manufacturer's instructions. cDNA (2 μL) was used as the template for qRT-PCR. Plasma expression of miRs was detected using SYBR Green miRNA qRT-PCR kits (Tiangen, China), according to the manufacturer's protocol with a Real-Time PCR System (Bio-Rad, USA). A melting curve analysis was performed at the end of the PCR cycle to validate the specificity of the expected PCR product. U6 was used as an internal control due to its prolonged and stable expression throughout all the evaluated samples. The relative level of expression of each miRNA was determined using the comparative CT method, which was defined as $2^{-\Delta Ct}$. For mRNA analysis, cDNA was synthesized using a cDNA Synthesis Kit (Bio-Rad, USA) and was subjected to 40 cycles of quantitative PCR with SYBR Premix (Takara, Japan) in the Real-Time PCR Detection System. Glyceraldehyde-3-phosphate dehydrogenase (GAPDH) was used as an internal control. Each sample from each study subject was analyzed with PCR in triplicate. The primers for analysis are summarized in Table 1.

2.5. *Biochemical and clinical assays*

Levels of IL-6, IL-8, IL-2R, TNF-alpha, IL-10 and IL-1beta were measured using ELISA kits (IBL-America, USA). Related health parameters, clinical history, personal history, and family history were recorded.

2.6. *Statistical analysis*

Results are expressed as the mean ± SD. A two-tailed Student's t test was used to compare two groups. Two-way ANOVA was used to compare multiple groups, and analyses were performed using GraphPad Prism 6.0. Logistics regression analysis was performed to evaluate risk factors for ISR, and receiver operating characteristic (ROC) analysis was perform to access the efficiency of distinguishing patients with ISR from patients without ISR (using STATA 14.0). A p-value of < 0.05 was considered statistically significant.

3. Results

3.1. *Clinical characteristics of subjects*

The general characteristics of patients with ISR (n = 14) and patients without ISR (n = 28), including gender, age, BMI, a family history of cardiovascular disease, a history of hypertension, hypercholesterolemia, or diabetes, and related risk factors are summarized in Table 2. More than half of the patients had hypertension, hypercholesterolemia, or a family history of cardiovascular disease. Similar characteristics were noted in patients with or without restenosis ($p > 0.05$ for all). The BMI of patients with restenosis (24.22 ± 0.58 kg/m^2) was slightly higher than that of patients without restenosis (23.66 ± 0.48 kg/m^2), and patients without restenosis were 1 year older than patients with restenosis; these differences were not significant.

3.2. *Circulating miRs and corresponding target gene levels in patients with or without ISR*

Real-time PCR analysis was used to measure plasma

levels of miR-17, miR-21, miR-125, and miR-126. The miR-17 level was significantly higher in patients with ISR compared to patients without ISR ($p < 0.01$), as shown in Figure 1. The average level of miR-17 was 3.13 ± 0.22 in patients with ISR and 1.06 ± 0.04 in patients without ISR. There was no significant difference in the levels of miR-21, miR-125, and miR-126 between the two groups. TIMP-1, as the downstream target of miR-17, was expressed at a lower level in patients with ISR compared to that in patients without ISR ($p < 0.05$). The TIMP-1 level was 0.33 ± 0.04 in patients with ISR and 1.00 ± 0.05 in patients without ISR. A logistic regression model indicated that miR-17 was significantly associated with a risk of ISR (odds ratio [OR]: 7.2254, $p < 0.01$, 95% confidence interval [CI]: 1.9825–26.3331), and TIMP-1 was also significantly related to ISR (OR: 0.002, $p < 0.01$, 95% CI: 0.00005–0.098).

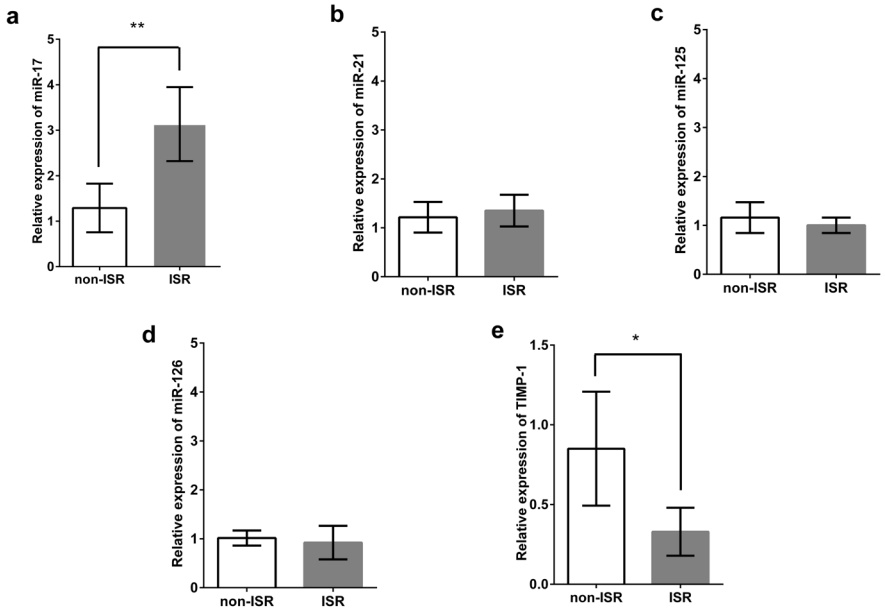

Figure 1. The expression of miR-17 (a), miR-21 (b), miR-125 (c), miR-126 (d), and TIMP-1(e) in plasma was evaluated with real-time PCR.

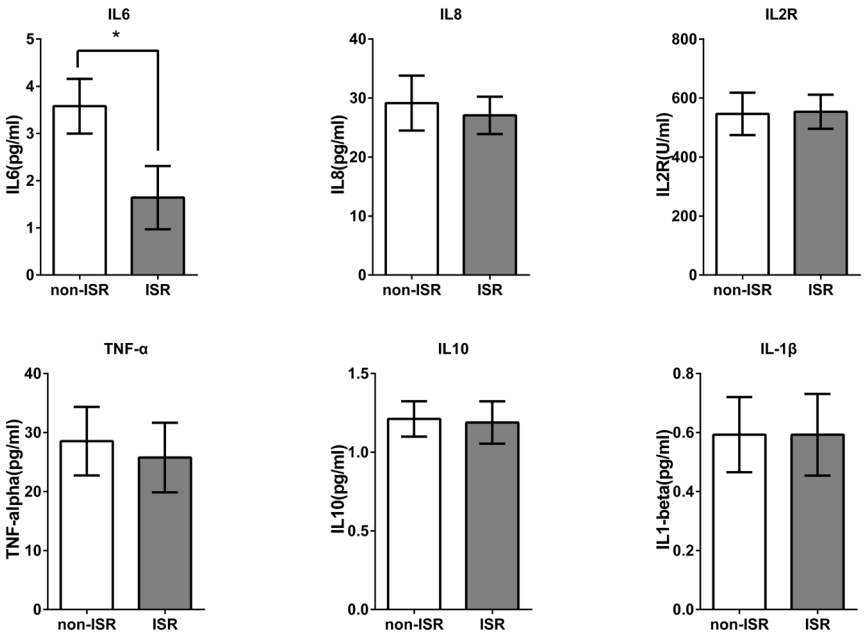

Figure 2. The plasma levels of IL-6 (a), IL-8 (b), IL-2R (c), TNF-alpha (d), IL-10 (e), and IL-1beta (f) were measured in patients with or without ISR.

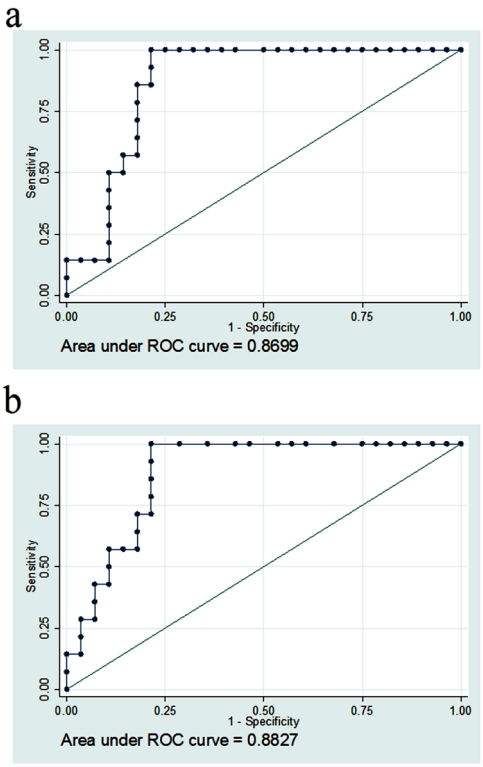

Figure 3. ROC curve analysis using plasma miR-17(a) and TIMP-1(b) to distinguish in-stent restenosis.

3.3. *Inflammatory marker levels in patients with or without ISR*

As shown in Figure 2, IL-6 levels were lower in patients with ISR than those in the patients without ISR ($p < 0.01$). The mean level of IL-6 in patients with ISR was 1.64 ± 0.18, while that in patients without ISR was 3.52 ± 0.11. However, significant differences in the levels of IL-8, IL-2R, TNF-alpha, IL-10, and IL-1beta were not noted in patients with or without ISR ($p > 0.05$ for all). The mean levels of IL-8, IL-2R, TNF-alpha, IL-10, and IL-1beta were 27.1 ± 3.17, 554 ± 57.9, 25.8 ± 5.9, 1.19 ± 0.13, and 0.50 ± 0.52 in patients with ISR and 29.1 ± 4.64, 546 ± 71.8, 28.5 ± 5.8, 1.21 ± 0.11, and 0.57 ± 0.50 in patients without ISR, respectively.

3.4. *ROC analysis of miR-17 and TIMP-1*

To investigate the relationship between the miR-17, TIMP-1, and ISR, ROC analyses were performed to evaluate the diagnostic ability of miR-17 and TIMP-1. As shown in Figure 3, the ROC curves for miR-17 and TIMP-1 reflected a strong distinction between patients with or without ISR, with an AUC of 0.8699 (95% CI: 0.75868–0.98112, $p < 0.001$) and 0.8827 (95% CI: 0.78159–0.98372, $p < 0.001$), respectively. miR-17 and TIMP-1 had a specificity of 78.57% and 78.57% in patients with ISR. miR-17 and TIMP-1 had a specificity of 85.71% and 92.86% in patients without ISR. miR-17 and TIMP-1 displayed acceptable sensitivity and specificity for the diagnosis of ISR.

4. Discussion

Recent studies have suggested that circulating miRNAs are useful biomarkers for the diagnosis of CVD. Several miRNAs have been found to take part in the pathogenesis of coronary artery disease (*12*) and atherosclerosis (*13*), but few studies focused on specific miRNAs related to ISR, which can be detected in circulating blood. miR-17, miR-21, miR-125, and miR-126 are commonly mentioned as corresponding to the pathologic process of ISR. One study found a higher level of expression of circulating miR-21 in patients with ISR (*14*). A point worth noting is that miR-21 and miR-126 are respectively related to ACS (*15*) and AMI (*16*), which may preclude their suitability for a specific diagnosis. On the basis of widely reported chip screening of miRNAs, the current study detected significantly higher plasma levels of miR-17 in patients with ISR *via* quantitative detection of real-time PCR. Given its clinical use, miR-17 is one biomarker with a higher specificity but not lower circulating expression, and it is more suitable for use as a diagnostic method.

Previous studies focused on the screening of miRs, since their levels of expression change in ISR, but little attention was paid to the corresponding downstream target gene levels or related effective factors, as a change at one point is usually not sufficient to support a potential diagnosis. The current study found that TIMP-1, a downstream target of miR-17, was expressed at lower levels in patients with ISR compared to levels in patients without ISR. Levels of expression of the inflammatory biochemical factor IL-6 were also lower in patients with ISR. These results indicated changes in the circulating cascade of miR-17/TIMP-1/IL-6 in patients with ISR, which closely coincide with the inflammatory response signaling pathway revealed by basic research. These observations indicate that miR-17 and its downstream factors are likely to allow predictive tests to diagnose ISR.

miR-17 has been widely studied. The coding area of miR-17 is located within an 800 base-pair region of human chromosome 13. miR-17 plays an essential role in the development of the human heart, lungs, and immune system (*17*). A study has revealed that miR-17 is involved in inflammation and oxidative stress, which are mechanisms relevant to macrophage polarization (*18*). miR-17 is also hypoxia-responsive; it may induce protective autophagy and counter apoptosis in vascular smooth muscle cells and contributes to vascular smooth muscle cell proliferation (*19,20*).

Based on bioinformatic analysis and experimental validation, TIMP-1 was identified as a target gene of miR-17. As previously reported, a functional study indicated that a decrease in TIMP-1 was responsible for

the upregulation of miR-17 (*21*).

ISR has been associated with the activation of matrix metalloproteinases (MMPs) and downregulation of their endogenous inhibitors (tissue inhibitor of matrix metalloproteinases [TIMPs]), which results in degradation of the artery wall matrix and decreased elasticity and which contributes to endothelial inflammation and vascular hyperpermeability (*22*). Expression of miR-17 is higher during ISR, resulting in decreased expression of its target-TIMPs and thus limiting potent inhibition of MMP-2 activity by TIMPs. Because TIMPs are essential to reducing inflammation, TIMP-1 (as a tissue inhibitor of MMPs) is expected to be lower in the pathologic process of ISR. The current study further demonstrated that these changes in levels of expression, according to the inflammatory pathway, can be readily detected in the circulation.

IL-6 is considered to be a pro-inflammatory lipocytokine. From molecular biology perspective, there is a negative correlation between TIMPs and IL-6. Mechanistic studies indicated that loss of TIMPs promoted production of IL-6, and recombinant adenovirus Ad-hTIMP-1 inhibited the inflammatory response and downregulated the expression of IL-6 (*23*). Blood levels of IL-6 were higher while blood levels of TIMP-1 were lower in individuals with unstable atherosclerotic plaque in their coronary arteries compared to individuals with stable atherosclerotic plaque (*24*). One year after PCI, IL-6 was lower than normal; this is because the inflammatory response in ISR was not merely equal to that in atherosclerotic injury. In the process of vascular wall repair after stent implantation, IL-6 changes nonlinearly, and only IL-6 plays an important role in the inflammatory response phase. IL-6 peaks 24 hours after drug-eluting stent implantation and then begins to decline (*25*). After restenosis occurs, the peak period of traumatic inflammation passes and the stable stage of an inflammatory reaction begins.

Previous studies on the primary mechanism underlying ISR mainly focused on the exaggerated neointimal proliferative response. Research has firmly established that proliferation and migration of VSMCs are critical cellular events responsible for the development of neointimal hyperplasia and that phenotypic modulation (transformation from a contractile to synthetic phenotype) of VSMCs plays an important role in this process. The current study verified the inflammatory cascade of ISR from another angle. Commonly, inflammatory-related factors are more widely distributed in the circulation. The current study quantitative measured key markers of the ISR cascade based on reported chip screening, and these findings are highly consistent with results of previous mechanistic studies.

The current study provides clinical evidence that circulating miR-17, TIMP-1, and IL-6 can serve as specific biomarkers for ISR. However, the small number of enrolled patients from a single center is a major limitation that must be considered. Further large-scale studies are needed to validate the clinical utility of miRs and their downstream target genes as practical biomarkers for ISR. Moreover, this study is a cross-sectional case-control study, and prospective follow-up studies should be conducted to better assess the predictive value of biomarkers for ISR.

Acknowledgements

This work was supported by the National Natural Science Foundation of China [81974022], the Clinical Research Project of Shanghai Municipal Health Committee [201940206] and the fund of Chongming Branch of Xinhua Hospital [YL201801].

References

1. Stettler C, Wandel S, Allemann S, *et al*. Outcomes associated with drug-eluting and bare-metal stents: A collaborative network meta-analysis. Lancet. 2007; 370:937-948.
2. Luscher TF, Steffel J, Eberli FR, Joner M, Nakazawa G, Tanner FC, Virmani R. Drug-eluting stent and coronary thrombosis: Biological mechanisms and clinical implications. Circulation. 2007; 115:1051-1058.
3. Joner M, Finn AV, Farb A, Mont EK, Kolodgie FD, Ladich E, Kutys R, Skorija K, Gold HK, Virmani R. Pathology of drug-eluting stents in humans: Delayed healing and late thrombotic risk. J Am Coll Cardiol. 2006; 48:193-202.
4. Zhang Y, Yun Z, Gong L, Qu H, Duan X, Jiang Y, Zhu H. Comparison of miRNA Evolution and Function in Plants and Animals. Microrna. 2018; 7:4-10.
5. Gao J, Ma X, Zhang Y, Guo M, Shi D. The role of microRNAs in prethrombotic status associated with coronary artery disease. Thromb Haemost. 2017; 117:429-436.
6. Backes C, Meese E, Keller A. Specific miRNA disease biomarkers in blood, serum and plasma: Challenges and prospects. Mol Diagn Ther. 2016; 20:509-518.
7. Kondkar AA, Abu-Amero KK. Utility of circulating microRNAs as clinical biomarkers for cardiovascular diseases. Biomed Res Int. 2015; 2015:821823.
8. Gareri C, De Rosa S, Indolfi C. MicroRNAs for restenosis and thrombosis after vascular injury. Circ Res. 2016; 118:1170-1184.
9. Staszel T, Zapala B, Polus A, Sadakierska-Chudy A, Kiec-Wilk B, Stepien E, Wybranska I, Chojnacka M, Dembinska-Kiec A. Role of microRNAs in endothelial cell pathophysiology. Pol Arch Med Wewn. 2011; 121:361-366.
10. Zhuang Y, Peng H, Mastej V, Chen W. MicroRNA regulation of endothelial junction proteins and clinical consequence. Mediators Inflamm. 2016; 2016:5078627.
11. Pereira-da-Silva T, Coutinho Cruz M, Carrusca C, Cruz Ferreira R, Napoleao P, Mota Carmo M. Circulating microRNA profiles in different arterial territories of stable atherosclerotic disease: A systematic review. Am J Cardiovasc Dis. 2018; 8:1-13.

12. Small EM, Olson EN. Pervasive roles of microRNAs in cardiovascular biology. Nature. 2011; 469:336-342.
13. Huber HJ, Holvoet P. Exosomes: Emerging roles in communication between blood cells and vascular tissues during atherosclerosis. Curr Opin Lipidol. 2015; 26:412-419.
14. He M, Gong Y, Shi J, *et al*. Plasma microRNAs as potential noninvasive biomarkers for in-stent restenosis. PLoS One. 2014; 9:e112043.
15. Oerlemans MI, Mosterd A, Dekker MS, de Vrey EA, van Mil A, Pasterkamp G, Doevendans PA, Hoes AW, Sluijter JP. Early assessment of acute coronary syndromes in the emergency department: the potential diagnostic value of circulating microRNAs. EMBO Mol Med. 2012; 4:1176-1185.
16. Zampetaki A, Willeit P, Tilling L, Drozdov I, Prokopi M, Renard JM, Mayr A, Weger S, Schett G, Shah A, Boulanger CM, Willeit J, Chowienczyk PJ, Kiechl S, Mayr M. Prospective study on circulating MicroRNAs and risk of myocardial infarction. J Am Coll Cardiol. 2012; 60:290-299.
17. Mogilyansky E, Rigoutsos I. The miR-17/92 cluster: A comprehensive update on its genomics, genetics, functions and increasingly important and numerous roles in health and disease. Cell Death Differ. 2013; 20:1603-1614.
18. Zhu D, Pan C, Li L, Bian Z, Lv Z, Shi L, Zhang J, Li D, Gu H, Zhang CY, Liu Y, Zen K. MicroRNA-17/20a/106a modulate macrophage inflammatory responses through targeting signal-regulatory protein alpha. J Allergy Clin Immunol. 2013; 132:426-436 e428.
19. Hao MX, Wang X, Jiao KL. MicroRNA-17-5p mediates hypoxia-induced autophagy and inhibits apoptosis by targeting signal transducer and activator of transcription 3 in vascular smooth muscle cells. Exp Ther Med. 2017; 13:935-941.
20. Chen T, Zhou Q, Tang H, Bozkanat M, Yuan JX, Raj JU, Zhou G. miR-17/20 controls prolyl hydroxylase 2 (PHD2)/hypoxia-inducible factor 1 (HIF1) to regulate pulmonary artery smooth muscle cell proliferation. J Am Heart Assoc. 2016; 5. pii: e004510.
21. Shi J, Bei Y, Kong X, *et al*. miR-17-3p contributes to exercise-induced cardiac growth and protects against myocardial ischemia-reperfusion injury. Theranostics. 2017; 7:664-676.
22. Kumar S, Kim CW, Simmons RD, Jo H. Role of flow-sensitive microRNAs in endothelial dysfunction and atherosclerosis: Mechanosensitive athero-miRs. Arterioscler Thromb Vasc Biol. 2014; 34:2206-2216.
23. Zhao LL, Song YQ, Zhang Y, Shi Y, Ren M, Liu S, Mao YM. Effects of overexpression of human tissue inhibitor of metalloproteinase-1 on the inflammatory response in rats with myocardial infarction and related mechanisms. Zhonghua Xin Xue Guan Bing Za Zhi. 2017; 45:513-518. (in Chinese)
24. Ragino Iul, Cherniavskii AM, Polonskaia Ia V, Volkov AM, Kashtanova EV, Tsymbal S, Polovnikova EM. Inflammatory-destructive biomarkers of atherosclerotic plaques instability. Study of arterial wall and blood. Kardiologiia. 2012; 52:37-41. (in Russian)
25. Guimaraes TS, da Rocha LA, Becari C, Piccinato CE, Joviliano RD, Ribeiro MS, Joviliano EE. The role of interleukins and inflammatory markers in the early restenosis of covered stents in the femoropopliteal arterial segment. Ann Vasc Surg. 2018; 50:88-95.

(Received August 28, 2019; Revised October 21, 2019; Accepted October 25, 2019)

Original Article

DOI: 10.5582/bst.2019.01190

Neuron loss and dysfunctionality in hippocampus explain aircraft noise induced working memory impairment: a resting-state fMRI study on military pilots

Huijuan Cheng[1,2,§], Guodong Sun[1,3,§], Mei Li[1], Minhong Yin[1], Hao Chen[1,2,*]

[1] *Lanzhou University Second Hospital, Lanzhou, Gansu, China;*
[2] *The Key Laboratory of the Digestive System Tumors of Gansu Province, Lanzhou, Gansu, China;*
[3] *The Regiment Medical Company, 96875 Army of PLA, Baoji, Shaanxi, China.*

Summary **Long-term aircraft noise exposure may cast a detrimental effect upon the working memory of military pilots, and the brain structural and functional bases of noise related cognitive impairment remains unclear. In this study, we enrolled 30 fighter jet pilots and 30 matched controls. The working memory performance of the subjects was measured with a neurobehavioral test battery including immediate verbal/visual memory and delayed verbal/visual memory tests. Structural MRI and resting-state functional magnetic resonance imaging (rs-fMRI) were utilized to quantify brain grey matter volumes (GMV), regional homogeneity (ReHo), amplitude of low-frequency fluctuation (ALFF) and fractional ALFF (fALFF) differences between the two groups. Furthermore, correlation analyses were performed to find the association between the neural imaging changes with individual neurobehavioral performance. The military pilots showed significantly lower accuracy in delayed verbal and visual memory tests in comparison to the controls, indicating a potential working memory deficit in this population. Structural MRI data and rs-fMRI data showed that the pilots displayed markedly decreased GMVs, ReHo and ALFF signals in the left hippocampus, suggesting neuron dysfunction of the hippocampus. Besides, ReHo and ALFF/fALFF analysis also revealed reduced ReHo in the left amygdala, left thalamus, left superior temporal gyrus and right superior/middle frontal gyrus, indicating disrupted local neural activity under chronic noise exposure. Furthermore, Spearman correlation analysis proved that the GMV and ReHo of left hippocampus were significantly associated with working memory accuracy. This study provided direct evidence of dysfunctional hippocampus serving as the structural and functional bases for neuropsychological impairment under aircraft noise exposure.**

Keywords: Aircraft noise, working memory, hippocampus, MRI

1. Introduction

The detrimental effects of aircraft noise on cognitive function and working memory are well documented (*1*). For instance, previous studies reported that aircraft noise may impair cognitive function of schoolchildren around airports, including recognition memory, attention and reading comprehension (*2*). Another study reported that nocturnal aircraft noise exposure induces significant delayed significant, linear impairments in reaction times (*3*). Compared with residents near airports, military pilots encounter more excessive aircraft noise while on duty. Noise levels generated by aircraft vary according to phase of flight as well as environmental factors, and ambient noise in the cockpit can reach as high as 80-120 dB along the flight. Previous studies have proved that ambient aircraft noise exposure injured hearing acuity of pilots and leads to hearing loss (*4*). Compared to the studies about hearing

Released online in J-STAGE as advance publication October 11, 2019.

[§]These authors contributed equally to this work.

**Address correspondence to:*
Dr. Hao Chen, The Key Laboratory of the Digestive System Tumors of Gansu Province, Lanzhou University Second Hospital, Lanzhou 730030, China.
E-mail: chenhao3996913@163.com

acuity, there are fewer studies on the cognitive and memory impairments associated with aircraft noise in the military pilot population.

Studies demonstrated that noise can lead to structural damages to the cochlea and hyperactivity in the central auditory pathway, including cochlear nucleus, inferior colliculus and auditory cortex at its traumatic levels (*5*). Besides, noise also triggers non-classical auditory-responsive brain areas (*e.g.* the lateral amygdala and striatum) and directly activates the emotion/fear system of the brain via the thalamus. In this way, noise can activate defense responses leading to activation of the hypothalamic–pituitary–adrenal (HPA) axis (*6*). Long-lasting activation of the HPA axis can lead to disturbed hormonal balance as well as morphometric and functional alteration of brain, which may be the potential mechanism of noise induced cognitive impairment (*7*). In a recent study in mice, chronic noise exposure adversely influenced the animals' behavior and brain structure. The noise stress caused HPA-axis hyperactivity, a reduction of size in the hippocampus, medial prefrontal cortex (mPFC), and amygdala, a reduced neuronal density in the mPFC and dentate gyrus (DG), and lower performance in all cognitive and motor tasks (*8*). Similarly, another study in mice revealed that noise may alter the long-term potentiation (LTP) and place cell activity in the hippocampus, and thus lead to spatial memory impairment (*9*). However, although a series of animal studies declared the brain morphometric with functional alteration under noise exposure, there's still a lack of direct human evidence of brain structural and functional bases of cognitive impairment.

In order to solve this problem, we focus on the military pilot population and try to reveal structural and functional alteration of the human brain under excessive aircraft noise exposure. Neuroimaging techniques, including anatomical T1-weighted MRI and resting-state functional MRI (rs-fMRI), allow us to accomplish this purpose. Anatomical T1-weighted MRI was routinely used for voxel-based morphology (VBM) to explore possible changes in grey matter volume (GMV); in turn, regional homogeneity (ReHo) analysis based on rs-fMRI can reflect the intrinsic functional organization and the endogenous neurophysiological process of the human brain, providing pertinent information on core mechanisms of neuropsychological disorders (*10*). We hypothesized that modified GMV and ReHo in certain brain regions will be revealed in comparison to those of the control population and these brain regions with differences may be associated with the working memory function of the subjects. To our knowledge, this is the first neuroimaging study comprehensively clarifing the potential cognitive and neuroimaging status in military pilots, which will help to elucidate the core mechanism of neuropsychological impairment under chronic aircraft noise exposure.

2. Materials and Methods

2.1. *Subjects*

30 male subjects in exposure group were randomly extracted from the 105 fighter jet pilots aged between 30-35 in an air force base in Gansu, China, while 30 male subjects in the control group were enrolled from the 429 military officers in an air force hospital in Gansu. All subjects in the two groups were matched by age, working life and education status. Excluded from the study were subjects who had a history of smoking and alcohol drinking, family history of neuropsychological diseases and exposure to audiological risk factors outside work (noise trauma, bomb, mine or other explosions, and use of firearms). For pilots in the exposure group, a Class-1 sound level meter (Brüel & Kjær, Denmark) was used to measure the equivalent continuous noise level in the cockpit of the fighter jet during the latest fight. The flight hours from the start of the pilot's working life were calculated by means of a questionnaire and a check on personal archives.

The protocol of this study was approved by the Ethics Committee of the Medical Faculty of Second Hospital of Lanzhou University (registry no. 2017A-074) and all study elements were conducted in accordance with ethical principles for medical research involving human subjects as defined in the Declaration of Helsinki. All subjects were fully aware of the study procedures and signed informed consent forms (ICFs).

2.2. *Working memory tests*

A neuropsychological test battery consisting of four computerized tests, were employed to assess the immediate verbal memory (IVBM), immediate visual memory (IVIM), delayed verbal memory (DVBM) and delayed visual memory (DVIM) of the subjects. All the verbal/visual memory tests were performed in the system of CNS Vital Signs (*http://www.cnsvs.com/*) (11,12).

2.3. *MRI image acquisition*

MRI were acquired using the General Electric Discovery MR750 3.0T systems (General Electric Co. Ltd., Connecticut, USA) in the Second Hospital of Lanzhou University. Standard T1-weighted 3D anatomical data were acquired using the 3D magnetization-prepared rapid gradient echo (3D MPRAGE) sequence (repetition time: 2530 ms; echo time: 3.5 ms; flip angle: 7°; field of view: 256 mm × 256 mm; matrix: 256 × 256; slice thickness: 1 mm; section gap: 0 mm; number of slices: 192, voxel size = 1 × 1 × 1 mm^3).

Rs-fMRI data were acquired with echo planar imaging (EPI) sequence (repetition time: 2000 ms;

echo time: 30 ms; flip angle: 90°; field of view: 220 mm × 220 mm; acquisition/reconstruction matrix: 128 × 128; slice thickness: 4 mm; section gap: 0.6 mm; number of slices: 30, scam time: 6min; voxel size = 3 × 3 × 3 mm^3) covering the entire brain. A custom-built head coil cushion and earplugs were used to minimize head motion and dampen scanner noise. During data acquisition, subjects were asked to remain alert with eyes closed and keep their head still.

2.4. *Structural MRI analysis*

Structural MRI data was analyzed by voxel-based morphometry (VBM) in Statistical Parametric Mapping software (SPM8, Wellcome Department of Cognitive Neurology, London, UK; *http://www.fil.ion.ucl.ac.uk/spm/*) in MATLAB R2014a (MathWorks Inc., Natick, MA, USA) (*13*). Data processing steps were performed according to Ashburner. We applied Diffeomorphic Anatomical Registration through Exponentiated Lie Algebra (DARTEL), which is implemented as a toolbox for SPM8 and enables the creation of a set of group-specific templates. Its performance on non-linear registration algorithms is better than that of other similar toolboxes. Brain images were segmented, normalized and modulated by using these templates. Registered images were then transformed to Montreal Neurological Institute (MNI) space, and finally, the normalized and modulated images were smoothed with a 6 mm full-width at half-maximum (FWHM) Gaussian kernel (*14,15*).

2.5. *Rs-fMRI preprocessing and analysis*

Rs-fMRI data pre-processing was then performed using the SPM8 and Data Processing Assistant for Resting-state fMRI Advanced (DPARSFA) tools. Prior to pre-processing, the first 10 volumes were discarded to reach a steady-state magnetization and allow participants to adapt to the scanning noise. For each subject, fMRI data were first adjusted for slice timing and head-motion (exclusion criteria: N 2.5 mm translation and/or N3.0° rotation). Then, the standard MNI template provided by SPM was further used for normalization with resampling to 3 mm × 3 mm × 3 mm voxels and spatially smoothed using a 4 mm × 4 mm × 4 mm full with a half-maximum Gaussian kernel. Next, a band-pass filter of 0.01 to 0.08 Hz was applied to the data in temporal frequency space to minimize low-frequency signal drift and high frequency variations due to cardiac and respiratory effects. In nuisance covariates regression, we selected the 6 head motion parameters, white matter signal, global mean signal, and cerebrospinal fluid signal as nuisance variables and regressed them out (*16,17*). The results are shown at $p < 0.05$ using false discovery rate (FDR) correction (with a combination of a threshold of $p < 0.001$ and a mini-mum cluster size of 65 voxels).

Voxel-based comparison of ReHo were conducted in Resting State fMRI Data Analysis Toolkit (REST) Version 2.0 (*http://restfmri.net/forum/REST_V2.0*). Computation of ReHo at resting state was performed as previously described. Briefly, Kendall's coefficient of concordance (KCC) for each voxel in the brain was calculated voxel-wise by applying a cluster size of 26 voxels. For standardization purposes, each individual ReHo map was divided by that subject's global mean brain KCC value to minimize inter-individual variability for statistical analysis within the whole-brain mask. Results are shown at $p < 0.05$ using AlphaSim correction (with a combination of a threshold of $p < 0.01$ and a mini- mum cluster size of 65 voxels) (*18,19*).

Using the preprocessed images, very low-frequency drift and high-frequency noise was first filtered (band-pass, 0.01~0.08Hz), then amplitude of low-frequency fluctuation (ALFF) were built according to standard procedures established by previous research (*20*). The filtered time series was transformed to the frequency domain using the fast Fourier transform (FFT) and the power spectrum was then obtained. The square root was calculated at each frequency of the power spectrum and taken as the ALFF. Furthermore, in order to eliminate physiological signals, fractional ALFF (fALFF) was also performed (*21*). Similar to ALFF, the square root was calculated at each frequency of the power spectrum. The sum of amplitude across 0.01-0.08 Hz was divided by that across the entire frequency range, *i.e.*, 0-0.25 Hz. Both the subject-level ALFF and fALFF were converted into a z-score map by subtracting the mean ALFF of the whole brain and dividing by the standard deviation (*22,23*). Results are shown at $p < 0.05$ using AlphaSim correction (with a combination of a threshold of $p < 0.01$ and a mini- mum cluster size of 65 voxels) (*18,19*).

2.6. Statistical analysis

Student *t* test was applied to assess differences of demographic and neurobehavioral parameters between the two groups. Spearman correlation coefficients were separately computed to examine correlations between GMV/ReHo and neuropsychological parameters. All statistical analyses were performed with R 3.1.3 (*https://www.r-project.org*). $p < 0.05$ was considered statistically significant.

3. Results

3.1. *Demographic information and noise exposure level*

Demographic information of the military pilots in the exposure group and controls are listed in Table 1. There were no significant difference between age, work lives and education status of the two groups. The flight hours

Table 1. Demographic information of the subjects in the exposure and control groups

Parameters	Exposure group (Military pilots of fighter jets) $n = 30$	Control group (Military officers in hospital) $n = 30$	t value	p value
Age (year)				
Mean (SD)	32.67 ± 1.19	33.07 ± 1.37	– 1.230	0.224
Range	30.1 – 34.4	30.6 – 34.9		
Working life (year)				
Mean (SD)	10.00 ± 1.72	10.37 ± 1.96	– 0.771	0.444
Range	7 – 12	7 – 14		
Education status (year)				
Mean (SD)	16.27 ± 0.69	16.07 ± 0.94	0.936	0.353
Range	15 – 18	15 – 19		

Table 2. Descriptive values (mean ± SD) and statistics of the working memory tests

Tests	Numbers of correct responses		t value	p value
	Exposure group	Control group		
IVBM	26.13 ± 2.65	26.40 ± 2.11	0.431	0.668
IVIM	22.67 ± 2.23	23.17 ± 2.23	0.868	0.389
DVBM*	24.60 ± 3.13	26.23 ± 2.70	2.166	0.034
DVIM**	19.00 ± 3.27	21.47 ± 3.25	2.933	0.005

IVBM, immediate verbal memory; IVIM, immediate visual memory; DVBM, delayed verbal memory; DVIM, delayed visual memory. *, $p < 0.05$; **, $p < 0.01$.

of the pilots in the exposure group were 840-1520 h, while the average equivalent continuous noise level in the cockpit was 108.6 ± 2.4 dB.

3.2. *Working memory measurements*

The results of the working memory tests are displayed in Table 2. There was no significant difference between the exposure and control group for the numbers of correct responses in IVBM and IVIM tests ($p = 0.668$ & 0.389, respectively). However, the numbers of correct responses in DVBM and DVIM tests were significantly less in the exposure group compared to control group ($p = 0.034$ & 0.005, respectively).

3.3. *VBM analysis of GMV changes*

Structural imaging analysis using VBM revealed brain structural differences between exposure and control group. Exposure group was observed to have less GMV in the left hippocampus, right middle frontal gyrus and right inferior parietal lobule compared with control group (t-test, $|t| > 3.02$, $p < 0.002$, $p < 0.05$ FDR corrected). What's more, exposure group was also found to have more GMV in the left caudate body. See details in Figure 1 and Table 3.

3.4. *ReHo analysis of rs-fMRI data*

Functional imaging analysis based on rs-fMRI was performed to investigate the ReHo differences between the two groups. Compared to control group, exposure group showed significantly lower ReHo values in the left amygdala, left hippocampus, left thalamus and right middle/superior frontal gyrus (t-test, $|t| > 2.70$, $p < 0.01$, AlphaSim corrected). In the meantime, exposure group showed higher ReHo values in the left cingulate and the right inferior temporal gyrus, compared to the control group. See details in Figure 2 and Table 4.

3.5. *ALFF/fALFF analysis of rs-fMRI data*

Furthermore, we used the ALFF/fALFF analysis based on rs-fMRI to examine neural activity changes after noise exposure. As shown in Table 5 and Figure 3, significantly lower ALFF signals were found in the left hippocampus, thalamus and the superior temporal gyrus, and significantly lower fALFF signals were observed in left middle temporal gyrus and left superior frontal gyrus, by which we confirmed that noise causes disrupted local neural activity in these regions, exactly. What's more, our analysis also showed significantly increased ALFF signals in the postcentral gyrus (Brodmann area 6, 22, 42, 43) and posterior cerebellum lobe. See details in Figure 3 and Table 5.

3.6. *Correlation between neurobehavioral performance and neuroimaging parameters*

In order to understand the effects of aircraft noise exposure on brain structure and function, we conducted correlation analyses between the performance of working memory tests and the corresponding GMV and ReHo of brain regions with significant differences between the two groups. As a result, the GMV of left hippocampus showed significantly positive associations with the DVIM accuracy (Figure 4A, $p = 0.0278$, $r = 0.3122$), while the ReHo of left hippocampus were

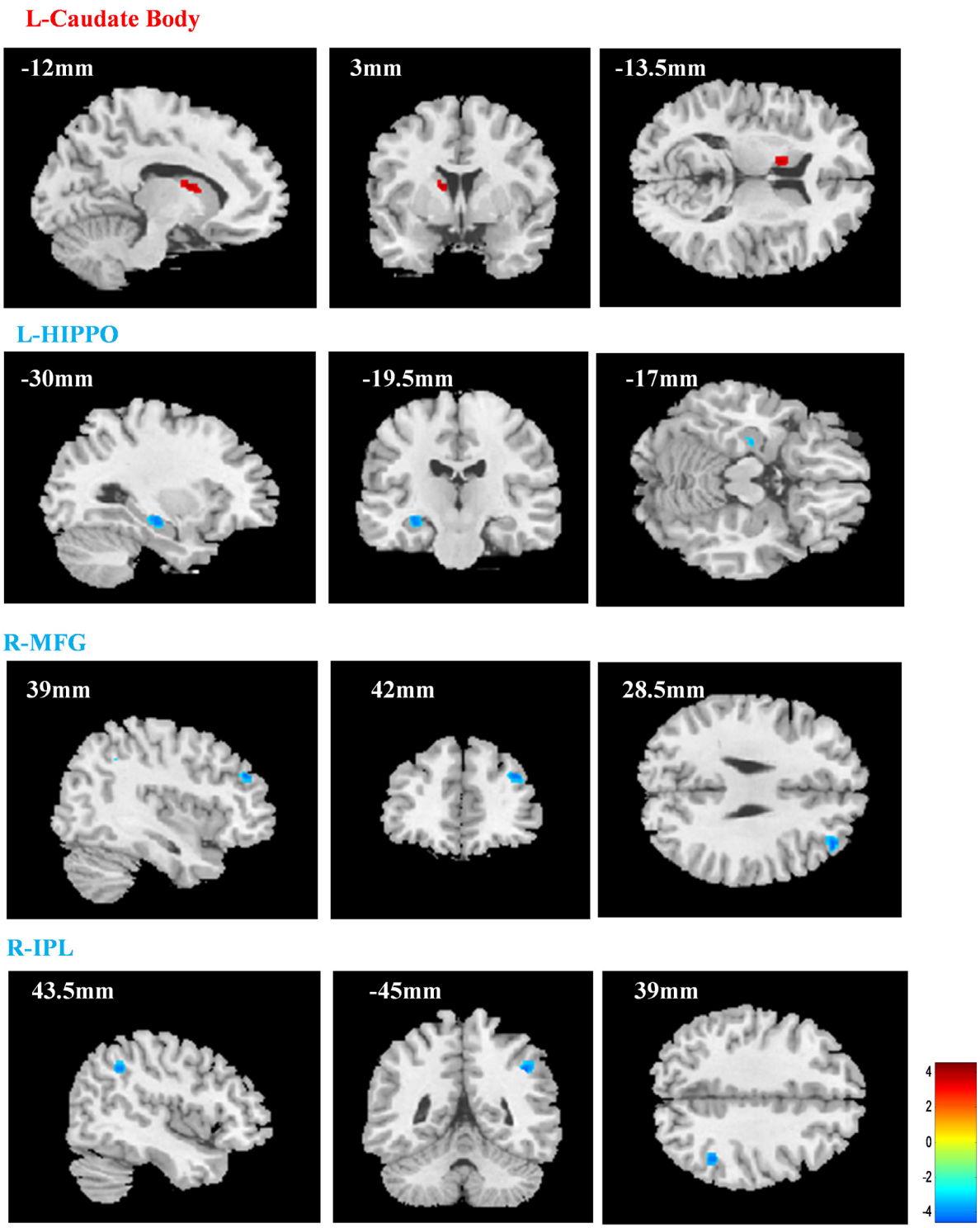

Figure 1. Regional GMV changes in subjects of exposure group compared with those of control group. Significantly increased GMV were seen in left caudate body (L-Caudate Body); significantly decreased areas were observed in the left hippocampus (L-HIPPO), the right middle frontal gyrus (R-MFG), and the right inferior parietal lobule (R-IPL). The red areas indicate high GMV brain regions and the blue areas indicate lower ones. The significance level was set at $p < 0.002$, $p < 0.05$ FDR corrected.

positively associated with DVBM accuracy (Figure 4B, $p = 0.0016$, $r = 0.434$) and DVIM accuracy (Figure 4C, $p = 0.0036$, $r = 0.4046$), respectively. What's more, as for the DVIM accuracy, we also found that it negatively associated with ReHo of the right superior frontal gyrus (Figure 4D, $p = 0.0178$, $r = -0.3362$) and the left amygdala (Figure 4E, $p = 0.0444$, $r = -0.2862$), respectively.

4. Discussion

Considering that the principal confounding factors were

Table 3. Regions showing significantly different GMV by comparing exposure and control group

Brain region	R/L	MNI coordinate (mm)			Volume (m^3)	Peak T value
		x	y	z		
Exposure < Control						
Hippocampus/Hippocampus_L (aal)	L	-30	-19.5	-17	151	-4.219
Middle Frontal Gyrus/Frontal_Mid_R (aal)	R	39	42	28.5	140	-4.373
Inferior Parietal Lobule/Parietal_Inf_R (aal)	R	43.5	-48	39	109	-4.377
Exposure < Control						
Caudate Body/Caudate_L (aal)	L	-12	3	13.5	131	3.715

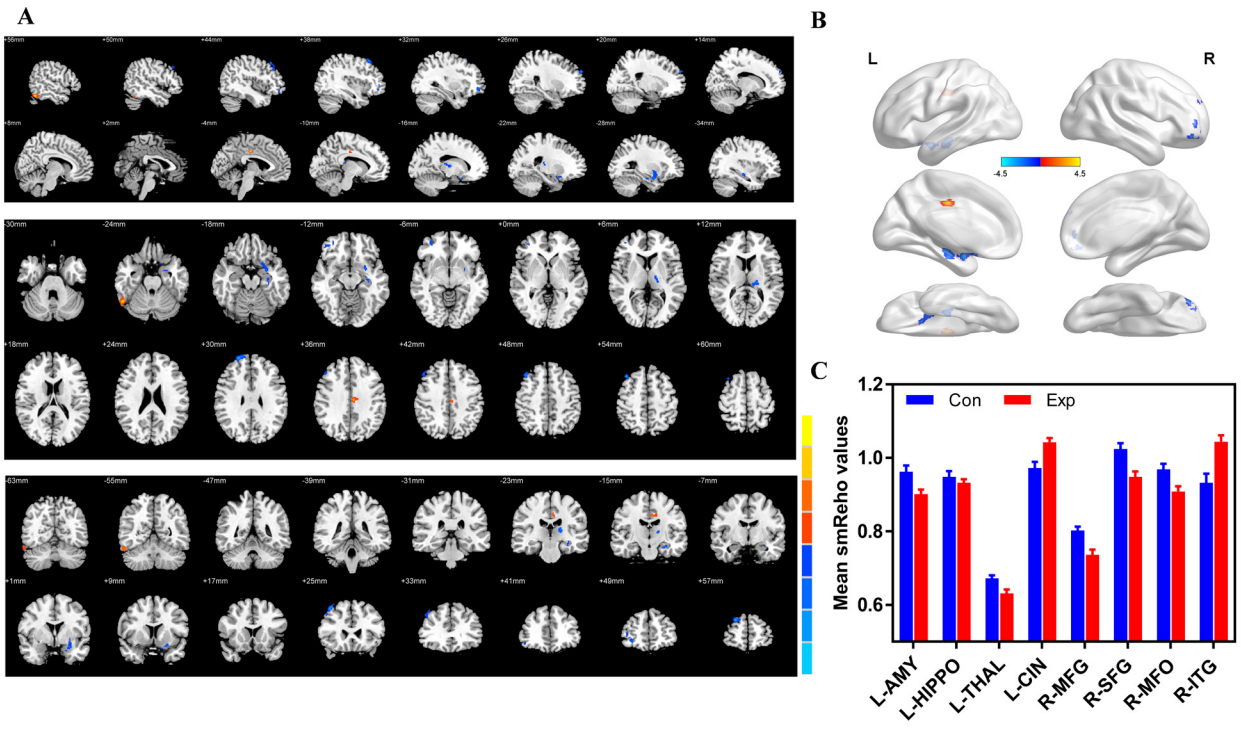

Figure 2. Regional ReHo value changes in subjects in exposure groups compared with control group. (A) MNI x,y,z plot and **(B)** BrainNet surface model shows that significantly increased areas were seen in Inferior Temporal Gyrus (R-ITG) and the left Cingulate Gyrus (L-CIN). Significantly decreased areas were observed in the left hippocampus (L-HIPPO), the left amygdala (L-AMY), the left thalamus (L-TH), the right middle frontal gyrus (R-MFG) and the right superior frontal gyrus (R-SFG). The red areas indicate high GMV brain regions and the blue areas indicate lower ones (*t*-test, $|t| > 2.70$, $p < 0.01$, AlphaSim corrected). **(C)** The mean smoothed ReHo values between the exposure and the control group subjects.

Table 4. Regions showing significantly different ReHo by comparing Control and Experiment group

Brain region	R/L	MNI coordinate (mm)			Volume (m^3)	Peak T value
		x	y	z		
Exposure < Control						
Amygdala/Amygdala_L (aal)	L	-28	0	-20	3645	-3.440
Hippocampus/Hippocampus_L (aal)	L	-32	-18	-12	1863	-3.369
Thalamus/Thalamus_L (aal)	L	-20	-20	12	2727	-3.369
Middle Frontal Gyrus/Frontal_Mid_R (aal)	R	42	28	50	4266	-4.108
Superior Frontal Gyrus/Frontal_Sup_R (aal)	R	24	58	30	2187	-4.021
Middle Frontal Gyrus/Frontal_Mid_Orb_R (aal)	R	32	48	-8	2592	-3.269
Exposure > Control						
Cingulate Gyrus/Cingulum_Mid_L (aal)	L	-6	-18	38	2160	4.118
Inferior Temporal Gyrus/Temporal_Inf_R (aal)	R	56	-58	-22	2727	4.082

Table 5. Regions showing significantly different ALFF/fALFF by comparing Control and Experiment group

Brain region	R/L	MNI coordinate (mm)			Volume (m^3)	Peak T value
		x	y	z		
ALFF						
Exposure < Control						
Superior Temporal Gyrus/Temporal_Sup_L (aal)	L	-46	-18	-20	149	-3.711
Hippocampus/Hippocampus_L (aal)	L	-28	2	-10	255	-4.561
Thalamus/Thalamus_L (aal)	L	-18	-24	10	200	-3.956
Exposure > Control						
Postcentral Gyrus/Postcentral_R (aal) (Brodmann area 6, 22, 42, 43)	R	62	-4	12	126	3.935
fALFF						
Exposure < Control						
Pons/Brainstem	-	-4	-18	-40	132	-4.940
Occipital Lobe/Occipital_Mid_L (aal)	L	-22	-68	16	150	-4.061
Middle Temporal Gyrus/Temporal_Mid_L (aal)	L	-48	-76	8	128	-3.761
Superior Frontal Gyrus/Frontal_Sup_L (aal)	L	-14	28	58	198	-4.786
Exposure > Control						
Cerebellum Posterior Lobe/Cerebelum_Crus1_R (aal)	R	26	-92	-30	218	4.316

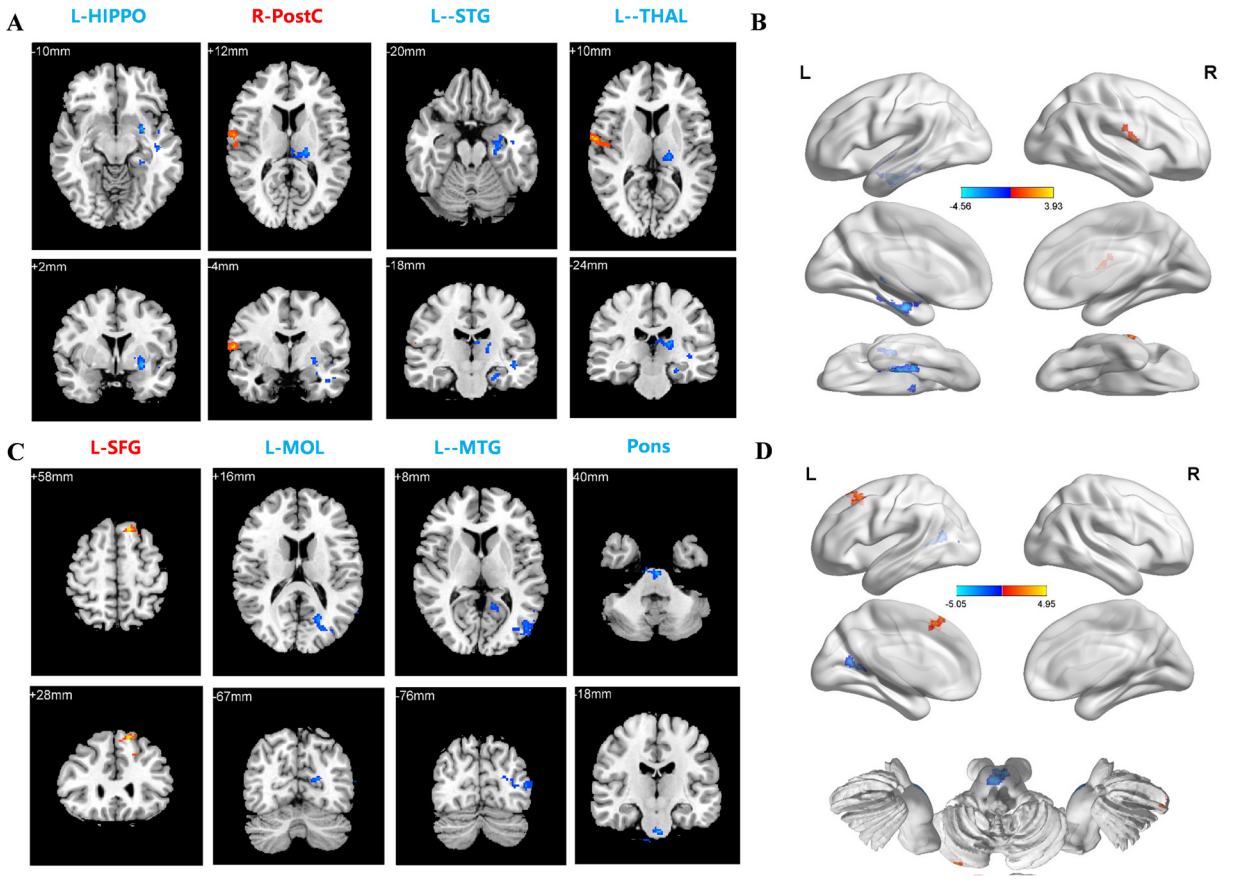

Figure 3. ALFF/fALFF signal changes in subjects in exposure group compared with control group. (A) MNI x,y,z plot and **(B)** BrainNet surface model showed that significantly decreased areas in ALFF analysis were found in the left superior temporal gyrus (L-STG), the left hippocampus (L-HIPPO) and the left thalamus (L-TH); And that significantly decreased areas in ALFF analysis were found in the postcentral gyrus (Brodmann area 6, 22, 42, 43). **(C)** MNI x,y,z plot and **(D)** BrainNet surface model showed that significantly decreased areas in fALFF analysis were found in Pons, the right occipital Lobe (L-MOL), and also the left middle temporal gyrus (L-MTG) and the superior frontal gyrus (L-STG); significantly increased areas in fALFF analysis were found in the cerebellum posterior lobe.

excluded from the study and that pilots and controls investigated were matched by age, working life and education status, the above-mentioned results suggest that exposure to aircraft noise in military pilots may lead to working memory impairment as well as brain structural and functional alteration.

In this study, we found that the DVBM and DVIM accuracies of military pilots were significantly lower than those of control military officers, indicating that long-term aircraft noise exposure may cast a detrimental

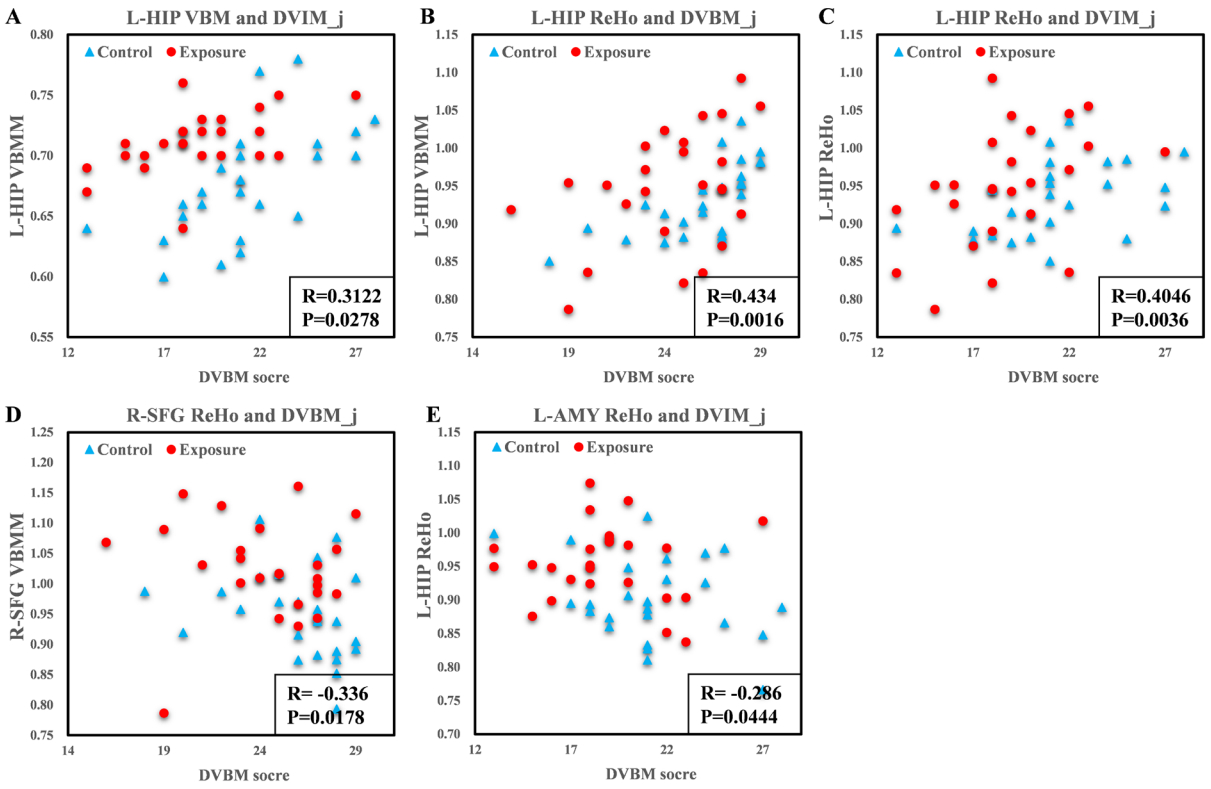

Figure 4. Scatterplots of significantly correlated DVBM/DVIM scores derived from the behavioral experiment against the neuroimaging parameters. (A) Scatterplot of DVIM scores against the GMV of left hippocampus (L-HIP). **(B)** Scatterplot of DVBM scores against the ReHo value of left hippocampus (L-HIP) **(C)** Scatterplot of DVIM scores against the ReHo value of left hippocampus (L-HIP) **(D)** Scatterplot of DVBM scores against the ReHo value of the right superior frontal gyrus (R-SFG). **(E)** Scatterplot of DVIM scores against the ReHo value of the left amygdala (L-AMY).

influence upon the working memory of humans. This result is consistent with earlier studies corroborating that noise exposure leads to memory impairment for both humans and non-human animals. Kempen *et al.* demonstrated that children attending schools with higher road or aircraft noise levels made significantly more errors in switching attention tests and digit memory span tests (*24*). Similarly, Loganathan *et al.* found an adverse effect of noise exposure on working memory in rodents exposed to simulated noise (*25*). Interestingly, significant differences between the two groups were only found in DVBM\DVIM tests rather than IVBM/IVIM tests. According to earlier studies, in the Munich Airport Study, Evans *et al.* found that children from noise exposed communities had more errors on a difficult subscale of German standardized reading tests than children from quiet communities; while the two groups did not differ on easy and intermediate portions of the test (*26*). Considering that DVBM\DVIM tests were more difficult than IVBM/IVIM, it can be concluded that performance on complex memory tasks is more susceptible to the effects of noise than performance on simple tasks.

By resting functional imaging analysis, we found decreased GMV, ReHo and ALFF in left hippocampi, indicating potential neuron loss and disrupted local functionality in these brain regions. Hippocampus is a medial temporal lobe structure which plays an important role in working memory (*27*). Adult hippocampal neurons are balanced by three main cellular events: cell proliferation, neuronal differentiation, and cell survival (*28*). According to previous studies, chronic hyperactivity of HPA-axis induced by noise stress can elevate the hippocampal corticosteroid receptors, lead to reduced hippocampal neurogenesis, cell proliferation, and impaired spatial memory in rodents (*29,30*). Besides, long-lasting elevated corticosterone levels also lead to increased apoptosis in the dentate gyrus of hippocampus, which has been shown in mice exposed to noise (*31*). Thus, we posit that neuron loss in hippocampi may be caused by reduced neurogenesis and proliferation as well as elevated cellular apoptosis under stress. Furthermore, noise exposure leads to abnormal synaptic plasticity in the structure and function of the hippocampus, temporal lobe, and amygdala. Noise also increases norepinephrine/noradrenaline (NE) and dopamine (DA) levels in hippocampus, while decreases serotonin 5 hydroxyindoleacetic acid (serotonin 5-HT) level (*32*). We inferred these alterations of synaptic plasticity and neurotransmitters may be contributing to the neural dysfunctionality in hippocampi we found in this study and lead to impaired learning and memory behavior.

The hippocampus is part of the limbic system, and plays important roles in the consolidation of information

from short-term memory to long-term memory, and in spatial memory that enables navigation (*27*). Neuron loss in hippocampus leads to memory impairment in aging and various neuropsychological disorders. For instance, previous VBM studies indicated that atrophy and neuron loss in hippocampus can significantly predict memory recall & storage performances in behavioral frontotemporal dementia, which is in accordance with our findings (*33*). Furthermore, similar to our results, decreased ReHo and ALFF in hippocampus were also observed in mild cognitive impairment patients compared to normal controls, which lead to increased errors in spatially-related memory tasks (*34*). Taken together, the structural and functional abnormalities noted in hippocampus in this study may be the key to working impairment under long-term aircraft noise exposure, which was further corroborated by the significant positive correlations between the DVBM\DVIM accuracies and the ReHo in the left hippocampus.

In this study, by resting functional imaging analysis, reduced neural activities were also found in left amygdala, left thalamus, left superior temporal gyrus and right superior/middle frontal gyrus. Amygdala, hippocampus, and frontal cortex are essential components of the neural circuitry mediating stress responses. The amygdala provides a primary association between subcortical areas, which are responsible for producing fear, and cerebral cortical areas receiving sensory information about the external environment (*35*). There is evidence of noise stress induced activation of the HPA-axis, amygdala, and other brain circuits and in producing abnormalities in timid and emotional or anxiety-like behaviors (*36*). Herein, we inferred that the functional alteration in these regions may be the result of HPA-axis hyperactivity.

In the meantime, we also found that the GMV of the left caudate body significantly increased in the exposure group. The basal ganglia have traditionally been viewed as motor processing nuclei; however, functional neuroimaging evidence has implicated these structures in more complex cognitive and affective processes that are fundamental for a range of human activities (*37*). In our analysis, however, the left caudate body GMV change did not correlate with the working memory score, suggesting that it may not function on working memory in cognitive function. Further research will discuss the possible relation of basal ganglia with other motor or cognitive function.

Interestingly, we found more noise induced neuron loss and neural dysfunction in left cerebrum, in comparison with the right side. Brain damage would be more likely to affect the left hemisphere in both childhood or adulthood, including epilepsy and stroke. According to radiological studies, there would be a biological basis for the higher vulnerability of the left hemisphere. The main pathogenetic factor seems to be a hemodynamic one, responsible for insufficient blood supply to the left hemisphere (*38*). The left hemisphere is also more vulnerable to traumatic stress and environmental stress. For example, Zhang *et al*. reported decreased GMV in the left hemisphere in flood disaster survivors with recent onset posttraumatic stress disorder (*39*), while Chen *et al*. observed both neuron loss and disrupted neural activities in the left hemisphere (rather than right hemisphere) after chronic hypoxia exposure (*10*), which is consistent with our results. We inferred that detrimental noise exposure may induce hemodynamic changes in the left hemisphere, and thus make it more vulnerable to the structural and functional abnormality.

Some limitations of the study must be recognized. First, like other population studies on noise stress, the neurobehavioral and neuroimaging findings in this study may be influenced by individual factors, ever-changing environments and co-exposure to other environmental pollutants or toxicants. To solve this problem, the potential confounding factors like age, work life and education status have been matched in the two groups. Besides, the subjects in exposure and control group were all enrolled from air force units and their education and work experience were quite similar to each other. A further study should be conducted to reveal the dose-effect relationship between the neurobehavioral impairment and neuroimaging abnormality. Second, the sample size of this study is relatively small, which should be expanded in future studies.

In conclusion, the current study demonstrates that long-term aircraft noise may lead to working memory impairment in jet fighter pilots. The hippocampus and other cognition region displayed both neuron loss and reduced local neural activities under chronic noise stress, which were further proved to be associated with neurobehavioral performance. Taken together, the detrimental impact of aircraft noise exposure on cognition should be considered in health maintenance of military pilots. A dysfunctional hippocampus may serve as structural and functional bases for neuropsychological impairment under exposure.

Acknowledgements

This study was financially supported by the National Science Foundation of China (No. 81470791, 81670594, 31770537).

References

1. Chen H, Kwong JC, Copes R, Tu K, Villeneuve PJ, van Donkelaar A, Hystad P, Martin RV, Murray BJ, Jessiman B, Wilton AS, Kopp A, Burnett RT. Living near major roads and the incidence of dementia, Parkinson's disease, and multiple sclerosis: A population-based cohort study. Lancet. 2017; 389:718-726.
2. van Kempen E, van Kamp I, Lebret E, Lammers J,

Emmen H, Stansfeld S. Neurobehavioral effects of transportation noise in primary schoolchildren: a cross-sectional study. Environ Health. 2010; 9:25.
3. Elmenhorst EM, Elmenhorst D, Wenzel J, Quehl J, Mueller U, Maass H, Vejvoda M, Basner M. Effects of nocturnal aircraft noise on cognitive performance in the following morning: Dose-response relationships in laboratory and field. Int Arch Occup Environ Health. 2010; 83:743-751.
4. Gordon B, Joachims Z, Cohen HB, Grossman A, Derazne E, Carmon E, Zilberberg M, Levy Y. Hearing loss in Israeli air force aviators: Natural history and risk factors. Mil Med. 2016; 181:687-692.
5. Jafari Z, Kolb BE, Mohajerani MH. Noise exposure accelerates the risk of cognitive impairment and Alzheimer's disease: Adulthood, gestational, and prenatal mechanistic evidence from animal studies. Neurosci Biobehav Rev. 2019. pii: S0149-7634(18)30897-2.
6. Burow A, Day HE, Campeau S. A detailed characterization of loud noise stress: Intensity analysis of hypothalamo-pituitary-adrenocortical axis and brain activation. Brain Res. 2005; 1062:63-73.
7. Rojas-Rueda D, Vrijheid M, Robinson O, Gunn Marit A, Grazuleviciene R, Slama R, Nieuwenhuijsen M. Environmental burden of childhood disease in Europe. Int J Environ Res Public Health. 2019; 16. pii: E1084.
8. Jafari Z, Kolb BE, Mohajerani MH. Chronic traffic noise stress accelerates brain impairment and cognitive decline in mice. Exp Neurol. 2018; 308:1-12.
9. Kim JJ, Lee HJ, Welday AC, Song E, Cho J, Sharp PE, Jung MW, Blair HT. Stress-induced alterations in hippocampal plasticity, place cells, and spatial memory. Proc Natl Acad Sci U S A. 2007; 104:18297-18302.
10. Chen X, Zhang Q, Wang J, *et al*. Cognitive and neuroimaging changes in healthy immigrants upon relocation to a high altitude: A panel study. Hu Hum Brain Mapp. 2017; 38:3865-3877.
11. Littleton AC, Register-Mihalik JK, Guskiewicz KM. Test-retest reliability of a computerized concussion test: CNS vital signs. Sports Health. 2015; 7:443-447.
12. Gualtieri CT, Johnson LG. Reliability and validity of a computerized neurocognitive test battery, CNS vital Signs. Arch Clin Neuropsychol. 2006; 21:623-643.
13. Matsuda H, Mizumura S, Nemoto K, Yamashita F, Imabayashi E, Sato N, Asada T. Automatic voxel-based morphometry of structural MRI by SPM8 plus diffeomorphic anatomic registration through exponentiated lie algebra improves the diagnosis of probable Alzheimer Disease. AJNR Am J Neuroradiol. 2012; 33:1109-1114.
14. Kim GW, Kim YH, Jeong GW. Whole brain volume changes and its correlation with clinical symptom severity in patients with schizophrenia: A DARTEL-based VBM study. PloS One. 2017; 12:e0177251.
15. Chen Z, Li L, Sun J, Ma L. Mapping the brain in type II diabetes: Voxel-based morphometry using DARTEL. Eur J Radiol. 2012; 81:1870-1876.
16. Yu E, Liao Z, Tan Y, Qiu Y, Zhu J, Han Z, Wang J, Wang X, Wang H, Chen Y, Zhang Q, Li Y, Mao D, Ding Z. High-sensitivity neuroimaging biomarkers for the identification of amnestic mild cognitive impairment based on resting-state fMRI and a triple network model. Brain Imaging Behav. 2019; 13:1-14.
17. Chao-Gan Y, Yu-Feng Z. DPARSF: A MATLAB toolbox for "Pipeline" data analysis of resting-state fMRI. Front Syst Neurosci. 2010; 4:13.
18. Cordova-Palomera A, Tornador C, Falcon C, Bargallo N, Nenadic I, Deco G, Fananas L. Altered amygdalar resting-state connectivity in depression is explained by both genes and environment. Hum Brain Mapp. 2015; 36:3761-3776.
19. Foster GE, Davies-Thompson J, Dominelli PB, Heran MK, Donnelly J, duManoir GR, Ainslie PN, Rauscher A, Sheel AW. Changes in cerebral vascular reactivity and structure following prolonged exposure to high altitude in humans. Physiol Rep. 2015; 3. pii: e12647.
20. Yan CG, Wang XD, Zuo XN, Zang YF. DPABI: Data processing & analysis for (resting-state) brain imaging. Neuroinformatics. 2016; 14:339-351.
21. Zou QH, Zhu CZ, Yang Y, Zuo XN, Long XY, Cao QJ, Wang YF, Zang YF. An improved approach to detection of amplitude of low-frequency fluctuation (ALFF) for resting-state fMRI: fractional ALFF. J Neurosci Methods. 2008; 172:137-141.
22. Cantou P, Platel H, Desgranges B, Groussard M. How motor, cognitive and musical expertise shapes the brain: Focus on fMRI and EEG resting-state functional connectivity. J Chem Neuroanat. 2018; 89:60-68.
23. Li Z, Kadivar A, Pluta J, Dunlop J, Wang Z. Test-retest stability analysis of resting brain activity revealed by blood oxygen level-dependent functional MRI. J Magn Reson Imaging. 2012; 36:344-354.
24. van Kempen EE, van Kamp I, Stellato RK, Lopez-Barrio I, Haines MM, Nilsson ME, Clark C, Houthuijs D, Brunekreef B, Berglund B, Stansfeld SA. Children's annoyance reactions to aircraft and road traffic noise. J Acoust Soc Am. 2009; 125:895-904.
25. Loganathan S, Rathinasamy S. Alteration in memory and electroencephalogram waves with sub-acute noise stress in albino rats and safeguarded by scoparia dulcis. Pharmacogn Mag. 2016; 12:S7-s13.
26. Bullinger M, Hygge S, Evans GW, Meis M, von Mackensen S. The psychological cost of aircraft noise for children. Zentralbl Hyg Umweltmed. 1999; 202:127-138.
27. Knierim JJ. The hippocampus. Curr Biol. 2015; 25:R1116-1121.
28. Kempermann G. Activity dependency and aging in the regulation of adult neurogenesis. Cold Spring Harb Perspect Biol. 2015; 7. pii: a018929.
29. Henckens MJ, van der Marel K, van der Toorn A, Pillai AG, Fernandez G, Dijkhuizen RM, Joels M. Stress-induced alterations in large-scale functional networks of the rodent brain. NeuroImage. 2015; 105:312-322.
30. Hu L, Yang J, Song T, Hou N, Liu Y, Zhao X, Zhang D, Wang L, Wang T, Huang C. A new stress model, a scream sound, alters learning and monoamine levels in rat brain. Physiol Behav. 2014; 123:105-113.
31. Gonzalez-Perez O, Chavez-Casillas O, Jauregui-Huerta F, Lopez-Virgen V, Guzman-Muniz J, Moy-Lopez N, Gonzalez-Castaneda RE, Luquin S. Stress by noise produces differential effects on the proliferation rate of radial astrocytes and survival of neuroblasts in the adult subgranular zone. Neurosci Res. 2011; 70:243-250.
32. Ravindran R, Rathinasamy SD, Samson J, Senthilvelan M. Noise-stress-induced brain neurotransmitter changes and the effect of Ocimum sanctum (Linn) treatment in albino rats. J Pharmacol Sci. 2005; 98:354-360.
33. Bertoux M, Flanagan EC, Hobbs M, Ruiz-Tagle A, Delgado C, Miranda M, Ibanez A, Slachevsky A, Hornberger M. Structural anatomical investigation of

long-term memory deficit in behavioral frontotemporal dementia. J Alzheimers Dis. 2018; 62:1887-1900.
34. Qing Z, Li W, Nedelska Z, Wu W, Wang F, Liu R, Zhao H, Chen W, Chan Q, Zhu B, Xu Y, Hort J, Zhang B. Spatial navigation impairment is associated with alterations in subcortical intrinsic activity in mild cognitive impairment: A resting-state fMRI study. Behav Neurol. 2017; 2017:6364314.
35. Wilson MA, Grillo CA, Fadel JR, Reagan LP. Stress as a one-armed bandit: Differential effects of stress paradigms on the morphology, neurochemistry and behavior in the rodent amygdala. Neurobiol Stress. 2015; 1:195-208.
36. Jafari Z, Mehla J, Kolb BE, Mohajerani MH. Prenatal noise stress impairs HPA axis and cognitive performance in mice. Sci Rep. 2017; 7:10560.
37. Arsalidou M, Duerden EG, Taylor MJ. The centre of the brain: Topographical model of motor, cognitive, affective, and somatosensory functions of the basal ganglia. Hum Brain Mapp. 2013; 34:3031-3054.
38. Taylor DC. Differential rates of cerebral maturation between sexes and between hemispheres. Evidence from epilepsy. Lancet. 1969; 2:140-142.
39. Zhang J, Tan Q, Yin H, Zhang X, Huan Y, Tang L, Wang H, Xu J, Li L. Decreased gray matter volume in the left hippocampus and bilateral calcarine cortex in coal mine flood disaster survivors with recent onset PTSD. Psychiatry Res. 2011; 192:84-90.

(Received July 22, 2019; Revised September 12, 2019; Accepted September 23, 2019)

Original Article

DOI: 10.5582/bst.2019.01282

Mutation analysis of the *SLC26A4* gene in three Chinese families

Cheng Wen[1,§], Shijie Wang[2,§], Xuelei Zhao[1], Xianlei Wang[1], Xueyao Wang[1], Xiaohua Cheng[1], Lihui Huang[1,*]

[1] *Beijing Tongren Hospital, Capital Medical University; Beijing Institute of Otolaryngology; Key Laboratory of Otolaryngology, Head and Neck Surgery, Ministry of Education, Beijing, China;*
[2] *No. 731 Hospital of China Aerospace Science and Industry Corp, Beijing, China.*

Summary **In order to investigate the genetic causes of hearing loss in a Chinese proband (in Family A) with enlarged vestibular aqueduct (EVA) and to investigate the genotype of two Chinese probands with *SLC26A4* singe-allelic mutation and normal hearing (in Families B and C, respectively), the three probands and their parents were clinically and genetically evaluated. Twenty exons and flanking splice sites of the *SLC26A4* gene were screened for pathogenic mutations *via* amplification with PCR and bidirectional sequencing. As controls, a group of 400 healthy newborns from the same ethnic background underwent *SLC26A4* gene screening using the same method. The three probands all harbored two mutations in the *SLC26A4* gene in the form of compound heterozygosity. The genotypes of mutations in Families A, B, and C are c.1211C>A/c.919-2A>G, c.1729G>A/c.919-2A>G, and c.1286C>A/c.919-2A>G, respectively. The missense mutations c.1211C>A (p.T430Q) in exon 10 and c.1729G>A (p.V577I) in exon 16 are both reported for the first time and were absent in 400 healthy newborns. c.1211C>A has Glutamine (Gln) at amino acid 430 instead of Threonine (Thr), and c.1729G>A has Isoleucine (Ile) at amino acid 577 instead of Valine (Val). c.1286C>A, a mutation previously reported in DVD and HGMD, was associated with Mondini deformity, but a proband with the c.1286C>A mutation in this study was normal. This study has demonstrated that the novel missense mutation c.1211C>A in compound heterozygosity with c.919-2A>G in the *SLC26A4* gene is likely to be the cause of deafness in Family A. A novel variant, c.1729G>A, was identified and is likely benign. The pathogenicity of the c.1286C>A mutation warrants more in-depth study. These findings will broaden the spectrum of known *SLC26A4* mutations in the Chinese population, providing more information for genetic counseling and diagnosis of hearing loss with EVA.**

Keywords: *SLC26A4*, novel mutation, enlarged vestibular aqueduct

1. Introduction

Deafness, which refers to various degrees of hearing loss, is one of the most common sensory disorders. The incidence of neonatal congenital deafness is approximately 1-3‰ (*1*). *SLC26A4* (OMIM 605646, also called the PDS gene, NM_000441.1) maps on 7q22-31 (DFNB4 locus) (*2*) and encodes a 780-amino-acid protein called pendrin, a member of the solute carrier 26 protein family that functions as a chloride iodide transporter in cell expression systems (*3*). Mutations in the *SLC26A4* gene are known to vary by region and ethnicity. Domestic data have indicated that *SLC26A4* is the second most common gene that causes nonsyndromic hearing loss (NSHL), accounting for 14.5% (4). To date, about 539 mutations have been identified. (*http://www.hgmd.cf.ac.uk/ac/gene.php?gene=SLC26A4*). Mutations in the SLC26A4 gene result in two typical phenotypes: *i*) the syndromic form, called Pendred syndrome (PS) (OMIM 274600), that

Released online in J-STAGE as advance publication October 27, 2019.

[§]These authors contributed equally to this work.

**Address correspondence to:*
Dr. Lihui Huang, Beijing Tongren Hospital, Capital Medical University; Beijing Institute of Otolaryngology; Key Laboratory of Otolaryngology, Head and Neck Surgery, Ministry of Education, No.17 Hougou Lane, Chongnei Street, Beijing 100005, China.
E-mail: huangpub@126.com

is characterized by hearing loss, goiter, and eventually hypothyroidism, with/without EVA or other inner ear malformations; *ii*) the nonsyndromic form, called DFNB4 or nonsyndromic EVA (OMIM 600791) (when EVA is present), that is characterized by hearing loss with/without EVA or other inner ear malformations (*5-7*).

Enlarged vestibular aqueduct (EVA) is an inner ear malformation of the temporal bone that predisposes patients to hearing loss from childhood as well as vestibular symptoms. Individuals with mutations in the *SLC26A4* may exhibit hearing loss, as well as EVA, at birth or during early childhood. Foreign data have revealed about 16-83.9% of patients with EVA have bi-allelic mutations in *SLC26A4* (including homozygous mutations and compound heterozygous mutations). Mono-allelic mutations in *SLC26A4* are found in about 16-36% of patients with EVA (*8-11*). NSHL with EVA is known to be typically characterized by congenital, bilateral sensorineural hearing loss (SNHL), which can be progressive and usually ranges from severe to profound (*12*).

Newborn genetic screening for deafness has been conducted in Beijing since 2012, and greater numbers of newborns with genes causing deafness have been detected. Dai and Huang reported that genetic screening of 180,469 infants revealed genes causing deafness in 8,136 (4.508%) (*13*). In 2017, the current authors' research team retrospectively analyzed 582 subjects with genetic mutations causing deafness and summarized the relationship between genotype and phenotype; results indicated that *SLC26A4* gene mutations were mainly associated with high-frequency hearing loss and profound-severe hearing loss (*14*). In addition, the *SLC26A4* gene is known to be closely associated with delayed-onset hearing loss and is often detected in deaf populations. Zhu *et al*. reported that the rate of homozygous and heterozygous mutations in the *SLC26A4* gene was 6.92% (22/318) and 18.55% (59/318), respectively, in 318 students with NSHL in Hebei Province, China (*15*). Later, the current authors' research group examined patients with a single-allele *SLC26A4* mutation revealed by newborn genetic screening for deafness. Zhao *et al*. found a variant of some type in 3.50% of these infants and a pathogenic mutation in 2.96% (*16*). The current authors examined patients with *SLC26A4* bi-allelic mutations and found a novel pathogenetic frameshift mutation, c.574delC (p.Leu192Ter), in 2018 (*17*). Later on, the current authors' team investigated how the *FOXI1* and *KCNJ10* genes were affected in infants with a single-allele mutation in the *SLC26A4* gene. Results suggested that individuals with an *SLC26A4* single-allele mutation, combined with *FOXI1* or *KCNJ10* gene mutations, do not suffer hearing loss during infancy (*18*).

Based on the studies mentioned above, the current authors noticed that three families warrant study and discussion. The current study investigated the *SLC26A4* gene in 4 members of one Chinese family with EVA and 6 members of two Chinese families with norming hearing. Two novel compound heterozygous mutations in *SLC26A4* were identified. The pathogenicity of the c.1286C>A (p.A429E) missense mutation warrants more in-depth study. The current findings will broaden the spectrum of *SLC26A4* mutations in the Chinese population.

2. Materials and Methods

Written informed consent was obtained from parents. The protocol was in accordance with the principles of the Declaration of Helsinki and was approved by the Ethics Committee of Beijing Tongren Hospital, Capital Medical University.

2.1. *Subjects and clinical evaluation*

One Chinese family with EVA and two Chinese families with normal hearing were recruited by Otolaryngology and Head and Neck Surgery, Beijing Tongren Hospital (Beijing, China). The proband had a c.919-2A>G single-allele mutation according to genetic screening for deafness (15 variants in 4 genes, including *GJB2* c.235delC, c.299delAT, c.176dell6, and c.35delG; *GJB3* c.538C>T; *SLC26A4* c.919-2A>G, c.2168A>G, c.1174A>T, C.1226G>A, c.1229C>T, c.1975G>C, c.2027T>A and c.IVS15+5G>A; and Mt 12SrRNA m.1555A>G and m.1494C>T). Clinical evaluation was performed and included family history, a detailed medical history, and a physical examination, including thyroid sonography and a high-resolution computed tomography (CT) scan of the temporal bone. Four hundred unrelated Chinese newborns with normal hearing were recruited as normal controls.

2.2. *Mutation analysis*

Genomic DNA was extracted from 2 mL of whole blood from each patient, using the Blood DNA kit (Tiangen Biotech, Beijing, China). Twenty exons and flanking splice sites of the *SLC26A4* gene were screened for mutations *via* amplification with PCR and bidirectional sequencing. Variants were interpreted in accordance with ACMG guidelines (*19*).

2.3. *Bioinformatics and validation of the variants*

Sequence data were analyzed by aligning them with the reference sequence of *SLC26A4* (NT_007933) from the National Center for Biotechnology Information (NCBI) using the software DNA Star 5.0. The 1000 Genomes Project database (*http://www.1000genomes.org/*), ClinVar (*https://www.st-va.ncbi.nlm.nih.gov/clinvar/*), the dbSNP database of NCBI (*http://www.ncbi.nlm.nih.*

gov/), and the Deafness Variation Database (*http://deafnessvariationdatabase.org/*) were used as references to assess the novelty of the mutations found in this study. Online tools including Mutation Taster, SIFT, CADD (v1.3.1) and PolyPhen-2 were used to predict the functional outcome of the variants. GERP and Phylop were used to score the conservation of the variants.

2.4. *Auditory evaluation*

Subjects underwent universal newborn hearing screening and had specific results. A comprehensive audiological evaluation was performed and included pure tone audiometry (PTA), auditory brainstem response (ABR), 40-Hz auditory event-related potential, distortion product otoacoustic emission (DPOAE), auditory steady-state response (ASSR), acoustic immittance, and pediatric behavioral audiometry. The hearing threshold was calculated as the average hearing level at 0.5, 1.0, 2.0, and 4.0 k Hz according to the 1997 World Health Organization standard. The severity of hearing impairment was defined as mild (26-40 dB), moderate (41-60 dB), severe (61-80 dB), or profound (> 80 dB). Owing to the young age of subjects, the ABR threshold and/or ASSR were recorded, and mean thresholds at frequencies in the 0.5-4 k Hz range were averaged to obtain an approximation for the directional conditioned reflex (*20,21*).

3. Results

3.1. *Clinical, audiological, and imaging data*

All members of the three families were negative for systemic and thyroid disease, and physical examination and otoscopy results were also normal. One subject 7 months of age in Family A had hearing loss, and pure-tone audiometry revealed normal hearing in the parents. This proband underwent universal neonatal hearing screening (UNHS) and was diagnosed with SNHL when first seen by a doctor at this Hospital at four months of age. The threshold of ABR air-conduction in the proband was 80 dB nHL on the right and 50 dB nHL on the left. The proband had a type "A" tympanogram, and the bilateral acoustic stapedial reflex was not elicited. DPOAE elicited no response from the patient in both ears. The results of objective audiometry and visual reinforcement audiometry (VRA) in the proband in Family A (4 months, 7 months, and

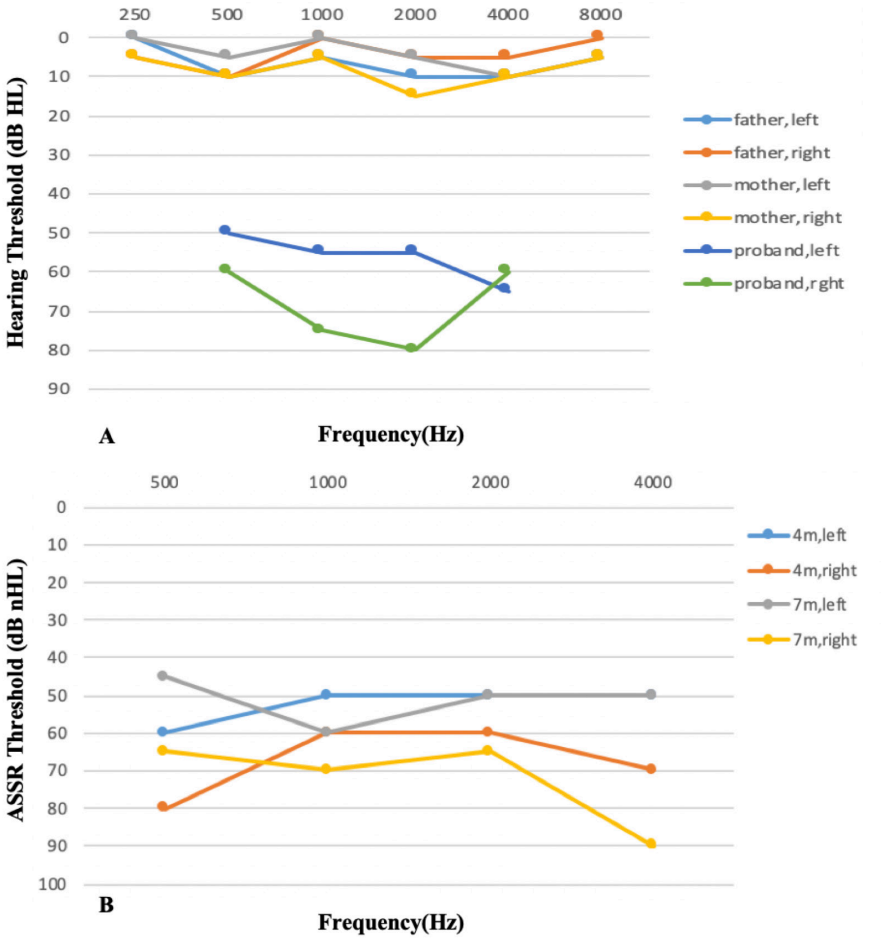

Figure 1. Audiograms of the proband in Family A and his parents. Frequency in Hertz (Hz) is plotted on the x-axis and the hearing level in decibels (dB HL and dB nHL) is plotted on the y-axis.

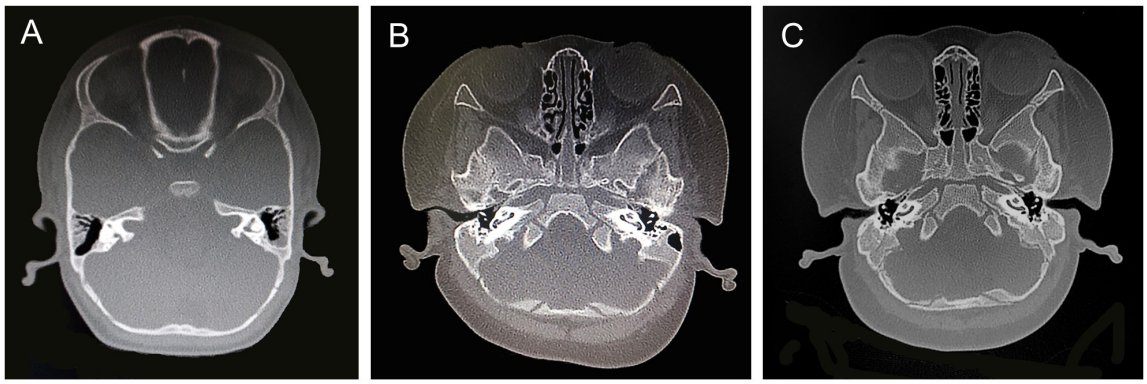

Figure 2. CT scan of the temporal bone of three probands. (A) A CT scan of the temporal bone of the proband in Family A (bilateral enlarged vestibular aqueducts); **(B)** A CT scan of the temporal bone of the proband in Family B; **(C)** A CT scan of the temporal bone of the proband in Family C.

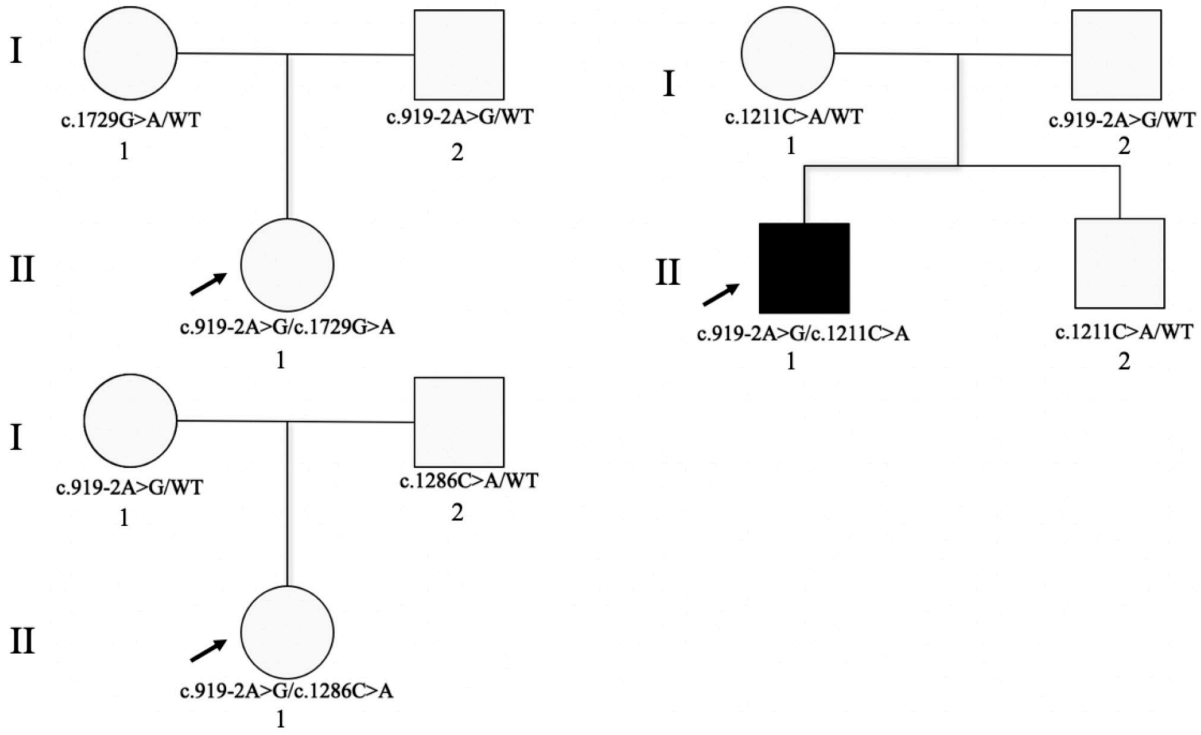

Figure 3. Pedigree map of the three families. Squares and circles denote male and female patients, respectively. WT, wild type.

11 months of age, respectively) and PTA in her parents are shown in Figure 1. A CT scan of the temporal bone of the proband revealed bilateral EVA with a vestibular aqueduct wider than 1.5 mm, pericochlear lucency, dilation around the bottom, parietal fusion, and paranasal sinusitis. She was diagnosed with bilateral large vestibular aqueduct syndrome at seven months of age according to the CT sacn (Figure 2A). The probands in Families B and C underwent UNHS, and were both found to have normal hearing at 3 and 6 months of age, respectively. These two probands both a type "A" tympanogram. A CT scan of the temporal bone was normal at 8 and 6 months of age, respectively (Figure 2B and 2C).

3.2. *Genetic analysis*

Sequencing of *SLC26A4* indicated that the proband in Family A had compound heterozygosity of a c.919-2A>G (IVS7-2A>G) (rs111033313) mutation in intron 7 and a c.1211C>A (p.T430Q) missense mutation in exon 10. In addition, the father was a heterozygous carrier of the c.919-2A>G mutation, and the mother was a heterozygous carrier of the c.1211C>A mutation. The genotypes of the proband in Families B and C were c.1729G>A/c.919-2A>G compound heterozygous mutations and c.1286C>A/c.919-2A>G compound heterozygous mutations, respectively. Figures 3 and 4 show the pedigree map of the three

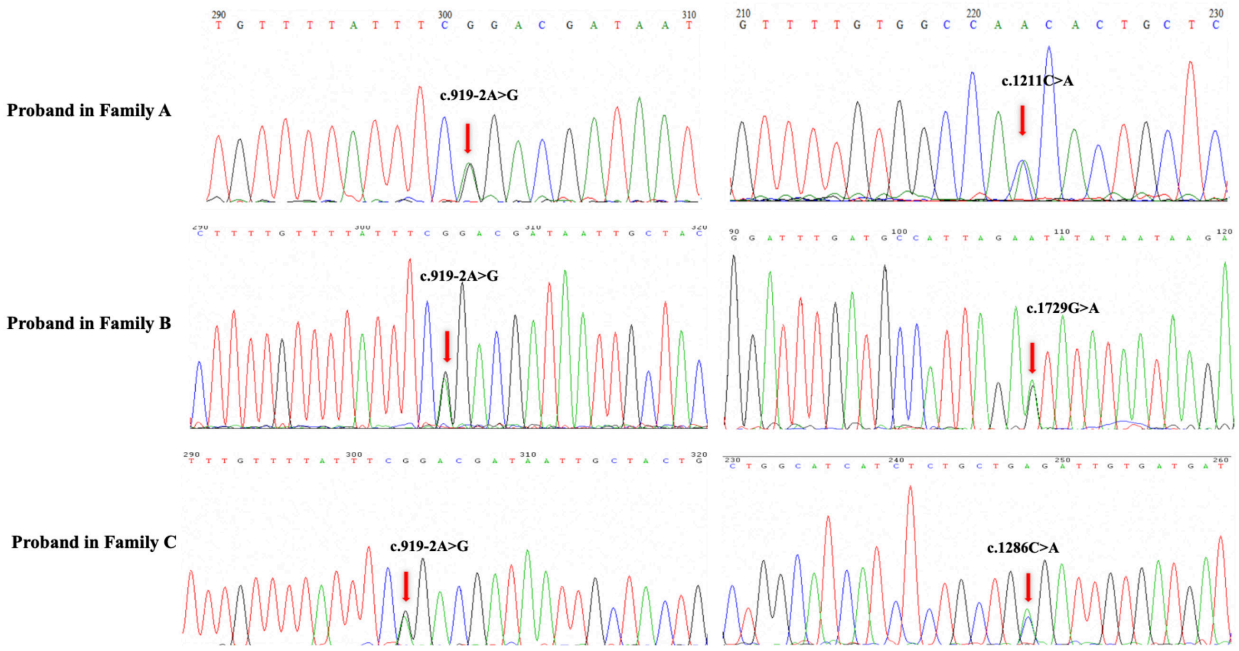

Figure 4. Sequence electropherograms of abnormal sequences from three probands in Families A, B and C.

Table 1. Prediction of variant effect using online tools

No	Variant	ACMG	SIFT score	Polyphen-2 score	Mutation Taster score	CADD score	GERP score	Phylop score
1	c.1211C>A	LP	0.003	0.949	0.998	28.4	5.1	3.261
2	c.1729G>A	LB	1.0	1.0	0.999	23.0	5.72	7.679
3	c.1286C>A	VUS	0.011	0.583	0.883	23.2	-1.65	-0.002

ACMG, American College of Medical Genetics; LP, likely pathogenic; LB, likely benign; VUS, variant of unknown significance.

families and sequence electropherograms of abnormal sequences from three probands in Families A, B, and C, respectively. The variants c.1211C>A (p.T430Q) and c.1729G>A (p.V577I) were not present in ClinVar, PubMed, Deafness Variation Database, dbSNP, the 1000 Genomes Project database, or HGMD and had never been described in clinical reports. These two novel mutations were not found in 400 healthy newborns. The variant c.1286C>A(rs753269996), which has previously been reported in DVD and HGMD, was associated with Mondini deformity. The variant c.1211C>A has Glutamine (Gln) at amino acid 430 instead of Threonine (Thr), and c.1729G>A has Isoleucine (Ile) at amino acid 577 instead of Valine (Val).

3.3. *Prediction of the functional outcome of variants*

The effect of variants was predicted using SIFT, Mutation Taster, Polyphen-2, CADD, GERP, and Phylop (Table 1). The mutation c.1211C>A was predicted to be "damaging" according to Polyphen-2 and SIFT, "disease causing" according to Mutation Taster, and "conserved" according to GERP and Phylop. The variant c.1729G>A was predicted to be "tolerated" according to SIFT and "nonconserved" according to GERP and Phylop.

4. Discussion

EVA is a genetically autosomal recessive disorder. Subjects with bi-allelic mutations have earlier age of onset, more severe deafness, more fluctuating hearing loss, and a larger vestibular aqueduct than those without mutations (*22,23*). EVA is known to be closely linked to *SLC26A4* mutations; variants are highly heterogenous and differ among ethnic groups. p.V138F (c.412G>T) is the most common mutation in the Czech population (*24*). p.L236P (c.707T>C), p.T416P (c.1246A>C), and IVS8+1G>A (c.1001+1G>A) are mainly detected in Caucasians (*25*), and p.H723R (c.2168A>G) is mainly detected in Koreans (*26*). The p.V609G (c.1826T>G) mutation and the IVS8+1G>A (c.1001+1G>A) mutation are predominantly found in the deaf population in South America and North America, respectively (*27*). An increasing number of novel mutations have been found in Chinese patients as more genetic studies are reported. c.919-2A>G (IVS7-2A>G) and p.H723R (c.2168A>G) account for the majority of mutations in China (*28*).

The current study found that the proband's father

and mother (the heterozygous carrier of c.919-2A>G and c.1211C>A mutation, respectively) both had normal hearing, and the proband with *SLC26A4* compound heterozygous mutations (c.1211C>A/c.919-2A>G) had bilateral SNHL as well as bilateral EVA. Therefore, genetic mutations were transmitted from the parents to the offspring, and a distinction between the genotype and phenotype was apparent. The splice-site mutation of c.919-2A>G mentioned above is the most prevalent pathogenic mutation of *SLC26A4* in China. Another mutation, c.1211C>A, is not present in ClinVar, PubMed, or HGMD and has never been described in clinical reports. Therefore, this is the first study to report that the mutation is associated with EVA. This mutation has highly conserved residues and is predicted to be pathogenic. This mutation leads to a p.T430Q switch at amino acid 430 in the cytoplasmic topological domain. Therefore, the novel mutation discovered in this study may impair the anion-transporting activity of pendrin by altering the structure of the pendrin protein. The c.1211C>A (p.T430Q) mutation is located in the STAS domain which is included in members of the SLC26A family to regulate the stability, trafficking, and anion transport function of SLC26A family proteins. The structural significance of this domain has been substantiated by the disease-causing nature of mutations in SLC26A family proteins. Therefore, the novel mutation discovered in this study may be closely related to hearing loss (*29,30*). According to ACMG guidelines, c.1211C>A is likely to be pathogenic.

The patient with c.1729G>A/c.919-2A>G compound heterozygous mutations had normal hearing and a normal CT scan of the temporal bone, and her father and mother (heterozygous carriers of the c.919-2A>G and c.1729G>A (p.V577I) mutations, respectively) also had normal hearing. This mutation in exon 16 had not been previously reported and was absent in 400 healthy newborns. It results in Isoleucine (Ile) taking the place of Valine (Val) at amino acid 577. The variant c.1729G>A was predicted to be "tolerated" according to SIFT and "nonconserved" according to GERP and Phylop. According to ACMG guidelines, c.1211C>A is likely to be benign.

The c.1286C>A (p.A429E) mutation is a documented SNP (rs753269996). It was first reported by Huang *et al*. in a study of extremely disparate mutations in *SLC26A4* among Chinese patients with an isolated Mondini deformity or EVA (*31*). They found that one of the patients with inner ear malformations carried the c.1286C>A mutation. The mutation affected residues that are conserved among *SLC26A4* orthologs [Mus (mouse)] and were not present in a screen of 50 patients without inner ear malformations and 200 normal Chinese controls in a study by Yuan *et al*., suggesting that this mutation is likely to be pathogenic (*32*). In the current study, however, the proband with c.1286C>A/c.919-2A>G compound heterozygous mutations currently has normal hearing and a normal CT scan of the temporal bone. His father and mother (heterozygous carriers of the c.1286C>A and c.919-2A>G mutations, respectively) also had normal hearing. Therefore, the pathogenicity of the c.1286C>A mutation warrants more in-depth study.

The current study analyzed the pathogenicity of three mutations in the *SLC26A4* gene in combination with clinical data. A possible follow-up would involve construction of a plasmid containing the corresponding *SLC26A4* mutants to verify protein expression at the cellular level.

5. Conclusion

This study has demonstrated that the novel missense mutation c.1211C>A in compound heterozygosity with c.919-2A>G in the *SLC26A4* gene is likely to be the cause of deafness in Family A. A novel variant, c.1729G>A, was identified and is likely benign. The pathogenicity of the c.1286C>A mutation warrants more in-depth study. The current findings have broadened the spectrum of known *SLC26A4* mutations in the Chinese population, providing more information for genetic counseling and diagnosis of hearing loss with EVA.

Acknowledgements

The authors wish to thank the patients and their family members for their participation in this study. This research was supported by the National Natural Science Foundation of China (grant number 81870730), the National Key R&D Program of China (grant number 2018YFC1002204), and the Beijing Natural Science Foundation (grant number 7172052).

References

1. Olusanya BO. Neonatal hearing screening and intervention in resource-limited settings: An overview. Arch Dis Child. 2012; 97:654-659.
2. Everett LA, Glaser B, Beck JC, Idol JR, Buchs A, Heyman M, Adawi F, Hazani E, Nassir E, Baxevanis AD, Sheffield VC, Green ED. Pendred syndrome is caused by mutations in a putative sulphate transporter gene (PDS). Nat Genet. 1997; 17:411-422.
3. Scott DA, Karniski LP. Human pendrin expressed in Xenopus laevis oocytes mediates chloride/format exchange. Am J Physiol Cell Physiol. 2000; 278:C207-C211.
4. Azaiez H, Yang T, Prasad S, Sorensen JL, Nishimura CJ, Kimberling WJ, Smith RJ. Genotype–phenotype correlations for SLC26A4-related deafness. Hum Genet. 2007; 122:451-457.
5. Martini A, Calzolari F, Sensi A. Genetic syndromes involving hearing. Int J Pediatr Otorhinolaryngol. 2009; 73:S2-S12.
6. Li XC, Everett LA, Lalwani AK, Desmukh D, Friedman

TB, Green ED, Wilcox ER. A mutation in PDS causes non-syndromic recessive deafness. Nat Genet. 1998; 18:215-217.
7. Royaux IE, Belyantseva IA, Wu T, Kachar B, Everett LA, Marcus DC, Green ED, Localization and functional studies of pendrin in the mouse inner ear provide insight about the etiology of deafness in Pendred syndrome. J Assoc Res Otolaryngol. 2003; 4:394-404.
8. Rah YC, Kim AR, Koo JW, Lee JH, Oh SH, Choi BY. Audiologic presentation of enlargement of the vestibular aqueduct according to the SLC26A4 genotypes. Laryngoscope. 2015; 125:E216-E222.
9. Tsukamoto K, Suzuki H, Harada D, Namba A, Abe S, Usami S. Distribution and frequencies of PDS (SLC26A4) mutations in Pendred syndrome and nonsyndromic hearing loss associated with enlarged vestibular aqueduct: A unique spectrum of mutations in Japanese. Eur J Hum Genet. 2003; 11:916-922.
10. Pryor SP, Madeo AC, Reynolds JC, Sarlis NJ, Arnos KS, Nance WE, Yang Y, Zalewski CK, Brewer CC, Butman JA, Griffith AJ. SLC26A4/PDS genotype-phenotype correlation in hearing loss with enlargement of the vestibular aqueduct (EVA): Evidence that Pendred syndrome and non-syndromic EVA are distinct clinical and genetic entities. J Med Genet. 2005; 42:159-165.
11. Albert S, Blons H, Jonard L, *et al*. *SLC26A4* gene is frequently involved in nonsyndromic hearing impairment with enlarged vestibular aqueduct in Caucasian populations. Eur J Hum Genet. 2006; 14:773-779.
12. Valvassori GE, Clemis JD. The large vestibular aqueduct syndrome. Laryngoscope. 1978; 88:723-728.
13. Dai P, Huang LH, Wang GJ, *et al*. Concurrent hearing and genetic screening of 180,469 neonates with follow-up in Beijing, China. Am J Hum Genet. 2019; 105:803-812.
14. Du Y, Huang L, Wang X, Cui Q, Cheng X, Zhao L, Ni T. Clinical data analysis of genotypes and phenotypes of deafness gene mutations in newborns: A retrospective study. Biosci Trends. 2017; 11:460-468.
15. Zhu J, Cao Q, Zhang N, Ge J, Sun D, Feng Q. A study of deafness-related genetic mutations as a basis for strategies to prevent hereditary hearing loss in Hebei, China. Intractable Rare Dis Res. 2015; 4:131-138.
16. Zhao X, Huang L, Wang X, Wang X, Zhao L, Cheng X, Ruan Y. Genotyping and audiological characteristics of infants with a single-allele SLC26A4 mutation. Int J Pediatr Otorhinolaryngol. 2019; 116:153-158.
17. Zhao X, Cheng X, Huang L, Wang X, Wen C, Wang X. Novel compound heterozygous mutations in *SLC26A4* gene in a Chinese family with enlarged vestibular aqueduct. Biosci Trends. 2018; 12:502-506.
18. Zhao X, Cheng X, Huang L, Wang X, Wen C, Wang X, Zhao L. Analysis of mutations in the FOXI1 and KCNJ10 genes in infants with a single-allele SLC26A4 mutation. Biosci Trends. 2019; 13:261-266.
19. Richards S, Aziz N, Bale S, Bick D, Das S, Gastier-Foster J, Grody WW, Hegde M, Lyon E, Spector E, Voelkerding K, Rehm HL; ACMG Laboratory Quality Assurance Committee. Standards and guidelines for the interpretation of sequence variants: A joint consensus recommendation of the American College of Medical Genetics and Genomics and the Association for Molecular Pathology. Genet Med. 2015; 17:405-424.
20. Kim SY, Park G, Han KH, Kim A, Koo JW, Chang SO, Oh SH, Park WY, Choi BY. Prevalence of p.V37I variant of GJB2 in mild or moderate hearing loss in a pediatric population and the interpretation of its pathogenicity. PLoS ONE. 2013; 8:e61592.
21. Liu J, Huang L, Fu X, Liu H, Yang Y, Cheng X, Ni T. The audiological characteristics of large vestibular aqueduct syndrome in infants and young children. Lin Chung Er Bi Yan Hou Tou Jing Wai Ke Za Zhi. 2016; 30:1702-1705. (in Chinese)
22. Xin F, Yuan Y, Deng X, Han M, Wang G, Zhao J, Gao X, Liu J, Yu F, Han D, Dai P. Genetic mutations in nonsyndromic deafness patients of Chinese minority and Han ethnicities in Yunnan, China. J Transl Med. 2013; 11:312.
23. Zhao FF, Lan L, Wang DY, Han B, Qi Y, Zhao Y, Zong L, Li Q, Wang QJ. Correlation analysis of genotypes, auditory function, and vestibular size in Chinese children with enlarged vestibular aqueduct syndrome. Acta Otolaryngol. 2013; 133:1242-1249.
24. Pourová R, Janousek P, Jurovcík M, Dvoráková M, Malíková M, Rasková D , Bendová O, Leonardi E, Murgia A, Kabelka Z, Astl J, Seeman P. Spectrum and frequency of SLC26A4 mutations among Czech patients with early hearing loss with and without enlarged vestibular aqueduct (EVA). Ann Hum Genet. 2010; 74:299-307.
25. Campbell C, Cucci RA, Prasad S, Green GE, Edeal JB, Galer CE, Karniski LP, Sheffield VC, Smith RJ. Pendred syndrome, DFNB4, and PDS/SLC26A4 identification of eight novel mutations and possible genotype–phenotype correlations. Hum Mutat. 2001; 17:403-411.
26. Park HJ, Lee SJ, Jin HS, Lee JO, Go SH, Jang HS, Moon SK, Lee SC, Chun YM, Lee HK, Jung SC, Griffith AJ, Koo SK. Genetic basis of hearing loss associated with enlarged vestibular aqueducts in Koreans. Clin Genet. 2005; 67:160-165.
27. Lin Z, Lu Y, Qian X, Yao J, Wei Q, Cao X. Study on molecular structure and racial difference of high frequency pathological SLC26A4 mutations in hearing loss. J Nanjing Medical University. 2015; 9:1185-1194. (in Chinese)
28. Yuan Y, Huang S, Wang G, Kang D, Han D, Huang D, Dai P. Sequencing analysis of entire *SLC26A4* gene with focus on IVS7- 2A>G mutation in 2352 patients with moderate to profound SNHL in China. Chin J Otology. 2011; 9:17-23. (in Chinese)
29. Sharma AK, Rigby AC, Alper SL. STAS domain structure and function. Cell Physiol Biochem. 2011; 28:407-422.
30. Sharma AK, Ye L, Baer CE, Shanmugasundaram K, Alber T, Alper SL, Rigby AC. Solution structure of the guanine Nucleotide-binding STAS domain of SLC26-related SulP protein Rv1739c from Mycobacterium tuberculosis. J Biol Chem. 2011; 286:8534-8544.
31. Huang S, Han D, Yuan Y, Wang G, Kang D, Zhang X, Yan X, Meng X, Dong M, Dai P. Extremely discrepant mutation spectrum of SLC26A4 between Chinese patients with isolated Mondini deformity and enlarged vestibular aqueduct. J Transl Med. 2011; 9:167.
32. Yuan Y, You Y, Huang D, Cui J, Wang Y, Wang Q, Yu F, Kang D, Yuan H, Han D, Dai P. Comprehensive molecular etiology analysis of nonsyndromic hearing impairment from typical areas in China. J Transl Med. 2009; 7:79.

(Received October 4, 2019; Revised October 23; Accepted October 25, 2019)

Original Article

DOI: 10.5582/bst.2019.01283

Hepatitis B virus recurrence after living donor liver transplantation of anti-HBc-positive grafts: A 22-year experience at a single center

Sung Kwan Bae[1], Nobuhisa Akamatsu[1,2], Junichi Togashi[1,2], Akihiko Ichida[2], Takuya Kawahara[3], Harufumi Maki[2], Yujiro Nishioka[2], Takashi Kokudo[2], Yuichiro Mihara[2], Yoshikuni Kawaguchi[2], Takeaki Ishizawa[2], Junichi Arita[2], Junichi Kaneko[2], Sumihito Tamura[2], Kiyoshi Hasegawa[1,2,*]

[1] *Organ Transplantation Service, The University of Tokyo Hospital, Tokyo, Japan;*
[2] *Artificial Organ and Transplantation Division, Department of Surgery, The University of Tokyo, Tokyo, Japan;*
[3] *Biostatistics Division, Clinical Research Support Center, The University of Tokyo Hospital, Tokyo, Japan.*

Summary **The use of hepatitis B core antibody (anti-HBc)-positive grafts is one strategy for expanding the donor pool for liver transplantation (LT). The aim of this study was to determine the risk factors associated with hepatitis B virus (HBV) recurrence after living donor LT (LDLT) of anti-HBc-positive grafts. From January 1996 to December 2018, a total of 609 LDLT procedures were performed at our center. A retrospective review was performed for 31 patients (23 males and 8 females; median age = 47 years) who underwent LDLT for HBV-unrelated liver disease from anti-HBc-positive donors. The factors associated with HBV recurrence were evaluated and compared between the HBV recurrence and non-recurrence groups. The median follow-up period after LT was 135 months (range, 6-273 months). Four of 31 patients (12.9%) developed post-LT HBV recurrence. All four cases were HBV-naïve patients (anti-HBc-negative and Hepatitis B surface antibody-negative). The median interval between LDLT and HBV recurrence was 42 months (range, 20-51). The overall actuarial rates of HBV recurrence at 1, 3, 5, 10, and 20 years were 0%, 7.2%, 15.7%, 15.7%, and 15.7%, respectively. Although there were no significant differences between the HBV recurrence and non-recurrence groups, HBV recurrence tended to occur in HBV-naïve recipients ($P = 0.093$). HBV-naïve status may contribute to HBV recurrence after LDLT for HBV-unrelated liver disease from anti-HBc-positive donors. Careful monitoring for serological HBV markers is needed, particularly in this group.**

Keywords: Liver transplantation, HBV recurrence, anti-HBc, HBIG, HBV-naïve

1. Introduction

The current efforts to overcome the issue of organ shortage include the use of marginal liver grafts, such as those from hepatitis B core antibody (anti-HBc)-positive donors. In Japan, the prevalence of resolved hepatitis B virus (HBV) infection is 23.2%, which is much higher than that in Western countries (*1*). However, resolved HBV infections in donor livers may be reactivated in hepatitis B s antigen (HBsAg)-negative recipients due to post-liver transplantation (LT) immunosuppressive therapy. Ideally, in order to prevent HBV transmission, anti-HBc-positive donors should not be used at all. However, one possible strategy for expanding the donor pool is the use of anti-HBc-positive grafts for LT.

Previous studies have reported that, in the absence of any prophylaxis, the probability of HBV infection depends on the HBV serological status of the recipient (*2*). A variety of prophylactic strategies have been used in small patient series; however, an adequate consensus has not been reached (*3*). Prophylactic strategies that are currently used for LT from anti-HBc-positive donors vary from the administration of hepatitis B

Released online in J-STAGE as advance publication October 30, 2019.

*Address correspondence to:
Dr. Kiyoshi Hasegawa, Artificial Organ and Transplantation Division, Department of Surgery, The University of Tokyo, 7-3-1 Hongo, Bunkyo-ku, Tokyo 113-8655, Japan.
E-mail: kihase-tky@umin.ac.jp

immunoglobulin (HBIG) or nucleoside/tide analogues (NAs) alone to combination therapy, depending on the liver transplant centers (*2,3*). We previously reported that HBIG monotherapy can prevent HBV infection from anti-HBc-positive donors (*4*). However, the recent practice guidelines indicate that lamivudine monotherapy is the most cost-effective treatment, due to the low rates of graft infection (< 3%) (*5,6*).

The aim of this study was to assess the incidence and risk factors associated with HBV recurrence in HBsAg-negative LDLT recipients of anti-HBc-positive grafts over a period of 20 years.

2. Methods

2.1. *Patients*

From January 1996 to December 2018, a total of 609 LDLT procedures were performed at the University of Tokyo Hospital. We retrospectively reviewed all demographics and radiologic and laboratory data, which had been gathered into a computerized database, collected over this period. All donors were HBsAg-negative. Among them, 55 (9.0%) were anti-HBc-positive donors. Of the recipients of anti-HBc-positive grafts, 33 were HBV-unrelated recipients. After 2 patients who were not followed up for at least 6 months were excluded, 31 patients were enrolled in this study (Figure 1). Patient data were censored at death or the time of the last follow-up.

The study protocol complied with the Good Clinical Practice Guidelines and the 1975 Declaration of Helsinki and was approved by the Institutional Review Board at the University of Tokyo Hospital.

2.2. *Immunoprophylaxis*

Postoperative prophylaxis consisted of HBIG monotherapy. HBIG was administered at 10,000 IU intravenously during the anhepatic phase. HBIG was administered once a month to keep the HBsAb level above 200 IU/L during the first year and above 100 IU/L thereafter (*4*).

2.3. *Immunosuppression protocol*

The details of the immunosuppression protocol are described elsewhere (*7*). The post-transplant immunosuppression regimen consisted of steroid and tacrolimus, both of which were tapered gradually. The targeted serum trough level of tacrolimus was 5 ng/mL, and methylprednisolone was prescribed at a dose of 0.05 mg/kg more than 1 year after LT.

2.4. *Serological monitoring*

The recurrence of the HBV was defined as the development of positive HBsAg and/or HBV DNA after LT (*2*). Standard biochemical tests of the liver function were performed at each follow-up visit. Measurements of HBsAg, Hepatitis B surface antibody (anti-HBs), and anti-HBc were carried out in the University of Tokyo Hospital using commercial chemiluminescent immunoassay (CLIA) kits in the ARCHITECT ANALYSER i2000 (Abbott Japan Co., Ltd., Tokyo, Japan). The sensitivity of the HBsAg assay ranged from 0.05 to 250 IU/mL. Specimens with an HBsAg value exceeding 250 IU/mL were diluted to 1:500 using a diluent recommended by the manufacturer, and the exact concentration of the samples has been measured since 2014. The sensitivity of the anti-HBs assay ranged from 6.0 to 1,000 mIU/mL. Until 2006, anti-HBc was measured using a microparticle enzyme immunoassay (MEIA, AxSYM System; Abbott Japan Co., Ltd.) in which samples with INH% values > 61% were regarded as positive, while those with values < 40% were regarded as negative. Between 2006 and 2008, anti-HBc was measured by a chemiluminescence enzyme-immunoassay (CLEIA) (Fujirebio, Tokyo, Japan), in which samples with INH% values > 50% were regarded as positive, while those with values < 50% were regarded as negative. Since 2008, anti-HBc was measured using the CLIA method, in which samples with S/CO values > 1.0 were regarded as positive, while those with values < 1.0 were regarded as negative. The HBV DNA levels were quantified with a transcription-mediated amplification assay (Mitsubishi Chemical Medience, Tokyo, Japan), which has a detection range of 3.7-8.7 log genome equivalents (LGE)/mL, until March 2004. Thereafter, all HBV DNA levels were quantified using the COBAS Amplicor HBV Monitor

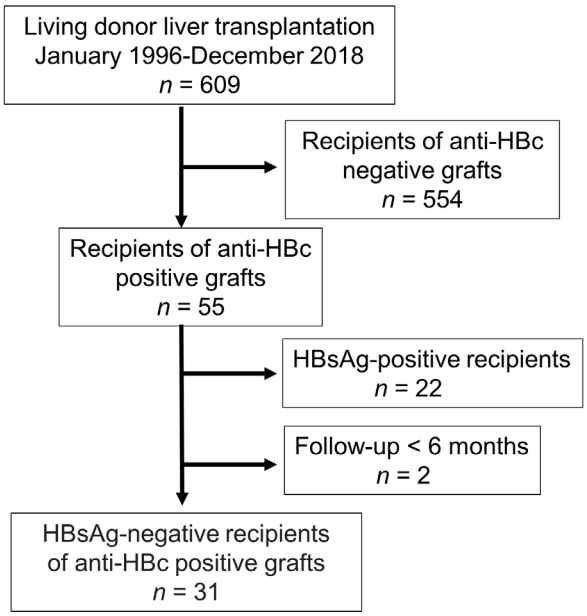

Figure 1. Flow diagram of the patients enrolled in the present study.

Test (Roche Diagnostics, Tokyo, Japan), which has a dynamic range of 2.6 to 7.6 log copies/mL, or COBAS TaqMan HBV Test v2.0 (Roche Diagnostics), which has a dynamic range of 2.1 to 9.0 log copies/mL (1.3 to 8.2 log IU/mL).

2.5. *Vaccination*

Among the subjects of the study, five patients were vaccinated in accordance with the one-year HBV vaccination protocol (*8*). After completion of the one-year vaccination protocol, patients were followed for an additional two years, with monthly measurements of the HBsAb titer and records of the required dose of HBIG for each patient in order to clarify the long-term efficacy of vaccination.

2.6. *Statistical analyses*

We assessed the cumulative incidence of HBV recurrence after LT and the overall survival with a Kaplan-Meier curve. We calculated the hazard ratios (HRs) for the time to HBV recurrence with the Cox proportional hazards model using each potential predictor as a covariate. The difference in the cumulative incidence of HBV recurrence was evaluated by the log-rank test. $p < 0.05$ was considered to indicate statistical significance, and $p < 0.1$ was considered to indicate a candidate potential predictor. Statistical analyses were performed using the SPSS statistics version 23.0 software package (SPSS Inc., Chicago, IL, USA).

Table 1. Patient demographics

Items	Recipients of anti-HBc-positive grafts ($n = 31$)
Age (years)	47 (0-64)
Sex, male/female	23/8
Primary disease	
HCV-cirrhosis	13 (42%)
Primary biliary cirrhosis	6 (19%)
Biliary atresia	4 (13%)
Alcoholic cirrhosis	3 (10%)
Others	5 (16%)
Pretransplant HBV status	
HBsAg positivity	0 (0%)
Anti-HBc/anti-HBs	
-/- (HBV naïve)	18 (58%)
+/+	6 (19%)
+/-	4 (13%)
-/+	3 (10%)
HBIG prophylaxis, yes/no	24/7
HBV vaccination, yes/no	5/26
Median follow-up period (months)	135 (6-273)

Qualitative variables are expressed as the numbers of patients, with percentages in parentheses, and quantitative variables are expressed as the medians, with ranges in parentheses. HCV, hepatitis C virus; HBV, hepatitis B virus; HBsAg, Hepatitis B surface Antigen; Anti-HBc, hepatitis B core antibody; Anti-HBs, hepatitis B surface antibody; HBIG, hepatitis B immunoglobulin.

3. Results

3.1. *Patient demographics*

The patient characteristics are shown in Table 1. The population comprised 23 men and 8 women, with median age of 47 years old (range, 0-64 years old). Primary diseases for LT in these patients were hepatitis C virus-cirrhosis ($n = 13$), primary biliary cholangitis ($n = 6$), biliary atresia ($n = 4$), alcoholic cirrhosis ($n = 3$), and others ($n = 5$). At the time of transplantation, 18 were HBV-naïve (anti-HBc-negative and anti-HBs-negative), 6 were anti-HBc-positive and anti-HBs-positive, 4 were anti-HBc-positive, and 3 were anti-HBs-positive. The median follow-up period after LT was 135 months (range, 6-273 months).

3.2. *Risk factors for HBV recurrence after LDLT*

Four of the 31 patients (12.9%) developed post-LT HBV recurrence (Table 2). All cases of HBV recurrence were in HBV-naïve patients and those under HBIG prophylaxis. The overall actuarial rates of HBV recurrence after LT at 1, 3, 5, 10, and 20 years were 0%, 7.4%, 15.7%, 15.7%, and 15.7%, respectively (Figure 2). Although there were no significant differences between the HBV recurrence and non-recurrence groups, HBV recurrence tended to occur in HBV-naïve recipients (Log-rank, $P = 0.093$) (hazard ratio [HR] and confidence interval [CI]: not estimable due to non-

Table 2. The outcomes of patients with HBV recurrence after LT

No.	Age/ gender	Primary disease	Pre-LT HBV status Anti-HBs/ anti-HBc	Anti-HBc titer of donor (INH%)	HBV Prophylaxis	At the time of HBV recurrence				
						Duration from LT (months)	Anti-HBs (mIU/mL)	HBsAg (IU/mL)	HBV DNA (LC/mL)	Peak ALT (IU/l)
1	29/F	AIH	-/-	95	HBIG	35	15	26.67	> 7.6	116
2	53/M	PBC	-/-	92	HBIG, vaccination	20	90.7	1.18	8.9	186
3	52/M	Alcoholic	-/-	78	HBIG	49	15.7	197.04	3.9	125
4	47/M	PBC	-/-	91	HBIG	51	10	8.8	8.0	199

LT, liver transplantation; HBV, hepatitis B virus; Anti-HBs, hepatitis B surface antibody; Anti-HBc, hepatitis B core antibody; INH, inhibition; HBsAg, Hepatitis B surface Antigen; PBC, primary biliary cholangitis; AIH, autoimmune hepatitis; HBIG, hepatitis B immunoglobulin; LAM, lamivudine; ADV, adefovir; ETV, entecavir.

convergence) (Table 3). The cumulative rates of post-LT HBV recurrence in HBV naïve recipients (n = 18) at 1, 3, 5, 10, and 20 years were 0%, 12.2%, 25.7%, 25.7%, and 25.7%, respectively. By contrast, in the anti-HBc- and/or anti-HBs-positive recipients (n = 13), there were no cases of HBV recurrence throughout the follow-up period (Figure 3). In the 24 recipients receiving HBIG prophylaxis according to our center's protocol, there were no significant differences between the HBV recurrence group and the non-recurrence group (Table 4).

3.3. *The overall survival after LT*

The overall survival of the 31 recipients of anti-HBc-positive grafts at 1, 3, 5, 10, and 20 years were 96.6%, 89.7%, 85.9%, 81.1%, and 81.1%, respectively (Figure 4). During the study period, five recipients died: one from pulmonary embolism, and the remaining four from HBV-unrelated graft failure.

3.4. *Clinical course of the recipients with HBV recurrence*

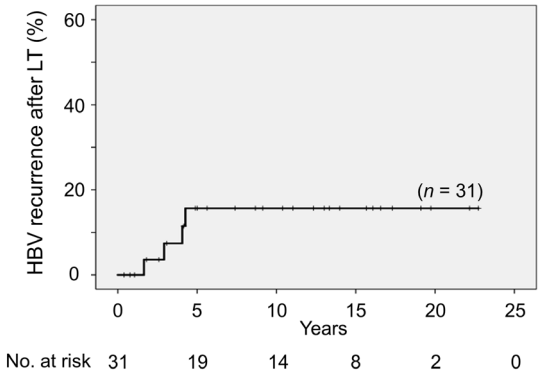

Figure 2. The cumulative overall rates of HBV recurrence after LDLT of anti-HBc-positive grafts.

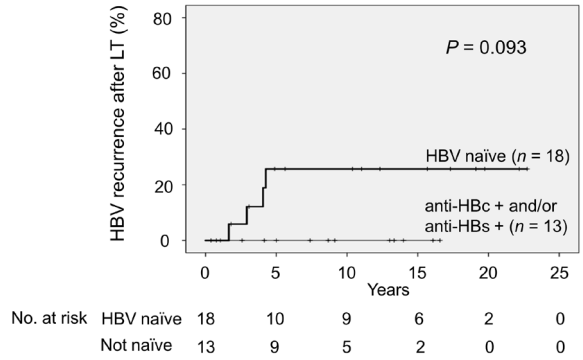

Figure 3. The cumulative rates of HBV recurrence after LDLT of anti-HBc-positive grafts.

Table 3. Predictive factors associated with HBV recurrence after LT

Items	HBV recurrence (n = 4)	HBV non-recurrence (n = 27)	HR	95% CI	P
Age, < 50/> 50 years	2/2	14/13	0.975	0.137-6.928	0.980
Sex, male/female	3/1	20/7	0.905	0.094-8.711	0.931
HBIG prophylaxis, yes/no	4/0	20/7	NE	NE	0.225
HBV vaccination, yes/no	1/3	4/23	0.639	0.066–6.154	0.699
Pre-LT HBV status					
HBV-naïve, yes/no	4/0	14/13	NE	NE	0.093
Anti-HBc positive, yes/no	0/4	10/17	NE	NE	0.148
Anti-HBs positive, yes/no	0/4	9/18	NE	NE	0.212

Qualitative variables are expressed as the numbers of patients, with percentages in parentheses, and quantitative variables are expressed as the medians, with ranges in parentheses. HBV, hepatitis B virus; HR, hazard ratio; CI, confidence interval; HBIG, hepatitis B immunoglobulin; LT, liver transplantation; Anti-HBc, hepatitis B core antibody; Anti-HBs, hepatitis B surface antibody; NE, not estimable due to non-convergence.

Table 4. Predictive factors associated with HBV recurrence after LT under HBIG prophylaxis

Items	HBV recurrence (n = 4)	HBV non-recurrence (n = 20)	HR	95% CI	P
Age, < 50/> 50 years	2/2	8/12	0.572	0.080–4.068	0.576
Sex, male/female	3/1	14/6	1.359	0.141–3.093	0.791
HBV vaccination, yes/no	1/3	4/16	1.052	0.109–10.134	0.965
Pre-LT HBV status					
HBV-naïve, yes/no	4/0	10/10	NE	NE	0.106
Anti-HBc positive, yes/no	0/4	8/12	NE	NE	0.137
Anti-HBs positive, yes/no	0/4	7/13	NE	NE	0.224

Qualitative variables are expressed as the numbers of patients, with percentages in parentheses, and quantitative variables are expressed as the medians, with ranges in parentheses. HBV, hepatitis B virus; HR, hazard ratio; CI, confidence interval; HBIG, hepatitis B immunoglobulin; LT, liver transplantation; Anti-HBc, hepatitis B core antibody; Anti-HBs, hepatitis B surface antibody; NE, not estimable due to non-convergence.

The clinical courses and outcomes of the recipients with HBV recurrence are shown in Table 2 and Figure 5. The median interval between LDLT and the development of HBV recurrence was 42 months (range, 20-51 months). At the time of HBV recurrence, anti-HBs titers were maintained at 10-90.7 mIU/mL despite positivity for HBsAg and HBV DNA. All cases of HBV recurrence were treated with lamivudine (LAM) or entecavir (ETV), with or without adefovir. No grafts were lost due to post-LT HBV recurrence-related events, and all cases were alive. Case 1 achieved HBsAg seroconversion after 18 months of LAM administration. In cases 2 and 3, HBsAg turned negative after 44 and 48 months of ETV administration respectively. However, HBsAg seroconversion was not achieved, and ETV was not discontinued. Case 4 remained HBsAg-positive throughout the study period. HBV DNA in these four cases was negative at the last follow-up.

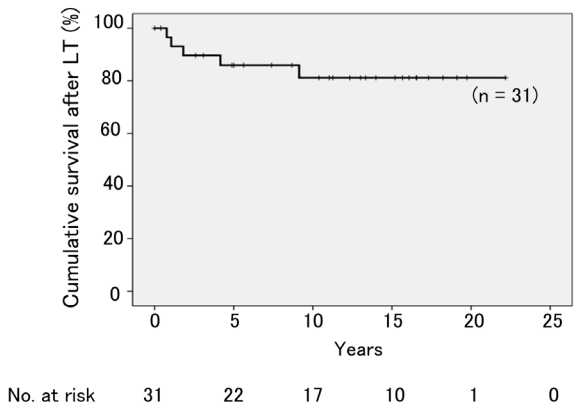

Figure 4. The cumulative survival in LDLT recipients.

3.5. *Outcomes of recipients not receiving HBIG prophylaxis*

Among the 31 patients, 7 did not receive HBIG prophylaxis according to our center's protocol after LDLT (Table 5). Of note, none of the 7 recipients developed HBV recurrence after a median interval of 160 months (range, 37-273 months) post-LT. At the time of transplantation, four were HBV-naïve, one was anti-HBs-positive, one was anti-HBc-positive, and one was anti-HBs-positive and anti-HBc-positive. Cases 1-4 were the patients who underwent LT before starting our HBIG prophylaxis protocol. Case 1 had achieved immunotorelance after LT and has since discontinued immunosuppressive drug use. Cases 2 and 3 were censored because of transfer to another hospital with no HBV recurrence. Cases 5-7 had incidentally not been administered HBIG prophylaxis; however, no patients had HBV recurrence under immunosuppression. They are now under close monitoring for HBV DNA according to the Japanese guideline for preventing HBV reactivation in patients receiving immunosuppressive therapy or chemotherapy (*9*).

3.6. *Vaccination*

All five vaccinated patients received HBIG prophylaxis

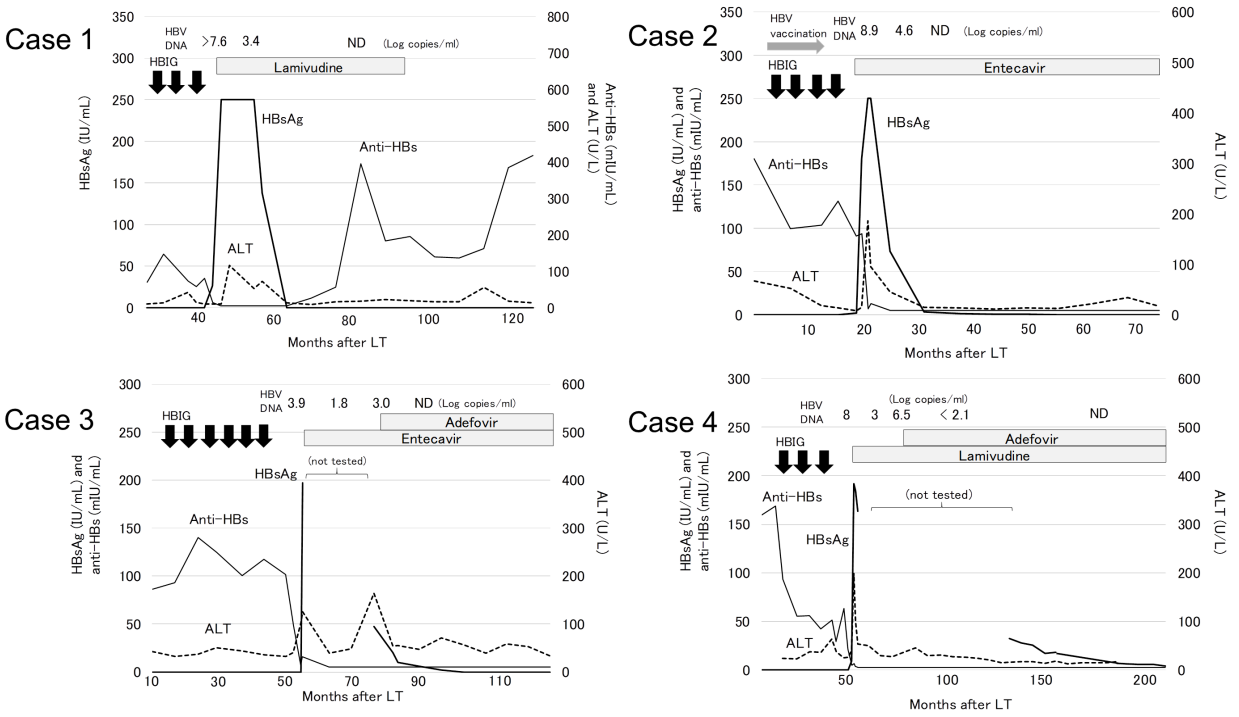

Figure 5. Clinical course of four patients with HBV recurrence after LDLT.

Table 5. Characteristics of patients without HBV prophylaxis

No.	Age/ gender	Primary disease	Pret-LT HBV status Anti-HBs (mIU/ml) / Anti-HBc (INH%)	Anti-HBc titer of donor	Immuno-suppression drug	Follow-up period (months)	HBV recurrence	Outcome
1	4/F	AGS	-/-	+	Withdrawal	273	None	Alive
2	0/M	BA	-/+	+	CyA	59	None	Transfer
3	0/M	BA	-/-	+	CyA	60	None	Transfer
4	8/M	BA	-/-	+	FK	266	None	Alive
5	46/M	PBC	150/-	51 INH%	FK	199	None	Alive
6	55/M	HCV	741/86	97 INH%	CyA	160	None	Alive
7	33/M	BCS	-/-	1.9 S/CO	FK	37	None	Alive

HBV, hepatitis B virus; LT, liver transplantation; Anti-HBs, hepatitis B surface antibody; Anti-HBc, hepatitis B core antibody; AGS, Alagille syndrome; BA, biliary atresia; PBC, primary biliary cholangitis; HCV, hepatitis C virus; BCS, Budd-Chiari syndrome; INH, inhibition; S/CO, sample/cut-off; CyA, cyclosporine; FK, tacrolimus.

(*8*). Of them, 2 showed a good response to the vaccination with an increase in the HBsAb titer (312 and 244 mIU/mL), and HBIG was discontinued successfully. However, the remaining three patients were poor responders, including one who had HBV recurrence after vaccination (Figure 5, case 2).

4. Discussion

It is well known that HBV infection can be reactivated in grafts from anti-HBc-positive donors at a frequency that is related to the HBV serological status of the recipient: in the absence of prophylaxis, this frequency was highest in HBV-naïve recipients (47.8%) and lowest in anti-HBc and/or anti-HBs positive recipients (1.4-13.1%) (*2*). However, with HBIG monoprophylaxis, the risk was decreased to 27% in HBV-naïve recipients and 0-5.8% in anti-HBc- and/or anti-HBs-positive recipients. Furthermore, with lamivudine monoprophylaxis, the risk was decreased to 3.4% in naïve recipients and 0-4% in anti-HBc- and/or anti-HBs-positive recipients (*2*).

In our center, HBIG monoprophylaxis has been the conventional strategy for LT from anti-HBc-positive donors (*4*). In the present study, the rate of HBV recurrence under HBIG monoprophylaxis was 16.7% (4 out of 24 patients) (Table 4), which was consistent with the findings of previous reports (*2*). Overall results showed that HBV recurrence tended to occur in HBV-naïve patients (Log-rank, $P = 0.093$) (Table 3). The rate of HBV recurrence was 22.2% (4 out of 18 patients) in the HBV-naïve group and 0% in the anti-HBc- and/or anti-HBs-positive group (0 out of 13 patients). These results are also consistent with those of previous reports (*2*).

Two main reasons have been proposed for HBV recurrence after LT: the discontinuation of HBIG (*10*) and the emergence of anti-HBs escape mutants (*11,12*). The mechanisms by which HBIG protects the transplanted liver against HBV reinfection are still unclear. One of the most prevalent theories is that HBIG protects naïve hepatocytes against HBV by blocking a putative HBV receptor (*13,14*). Previous studies have shown that recurrent hepatitis B during the first six months after LT develops mainly due to inadequate HBIG doses, whereas late recurrence is caused usually by the selection of immune escape mutants (*15-17*). The most common escape mutation is a glycine-to-arginine substitution at codon 145 of the HBV S protein (G145R) (*18*), which results in reduced binding to anti-HBs, allowing such viruses to escape neutralization by HBIG. In our study, 4 patients had HBV recurrence after a median interval of 42 months (range, 20-51 months) post-LT despite the continuous administration of HBIG. In that respect, our results suggest that all four of these cases may have had anti-HBs escape mutations. However, our study is limited by the fact that a sequence analysis of serum HBV DNA was not performed at the time of HBV recurrence.

In our study, seven recipients did not receive the HBIG prophylaxis protocol, as shown in Table 5. Remarkably, however, HBV recurrence did not occur in any of the seven cases. Cases 5 and 6 were patients who had adequate anti-HBs titers before LT (150 and 741 mIU/mL, respectively) (*19*). The latest EASL clinical practice guideline recommends that prophylaxis for HBV recurrence be performed immediately after LT if recipients do not have anti-HBs (*5*). Furthermore, Cholongitas *et al*. showed that recipients positive for both anti-HBc and anti-HBs represent a group that can safely receive anti-HBc-positive grafts without any post-transplant HBV prophylaxis (*2,20*). In that respect, cases 5 and 6 were recipients who did not need early HBV prophylaxis after LT. One proposed reason for this is that patients with resolved HBV infection have memory T-cells and various antibodies protecting against the proliferation of HBV, including anti-HBs-escape mutations (*16*). However, case 7, who did not have anti-HBs or anti-HBc, incidentally had not been receiving HBV prophylaxis and yet experienced no recurrence of HBV during the follow-up period. In that case, the anti-HBc titer of the donor was relatively low (1.9 S/CO). We previously reported that the titer of anti-HBc may reflect the potential activity of HBV,

even after HBsAg disappearance (*21*). The relationship between the anti-HBc titer of the donor and HBV recurrence after LT is still unclear, and further studies will be necessary to clarify this issue.

The feasibility of HBV vaccination in post-LT recipients is highly controversial. We previously reported that a limited number of patients were able to establish active immunity with our extended one-year vaccination protocol, and the clinical indication for HBV vaccination in LT recipients is currently minimal (*8*). Ishigami *et al*. reported that although the HBV vaccine is an effective substitute for prophylaxis against HBV reactivation after LT, frequent vaccination may be a risk factor for producing escape mutants (*12*). In our study, two of five patients demonstrated a good response to HBV vaccination. However, in Table 2 and Figure 5, case 2 developed HBV recurrence after receiving the HBV vaccination protocol. Although post-transplant HBV vaccination is an alternative that may provide a chance to discontinue prophylaxis by producing anti-HBs, close monitoring of serum HBV markers is needed. Furthermore, based on the fact that Japanese adults are not obligated to undergo HBV vaccination (*22*), pre-transplant HBV vaccination is crucial for potential recipients of LT in Japan (*19*).

In Japan, although the use of HBIG is associated with several issues, such as a high cost and the emergence of escape mutant, HBIG monotherapy is the dominant form of prophylaxis for HBV recurrence after LT from anti-HBc-positive donors (*4,16,23,24*). However, recent clinical practice guidelines of AASLD and EASL recommend the administration of antiviral therapy, such as LAM, ETV, tenofovir disoproxil fumarate (TDF), or tenofovir alafenamide (TAF), as these antiviral drugs function as cost-effective treatments due to the low rates of HBV recurrence (< 3%) (*5,6,25*). We are still cautious for NAs especially in the young for the potential risk of the emergence of drug-resistant variants and unknown adverse reactions due to their long-term use.

There are some limitations associated with our study, including its retrospective design and relatively small sample size. However, to our knowledge, this study has the longest duration of follow-up among studies analyzing LDLT recipients with anti-HBc-positive grafts. Furthermore, our results indicated the possibility of a tailor-made prophylactic antiviral therapy for this specific group (*20,26*).

In conclusion, an HBV-naïve status may contribute to HBV recurrence after LDLT of anti-HBc-positive grafts. We should remain cautious concerning the risk of HBV recurrence, particularly in this group. In this respect, pre-transplant HBV vaccination should be recommended for candidate recipients of LT. Further multicenter studies are needed in order to standardize the prophylactic regimen for HBV recurrence after LT with anti-HBc-positive grafts.

Acknowledgements

We gratefully acknowledge the work of past and present members of our department.

References

1. Tanaka J, Kumagai J, Katayama K, Komiya Y, Mizui M, Yamanaka R, Suzuki K, Miyakawa Y, Yoshizawa H. Sex- and age-specific carriers of hepatitis B and C viruses in Japan estimated by the prevalence in the 3,485,648 first-time blood donors during 1995-2000. Intervirology. 2004; 47:32-40.
2. Cholongitas E, Papatheodoridis GV, Burroughs AK. Liver grafts from anti-hepatitis B core positive donors: A systematic review. J Hepatol. 2010; 52:272-279.
3. Perrillo R. Hepatitis B virus prevention strategies for antibody to hepatitis B core antigen-positive liver donation: a survey of North American, European, and Asian-Pacific transplant programs. Liver Transpl. 2009; 15:223-232.
4. Takemura N, Sugawara Y, Tamura S, Makuuchi M. Liver transplantation using hepatitis B core antibody-positive grafts: review and university of Tokyo experience. Dig Dis Sci. 2007; 52:2472-2477.
5. European Association for the Study of the Liver. EASL Clinical Practice Guidelines: Liver transplantation. J Hepatol. 2016; 64:433-485.
6. Terrault NA, Lok ASF, McMahon BJ, Chang KM, Hwang JP, Jonas MM, Brown RS Jr, Bzowej NH, Wong JB. Update on prevention, diagnosis, and treatment of chronic hepatitis B: AASLD 2018 hepatitis B guidance. Hepatology. 2018; 67:1560-1599.
7. Waki K, Sugawara Y, Mizuta K, Fujita H, Kadowaki T, Kokudo N. Living-donor liver transplantation at the University of Tokyo, 1996-2011: the impact of HLA matching and a positive crossmatch on long-term survival and tolerance. Clin Transpl. 2011;223-235.
8. Togashi J, Akamatsu N, Sugawara Y, Kaneko J, Tamura S, Tanaka T, Arita J, Sakamoto Y, Hasegawa K, Kokudo N. One-year extended, monthly vaccination prophylaxis combined with hepatitis B immune globulin for hepatitis B after liver transplantation. Hepatol Res. 2016; 46:E51-59.
9. Oketani M, Ido A, Uto H, Tsubouchi H. Prevention of hepatitis B virus reactivation in patients receiving immunosuppressive therapy or chemotherapy. Hepatol Res. 2012; 42:627-636.
10. Bae SK, Shimoda S, Ikegami T, Yoshizumi T, Harimoto N, Itoh S, Soejima Y, Uchiyama H, Shirabe K, Maehara Y. Risk factors for hepatitis B virus recurrence after living donor liver transplantation: A 17-year experience at a single center. Hepatol Res. 2015; 45:1203-1210.
11. Cooreman MP, van Roosmalen MH, te Morsche R, Sünnen CM, de Ven EM, Jansen JB, Tytgat GN, de Wit PL, Paulij WP. Characterization of the reactivity pattern of murine monoclonal antibodies against wild-type hepatitis B surface antigen to G145R and other naturally occurring "a" loop escape mutations. Hepatology. 1999; 30:1287-1292.
12. Ishigami M, Honda T, Ishizu Y, Onishi Y, Kamei H, Hayashi K, Ogura Y, Hirooka Y, Goto H. Frequent incidence of escape mutants after successful hepatitis B vaccine response and stopping of nucleos(t)ide analogues

in liver transplant recipients. Liver Transplant. 2014; 20:1211-1220.
13. Markowitz JS, Martin P, Conrad AJ, *et al*. Prophylaxis against hepatitis B recurrence following liver transplantation using combination lamivudine and hepatitis B immune globulin. Hepatology. 1998; 28:585-589.
14. Marzano A, Salizzoni M, Debernardi-Venon W, Smedile A, Franchello A, Ciancio A, Gentilcore E, Piantino P, Barbui AM, David E, Negro F, Rizzetto M. Prevention of hepatitis B virus recurrence after liver transplantation in cirrhotic patients treated with lamivudine and passive immunoprophylaxis. J Hepatol. 2001; 34:903-910.
15. Ghany MG, Ayola B, Villamil FG, Gish RG, Rojter S, Vierling JM, Lok AS. Hepatitis B virus S mutants in liver transplant recipients who were reinfected despite hepatitis B immune globulin prophylaxis. Hepatology. 1998; 27:213-222.
16. Ueda Y, Marusawa H, Egawa H, Okamoto S, Ogura Y, Oike F, Nishijima N, Takada Y, Uemoto S, Chiba T. De novo activation of HBV with escape mutations from hepatitis B surface antibody after living donor liver transplantation. Antivir Ther. 2011; 16:479-487.
17. Terrault NA, Zhou S, McCory RW, Pruett TL, Lake JR, Roberts JP, Ascher NL, Wright TL. Incidence and clinical consequences of surface and polymerase gene mutations in liver transplant recipients on hepatitis B immunoglobulin. Hepatology. 1998; 28:555-561.
18. Zuckerman JN, Zuckerman AJ. Mutations of the surface protein of hepatitis B virus. Antiviral Res. 2003; 60:75-78.
19. Wang SH, Loh PY, Lin TL, Lin LM, Li WF, Lin YH, Lin CC, Chen CL. Active immunization for prevention of De novo hepatitis B virus infection after adult living donor liver transplantation with a hepatitis B core antigen-positive graft. Liver Transplant. 2017; 23:1266-1272.
20. Cholongitas E, Papatheodoridis G V. Liver transplantation using hepatitis B core positive grafts: Which is the optimal antiviral prophylaxis? J Hepatol. 2019; 71:635-636.
21. Bae SK, Gushima T, Saito N, Yamanaka I, Shimokawa T, Matsuo Y, Yoshida S, Kawano I, Henzan H, Shimoda S, Eto T, Takahashi K. The impact of hepatitis B core antibody levels on HBV reactivation after allogeneic hematopoietic SCT: an 11-year experience at a single center. Bone Marrow Transplant. 2016; 51:1496-1498.
22. Bae SK, Yatsuhashi H, Takahara I, Tamada Y, Hashimoto S, Motoyoshi Y, Ozawa E, Nagaoka S, Yanagi K, Abiru S, Komori A, Ishibashi H. Sequential occurrence of acute hepatitis B among members of a high school Sumo wrestling club. Hepatol Res. 2014; 44:E267-272.
23. Yamashiki N, Yoshizawa A, Ueda Y, Kaido T, Okajima H, Marusawa H, Seno H, Uemoto S. The use of hepatitis B immunoglobulin with or without hepatitis B vaccine to prevent de novo hepatitis B in pediatric recipients of anti-HBc-positive livers. Pediatr Transplant. 2018; 22:e13227.
24. Kogiso T, Tokushige K. Key roles of hepatologists in successful liver transplantation. Hepatol Res. 2018; 48:608-621.
25. Wong TC, Fung JY, Cui TY, Lam AH, Dai JW, Chan AC, Cheung TT, Chok KS, Ng KK, Lo CM. Liver transplantation using hepatitis B core positive grafts with antiviral monotherapy prophylaxis. J Hepatol. 2019; 70:1114-1122.
26. Verna EC. Vaccination to prevent de novo hepatitis B: Are there patients who do not need antiviral prophylaxis? Liver Transplant. 2017; 23:1253-1254.

(Received October 14, 2019; Revised October 24, 2019; Accepted October 26, 2019)

Brief Report

DOI: 10.5582/bst.2019.01271

Laparoscopic duodenum and spleen-preserving total pancreatectomy: A novel surgical technique for pancreatic intraductal papillary mucinous neoplasms

Jia Wu[1,§], Qirong Hu[2,§], Liming Jin[1], Weifeng Yao[1], Chengwu Zhang[1], Zhiming Hu[1], Yuhua Zhang[1,*]

[1] *Department of Hepatobiliary and Pancreatic Surgery, Zhejiang Provincial People's Hospital and Hangzhou Medical College Affiliated Hospital, Zhejiang, China;*
[2] *Department of Surgery, Yongkang First People's Hospital, Zhejiang, China.*

Summary **Intraductal papillary mucinous neoplasm (IPMN) of the pancreas is no longer a rarely diagnosed disease, because of the development of medical imaging. With a high incidence of canceration, especially in the main duct type, surgery is strongly recommended. Pancreatoduodenectomy, distal pancreatectomy and central pancreatectomy are applied in those cases. For this potentially malignant disease, function-preserving surgery seems more appropriate. An old female was enrolled in our research, who was diagnosed with IPMN. Diameter of the main pancreatic duct (MPD) was > 5 mm and lesions distributed to the whole pancreas. laparoscopic duodenum and spleen-preserving total pancreatoduodenectomy was carried out, which has not reported previously. We successfully performed laparoscopic duodenum and spleen-preserving total pancreatectomy, without major complications such as severe pancreatic fistula, postoperative bleeding, and delayed ischemia of duodenum and spleen. We consider laparoscopic duodenum and spleen-preserving total pancreatectomy is technically feasible, but a large sample of randomized controlled trials is needed to evaluate its safety, effectiveness and long-term outcome.**

Keywords: Laparoscopy, function-preserving, total pancreatectomy, IPMN, pancreatoduodenectomy

1. Introduction

Although some consensus defined the surgical indication for intraductal papillary mucinous neoplasm (IPMN) as diameter of main pancreatic duct more than 10 mm (*1*). However, it is still controversial, Hackert *et al*. reported main duct type IPMN of the pancreas is potentially malignant, especially when the diameter of the main pancreatic duct (MPD) is > 5 mm (*2*). To achieve radical resection in these cases, total pancreatectomy (TP) is indicated. Laparoscopic TP is a complicated procedure that has been described recently with resection of the spleen and/or duodenum (*3-6*). However, function-preserving surgery, such as pylorus-preserving pancreatoduodenectomy, is widely used for benign, potentially malignant and even malignant tumors of the pancreas (*7*). Laparoscopic spleen-preserving distal pancreatectomy and laparoscopic duodenum-preserving pancreatic head resection (*8,9*) have been reported to treat benign or low-grade malignant tumors respectively.

Here, we present a patient with main duct IPMN treated with laparoscopic duodenum and spleen-preserving TP, which has not published previously.

2. Materials and Methods

2.1. *Characteristic of patient*

A 68-year-old female patient was admitted to our hospital because preoperative examination revealed

Released online in J-STAGE as advance publication October 15, 2019.

[§]These authors contributed equally to this work.

**Address correspondence to:*
Dr. Yuhua Zhang, Department of Hepatobiliary and Pancreatic Surgery, Zhejiang Provincial People's Hospital and Hangzhou Medical College Affiliated Hospital, 158 Shangtang Rd, Xiacheng, Hangzhou, Zhejiang 310014, China.
E-mail: zhangyuhua1013@126.com

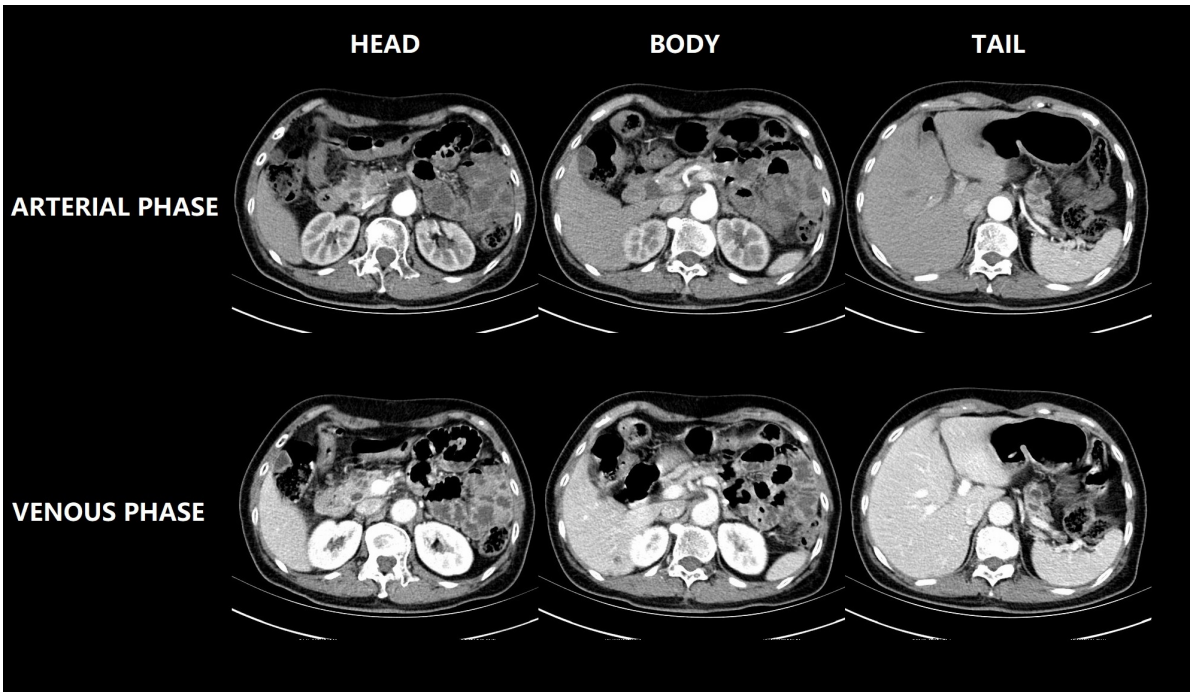

Figure 1. Enhanced CT showed the lesions in different parts of pancreas in each phase.

pancreatic cystic lesions when she underwent endoscopic submucosal dissection (ESD) for early gastric cancer in another hospital 3 months previously. Physical examination and laboratory workup, including tumor markers, were all negative and she denied a history of alcohol abuse.

2.2. *Imaging outcome*

Enhanced computed tomography (CT) demonstrated (Figure 1) that there was a cystic solid lesion in the pancreatic head, which connected with the MPD, which was dilated. The lesion was not enhanced after injection of contrast agent, and the left renal anterior fascia was not thickened. The common bile duct (CBD) was not dilated and no significantly enlarged lymph nodes were found in the retroperitoneum. Endoscopic ultrasonography (EUS) revealed that the pancreatic duct at the tail of the pancreas was significantly dilated, with a maximum inner diameter of 6.5 mm. The pancreatic neck had a honeycomb-like non-echo structure, smooth cystic wall, no mural nodules, and the cystic solid lesion communicated with the MPD. The diameter of pancreatic head MPD expanded to 5.5 mm, and duodenal papilla were normal, and similar changes were found on magnetic resonance imaging.

According to enhanced CT and EUS, the patient was diagnosed with pancreatic IPMN of mixed type. The lesion spread throughout the whole pancreas and TP was indicated. However, for this borderline tumor, function-preserving surgery was more appropriate than TP. Based on our experience with laparoscopic pancreatoduodenectomy and spleen-preserving distal pancreatectomy, we decided to perform laparoscopic duodenum and spleen-preserving TP. It was approved by Ethics Committee of Zhejiang Provincial People's Hospital and had gotten written informed consent from the patient.

2.3. *Surgical procedure*

The patient was placed in the reverse Trendelenburg position with head raised to 30°. Pneumoperitoneum was established in the umbilical incision with setting pressure at 14 mmHg. The 5 trocars were placed in a V shape. The gastrocolic and hepatogastric ligaments were opened to visualize the pancreas. A catheter was used to hang up the stomach through the abdominal wall. Our procedure started with opening the retroperitoneum at the upper edge of the pancreatic neck, and dividing the initial part of the splenic artery and suspending it with a fine rubber tape. Then, we opened the retroperitoneum at the lower edge of the pancreas, near the superior mesenteric vein (SMV). After establishing a retropancreatic tunnel, the pancreatic neck was suspended by a tape and transected by an ultrasonic scalpel. After transection of the pancreatic neck, the operation was divided into two steps: spleen-preserving distal pancreatectomy and duodenum-preserving pancreatic head resection.

2.3.1. *Spleen-preserving distal pancreatectomy*

After hanging the pancreatic neck by the atraumatic grasper, we opened the pancreatic capsule along the lower edge from proximal to distal, visualized the

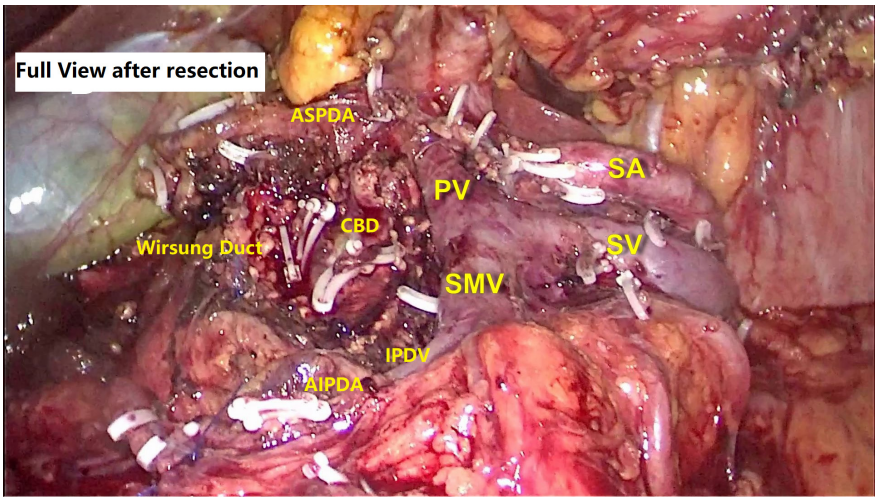

Figure 2. The structure after duodenum and spleen preserving total pancreatectomy.

splenic vein, and carefully dissected the branches of the vein toward the pancreas and ligated them with a hem-o-lok (Teleflex, USA.) clip. After disconnecting all the branches attached to the splenic vein, we pulled the pancreas to the tail side, which made it clearer to expose the upper edge of the pancreas. We opened the pancreatic capsule along the upper edge from proximal to distal and pulled the initial part of the splenic artery, which was suspended by a tape in the direction of the head side, which ensured proper tension between the distal pancreas and the splenic artery. As with the splenic vein, we disconnected the branches from the splenic artery to the pancreas. The distal pancreas was resected completely.

2.3.2. *Duodenum-preserving pancreatic head resection*

After finishing distal pancreatectomy, we started duodenum-preserving pancreatic head resection. We turned the pancreatic neck to the right side, and divided the space between the portal vein-SMV and pancreatic head, some collateral branches toward the uncinate process were dissected and sealed by hem-o-lok. We dissected the tissue between the superior mesenteric artery (SMA) and uncinate process, bipolar coagulation and hem-o-lok were used to ligate or seal the small branches from the SMA to the uncinate process. The anterior capsule of the pancreas was opened at the lower part of the pancreatic neck, and subcapsular dissection was carried out. After the anterior inferior pancreatoduodenal artery (AIPDA) was dissected and ligated by hem-o-lok, the lower part of the pancreatic head and uncinate process were separated by preserving a small amount of pancreatic tissue to ensure the integrity of the posterior inferior pancreatoduodenal arterial (PIPDA) arcade. When the upper part of the pancreatic head was separated, the lower CBD was exposed and the terminal CBD was embedded in the pancreas. The blood supply of the lower CBD came from the posterior superior pancreatoduodenal artery (PSPDA), which came from the gastroduodenal artery. Maintenance of the integrity of the PSPDA was the key to avoiding ischemia of the CBD and postoperative bile leakage.

We followed the principle that from left to right, from ventral to dorsal, preservation of some pancreatic tissue would avoid injury to the posterior arcade along the duodenum. When we reached the descending duodenum, the MPD to the ampulla of Vater was visualized, ligated and cut off. The pancreatic head including the uncinate process was resected completely (Figure 2), and the specimen was placed in a bag and retrieved by an enlarged trocar incision. Two drainage tubes were positioned on the wound surface of the pancreas and Winslow hole, respectively.

3. Results and Discussion

Spleen-preserving and duodenum-preserving laparoscopic TP was performed in 270 min, with 250 ml blood loss, without major complications including postoperative bleeding, duodenal or splenic necrosis, or delayed gastric emptying. On postoperative day (POD) 1, the nasogastric tube was discontinued, and diabetic fluid was started on POD 3. The drainage tube was withdrawn on POD 7, when there was no evidence of bile and pancreatic leakage. The patient's hospital course was uncomplicated and she was discharged home on POD 9. Pathological examination demonstrated mixed type of IPMN with mild to moderate dysplasia. For insulin regimen, we gave continuous insulin infusion during fasting and adjusted the dosage according to the level of fasting blood glucose. When oral feeding was resumed, we gave quick-acting insulin before three meals and long-acting insulin before bedtime, after obtaining the opinion of an endocrinology consultant. Compound digestive enzyme capsules were used in the substitution therapy of external secretion function.

We followed up the patient for 3 months, and routine blood, biochemical and other indicators, and glycosylated hemoglobin were in the normal range. Enhanced CT was repeated 1 month after surgery, which showed a small amount of normal pancreatic tissue left surrounding the CBD, and no duodenal or splenic ischemia.

MPD diameter 5-9.9 mm is the single best predictor of high-grade or invasive main duct type IPMN, and is a key indicator of surgical candidates (*10*). MPD diameter > 10 mm is identified as a high-risk stigmata for malignancy in the Fukuoka guidelines (*1*). According to the location of the lesion, pancreatoduodenectomy, central pancreatectomy, distal pancreatectomy and TP are available surgical procedures.

TP is a complicated and highly technically demanding procedure, especially when performed laparoscopically. Several studies have focused on laparoscopic TP and demonstrated that it is a safe procedure in selected patients. Chapman *et al*. reported laparoscopic TP with spleen preservation for main duct IPMN (*3*). Peng *et al*. reported 3 cases of TP for IPMN and pancreatic neuroendocrine tumor, they resected the whole pancreas and duodenum with preservation of the pylorus and spleen (*6*).

Function-preserving pancreatic surgery was launched recently, and provided patients with enhanced recovery and low rate of postoperative complications (*7*). Beger *et al*. reported duodenum-preserving pancreatic head resection for pancreatic benign or low-grade malignant lesions (*11*). Cao *et al*. reported 12 cases of laparoscopic duodenum-preserving total pancreatic head resection (*8*). They transected the pancreatic neck and performed subcapsular dissection to mobilize the pancreatic head, and paid close attention to preserving the anterior and/or posterior pancreatic duodenal arterial arcade. Furthermore, Yamashita *et al*. reported the case of resection of the second portion of the duodenum but preserving the pancreas for a recurrent duodenal adenocarcinoma patient (*12*).

However, in most of the published studies, TP was combined with duodenal and/or splenic resection, even in some patients with benign or potentially malignant lesions. There are no reports of laparoscopic TP with both spleen and duodenum preservation.

Our center has experience of laparoscopic spleen-preserving distal pancreatectomy and laparoscopic duodenum-preserving pancreatic head resection over 100 cases in the past 5 years. These procedures have been proved to be minimally invasive and patients have better survival and quality of life postoperatively.

In the present case, we performed duodenum and spleen-preserving TP. The duodenal papilla could be seen at the intersection of the biliary, pancreatic and alimentary tracts. Our procedure starts with transection of the pancreatic neck, followed by two steps of spleen-preserving distal pancreatectomy and duodenum-preserving pancreatic head resection. The key feature of spleen-preserving distal pancreatectomy is accurately identifying the arterial branches of the splenic artery (*e.g*. great pancreatic artery, transverse pancreatic artery, or dorsal pancreatic artery) and venous branches toward the pancreas. The small branches usually tear easily if we hang the distal pancreas with too much tension, and this is the most common reason for conversion to or combination with splenectomy. We strongly recommend transection of the pancreatic neck first, which facilitates hanging the distal pancreas to visualize the space between the splenic vessels and distal pancreas, by excluding the limitation of the immobilized pancreatic head. But in potentially malignant cases, the principle of En bloc resection should be applied strictly.

Duodenum-preserving pancreatic head resection is the best choice for treatment of benign and low-grade malignant tumors, but it only can be carried out in large centers. The duodenum has a poor blood supply. Its feeding arteries are the anterior and posterior arcades, which are formed by branches of the superior pancreatoduodenal artery (SPDA) and IPDA. The anterior SPDA (ASPDA) and AIPDA derive from the anterior arcade, and the PSPDA and PIPDA from the posterior arcade. Compared with the concomitant artery, preservation of venous arcade is tougher because of thin wall. The pancreatic head is covered by a capsule to the front and in the rear, and this capsule is continuous with the retroperitoneum, and surrounded by the C-shaped duodenum and left margin of the portal vein. In this space, we must preserve at least one arcade. The anterior arcade is usually detached for further deep dissection, and the posterior arcade must be preserved carefully. Takada (*13*) mentioned that the PSPDA is important to avoid ischemia, and the retropancreatic fascia (posterior capsule) and fibrotic tissue along the CBD were preserved to ensure the blood supply. The anterior capsule should be opened with ligation of the initial part of the ASPDA and AIPDA, the posterior capsule should be kept integrally for preserving PSPDA and PIPDA. In addition, the segment of the Wirsung duct (MPD) that converges into the ampulla should be identified and sealed.

Laparoscopic duodenum and spleen-preserving TP is a safe, feasible, function-preserving, novel surgical procedure, and surgeons should implement spleen-preserving distal pancreatectomy and duodenum-preserving pancreatoduodenectomy. Surgeons who want to implement this procedure should perform laparoscopic spleen-preserving distal pancreatectomy or laparoscopic duodenum-preserving pancreatic head resection, and then laparoscopic duodenum and spleen-preserving TP. The outcome from present single case or small numbers of cases can only be suggestive, and further prospective randomized studies are needed to obtain an objective assessment of laparoscopic duodenum and spleen-preserving TP.

References

1. Tanaka M, Fernández-Del Castillo C, Kamisawa T, Jang JY, Levy P, Ohtsuka T, Salvia R, Shimizu Y, Tada M, Wolfgang CL. Revisions of international consensus Fukuoka guidelines for the management of IPMN of the pancreas. Pancreatology. 2017; 17:738-753.
2. Hackert T, Fritz S, Klauss M, Bergmann F, Hinz U, Strobel O, Schneider L, Büchler MW. Main-duct intraductal papillary mucinous neoplasm: High cancer risk in duct diameter of 5 to 9 mm. Ann Surg. 2015; 262:875-880.
3. Chapman BC, Paniccia A, Ryan C, Schulick RD, Edil BH. Laparoscopic spleen-preserving total pancreatectomy for a main-duct intraductal papillary mucinous neoplasm. Ann Surg Oncol. 2017; 24:560.
4. Dallemagne B, de Oliveira AT, Lacerda CF, D'Agostino J, Mercoli H, Marescaux J. Full laparoscopic total pancreatectomy with and without spleen and pylorus preservation: A feasibility report. J Hepatobiliary Pancreat Sci. 2013; 20:647-653.
5. Gumbs AA, Daskalaki D, Milone L. Laparoscopic total pancreatectomy for chronic pancreatitis. Surg Laparosc Endosc Percutan Tech. 2018; 28:e62.
6. Wang X, Li Y, Cai Y, Liu X, Peng B. Laparoscopic total pancreatectomy: Case report and literature review. Medicine (Baltimore). 2017; 96:e5869
7. Klaiber U, Probst P, Hüttner FJ, Bruckner T, Strobel O, Diener MK, Mihaljevic AL, Büchler MW, Hackert T. Randomized trial of pylorus-preserving vs. pylorus-resecting pancreatoduodenectomy: Long-term morbidity and quality of life. J Gastrointest Surg. 2019; doi: 10.1007/s11605-018-04102-y.
8. Cao J, Li GL, Wei JX, Yang WB, Shang CZ, Chen YJ, Lau WY, Min J. Laparoscopic duodenum-preserving total pancreatic head resection: a novel surgical approach for benign or low-grade malignant tumors. Surg Endosc. 2019; 33:633-638.
9. Dai MH, Shi N, Xing C, Liao Q, Zhang TP, Chen G, Wu WM, Guo JC, Liu ZW, Zhao YP. Splenic preservation in laparoscopic distal pancreatectomy. Br J Surg. 2017; 104:452-462.
10. Del Chiaro M, Beckman R, Ateeb Z, *et al*. Main duct dilatation is the best predictor of high-grade dysplasia or invasion in intraductal papillary mucinous neoplasms of the pancreas. Ann Surg. 2019; doi: 10.1097/SLA.0000000000003174.
11. Beger HG, Rau BM, Gansauge F, Poch B. Duodenum-preserving subtotal and total pancreatic head resections for inflammatory and cystic neoplastic lesions of the pancreas. J Gastrointest Surg. 2008; 12:1127-1132.
12. Yamashita S, Sakamoto Y, Kaneko J, Tamura S, Aoki T, Sugawara Y, Hasegawa K, Kokudo N. Resection of the second portion of the duodenum sacrificing the minor papilla but preserving the pancreas for a recurrent duodenal adenocarcinoma: Report of a case. Biosci Trends. 2012; 6:44-47.
13. Takada T, Yasuda H, Amano H, Yoshida M. A duodenum-preserving and bile duct-preserving total pancreatic head resection with associated pancreatic duct-to-duct anastomosis. J Gastrointest Surg. 2004; 8:220-224.

(Received September 2, 2019; Revised October 8, 2019; Accepted October 10, 2019)

Communication

DOI: 10.5582/bst.2019.01243

Rapid advances in research on and development of anticancer drugs in China

Xu Yao[1], Nan Du[2], Shasha Hu[3], Lei Wang[1], Jianjun Gao[1,*]

[1] *Department of Pharmacology, School of Pharmacy, Qingdao University, Qingdao, Shandong, China;*
[2] *Department of Otolaryngology, Liaocheng Dongchangfu District Hospital, Liaocheng, Shandong, China;*
[3] *Department of Pathology, the Affiliated Hospital of Qingdao University, Qingdao, Shandong, China.*

Summary **Cancer is a major public health issue in China, and effective anticancer drugs remain a huge unmet need. Generic drugs have long been the main products of pharmaceutical companies in China. In this decade, research on and development of innovative drugs has greatly advanced thanks to policy reforms and economic growth. Five innovative anticancer drugs - anlotinib, pyrotinib, fruquintinib, sintilimab, and toripalimab - that were developed by Chinese domestic pharmaceutical companies were approved by the National Medical Products Administration (NMPA) of China in 2018. Several novel anticancer drugs such as avitinib, flumatinib, zanubrutinib, and ensartinib may also receive approval for marketing in China in the near future. There are unprecedented opportunities for development of innovative drugs in China. In the future, innovative drug development in China is poised to shift from "me too" or "me better" drugs to "first-in-class" or "best-in-class" drugs.**

Keywords: China, anticancer drug, molecularly targeted drug, immune checkpoint inhibitor

Cancer is the second leading cause of death globally and was responsible for an estimated 9.6 million deaths in 2018 according to data from the World Health Organization (*1*). In China, there were approximately 4.3 million new cancer cases and 2.9 million cancer deaths in 2018 (*2*). This represents a substantial demand for novel anticancer drugs. Generic drugs have long been the main products of pharmaceutical companies in China due to their limited financial resources and government drug policies. In this decade, economic growth and the reform of drug policies have led to a rapid increase in the number of innovative drugs, and especially anticancer drugs, developed by Chinese domestic pharmaceutical companies.

Molecularly targeted drugs (MTDs) and immune checkpoint inhibitors (ICIs) are the focus of research on and development of anticancer drugs. Since the year 2010, 6 MDTs - icotinib, apatinib, chidamide, anlotinib, pyrotinib, and fruquintinib - and 3 ICIs - sintilimab, toripalimab, and camrelizumab - have been approved by the National Medical Products Administration (NMPA) of China (Table 1). Icotinib, a first-generation epidermal growth factor receptor (EGFR) tyrosine kinase inhibitor, was approved in 2011 for use as monotherapy in patients with non-small-cell lung cancer (NSCLC) with somatic EGFR mutations. Icotinib won the State Scientific and Technological Progress Award in 2015, and this success represents a landmark in the field of drug research and development in China. In 2017, icotinib appeared to account for over a third of the Chinese market share in lung cancer therapies since attaining approval (*3*). In 2014, the NMPA approved apatinib to treat late-stage gastric carcinoma and chidamide to treat peripheral T-cell lymphoma. Both drugs are now undergoing clinical trials for additional indications. A recently completed phase 3 clinical trial showed that chidamide plus exemestane achieved the primary endpoint in patients with advanced, hormone receptor-positive, HER2-negative breast cancer that progressed after previous endocrine therapy (*4*). Based on these promising results, an application for a new indication of chidamide was submitted to the NMPA in November

Released online in J-STAGE as advance publication September 10, 2019.

**Address correspondence to:*
Dr. Jianjun Gao, Department of Pharmacology, School of Pharmacy, Qingdao University, 38 Dengzhou Road, Qingdao, Shandong, China 266021.
E-mail: gaojj@qdu.edu.cn

Table 1. The approved anticancer drugs originally developed by Chinese pharmaceutical companies since 2010

Drug	Target(s)	Indication(s)	Developer	Year
Icotinib	EGFR	Non-small-cell lung cancer	Betta Pharmaceuticals	2011
Apatinib	VEGFR	Gastric cancer	Hengrui Medicine	2014
Chidamide	HDAC	Peripheral T-cell lymphoma	Chipscreen Biosciences	2014
Anlotinib	VEGFR, PDGFR, c-Kit	Non-small-cell lung cancer, alveolar soft part sarcoma, clear cell sarcoma	Chiatai Tianqing	2018
Pyrotinib	EGFR, HER2	Breast cancer	Hengrui Medicine	2018
Fruquintinib	VEGFR	Colorectal cancer	Hutchison MediPharma	2018
Sintilimab	PD-1	Hodgkin's lymphoma	Innovent Biologics	2018
Toripalimab	PD-1	Melanoma	Suzhou Union Biopharm Biosciences	2018
Camrelizumab	PD-1	Hodgkin's lymphoma	Hengrui Medicine	2019

EGFR, epidermal growth factor receptor; VEGFR, vascular endothelial growth factor receptor; HDAC, histone deacetylase; PDGFR, platelet-derived growth factor receptor; HER2, human epidermal growth factor receptor 2; PD-1, programmed cell death protein 1.

2018. The year 2018 was a fruitful one for the Chinese pharmaceutical industry since 5 innovative anticancer drugs - anlotinib, pyrotinib, fruquintinib, sintilimab, and toripalimab - were approved by the NMPA (Table 1). Clinical trials of pyrotinib, fruquintinib, and toripalimab are currently underway in the United States.

Good results are also expected in 2019. Camrelizumab has already been approved. Applications for marketing approval that were submitted in 2018 for several anticancer drugs such as avitinib, flumatinib, zanubrutinib, and ensartinib may soon receive approval. Avitinib is a third-generation EGFR inhibitor designed to treat patients with NSCLC who have developed resistance to first-generation EGFR inhibitors and who have the gatekeeper mutation of EGFR, T790M (*5*). The recently disclosed results of a phase 2 clinical trial of avitinib showed that the objective response rate was 50.2% and the disease control rate was 88% in patients with EGFR T790M+ NSCLC (*6*). An application for conditional approval of avitinib was submitted to the NMPA. Flumatinib is a selective inhibitor of BCR-ABL1 designed for treatment of Philadelphia chromosome-positive chronic myeloid leukemia in the chronic phase (CML-CP) (*7*). Results from a phase 3 clinical trial showed that flumatinib is comparable to imatinib in its safety and superior in its efficacy profile at 3, 6, and 12 months, supporting flumatinib as a frontline treatment option for patients with newly diagnosed CML-CP (*7*). Zanubrutinib is an inhibitor of Bruton tyrosine kinase (BTK) targeting B-cell malignancies such as mantle cell lymphoma (MCL), chronic lymphocytic leukemia, small lymphocytic lymphoma, Waldenstrom's macroglobulinemia, and follicular lymphoma (*8*). Zanubrutinib treatment had an overall response rate of 84%, including a complete response rate of 59% in patients with relapsed or refractory MCL in a phase 2 trial (*9*). Based on these findings, an application for use of zanubrutinib to treat relapsed/refractory MCL was submitted to the NMPA. Zanubrutinib was also designated as a breakthrough therapy by the US Food and Drug Administration in January 2019. Ensartinib is a potent anaplastic lymphoma kinase (ALK) inhibitor for potential treatment of NSCLC (*10*). A phase 1/2 clinical trial showed that ensartinib treatment resulted in a response rate of 60% and median progression-free survival of 9.0 months in patients with ALK-positive NSCLC (*11*). All of these drugs showing promising clinical activity and manageable toxicity may benefit select patients in the near future.

Rapid advances in the research on and development of innovative drugs in China may be ascribed to the following factors. From the perspective of national policies, in recent years China has issued a series of supporting policies in the field of innovative drugs, such as reform of drug registration and classification, implementation of a Marketing Authorization Holder (MAH) system, priority review of innovative drugs, compensation of the duration of a drug patent, and enhancement of the protection of drug test data. A point worth noting is that the government also implemented a National Major Scientific and Technological Special Project for "Significant New Drugs Development" in 2008 (*12*). All of these reforms have eliminated policy obstacles and accelerated the speed of research on and development of innovative drugs. In the eyes of pharmaceutical companies, innovative drugs and technologies have become a hot spot for capital investment in China. Pharmaceutical companies such as Chipscreen Biosciences, BeiGene, and Innovent have announced obtaining a large amount of financing to provide capital investment for novel drug development. In addition, a large number of native and returning Chinese professionals have become a reliable human resource for drug development. Thus, there are unprecedented opportunities in China for innovative drug development thanks to the promotion of policies, capital, and qualified personnel. In the future, drug development in China is poised to shift from generic, "me too" or "me better" drugs to "first-in-class" or "best-in-class" drugs.

References

1. World Health Organization. Key Facts of Cancer. *https://*

www.who.int/news-room/fact-sheets/detail/cancer. (accessed August 21, 2019).
2. World Health Organization. Globocan 2018. *https://gco.iarc.fr/today/data/factsheets/populations/160-china-fact-sheets.pdf*. (accessed August 21, 2019).
3. BetaPharma: About Us: Icotinib Hydrochloride. *http://betapharma.com/about-us/icotinib/* (Accessed August 22, 2019)
4. Jiang Z, Li W, Hu X, *et al*. Tucidinostat plus exemestane for postmenopausal patients with advanced, hormone receptor-positive breast cancer (ACE): A randomised, double-blind, placebo-controlled, phase 3 trial. Lancet Oncol. 2019; 20:806-815.
5. Wang H, Zhang L, Hu P, Zheng X, Si X, Zhang X, Wang M. Penetration of the blood-brain barrier by avitinib and its control of intra/extra-cranial disease in non-small cell lung cancer harboring the T790M mutation. Lung Cancer. 2018; 122:1-6.
6. Zhou Q WL, Feng L, *et al*. Safety and efficacy of abivertinib (AC0010), a third-generation EGFR tyrosine kinase inhibitor, in Chinese patients with EGFR-T790M positive non-small cell lung cancer (NCSLC). J Clin Oncol. 2019; 37(Suppl. 15):9091-9091.
7. Zhang L LM, Zhang Y, *et al*. Frontline flumatinib versus imatinib in patients with chronic myeloid leukemia in chronic phase: Results from the China randomized phase III study. J Clin Oncol. 2019; 37(Suppl. 15):7004-7004.
8. Guo Y, Liu Y, Hu N, et al. Discovery of zanubrutinib (BGB-3111), a novel, potent, and selective covalent inhibitor of Bruton's tyrosine kinase. J Med Chem. 2019. doi: 10.1021/acs.jmedchem.9b00687.
9. Song Y, Zhou K, Zou D, *et al*. Safety and activity of the investigational Bruton tyrosine kinase inhibitor zanubrutinib (BGB-3111) in patients with mantle cell lymphoma from a phase 2 trial. Blood. 2018; 132(Suppl. 1):148.
10. Li T, Ma W, Tian EC. Ensartinib (X-396): What does it add for patients with ALK-rearranged NSCLC. Chin Clin Oncol. 2018. doi: 10.21037/cco.2018.10.12.
11. Horn L, Infante JR, Reckamp KL, *et al*. Ensartinib (X-396) in ALK-positive non-small cell lung cancer: Results from a first-in-human phase I/II, multicenter study. Clin Cancer Res. 2018; 24:2771-2779.
12. State Council of the People's Republic of China. *http://www.gov.cn/xinwen/2019-02/22/content_5367843.htm* (accessed August 22, 2019). (in Chinese).

(Received August 25, 2019; Accepted August 28, 2019)

BioScience Trends. 2019; 13(5):E1.

DOI: 10.5582/bst.2019.E1

RETRACTED: Polyphosphate-induced matrix metalloproteinase-3-mediated differentiation in rat dental pulp fibroblast-like cells.

This article entitled “Polyphosphate-induced matrix metalloproteinase-3-mediated differentiation in rat dental pulp fibroblast-like cells” (*1*) has been retracted at the request of the authors due to research misconduct.

Reference

1. Hiyama T, Ozeki N, Hase N, Yamaguchi H, Kawai R, Kondo A, Mogi M, Nakata K. Polyphosphate-induced matrix metalloproteinase-3-mediated differentiation in rat dental pulp fibroblast-like cells. *Biosci Trends. 2015; 9(6):360-366.*

BioScience Trends. 2019; 13(5):E2.

DOI: 10.5582/bst.2019.E2

RETRACTED: Polyphosphate-induced matrix metalloproteinase-13 is required for osteoblast-like cell differentiation in human adipose tissue derived mesenchymal stem cells.

This article entitled "Polyphosphate-induced matrix metalloproteinase-13 is required for osteoblast-like cell differentiation in human adipose tissue derived mesenchymal stem cells" (*1*) has been retracted at the request of the authors due to research misconduct.

Reference

1. Ozeki N, Mogi M, Hase N, Hiyama T, Yamaguchi H, Kawai R, Nakata K. Polyphosphate-induced matrix metalloproteinase-13 is required for osteoblast-like cell differentiation in human adipose tissue derived mesenchymal stem cells. *BioScience Trends. 2016; 10(5):365-371.*

BST
BioScience Trends

Guide for Authors

1. Scope of Articles

BioScience Trends is an international peer-reviewed journal. BioScience Trends devotes to publishing the latest and most exciting advances in scientific research. Articles cover fields of life science such as biochemistry, molecular biology, clinical research, public health, medical care system, and social science in order to encourage cooperation and exchange among scientists and clinical researchers.

2. Submission Types

Original Articles should be well-documented, novel, and significant to the field as a whole. An Original Article should be arranged into the following sections: Title page, Abstract, Introduction, Materials and Methods, Results, Discussion, Acknowledgments, and References. Original articles should not exceed 5,000 words in length (excluding references) and should be limited to a maximum of 50 references. Articles may contain a maximum of 10 figures and/or tables.

Brief Reports definitively documenting either experimental results or informative clinical observations will be considered for publication in this category. Brief Reports are not intended for publication of incomplete or preliminary findings. Brief Reports should not exceed 3,000 words in length (excluding references) and should be limited to a maximum of 4 figures and/or tables and 30 references. A Brief Report contains the same sections as an Original Article, but the Results and Discussion sections should be combined.

Reviews should present a full and up-to-date account of recent developments within an area of research. Normally, reviews should not exceed 8,000 words in length (excluding references) and should be limited to a maximum of 100 references. Mini reviews are also accepted.

Policy Forum articles discuss research and policy issues in areas related to life science such as public health, the medical care system, and social science and may address governmental issues at district, national, and international levels of discourse. Policy Forum articles should not exceed 2,000 words in length (excluding references).

Case Reports should be detailed reports of the symptoms, signs, diagnosis, treatment, and follow-up of an individual patient. Case reports may contain a demographic profile of the patient but usually describe an unusual or novel occurrence. Unreported or unusual side effects or adverse interactions involving medications will also be considered. Case Reports should not exceed 3,000 words in length (excluding references).

News articles should report the latest events in health sciences and medical research from around the world. News should not exceed 500 words in length.

Letters should present considered opinions in response to articles published in BioScience Trends in the last 6 months or issues of general interest. Letters should not exceed 800 words in length and may contain a maximum of 10 references.

3. Editorial Policies

Ethics: BioScience Trends requires that authors of reports of investigations in humans or animals indicate that those studies were formally approved by a relevant ethics committee or review board.

Conflict of Interest: All authors are required to disclose any actual or potential conflict of interest including financial interests or relationships with other people or organizations that might raise questions of bias in the work reported. If no conflict of interest exists for each author, please state "There is no conflict of interest to disclose".

Submission Declaration: When a manuscript is considered for submission to BioScience Trends, the authors should confirm that 1) no part of this manuscript is currently under consideration for publication elsewhere; 2) this manuscript does not contain the same information in whole or in part as manuscripts that have been published, accepted, or are under review elsewhere, except in the form of an abstract, a letter to the editor, or part of a published lecture or academic thesis; 3) authorization for publication has been obtained from the authors' employer or institution; and 4) all contributing authors have agreed to submit this manuscript.

Cover Letter: The manuscript must be accompanied by a cover letter signed by the corresponding author on behalf of all authors. The letter should indicate the basic findings of the work and their significance. The letter should also include a statement affirming that all authors concur with the submission and that the material submitted for publication has not been published previously or is not under consideration for publication elsewhere. The cover letter should be submitted in PDF format. For example of Cover Letter, please visit http://www.biosciencetrends.com/downcentre.php (Download Centre).

Copyright: A signed JOURNAL PUBLISHING AGREEMENT (JPA) form must be provided by post, fax, or as a scanned file before acceptance of the article. Only forms with a hand-written signature are accepted. This copyright will ensure the widest possible dissemination of information. A form facilitating transfer of copyright can be downloaded by clicking the appropriate link and can be returned to the e-mail address or fax number noted on the form (Please visit Download Centre). Please note that your manuscript will not proceed to the next step in publication until the JPA Form is received. In addition, if excerpts from other copyrighted works are included, the author(s) must obtain written permission from the copyright owners and credit the source(s) in the article.

Suggested Reviewers: A list of up to 3 reviewers who are qualified to assess the scientific merit of the study is welcomed. Reviewer information including names, affiliations, addresses, and e-mail should be provided at the same time the manuscript is submitted online. Please do not suggest reviewers with known conflicts of interest, including participants or anyone with a stake in the proposed research; anyone from the same institution; former students, advisors, or research collaborators (within the last three years); or close personal contacts. Please note that the Editor-in-Chief may accept one or more of the proposed reviewers or may request a review by other qualified persons.

Language Editing: Manuscripts prepared by authors whose native language is not English should have their work proofread by a native English speaker before submission. If not, this might delay the publication of your manuscript in BioScience Trends.

The Editing Support Organization can provide English proofreading, Japanese-English translation, and Chinese-English translation services to authors who want to publish in BioScience Trends and need assistance before submitting a manuscript. Authors can visit this organization directly at http://www.iacmhr.com/iac-eso/support.php?lang=en. IAC-ESO was established to facilitate manuscript preparation by researchers whose native language is not English and to help edit works intended for international academic journals.

4. Manuscript Preparation

Manuscripts should be written in clear, grammatically correct English and submitted as a Microsoft Word file in a single-column format. Manuscripts must be paginated and typed in 12-point Times New Roman font with 24-point line spacing. Please do not embed figures in the text. Abbreviations should be used as little as possible and should be explained at first mention unless the term is a well-known abbreviation (*e.g.* DNA). Single words should not be abbreviated.

Title Page: The title page must include 1) the title of the paper (Please note the title should be short, informative, and contain the major key words); 2) full name(s) and affiliation(s) of the author(s), 3) abbreviated names of the author(s), 4) full name, mailing address, telephone/fax numbers, and e-mail address of the corresponding author; and 5) conflicts of interest (if you have an actual or potential conflict of interest to disclose, it must be included as a footnote on the title page of the manuscript; if no conflict of

interest exists for each author, please state "There is no conflict of interest to disclose"). Please visit Download Centre and refer to the title page of the manuscript sample.

Abstract: The abstract should briefly state the purpose of the study, methods, main findings, and conclusions. For article types including Original Article, Brief Report, Review, Policy Forum, and Case Report, a one-paragraph abstract consisting of no more than 250 words must be included in the manuscript. For News and Letters, a brief summary of main content in 150 words or fewer should be included in the manuscript. Abbreviations must be kept to a minimum and non-standard abbreviations explained in brackets at first mention. References should be avoided in the abstract. Key words or phrases that do not occur in the title should be included in the Abstract page.

Introduction: The introduction should be a concise statement of the basis for the study and its scientific context.

Materials and Methods: The description should be brief but with sufficient detail to enable others to reproduce the experiments. Procedures that have been published previously should not be described in detail but appropriate references should simply be cited. Only new and significant modifications of previously published procedures require complete description. Names of products and manufacturers with their locations (city and state/country) should be given and sources of animals and cell lines should always be indicated. All clinical investigations must have been conducted in accordance with Declaration of Helsinki principles. All human and animal studies must have been approved by the appropriate institutional review board(s) and a specific declaration of approval must be made within this section.

Results: The description of the experimental results should be succinct but in sufficient detail to allow the experiments to be analyzed and interpreted by an independent reader. If necessary, subheadings may be used for an orderly presentation. All figures and tables must be referred to in the text.

Discussion: The data should be interpreted concisely without repeating material already presented in the Results section. Speculation is permissible, but it must be well-founded, and discussion of the wider implications of the findings is encouraged. Conclusions derived from the study should be included in this section.

Acknowledgments: All funding sources should be credited in the Acknowledgments section. In addition, people who contributed to the work but who do not meet the criteria for authors should be listed along with their contributions.

References: References should be numbered in the order in which they appear in the text. Citing of unpublished results, personal communications, conference abstracts, and theses in the reference list is not recommended but these sources may be mentioned in the text. In the reference list, cite the names of all authors when there are fifteen or fewer authors; if there are sixteen or more authors, list the first three followed by *et al.* Names of journals should be abbreviated in the style used in PubMed. Authors are responsible for the accuracy of the references. Examples are given below:

Example 1 (Sample journal reference):
Inagaki Y, Tang W, Zhang L, Du GH, Xu WF, Kokudo N. Novel aminopeptidase N (APN/CD13) inhibitor 24F can suppress invasion of hepatocellular carcinoma cells as well as angiogenesis. Biosci Trends. 2010; 4:56-60.

Example 2 (Sample journal reference with more than 15 authors):
Darby S, Hill D, Auvinen A, *et al.* Radon in homes and risk of lung cancer: Collaborative analysis of individual data from 13 European case-control studies. BMJ. 2005; 330:223.

Example 3 (Sample book reference):
Shalev AY. Post-traumatic stress disorder: diagnosis, history and life course. In: Post-traumatic Stress Disorder, Diagnosis, Management and Treatment (Nutt DJ, Davidson JR, Zohar J, eds.). Martin Dunitz, London, UK, 2000; pp. 1-15.

Example 4 (Sample web page reference):
Ministry of Health, Labour and Welfare of Japan. Dietary reference intakes for Japanese. *http://www.mhlw.go.jp/houdou/2004/11/h1122-2a.html* (accessed June 14, 2010).

Tables: All tables should be prepared in Microsoft Word or Excel and should be arranged at the end of the manuscript after the References section. Please note that tables should not in image format. All tables should have a concise title and should be numbered consecutively with Arabic numerals. If necessary, additional information should be given below the table.

Figure Legend: The figure legend should be typed on a separate page of the main manuscript and should include a short title and explanation. The legend should be concise but comprehensive and should be understood without referring to the text. Symbols used in figures must be explained.

Figure Preparation: All figures should be clear and cited in numerical order in the text. Figures must fit a one- or two-column format on the journal page: 8.3 cm (3.3 in.) wide for a single column, 17.3 cm (6.8 in.) wide for a double column; maximum height: 24.0 cm (9.5 in.). Please make sure that the symbols and numbers appeared in the figures should be clear. Please make sure that artwork files are in an acceptable format (TIFF or JPEG) at minimum resolution (600 dpi for illustrations, graphs, and annotated artwork, and 300 dpi for micrographs and photographs). Please provide all figures as separate files. Please note that low-resolution images are one of the leading causes of article resubmission and schedule delays. All color figures will be reproduced in full color in the online edition of the journal at no cost to authors.

Units and Symbols: Units and symbols conforming to the International System of Units (SI) should be used for physicochemical quantities. Solidus notation (*e.g.* mg/kg, mg/mL, mol/mm^2/min) should be used. Please refer to the SI Guide www.bipm.org/en/si/ for standard units.

Supplemental data: Supplemental data might be useful for supporting and enhancing your scientific research and BioScience Trends accepts the submission of these materials which will be only published online alongside the electronic version of your article. Supplemental files (figures, tables, and other text materials) should be prepared according to the above guidelines, numbered in Arabic numerals (*e.g.*, Figure S1, Figure S2, and Table S1, Table S2) and referred to in the text. All figures and tables should have titles and legends. All figure legends, tables and supplemental text materials should be placed at the end of the paper. Please note all of these supplemental data should be provided at the time of initial submission and note that the editors reserve the right to limit the size and length of Supplemental Data.

5. Submission Checklist

The Submission Checklist will be useful during the final checking of a manuscript prior to sending it to BioScience Trends for review. Please visit Download Centre and download the Submission Checklist file.

6. Online Submission

Manuscripts should be submitted to BioScience Trends online at http://www.biosciencetrends.com. The manuscript file should be smaller than 5 MB in size. If for any reason you are unable to submit a file online, please contact the Editorial Office by e-mail at office@biosciencetrends.com.

7. Accepted Manuscripts

Proofs: Galley proofs in PDF format will be sent to the corresponding author via e-mail. Corrections must be returned to the editor (proof-editing@biosciencetrends.com) within 3 working days.

Offprints: Authors will be provided with electronic offprints of their article. Paper offprints can be ordered at prices quoted on the order form that accompanies the proofs.

Page Charge: Page charges will be levied on all manuscripts accepted for publication in BioScience Trends ($140 per page for black white pages; $340 per page for color pages). Under exceptional circumstances, the author(s) may apply to the editorial office for a waiver of the publication charges at the time of submission.

(*Revised February 2013*)

Editorial and Head Office:
Pearl City Koishikawa 603
2-4-5 Kasuga, Bunkyo-ku
Tokyo 112-0003 Japan
Tel: +81-3-5840-8764
Fax: +81-3-5840-8765
E-mail: office@biosciencetrends.com

BST
BioScience Trends

JOURNAL PUBLISHING AGREEMENT (JPA)

Manuscript No.:

Title:

Corresponding Author:

The International Advancement Center for Medicine & Health Research Co., Ltd. (IACMHR Co., Ltd.) is pleased to accept the above article for publication in BioScience Trends. The International Research and Cooperation Association for Bio & Socio-Sciences Advancement (IRCA-BSSA) reserves all rights to the published article. Your written acceptance of this JOURNAL PUBLISHING AGREEMENT is required before the article can be published. Please read this form carefully and sign it if you agree to its terms. The signed JOURNAL PUBLISHING AGREEMENT should be sent to the BioScience Trends office (Pearl City Koishikawa 603, 2-4-5 Kasuga, Bunkyo-ku, Tokyo 112-0003, Japan; E-mail: **office@biosciencetrends.com**; Tel: **+81-3-5840-8764**; Fax: **+81-3-5840-8765**).

1. Authorship Criteria

As the corresponding author, I certify on behalf of all of the authors that:
1) The article is an original work and does not involve fraud, fabrication, or plagiarism.
2) The article has not been published previously and is not currently under consideration for publication elsewhere. If accepted by BioScience Trends, the article will not be submitted for publication to any other journal.
3) The article contains no libelous or other unlawful statements and does not contain any materials that infringes upon individual privacy or proprietary rights or any statutory copyright.
4) I have obtained written permission from copyright owners for any excerpts from copyrighted works that are included and have credited the sources in my article.
5) All authors have made significant contributions to the study including the conception and design of this work, the analysis of the data, and the writing of the manuscript.
6) All authors have reviewed this manuscript and take responsibility for its content and approve its publication.
7) I have informed all of the authors of the terms of this publishing agreement and I am signing on their behalf as their agent.

2. Copyright Transfer Agreement

I hereby assign and transfer to IACMHR Co., Ltd. all exclusive rights of copyright ownership to the above work in the journal BioScience Trends, including but not limited to the right 1) to publish, republish, derivate, distribute, transmit, sell, and otherwise use the work and other related material worldwide, in whole or in part, in all languages, in electronic, printed, or any other forms of media now known or hereafter developed and the right 2) to authorize or license third parties to do any of the above.

I understand that these exclusive rights will become the property of IACMHR Co., Ltd., from the date the article is accepted for publication in the journal BioScience Trends. I also understand that IACMHR Co., Ltd. as a copyright owner has sole authority to license and permit reproductions of the article.

I understand that except for copyright, other proprietary rights related to the Work (*e.g.* patent or other rights to any process or procedure) shall be retained by the authors. To reproduce any text, figures, tables, or illustrations from this Work in future works of their own, the authors must obtain written permission from IACMHR Co., Ltd.; such permission cannot be unreasonably withheld by IACMHR Co., Ltd.

3. Conflict of Interest Disclosure

I confirm that all funding sources supporting the work and all institutions or people who contributed to the work but who do not meet the criteria for authors are acknowledged. I also confirm that all commercial affiliations, stock ownership, equity interests, or patent-licensing arrangements that could be considered to pose a financial conflict of interest in connection with the article have been disclosed.

Corresponding Author's Name (Signature):

Date: